การศึกษาทางเคมีของฟองน้ำทะเล

AXINYSSA SP., *PETROSIA* SP. และ *CACOSPONGIA MYCOFIJIENSIS*

นางสาว วีณา สาธิตปัตติพันธ์

CHEMICAL INVESTIGATIONS OF MARINE SPONGES,
AXINYSSA SP., *PETROSIA* SP. AND *CACOSPONGIA MYCOFIJIENSIS*

Miss Veena Satitpatipan

A Dissertation Submitted in Partial Fulfillment of the Requirements
for the Degree of Doctor of Philosophy in Pharmaceutical Chemistry and Natural Products
Faculty of Pharmaceutical Sciences
Chulalongkorn University
Academic Year 2003

Thesis Title   Chemical Investigations of Marine Sponges, *Axinyssa* sp., *Petrosia* sp., and *Cacospongia mycofijiensis*

By   Miss Veena Satitpatipan

Field of Study   Pharmaceutical Chemistry and Natural Products

Thesis Advisor   Khanit Suwanborirux, Ph.D.

Accepted by the Faculty of Pharmaceutical Sciences, Chulalongkorn University in Partial Fulfillment of the Requirements for the Doctor's Degree

…………………………………………..Dean of the Faculty of Pharmaceutical Sciences

(Associate Professor Boonyong Tantisira, Ph.D.)

THESIS COMMITTEE

…………………………………………………..Chairman

(Associate Professor Ekarin Saifah, Ph.D.)

…………………………………………………..Thesis Advisor

(Khanit Suwanborirux, Ph.D.)

…………………………………………………..Member

(Associate Professor Sunibhond Pummangura, Ph.D.)

…………………………………………………..Member

(Assistant Professor Chamnan Patarapanich, Ph.D.)

…………………………………………………..Member

(Assistant Professor Rutt Suttisri, Ph.D.)

…………………………………………………..Member

(Prasat Kittakoop, Ph.D.)

วีณา สาธิตปัตติพันธ์: การศึกษาทางเคมีของฟองน้ำทะเล *AXINYSSA* SP., *PETROSIA* SP. และ *CACOSPONGIA MYCOFIJIENSIS* (CHEMICAL INVESTIGATIONS OF MARINE SPONGES, *AXINYSSA* SP., *PETROSIA* SP. AND *CACOSPONGIA MYCOFIJIENSIS*) อาจารย์ที่ปรึกษา: ดร. คณิต สุวรรณบริรักษ์, 228 หน้า. ISBN 974-17-47942

จากการศึกษาทางเคมีของฟองน้ำ *Axinyssa* sp. สามารถแยกสารชนิดใหม่ในกลุ่ม nitrogenous germacrane sesquiterpenes ได้ 2 ชนิดคือ (1Z,4Z)-7αH-11-aminogermacra-1(10),4-diene และ *N,N'*-11-bis[(1Z,4Z)-7αH-germacra-1(10),4-dienyl]urea รวมทั้งสารพวกสเตอรอยด์ที่มีรายงานมาแล้ว 1 ชนิดคือ axinysterol ได้เป็นปริมาณโดยน้ำหนักที่คิดจากสิ่งสกัดเมธานอล คือ 0.06% 0.12% และ 0.03% ตามลำดับ พบว่าสาร (1Z,4Z)-7αH-11-aminogermacra-1(10),4-diene มีฤทธิ์ต้านเชื้อ *Staphylococcus aureus*, *Bacillus subtilis* และ *Candida albicans* โดยให้บริเวณยับยั้งเชื้อขนาดเส้นผ่านศูนย์กลาง 23 22 และ 27 มิลลิเมตรตามลำดับ ที่ความเข้มข้น 500 µg/disc

จากการศึกษาทางเคมีของฟองน้ำ *Petrosia* sp. สามารถแยกสารในกลุ่ม pyridoacridine alkaloids ได้ 2 ชนิด คือ สาร 2-bromoamphimedine ซึ่งเป็นสารชนิดใหม่ และสาร petrosamine ที่เคยมีรายงานแล้ว รวมทั้งสารชนิดใหม่ในกลุ่มของ isoguanines 1 ชนิดคือ สาร 1,3,9-trimethyl-8-hydroxyisoguanine ในปริมาณโดยน้ำหนักที่คิดจากสิ่งสกัดบิวธานอล คือ 0.03% 1.5% และ 0.01% ตามลำดับ สาร petrosamine แสดงฤทธิ์ต้านเชื้อ *Bacillus subtilis* โดยให้บริเวณยับยั้งเชื้อขนาดเส้นผ่านศูนย์กลาง 22 มิลลิเมตร ที่ความเข้มข้น 200 µg/disc และมีฤทธิ์ที่แรงในการยับยั้งการทำงานของเอนไซม์ acetylcholinesterase โดยมีค่า IC$_{50}$ เท่ากับ 91 nM ซึ่งมีฤทธิ์แรงกว่าสาร galanthamine ถึงหกเท่า จากการศึกษาโดยวิธีทาง molecular docking แสดงให้เห็นว่าหมู่ quaternary ammonium ของสาร petrosamine มีปฏิกิริยาที่แรงต่อกรดอะมิโนที่สำคัญในบริเวณ active site ของเอนไซม์ acetylcholinesterase ที่ได้จากปลาไหลชนิด *Torpedo californica*

เมื่อทำการแยกสารสกัดจากฟองน้ำ *Cacospongia mycofijiensis* ให้บริสุทธิ์ด้วยวิธีทางโครมาโตกราฟี ควบคู่กับการทดสอบฤทธิ์ทางชีวภาพ สามารถแยกสารที่มีรายงานแล้ว คือสาร latrunculin A และ laulimalide ได้เป็นปริมาณโดยน้ำหนักที่คิดจากสิ่งสกัดเมธานอล คือ 0.54% และ 0.02% ตามลำดับ สาร latrunculin A มีฤทธิ์ยับยั้งการเกิด actin polymerization และสาร laulimalide มีฤทธิ์ทำให้ไมโครทิวบูลคงตัว นอกจากนี้ได้ทำการสังเคราะห์สารอนุพันธ์ในส่วนของคาร์บอนที่ 1 ถึงคาร์บอนที่ 14 ของสาร laulimalide จำนวน 3 ชนิด คือ LAU13, LAU14 และ LAU16 ได้ในปริมาณที่ดี

สาขาวิชา เภสัชเคมีและผลิตภัณฑ์ธรรมชาติ ลายมือชื่อนิสิต...................................
ปีการศึกษา 2546 ลายมือชื่ออาจารย์ที่ปรึกษา........................

Two new nitrogenous germacrane sesquiterpenes, $(1Z,4Z)$-$7\alpha H$-11-aminogermacra-1(10),4-diene, and N,N'-11-bis[$(1Z,4Z)$-$7\alpha H$-germacra-1(10),4-dienyl]urea were isolated from the sponge *Axinyssa* sp., together with a known steroid axinysterol in 0.06, 0.12, and 0.03% w/w based on the MeOH extract, respectively. The compound $(1Z,4Z)$-$7\alpha H$-11-aminogermacra-1(10),4-diene showed significant antimicrobial activity against *Staphylococcus aureus*, *Bacillus subtilis,* and *Candida albicans* with inhibition zones of 23, 22, and 27 mm, respectively, at concentration of 500 μg/disc.

The chemical study of the sponge *Petrosia* sp. led to the isolation of two pyridoacridine alkaloids, including the new 2-bromoamphimedine and the known petrosamine, together with a new isoguanine derivative, namely 1,3,9-trimethyl-8-hydroxyisoguanine in 0.03, 1.5, and 0.01% w/w based on the n-butanol extract, respectively. Petrosamine exhibited antimicrobial activity against *Bacillus subtilis* with an inhibition zone of 22 mm at concentration of 200 μg/disc and possessed acetylcholinesterase inhibitory activity with an IC_{50} of 91 nM, which was six times more potent than the reference compound galanthamine. Molecular docking study indicated the quaternary ammonium group of petrosamine donated the major and strong interactions to the key amino acid residues in the active site of *Torpedo californica* acetylcholinesterase.

Bioassay-guided fractionation led to the isolation of the actin polymerization inhibitor latrunculin A and the microtubule-stabilizing agent laulimalide from the sponge, *Cacospongia mycofijiensis*. The yields of latrunculin A and laulimalide were 0.54 and 0.02% w/w based on the MeOH extract, respectively. In addition, three C1-C14 fragment analogs of laulimalide, LAU13, LAU14, and LAU16, were successfully synthesized in good yields.

Field of study Pharmaceutical Chemistry and Natural Products

Academic year 2003   Student's signature……………………...

                                     Advisor's signature……………………..

ACKNOWLEDGEMENTS

I would like to express my deepest gratitude to Dr. Khanit Suwanborirux of Deparment of Pharmacognosy, Faculty of Pharmaceutical Sciences, Chulalongkorn University, for being my advisor. I also greatly realize for his valuable advice, kindness, patience, and a constant encouragement throughout my research study.

I am so thankful to Assoc. Prof. Supot Hannongbua and Dr. Suwipa Saen-oon of Faculty of Science, Chulalongkorn University for kindly helping and valuable suggestions in molecular modeling experiment.

I wish to thank Assist. Prof. Kornkanok Ingkaninan of Faculty of Pharmaceutical Sciences, Naresuan University for performing bioassay of acetylcholinesterase activity.

I am very grateful to all thesis committees for their valuable advice and assistance. My sincere appreciation is conveyed as well to Bioassay Research Facilities of the National Center for genetic Engineering and Biotechnology (BIOTEC) for performing bioassay of cytotoxic activities and to the Scientific and Technology Research Equipment Center (STREC) and Pharmaceutical Research Equipment Center of Pharmaceutical Sciences, Chulalongkorn University for providing all research facilities.

My deepest appreciations are extended to Dr. Bradley S. Davidson of Department of Chemistry and Biochemistry, Utah State University, USA for his warm support and useful guidance in synthesis of analogs of laulimalide.

I am particularly indebted to the Thailand Research Fund (TRF) for financial support through the 1998 Royal Golden Jubilee Ph.D. program.

On the personal side, I would like to thank previous/present graduate students of the Department of Pharmacognosy, Chulalongkorn University and of Department of Chemistry and Biochemistry, Utah State University who all share the happy time together.

Finally, I would like to express my special deepest appreciation to my wonderful parents and my family for their love, understanding and encouragement.

CONTENTS

LIST OF TABLES

Table **Page**

LIST OF FIGURES

Figure		Page

SECTION 2 CHEMICALCONSTITUENTS FROM THE SPONGE,

PETROSIA SP.

SECTION 3 CHEMICAL CONSTITUENTS FROM THE SPONGE,
        CACOSPONGIA MYCOFIJIENSIS

Figure   **Page**

Figure **Page**

LIST OF SCHEMES

LIST OF ABBREVIATIONS AND SYMBOLS

$[\alpha]^{25}_D$	=	Specific rotation at 25° and sodium D line (589 nm)
α	=	Alpha
β	=	Beta
Bn	=	Benzyl
br	=	Broad (for NMR spectra)
Bu	=	Butyl
BuOH	=	Butanol
Bz	=	Benzoyl
°C	=	Degree Celsius
calcd	=	Calculated
$CDCl_3$	=	Deuterated chloroform
C_6D_6	=	Deuterated benzene
$CHCl_3$	=	Chloroform
CH_2Cl_2	=	Dichloromethane
^{13}C NMR	=	Carbon-13 Nuclear Magnetic Resonance
2D NMR	=	Two dimensional Nuclear Magnetic Resonance
d	=	Doublet (for NMR spectra)
dd	=	Doublet of doublets (for NMR spectra)
DCC	=	Dicyclohexylcarbodiimide
DMAP	=	4-*N,N*-dimethylaminopyridine
DEPT	=	Distortionless Enhancement by Polarization Transfer
DMSO	=	Dimethyl sulfoxide
DMSO-d_6	=	Deuterated dimethyl sulfoxide
δ	=	Chemical shift
EIMS	=	Electron Impact Mass Spectrometry
EtOAc	=	Ethyl acetate
g	=	Gram
hr	=	Hour
^1H NMR	=	Proton Nuclear Magnetic Resonance
H,H-COSY	=	Homonuclear (Proton-Proton) Correlation Spectroscopy
HMBC	=	^1H-detected Heteronuclear Multiple Bond Coherence

HMQC	=	^{1}H-detected Heteronuclear Multiple Quantum Coherence
HPLC	=	High Pressure Liquid Chromatography
H_2O	=	Water
HRFABMS	=	High Resolution Fast Atom Bombardment Mass Spectrometry
Hz	=	Hertz
IC_{50}	=	Median Inhibitory Concentration
IR	=	Infrared Spectrum
J	=	Coupling constant
Kg	=	Kilogram
l	=	Liter
Me	=	Methyl
μg	=	Microgram
μl	=	Microliter
μM	=	Micromolar
λ_{max}	=	Wavelength at maximal absorption
ε	=	Molar absorptivity
M^{+}	=	Molecular ion
m	=	Multiplet (for NMR spectra)
MeOH	=	Methanol
mg	=	Milligram
$[M+H]^{+}$	=	Protonated molecular ion
MHz	=	Megahertz
min	=	Minute
mL	=	Milliliter
MW	=	Molecular weight
m/z	=	Mass to charge ratio
MS	=	Mass Spectrometry
NaCl	=	Sodium chloride
nM	=	Nanomolar
NOE	=	Nuclear Overhauser Effect
Pet. Ether	=	Petroleum ether
Ph	=	Phenyl
ppm	=	Part-per-million

TFA	=	Trifluoroacetic acid
THF	=	Tetrahydrofuran
TLC	=	Thin Layer Chromatography
TMS	=	Trimethylsilyl
UV	=	Ultraviolet

GENERAL INTRODUCTION

Natural products are organic compounds produced by microbes, plants, and marine invertebrates. It is thought by some that toxic natural products are produced by the host as adaptations to deter predators (chemical defense) or to compete for space in their native environments (alleopathy). Some natural products also exhibit biological activities relevant to human physiology and disease states. Many terrestrial natural products have found uses in medicine and agriculture; however, exploration of marine natural products is relatively recent.

The unusal adaptations of marine organisms to their unique aquatic environment are of continuing excitement to scientists with diverse interests, including biologists, chemists, ecologists, and those involved in drug discovery and development (Faulkner, 2000). The secondary metabolites of these creatures, and the underlying biochemical systems responsible for their formation, are unlike those from terrestrial plants and microorganisms, and hence represent an exciting "treasure trove" of compounds for drug discovery and ensuing biochemical studies.

Marine natural products often possess chemical structures with exotic functional groups (e.g. isonitrile, multiple halogenation) or unique parent carbon skeletons that are without precedent among terrestrial natural products. In the early 1950's, Bergmann reported the first isolation of marine natural products (Bergmann and Feeney, 1951; Bergmann and Bruke, 1955). From the sponge *Cryptotethya crypta*, spongothymidine [1] and spongouridine [2], which possessed arabinose sugar instead of the more common ribose sugar, were isolated. This finding led to the development of the ara-nucleosides, such as ara-A [3] and ara-C [4] as anticancer agents, and ultimately to the development of the first, and still drug of choice, antiviral agent acyclovir [5] (Mayer, 1999).

[1] R = CH₃   [3]   [4]   [5]

[2] R = H
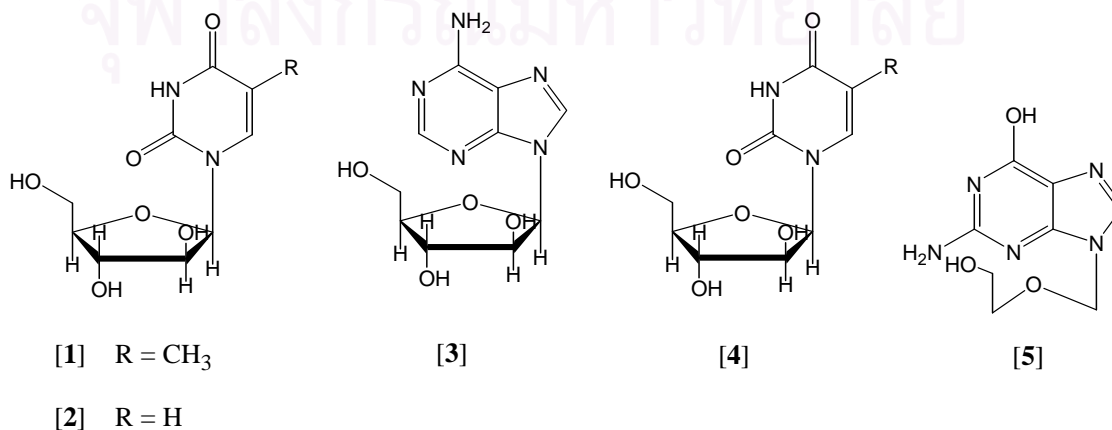
The ability of marine organisms to produce novel secondary metabolites that are unprecedented among terrestrial natural products, as well as the potential of these compounds for the medicinal and pharmaceutical applications, as seen in the ara-nucleosides, have both drawn scientists' attention to marine natural products. Investigations of secondary metabolites from marine organisms have focused particularly on their potential biomedical and agricultural applications (Faulkner, 2002).

Among the anticancer compounds currently under investigation, bryostatin 1 [**6**] serves as a good example of past and current trends in marine biomedical research. Bryostatin 1 was isolated in very small quantities from the bryozoan *Bugula neritina* and its structure was determined by x-ray crystallography in 1982 (Pettit *et al.*, 1982). It is currently in phase 2 clinical trials. Supply of material for clinical trials was a problem until it was demonstrated that *B. neritina* was amenable to aquaculture. Recently, evidence favouring a symbiotic origin for bryostatin 1 has been presented, opening the way for biotechnological manipulation of the biosynthetic genes (Faulkner, 2000.). Furthermore, it has been shown that semi-synthetic bryostatins retain the activity of the natural product (Batrakov *et al.*, 1998). Other marine natural products under intense investigation at present include the potential anticancer agents dehydrodidemnin B, dolastatin 10, ecteinascidin 743, discodermolide, eleutherobin, and sarcodictyin A (Faulkner, 2000).
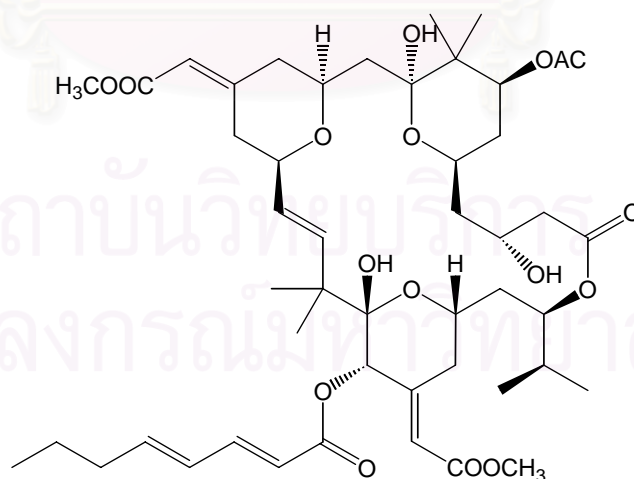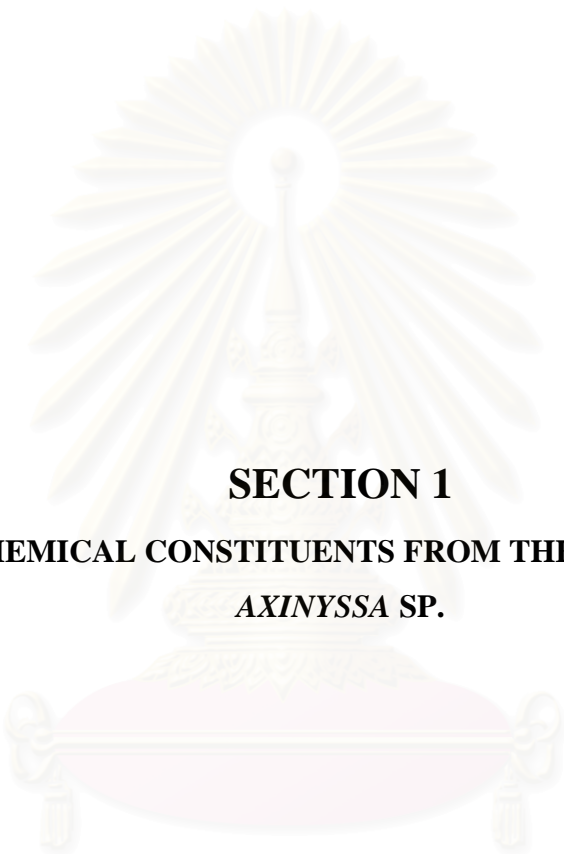
[**6**]

Secondary metabolites from marine organisms are diverse in their biosynthetic origins, including products from the mevalonate, polyketide, and amino acid biosynthetic pathways. The sources of marine natural products have included almost

every phylum of marine organisms, ranging from the prokaryotic microbes to hemichordates. However, not all phyla are equal in their production of numbers or types of compounds (Ireland *et al.*, 1993). During the early years of marine natural product studies, macroalgae were heavily studied, possibly because of their abundance and availability. For instance, during the decade from 1977 to 1987, approximately one third of the newly reported compounds were isolated from algae (Faulkner, 1988). However, marine invertebrates have gained increasing attention. Sponges, in particular, have become the dominant source of natural products because of not only their relative ease of collection, but also a wider range of biosynthetic capabilities than other groups of marine invertebrates (Ireland *et al.*, 1993). The study of sponges has, thereby, led to the discovery of a whole range of new structural classes.

As described above, marine organisms, particularly sponge, have been shown to be promising sources of biologically active and potentially useful natural products. In this dissertation, three separated research projects involving three marine sponges will be discussed. Each sponge was chosen based on promising biological activities and the observation of interesting compounds as detected in the NMR spectrum of its crude extract. The following three sections will describe the research results from these projects involving selected marine sponges. The three sections are: 1) chemical constituents from the sponge, *Axinyssa* sp., 2) chemical constituents from the sponge, *Petrosia* sp., 3) chemical constituents from the sponge, *Cacospongia mycofijiensis*. The isolation, structure determination, and biological testing of isolated compounds will be discussed. In addition, the synthesis of the C1-C14 fragment analogs of laulimalide will be conducted in section 3.

SECTION 1

CHEMICAL CONSTITUENTS FROM THE SPONGE,
***AXINYSSA* SP.**

CHAPTER I

INTRODUCTION

Marine sponges are proved to be a rich source of secondary metabolites with unusual structures as well as interesting biological activities. The marine sponges of the genus *Axinyssa* which belongs to order Halichondrida, Family Halichondriiidae, have attracted considerable research interest mainly due to the presence of sesquiterpenes containing unusual nitrogenous functional groups, such as isothiocyanates, isocyanides, and formamides (He *et al.*, 1989; Marcus *et al.*, 1989; Alvi, Tenenbaum, and Crews, 1991; He *et al.*, 1992; Compagnone and Faulkner, 1995; Patil *et al.*, 1997; Simpson *et al.*, 1997). Occasionally, sesquiterpene thiocyanates, ureas, or amines are encountered. These metabolites are thought to inhibit feeding by omnivorous browsers; however they do not deter nudibranches that are specific predators on the sponges. Since almost all compounds from the sponges of the genus *Axinyssa* are terpenes, the structure elucidation as well as stereochemistry determination is challenging due to the overlapping signals and chiral positions frequently found within the molecules. The secondary metabolites from the sponges of the genus *Axinyssa* have shown a variety of biological activities, such as antimicrobial activity, cytotoxicity (Simpson *et al.*, 1997), and anthelmintic activity (Alvi *et al.*, 1991).

As mentioned above, the combination of promising activities and challenging structures which contained unusual functional groups have made the search of the compounds from the sponge of the genus *Axinyssa* interesting.

During preliminary study, the EtOAc extract of the reddish brown sponge *Axinyssa* n. sp. collected from the Andaman Sea, Trang province, Thailand in 2002 exhibited significant antimicrobial activity against *Staphylococcus aureus, Bacillus subtilis,* and *Candida albicans*. These data led to the isolation of the active compounds from the sponge *Axinyssa* n. sp. In the following section, the isolation, purification and structure elucidation of the isolated compounds from the sponge *Axinyssa* n sp. will be discussed. In addition, the antimicrobial activity of the isolated compounds will also be described.

CHAPTER II

HISTORICAL

Marine sponges of the genus *Axinyssa* have provided an unprecedented array of sesquiterpene isonitriles, isothiocyanates, and formamides. In 1989, Faulkner's group reported the isolation of 5-isothiocyanatopupukeanane [1] from a sponge of the genus *Axinyssa* collected at Gun Beach, Guam (Marcus *et al.*, 1989). This compound was isolated along with the known metabolites 10-isothiocyanato-4-amorphene [2], calamanene [3], and zizanene [4]. The compound 2-isothiocyananopupukeanane [5] which has similar structure to that of [1] was reported from sponge of the genus *Hymeniacidon* (Hagadone *et al.*, 1979). The crude extract of the sponge *Axinyssa* deterred feeding in the common pufferfish *Canthigaster solandri*. However, when tested at a relatively high concentration of [1], it failed to deter feeding.

[1]   [5]

[2]   [3]   [4]
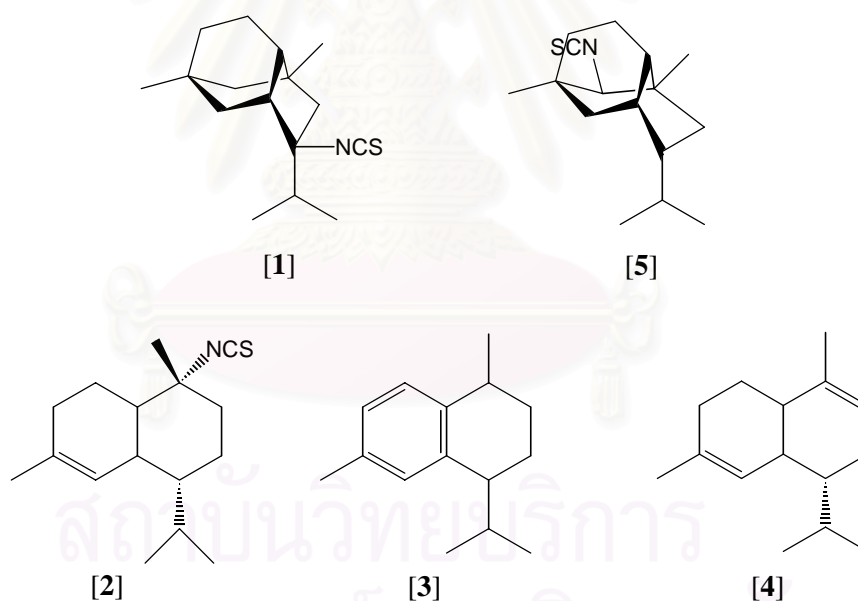
Although many marine sponges of the order Halichondrida produce sesquiterpene isonitriles, isothiocyanates, and formamides, the corresponding thiocyanates have rarely been encountered. A specimen of *Trachyopsis aplysinoides* from Palau, which has been later reclassified as *Axinyssa aplysinoides*, containing a sesquiterpene thiocyanate, (1S^*,4S^*,6S^*,7R^*)-4-thiocyanato-9-cadiene [6], in addition to three sesquiterpene isothiocyanates [7-9], and a sesquiterpene formamide [10] has been reported by Faulkner's group (He *et al.*, 1989). Reinvestigation of the same

sponge in 1992 yielded a second thiocyanate, $(1R^*,2R^*,3R^*,5R^*,6S^*,7S^*)$-2-thiocyanatopupukeanane [**10**], as a minor metabolite (He *et al.*, 1992).

[**6**] [**7**] [**8**]

[**9**] [**10**]
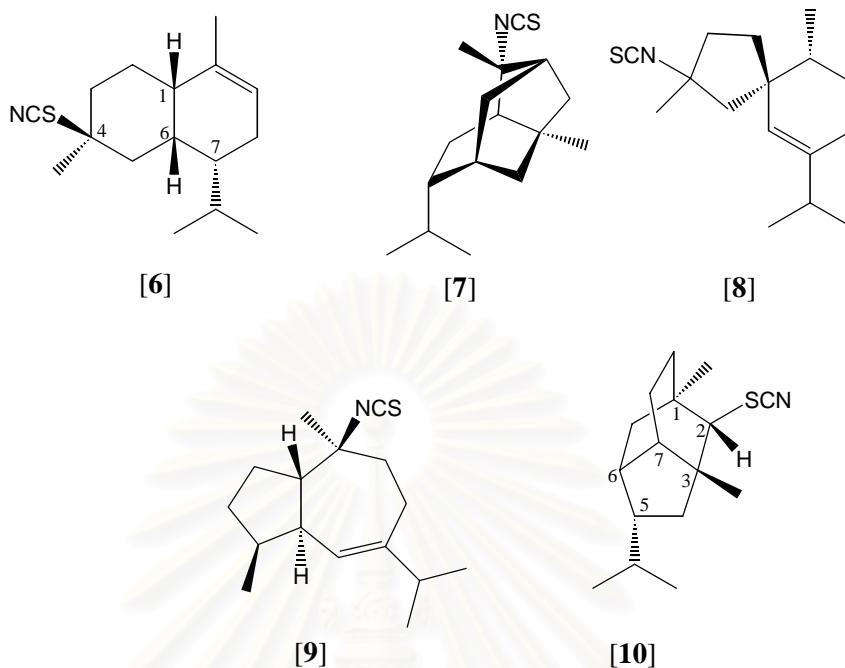
The same group also investigated a specimen of *A. aplysinoides* from another location, Pohnpei, which yielded two new isothiocyanates, $(1S^*,2R^*,5S^*,6S^*,7R^*,8S^*)$-13-isothiocyanatocubebane [**11**] and $(1R^*,4S^*,5R^*,6S^*,7S^*,10R^*)$-1-isothiocyanatoaroma dendrane [**12**]. A second specimen of *A. aplysinoides* from Pohnpei was isolated to obtain axisonitrile-3 [**13**] and a thiocyanate $(1S^*,2S^*,3R^*,6R^*,7S^*,9R^*)$-2-thiocyanatoneopupukaenane [**14**]. The relative configuration of these compounds was obtained from NOEDS experiments (He *et al.*, 1992).

[**11**] [**12**]

[**13**] [**14**]
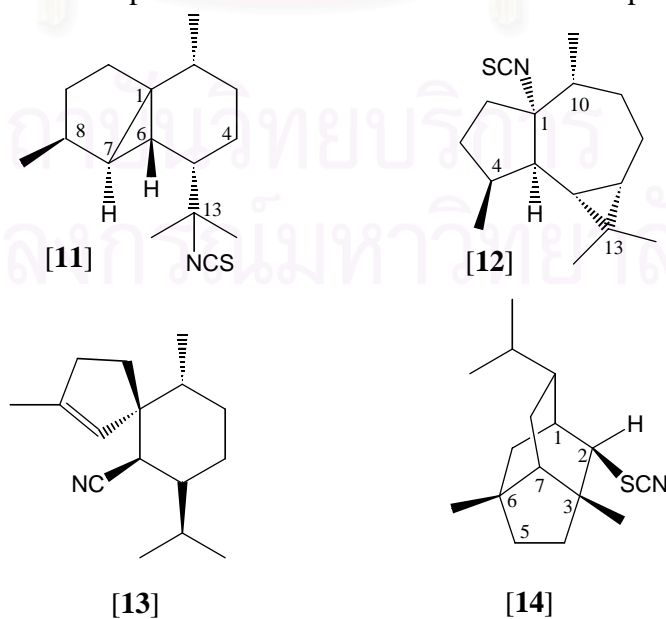
Bioassay-guided isolation of the Fiji sponge *Axinyssa fenestratus* based on anthelmintic activity resulted in four amorphane sesquiterpenes (1*R*,6*S*,7*S*,10*S*)-10-isothiocyanato-4-amorphene [(+)-**15**], (1*R**,4*S**,6*R**,7*S**)-4-isothiocyanato-9-amorphene [**16**], 10-isothiocyanato-4,6-amorphadiene [**17**], and 10-isothiocyanato-5-amorphen-4-ol [**18**] (Alvi, Tenenbaum, and Crews, 1991). Compound [(-)-**15**] was previously described by Burreson *et al* from a deep-water *Halichondria* sp. collected off Oahu Island, Hawaii (Burreson, Christophersen, and Scheuer, 1975). Compound [(+)-**15**], [**16**], [**17**] were active against *Nippostrongylus brasiliensis*.

[(+)-**15**]   [**16**]   [**17**]   [**18**]
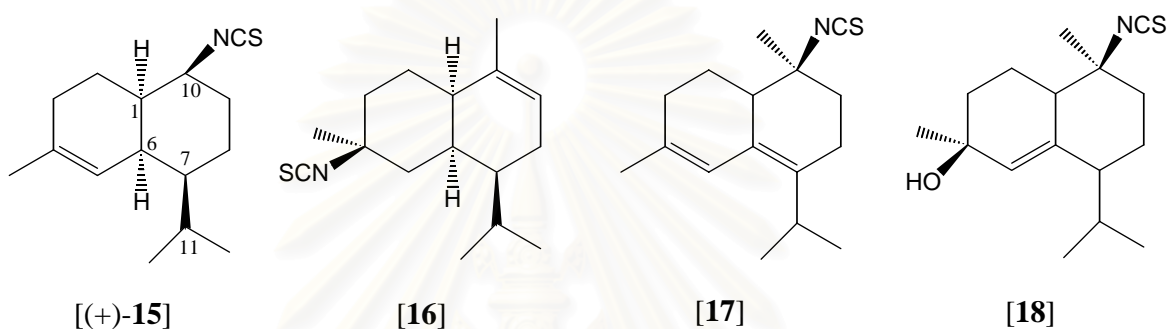
From the Palauan sponge *Ax*inyssa *aplysinoides*, was isolated compounds of different classes, (3*S**,5*R**,6*R**,9*R**)-3-isocyano-1(10)-cadiene [**19**], (3*S**,5*R**,6*R**,9*R**)-3-formamido-1(10)-cadinene [**20**], and (*E*)-(4-hydroxystyryl) trimethylammonium chloride [**21**], together with the known diterpenes (-) neoverrucosan-5β-ol [**22**] and (+)-homoverrucosan-5β-ol [**23**] (Compagnone and Faulkner, 1995). Although it is unusual to isolate different class of compounds from a single sponge, the authors stated that there was no obvious evidence of the presence of symbionts or other sponges in the sample. The antimicrobial activity of the crude extract was shown to be due to the formamide [**20**] that inhibited *Staphylococcus aureus* and *Bacillus subtilis* at 25 and 10 μg/disc, respectively.

[**19**]   R = NC   [**21**]   [**22**]   [**23**]

[**20**]   R = NHCHO
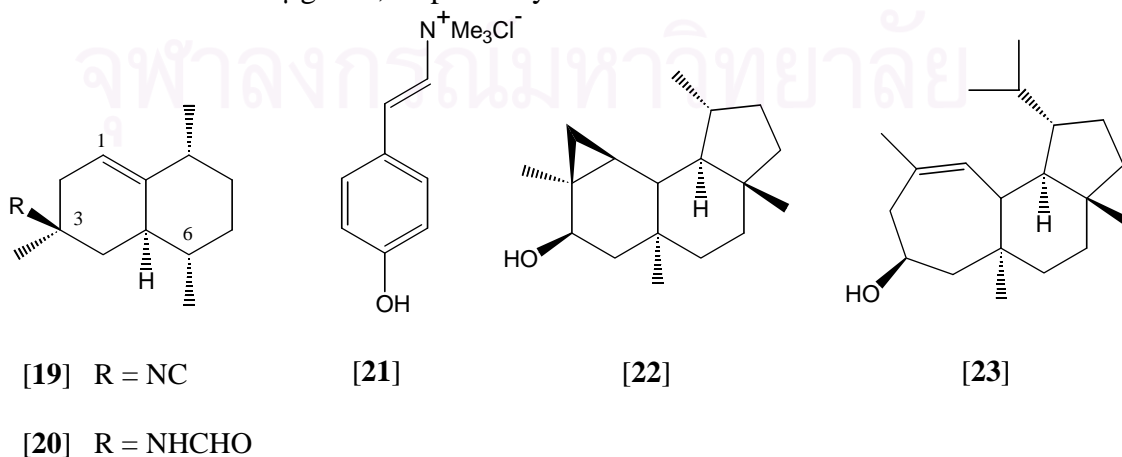
The crude EtOAc extract of the same sponge *A. aplysinoides* was subjected to bioassay-guided fractionation to yield two novel compounds, 2-(formylamino) trachyopsane [**24**] and *N*-phenethyl-*N′*-2-trachyopsanylurea [**25**] (Patil *et al*., 1997). Both compounds demonstrated activity against wild-type and DNA-repair-deficient yeast strains at concentrations in the range of 20-50 μg/100 μL.

[**24**]   R = H

[**25**]   R =
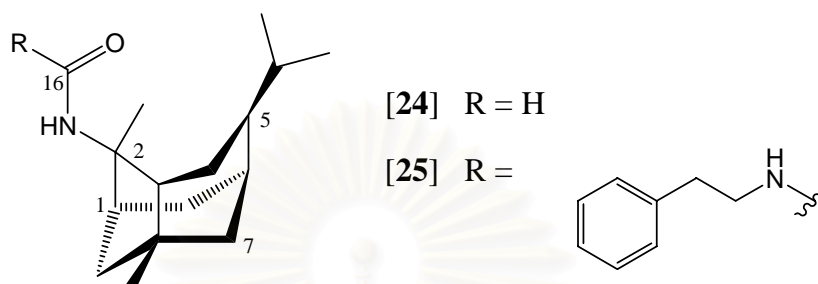
The first report of nitrogenous bisabolenes from sponges of the genus *Axinyssa* was recently described by Kelly's group from New Zealand. Three new formamido-substituted bisabolene sesquiterpenes, 3-formamidobisabolane-14(7),9-dien-8-one [**26**], 3-formamidobisabolane-14(7),9-dien-8-ol [**27**], and 3-formamido-8-methoxybisabolan-9-en-10-ol [**28**], together with the known compound 3-formamidotheonellin [**29**] were isolated from a Micronesian marine sponge *Axinyssa* sp (Li, Schmitz, and Kelly, 1999). Other nitrogenous bisabolenes have been found from sponges in other genus, such as *Theonella*, *Halichondrida*, *Acanthella*, and some mollusks.

[**26**]

[**27**]

[**28**]

[**29**]
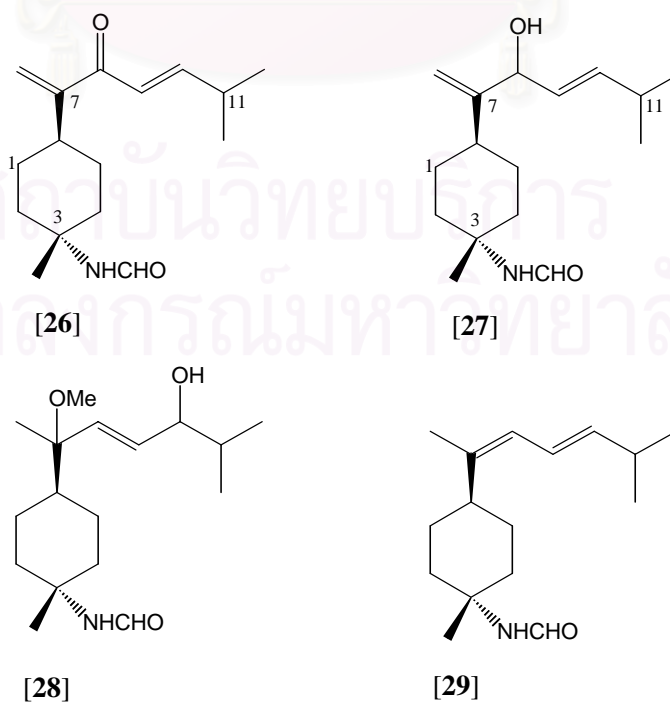
Recently, a novel diterpene, (-)-axinyssene [**30**], was isolated from the Japanese marine sponge *Axinyssa* sp. collected from Tsutsumi Island, Fukuoka prefecture, Japan, together with three known sesquiterpenes: isothicyanate [**31**], (+)-axisothiocyanate 2 [**32**], and epipolasin [**33**] (Kodama *et al*., 2003). The absolute configuration of axinyssene was determined by spectroscopic techniques and synthesis of (+)- and (-)-axinyssene from the commercially available (+)- and (-)-limonene and geraniol. The (+)- and (-)-axinyssene did not differ significantly in their cytotoxicity against acute promyelocytic leukemia, HL-60 cells (12.1 and 9.6 µg/mL).

[**30**]

[**31**]   [**32**]   [**33**]
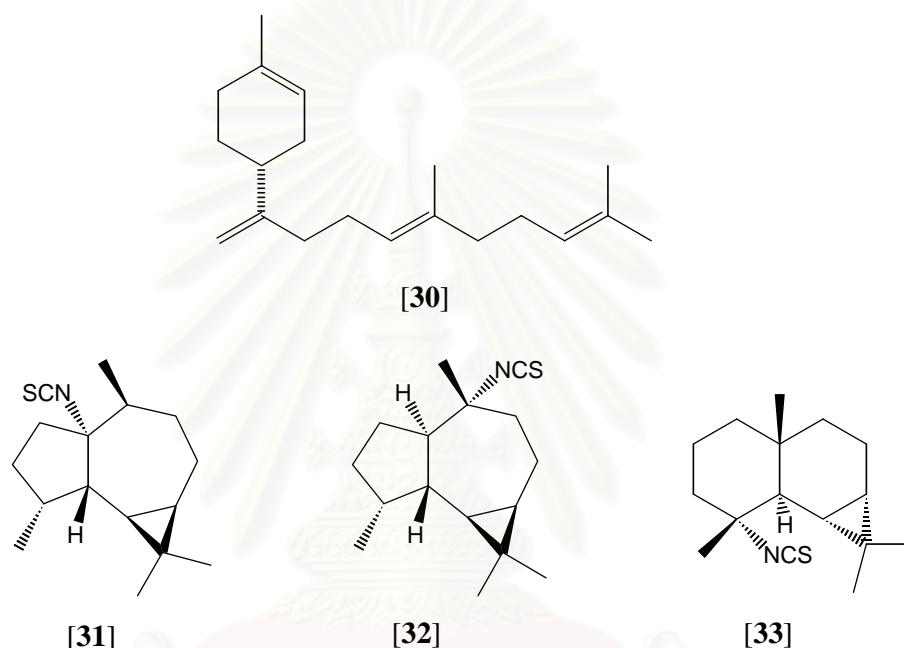
Most terpene isocyanides from sponges occur along with parallel isothiocyanates, formamides, and amines. Fookes *et al* have demonstrated that cyanide is important in the biosynthesis of diterpene diisocyanoadocianne (Fookes *et al*., 1988), while Karuso and Scheuer have proved that cyanide is a specific precursor for the isocyano function in selected sesqui- and diterpenes (Karuso and Scheuer, 1989). In an additional study, Hagadone *et al* have shown the interconversion of RNC to RNHCHO in sponges (Hagadone *et al*., 1984), but Tada *et al*. have also shown this same interconversion can occur during chromatography of an isocyanate. Recently, Simpson and Garson have demonstrated the conversion of inorganic cyanide into inorganic thiocyanate in the sponge *Axinyssa* n. sp. (Simpson and Garson, 1998). More recently, the same group has shown that the isocyano sesquiterpene can be interconverted to isothiocyanate by the sponge *Axinyssa* n. sp. (Simpson and Garson, 2001).

CHAPTER III

EXPERIMENTAL

1. Sample collection

The reddish brown sponges were collected from the Andaman Sea, Trang province, Thailand at the depth of 10-15 m in April 2002. This sponge was frozen on site, and preserved at -20 °C before extraction. The sponge was later identified as *Axinyssa* n. sp. (Class Demonspongiae, Order Halichondrida, Family Halichondriidae) by Dr. John N.A. Hooper of Queensland Museum, South Brisbane, Australia. The voucher specimens of this sponge are deposited at Queensland Museum under number QM G320224 and also at Bioactive Marine Natural Products Chemistry Research Unit, Department of Pharmacognosy, Faculty of Pharmaceutical Sciences, Chulalongkorn University under code number of TR98-16.

1.1 Identification and Characterization of the sponge *Axinyssa* n. sp.

The sponge was identified and characterized by Dr. John N. A. Hooper from Queensland Museum, South Brisbane, Australia. The identification and characterization of this sponge were conducted as follows:

Name : *Axinyssa* new species [QM species file number # 1939]

Phylum : Porifera

Class : Demospongiae

Order : Halichondrida

Family : Halichondriidae

Known Distribution : East coast of Queensland (Moreton Bay to northern Great Barrier Reef), Andaman Sea, Thailand

Habitat : Growing on rocks and dead coral, shallow subtidal

Grown form : Lobate, massive, and partially embedded in substratum

Color : Externally brownish violet; internally whitish brown

Oscules : several, discrete, small, flush with surface

Texture : Soft

Ectosomal skeleton   : Organic, tough, infrequently penetrated by ascending
                          choanosomal tracts of oxeas

Choanosomal skeleton: Deeper choanosome is comprised of vaguely ascending
                          tracts of oxeas amongst a scattered confusion of individual
                          oxeas; the peripheral choanosomal region lacks the confusion
                          of individual oxeas but is still transversed by ascending tracts

Megascleres   : Long slender oxeas with telescoped points, straight or slightly
                          curved

Length   : 340-(475)-585 μm

Width   : 6-(15)-22 μm

Microscleres   : Absent
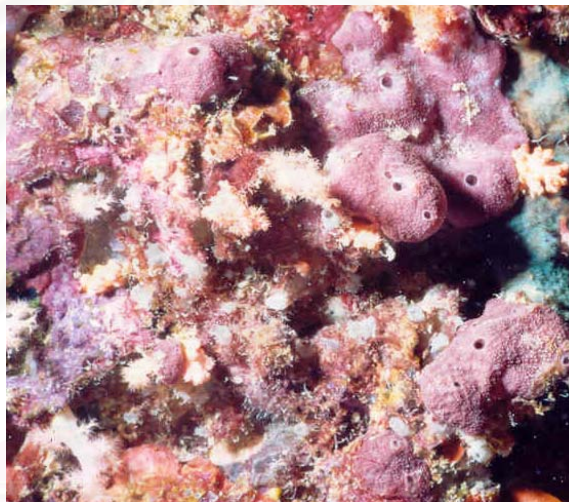
Figure 1 The sponge *Axinyssa* n. sp.

2. General Techniques

2.1 Solvents

Throughout this work, all organic solvents were of commercial grade and were redistilled prior to use.

2.2 Analytical Thin-Layer Chromatography (TLC)

Technique	:	One dimension, ascending
Adsorbent	:	Silica gel 60 F_{254} (E. Merck) pre-coated plate
Layer thickness	:	250 μm
Distance	:	5.0 cm
Temperature	:	Laboratory temperature (25-30 ^oC)
Detection	:	1. Visual detection under daylight
		2. Ultraviolet light (254 and 365 nm)
		3. Anisaldehyde and heating at 105 ^oC for 10 min

2.3 Column Chromatography

2.3.1 Flash Column Chromatography

Adsorbent	:	Silica gel 60 (No. 7734) particle size 0.063-0.200 nm (70-230 mesh ASTM) (E. Merck)
Packing method	:	Wet packing: the adsorbent was slurried in the eluent, and poured into a column and then allowed to settle.
Sample loading	:	The sample was dissolved in a small amount of the eluent, and then applied gently on top of the column.
Detection	:	Fractions were examined by TLC technique in the same manner as described in section 2.2

2.3.2 Gel Filtration Chromatography

Gel Filter	:	Sephadex LH-20 (Pharmacia Biotech AB)
Packing method	:	Gel filter was suspended in the eluent and left standing to swell for 24 hours prior to use. It was then poured into the column and allowed to set tightly.
Sample loading	:	The sample was dissolved in a small amount of eluent and then applied gently on top of the column.

Detection   :   Fractions were examined by TLC technique in the same
manner as described in section 2.2

2.4 Crystallization Technique

Compounds **TRF01** and **TRF03** were crystallized by dissolving in $CHCl_3$, until saturated and then MeOH was added. The solutions were left standing at room temperature until white crystals were formed.

2.5 Spectroscopy

2.5.1 Ultraviolet (UV) Spectra

UV spectra were obtained on a Milton Roy Spectronic 3000 Array spectrophotometer (Pharmaceutical Research Instrument Center, Faculty of Pharmaceutical Sciences, Chulalongkorn University).

2.5.2 Infrared (IR) Spectra

IR spectra were recorded on a Perkin Elmer FT-IR 1760X spectrometer (Pharmaceutical Research Instrument Center, Faculty of Pharmaceutical Sciences, Chulalongkorn University).

2.5.3 Mass Spectra

Mass spectra were obtained by an Electrospray Ionization Time of Flight mass spectra (ESI-TOF MS) made on a Micromass LCT mass spectrometer (The National Center for Genetic Engineering and Biotechnology, BIOTEC, Thailand), and the lock mass calibration was applied for the determination of accurate mass, Electron Impact mass spectrometry (EIMS) on a JEOL JMS-700 (Meiji University, Japan)

2.5.4 Proton and Carbon-13 Nuclear Magnetic Resonance (^{1}H and ^{13}C NMR) Spectra

^{1}H (300 MHz) and ^{13}C (75 MHz) NMR spectra were measured on a Bruker DPX-300 FT-NMR spectrometer (Pharmaceutical Research Instrument Center, Faculty of Pharmaceutical Sciences, Chulalongkorn University).

The solvents for NMR spectra were deuterated benzene (C_6D_6), and deuterated chloroform ($CDCl_3$). The chemical shifts were reported in ppm scale using

the chemical shift of residual undeuterated solvents as the reference signals at δ 7.15 ppm (^{1}H) and 128.0 ppm (^{13}C) for DMSO-$d_6$7.24 ppm (^{1}H) and 77.0 ppm (^{13}C) for CDCl$_3$.

2.6 Physical Properties

2.6.1 Melting Points

Melting points were obtained on a Fisher-John Melting Point Apparatus (Department of Pharmaceutical Botany, Faculty of Pharmaceutical Sciences, Chulalongkorn University).

2.6.2 Optical Rotations

Optical rotations were measured on a Perkin-Elmer 341 polarimeter using a sodium lamp operating at 589 nm (Pharmaceutical Research Instrument Center, Faculty of Pharmaceutical Sciences, Chulalongkorn University).

2.6.3 Circular Dichroism (CD) Spectra

CD spectra were recorded on a JASCO J-715 spectropolarimeter (Pharmaceutical Research Instrument Center, Faculty of Pharmaceutical Sciences, Chulalongkorn University).

3. Extraction and Isolation of Compounds from *Axinyssa* n. sp.

3.1 Extraction

Freshly thawed specimens of the sponge *Axinyssa* n. sp. (15 kg wet wt) were cut into small pieces and macerated three times with MeOH (14 L each). The combined extracts were concentrated *in vacuo*, and the residue was partitioned between EtOAc and H$_2$O to obtain the crude EtOAc extract (18 g) (Scheme 1).

The EtOAc extract exhibited strong antimicrobial activity; therefore it was further purified by chromatographic techniques.

3.2 Isolation

The crude EtOAc extract (**F03**) (18 g) was chromatographed on a silica gel column by eluting stepwise with hexane-CHCl$_3$, CHCl$_3$, CHCl$_3$-MeOH, and MeOH to give 5 fractions **F04**-**F08** (Scheme 2). The fraction **F05** was repeatedly purified by a

silica gel column using isocratic hexane- $CHCl_3$ (1:4) as an eluent to yield compound **TR02** (Scheme 3)**.** The fraction **F06** was successively separated with a Sephadex LH-20 column using $CHCl_3$-EtOAc (1:1) as solvent, followed by a silica gel column (stepwise, $CHCl_3$-MeOH) to yield compound **TR03** (Scheme 3)**.** The fraction **F07** was further chromatographed on a silica gel column by eluting with $CHCl_3$-MeOH (10:1) and on a Sephadex LH-20 column by eluting with MeOH to yield the active compound **TR01** (Scheme 2)**.**
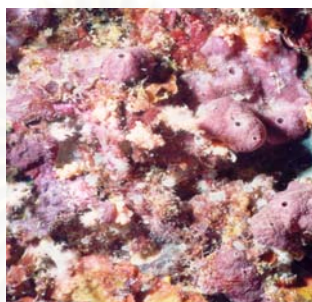
Sponge Axinyssa n. sp.
(15 kg wet wt.)

macerated with MeOH
filtered
evaporated

MeOH extract (**F01**)
(25 g)

Partitioned with EtOAc/H_2O

EtOAc extract (**F02**)   Aqueous extract
(18 g)

Scheme 1 Extraction of the Reddish Brown Sponge *Axinyssa* n. sp.

F03*
(18g)

silica gel
gradient Hexane:CHCl$_3$:MeOH

F04   **F05**   **F06**   **F07*** F08
(2.3 g)   (3.1 g)   (4.2 g)   (2.8 g)   (4.7 g)

Scheme 3

silica gel
CHCl$_3$:MeOH (10:1)

F09   F10   F11   **F12*** F14
(21 mg)   (45 mg)   (25 mg)   (42 mg)   (31 mg)

SephadexLH-20, MeOH

F15   F16   **F17*** F18
(7 mg)   (11 mg)   (4 mg)
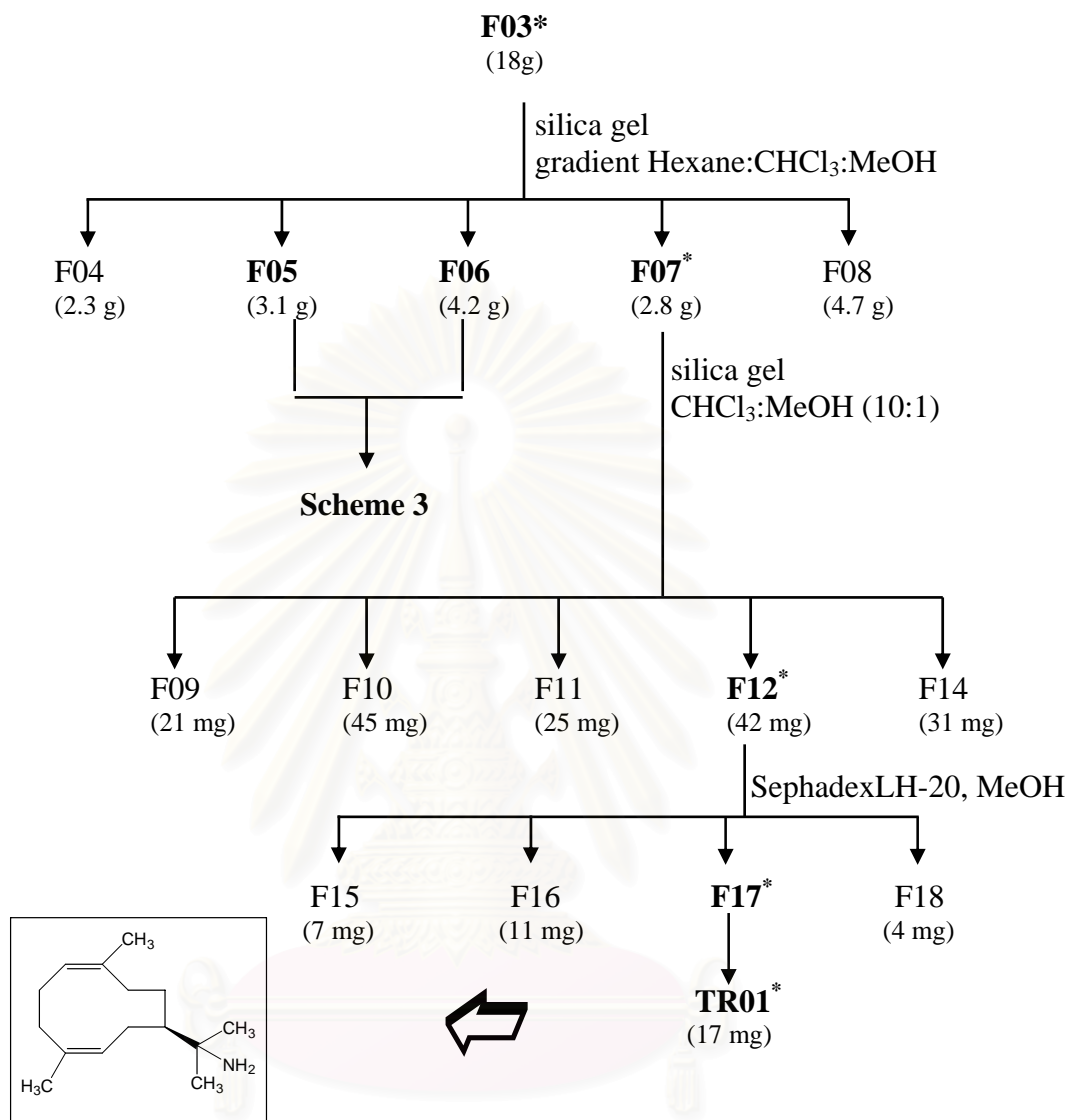
TR01*
(17 mg)

Scheme 2 Isolation of the EtOAc Extract from the sponge *Axinyssa* n. sp.

F05
(3.1 g)

F06
(4.2 g)

silica gel
hexane:CHCl₃
(1:4)

F19
(53 mg)

F20
(40 mg)

F21
(64 mg)

F22
(90 mg)

Sephadex LH-20
CHCl₃:EtOAc
(1:1)

recrystallized

TR02
(32 mg)

F23
(40 mg)

F24
(86 mg)

F25
(67 mg)

F26
(140 mg)

silica gel
CHCl₃:MeOH

F27
(12 mg)

F28
(25 mg)

F29
(11 mg)

F30
(8 mg)

recrystallized

TR03
(8 mg)
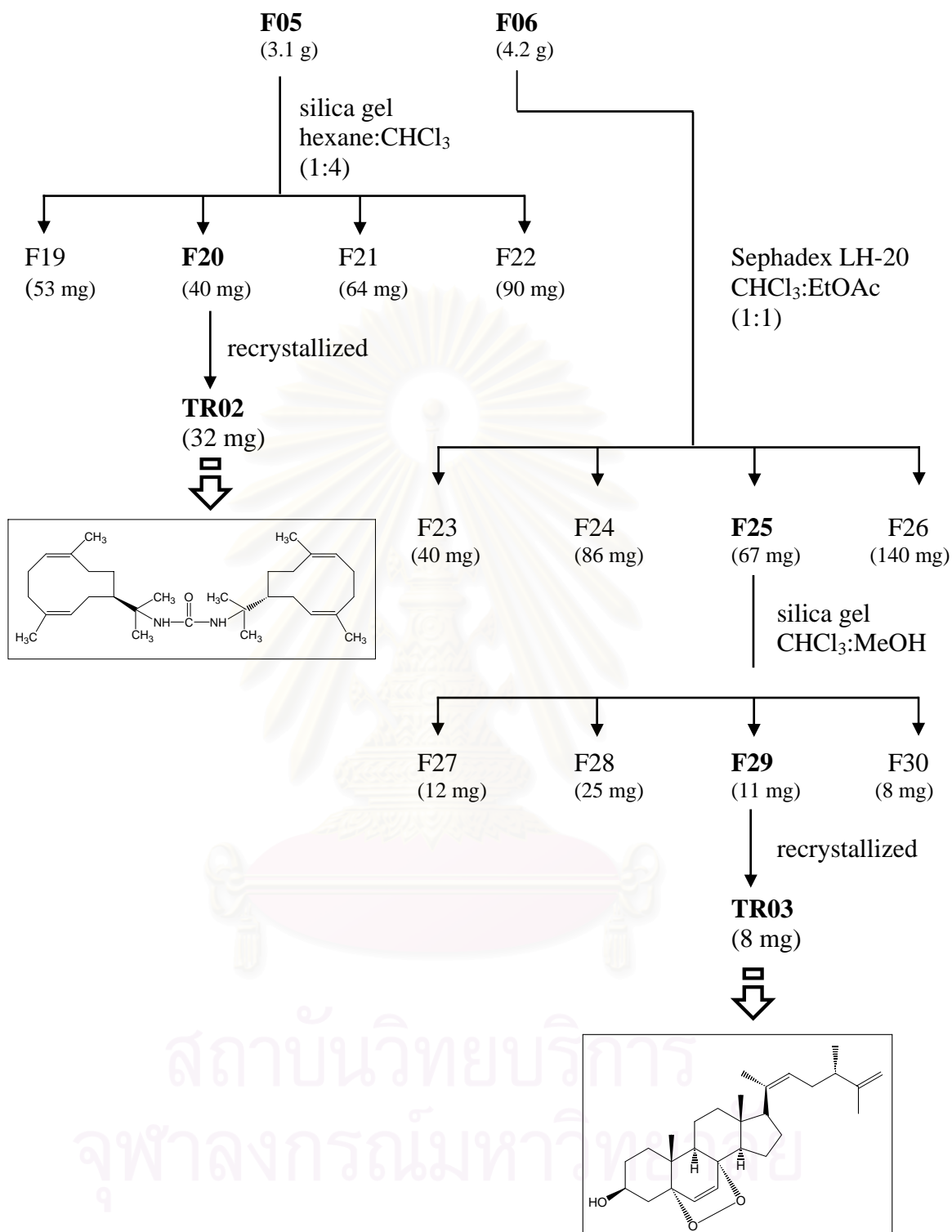
* positive antimicrobial

Scheme 3 Isolation of **F05** and **F06** from the Sponge *Axinyssa* n. sp.

4. Physical and Chemical Properties of the Isolated Compounds

4.1 Compound TR01 ((1Z,4Z)-7αH-11-Aminogermacra-1(10),4-diene)

Compound **TR01** was obtained as yellow oil.

HR ESI-TOF MS	: $[M+H]^+$ m/z 222.2232 (calcd for $C_{15}H_{28}$ N 222.2222); Figure 5
$[\alpha]^{25}_D$	: + 28.0° (c 0.2; $CHCl_3$)
UV	: λ_{max} nm (ε), in methanol; Figure 6
	208 (5,600)
IR	: ν_{max} cm^{-1}, Film; Figure 7
	3360, 3212, 2914, 1617
CD	: Figure 8
^{1}H NMR	: δ ppm, 300 MHz, in $CDCl_3$; Table 1, Figure 9
^{13}C NMR	: δ ppm, 75 MHz, in $CDCl_3$; Table 1, Figure 10

4.2 Compound TR02 (N,N′-11-Bis[(1Z,4Z)-7αH-germacra-1(10),4-dienyl] urea)

Compound **TR02** was obtained as colorless needles, soluble in $CHCl_3$, benzene.

HR ESI-TOF MS	: $[M+H]^+$ m/z 469.4151 (calcd for $C_{31}H_{53}$ N_2O 469.4168); Figure 14
$[\alpha]^{25}_D$	: + 32.5° (c 0.2; $CHCl_3$)
UV	: λ_{max} nm (ε), in methanol; Figure 15
	204 (9,600), 270 (920), 282 (890)
IR	: ν_{max} cm^{-1}, Film; Figure 16
	3368, 2921, 1642, 1557
CD	: Figure 17
^{1}H NMR	: δ ppm, 300 MHz, in $CDCl_3$; Table 2, Figure 18
^{13}C NMR	: δ ppm, 75 MHz, in $CDCl_3$; Table 2, Figure 19

4.3 Compound TR03 (Axinysterol)

Compound **TR03** was obtained as colorless needles, soluble in $CHCl_3$, benzene.

EIMS	: $[M]^+$ m/z 426; Figure 24
$[\alpha]^{25}_D$	: - 8.0° (c 0.2; $CHCl_3$)

UV	**:** λ_{max} nm (ϵ), in methanol; Figure 25
	206 (8,410), 383 (624)
IR	**:** ν_{max} cm^{-1}, Film; Figure 26
	3314, 2952, 2868, 1648, 1454, 1378, 1047, 968, 890
^{1}H NMR	**:** δ ppm, 300 MHz, in C$_6$D$_6$; Table 3, Figure 27
	δ ppm, 300 MHz, in CDCl$_3$; Table 3, Figure 28
^{13}C NMR	**:** δ ppm, 75 MHz, in C$_6$D$_6$; Table 3, Figure 29
	δ ppm, 75 MHz, in CDCl$_3$; Table 3, Figure 30

5. Determination of Antimicrobial Activity

Antimicrobial activity of the fractions and pure compounds were tested by using agar disc diffusion method (Lorian, 1980). Activity was tested against *Escherichia coli* ATCC 25922, *Staphylococcus aureus* ATCC 25923, *Bacillus subtilis* ATCC 6633 and *Candida albicans* ATCC 10231. All tested bacteria were cultivated on tryptic soy agar slant, TSA (Difco$^®$), and the yeast *Candida albicans* ATCC 10231 was cultivated on Sabouraud dextrose agar slant, SDA (Difco$^®$) at 37 ^{o}C for 24 hours. The cell cultures were washed from the agar surface and suspended in the steriled normal saline solution (NSS), and standardized to match a 0.5 turbidity standard of MacFarland No. 1, provided approximately 1×10^8 CFU (colony forming unit/mL). Each 20 mL of molten TSA and SDA was separated and poured into 9 cm diameter petri dish and allowed to solidify to form base layer. A loopful of each tested microorganisms was swabbed on the surface of TSA and SDA. plates. All tested samples were dissolved in the suitable solvent and then applied on sterile paper disc for disc diffusion assay. These paper discs were left in steriled petri dish until the solvent was completely dried. The dried paper discs were placed on the surface of the swabbed plates and incubated at 37 ^{o}C for 24 hours. The diameters of inhibition zones were measured. Fractions exhibited good antimicrobial activities were subsequently selected for further study.

CHAPTER IV

RESULTS AND DISCUSSION

In this study, the EtOAc extract of the reddish brown Thai marine sponge *Axinyssa* n. sp. have been found to possess strong antimicrobial activity. Further purification with chromatographic techniques yielded three pure compounds: (1*Z*,4*Z*)-7α*H*-11-aminogermacra-1(10),4-diene [**TR01**], *N*,*N*′-11-bis[(1*Z*,4*Z*)-7α*H*-germacra-1(10),4-dienyl]urea [**TR02**], and axinysterol [**TR03**]. All of the isolated compounds were also subjected to antimicrobial activity testing.

The structures of all isolated compounds were accomplished by interpretation of their IR, NMR and MS data, and further confirmed by comparison with those of literature values.

[**TR01**]   [**TR02**]

[**TR03**]
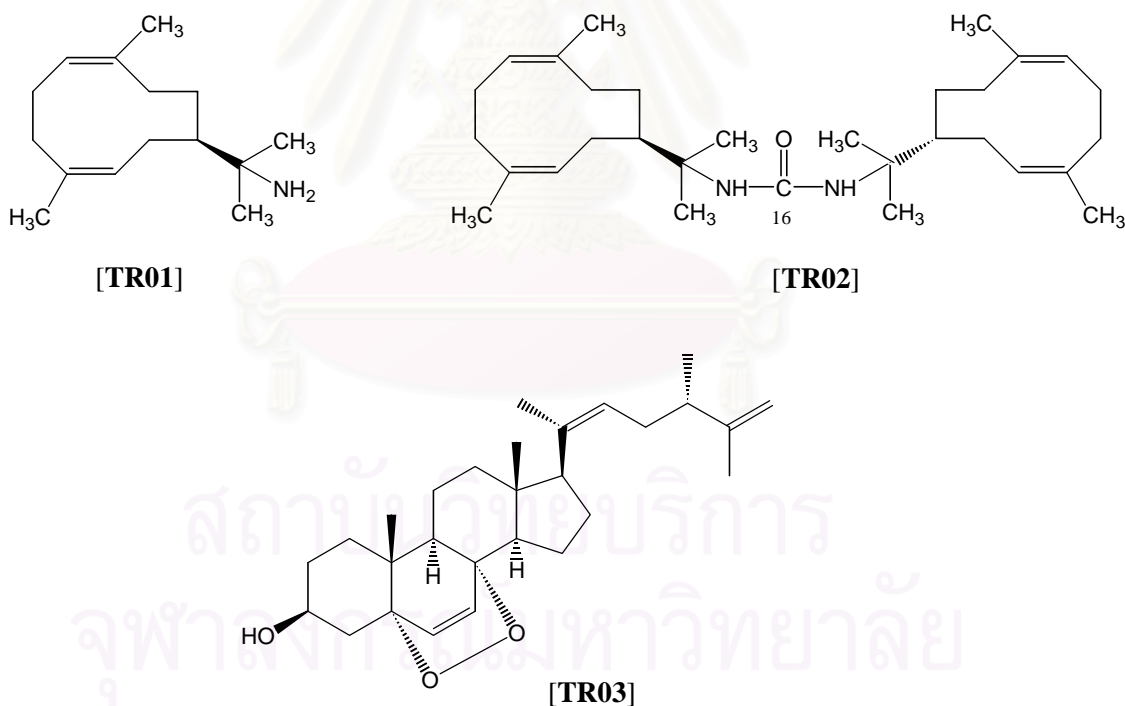
1. Structure Determination of the Isolated Compounds

1.1 Structure Determination of TR01 ((1Z,4Z)-7αH-11-Aminogermacra-1(10),4-diene)

Compound **TR01** was obtained as oil and its ESITOFMS showed an accurate mass [M+H]$^+$ at m/z 222.2232 (Figure 5), corresponding to a molecular formula of $C_{15}H_{27}N$ and therefore possessing three degrees of unsaturation.

The ^{1}H NMR spectrum (Figure 9) of **TR01** displayed signals of four singlet methyls (δ 1.25, 1.58, 1.61, and 1.63), two olefinic methines (δ 5.05 and 5.32), and a bundle of methine and methylene signals resonating at δ 1.77-2.05. The ^{13}C NMR spectrum (Figure 10) of **TR01** displayed 15 carbon signals which were classified into four methyl, five methylene, three methine, and three quaternary carbons by DEPT experiments. The ^{1}H and ^{13}C NMR data are summarized in Table 1. The presence of four sp^2 carbon resonances in the ^{13}C NMR spectrum at δ 123.4 (C-1), 133.6 (C-4), 119.9 (C-5), and 131.8 (C-10) represented two degrees of unsaturation, and hence compound **TR01** must contain a monocyclic ring. The germacrane skeleton, the position of substituents, and unsaturation were analyzed by 2D NMR experiments (Table 1). The H,H-COSY (Figure 11) and HMQC (Figure 12) NMR spectra indicated the partial structures =CH-CH$_2$-CH$_2$-, =CH-CH$_2$-CH-, and –CH$_2$-CH$_2$- in the molecule. The connectivity of these fragments with two allylic methyls (δ$_C$ 23.3/δ$_H$ 1.61, 14-CH$_3$ and δ$_C$ 25.7/δ$_H$ 1.63, 15-CH$_3$) and the olefinic quarternary carbons (δ 133.6, C-4 and δ 131.8, C-10) to construct a ten-membered ring of the germacrane skeleton was deduced by the following long range H-C correlations in the HMBC spectrum (Figure 13): H$_2$-8 to C-6; H$_3$-14 to C-3, C-4, and C-5; and H$_3$-15 to C-1, C-9, and C-10 (Figure 2).

The Z-orientation of both double bonds was assigned based on the following NOESY correlations: H$_3$-14 to H-5 and H$_3$-15 to H-1 (Figure 23). Furthermore, the downfield resonances of the allylic methyl carbons at δ 23.3 (C-14) and 25.7 (C-15) also confirmed the designated Z-double bonds (Ganber, Pollak, and Berger, 1995). The aminoisopropyl side chain was readily identified by the NMR signals of two tertiary methyls (δ$_C$ 22.2/δ$_H$ 1.25, 12-CH$_3$ and δ$_C$ 17.9/δ$_H$ 1.58, 13-CH$_3$) and a quaternary carbon attached to the amino group (δ 58.1, C-11). This was supported by the presence of the primary amine band at 3360 and 3212 cm^{-1} in its IR spectrum (Figure 7) and the ion peaks at m/z 205 [(M+H)-NH$_3$]$^+$ in the TOFMS. The placement

of the side chain at C-7 was based on the HMBC correlations of H-7 to C-13, H_3-12 and H_3-13 to C-7.

Attempts to form p-bromobenzoyl amide and dinitrobenzoyl amide derivatives of **TR01** for X-ray crystallographic study led to the decomposed products. Therefore, the stereochemistry of C-7 in **TR01** was mainly proposed by $[\alpha]_D$ comparison with similar known germacranes containing single chiral center at C-7. The germacranes with H-7 in β-orientation; for example (-)-germacrene A (Weinheimer *et al.*, 1970), (*E,S*)-germacra-1,4(15),11-triene-5-one (Suzuki *et al.*, 1990), and 7*S*-1*E*,4*E*-germacra-1(10),4-diene (Segawa, Yamano, and Shirahama, 1990); have been reported to show negative $[\alpha]_D$ of -3.2°, -167.0°, and -2.8°, respectively. In contrast, the H-7α germacranes; for example hedycaryol (Minnaard, Wijnberg, and de Groot, 1994), bacchascandon (Bohlmann *et al.*, 1979), and 6-oxo-germacra-1(10)*E*,4(15)-diene (Zdero *et al.*, 1989); have been reported to show positive $[\alpha]_D$ of +24.2°, +28.5°, and +53.0°, respectively. In addition, replacement of H-11 in the isopropyl side chain by a heteroatom (e.g. dilophol (Ishitsuka *et al.*, 1986) and hydroxydilophol (Sun and Fenical, 1979) and alteration of *E*- or *Z*-double bonds (e.g. kikkanol D and kikkanol F (Yoshikawa *et al.*, 2000)) affected only the magnitude of $[\alpha]_D$. From the above observation, **TR01** which exhibited a positive $[\alpha]_D$ of +28.0°, was established as (1*Z*,4*Z*)-7α*H*-11-aminogermacra-1(10),4-diene, based on the germacranolide nomenclature proposed by Rogers *et al* (Rogers, Moss, and Neidle, 1972).

TR01 is the first natural germacrane sesquiterpene containing an amino functional group and possessing *Z*-configuration at both C-1(10) and C-4 double bonds. Few *Z,Z*-germacranes have been reported in nature (Bohlmann and Ehlers, 1977). **TR01** may be biogenetically synthesized from the unusual precursor *Z,Z*-farnesyl pyrophosphate.

Germacrene-A
$[\alpha]_D$ -3.2°

hedycaryol
$[\alpha]_D$ +24.2°

(E,S)-germacra-1,4(15),11-triene-5-one
$[\alpha]_D$ -167.0°

bacchascandon
$[\alpha]_D$ +28.5°

7S-1E,4E-germacra-1(10),4-diene
$[\alpha]_D$ -2.8°

6-oxo-germacra-1(10)E,4(15)-diene
$[\alpha]_D$ +53.0°
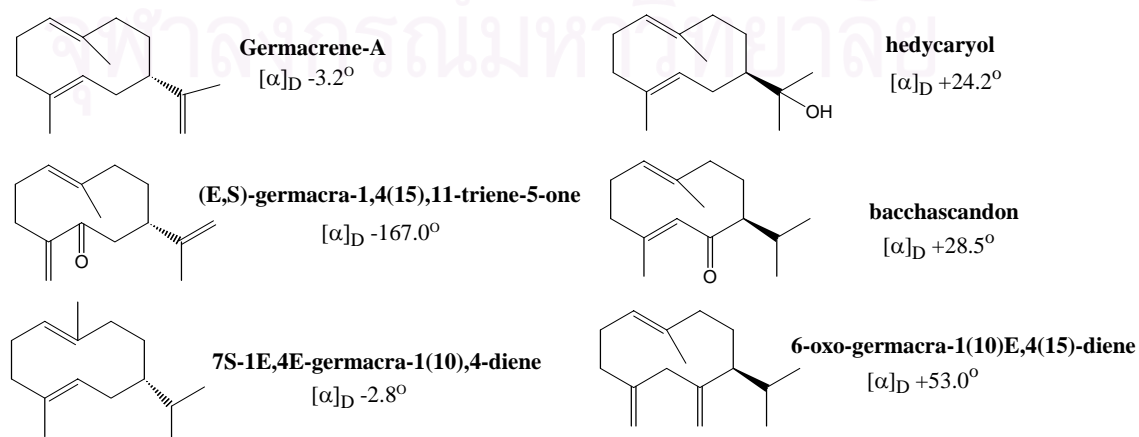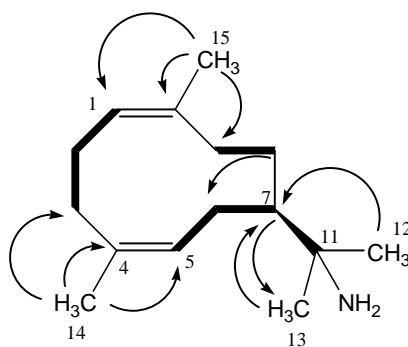
Figure 2 ¹H-¹³C Long Range Correlations (arrow) and H,H-COSY (bold) of **TR01** ((1Z,4Z)-7αH-11-Aminogermacra-1(10),4-diene)

Table 1 ¹H (300 MHz) and ¹³C (75 MHz) NMR, H,H-COSY, and HMBC Spectral Data of **TR01** ((1Z,4Z)-7αH-11-Aminogermacra-1(10),4-diene)

position	**TR01** (in CDCl₃)			
	¹H (mult., J in Hz)	¹³C (mult)	H,H COSY	HMBC (H-C long range correlation)
1	5.05 (br t, 6, 1H)	123.4 (d)	H₂-2	C-15
2	2.05 (m, 2H)	22.7 (t)	H-1, H₂-3	
3	1.60 (m, 2H)	37.2 (t)	H₂-2	C-1, C-10
4	-	133.6 d()		
5	5.32 (br s, 1H)	119.9, (d)	H₂-6	
6	2.00 (m, 2H)	26.3 (t)	H-5, H-7	
7	1.77 (m, 1H)	41.1 (d)	H₂-6	C-13
8	1.81 (m, 2H)	23.8 (t)	H₂-9	C-6
9	1.95 (m, 2H)	30.9, (t)	H₂-8	
10	-	131.8 (s)		
11	-	58.1 (s)		
12	1.25 (s, 3H)	22.2 (q)		C-7, C-11
13	1.58 (s, 3H)	17.9 (q)		C-7
14	1.61 (s, 3H)	23.3 (q)		C-3, C-4, C-5
15	1.63 (s, 3H)	25.7 (q)		C-1, C-9, C-10

1.2   Structure Determination of TR02 (*N,N′*-11-Bis-[(1*Z*,4*Z*)-7*αH*-germacra-1(10),4-dienyl]urea)

Compound **TR02** was isolated as colorless needles. The molecular formula of $C_{31}H_{52}N_2O$ was established by an accurate mass from the ESITOFMS of **TR02** showing the $[M+H]^+$ peak at m/z 469.4151 (Figure 14).

The ^1H (Figure 18) and ^{13}C (Figure 19) NMR spectra of **TR02** were quite similar to those of **TR01** (Table 2), suggesting that **TR02** was composed of two identical units of 1*Z*,4*Z*-11-aminogermacra-1(10),4-diene.   Further NMR studies, including H,H-COSY (Figure 20) , HMQC (Figure 21), HMBC (Figure 22), and NOESY experiments (Figure 23) confirmed this observation. Finally, the presence of the carbonyl carbon at δ 155.9 in the ^{13}C NMR spectrum and the absorption bands at 3368 and 1642 cm^{-1} in the IR spectrum (Figure 16), indicated that the two identical germacrane units were connected through urea functionality.

Attempts to crystallize compound **TR02** in several solvents produced no crystals suitable for X-ray crystallographic study. Since **TR02** exhibited an $[\alpha]_D$ of the same sign and similar magnitude ($+32.5^o$), the stereochemistry at C-7 and C-7′ should be the same as **TR01**. Compound **TR02** was therefore identified as *N,N′*-11-Bis-[(1*Z*,4*Z*)-7*αH*-germacra-1(10),4-dienyl]urea.

Both **TR01** and **TR02** were directly detected from the EtOAc crude extract as brown spots on a Si gel TLC plate with hR$_f$ values of 25 and 80, respectively [solvent system: C_6H_{14}-EtOAc (2:3), visualizing agent: anisaldehyde in H_2SO_4]. This result ruled out that **TR02** was a urea artifact of **TR01** and phosgene from chloroform decomposition during the purification process.
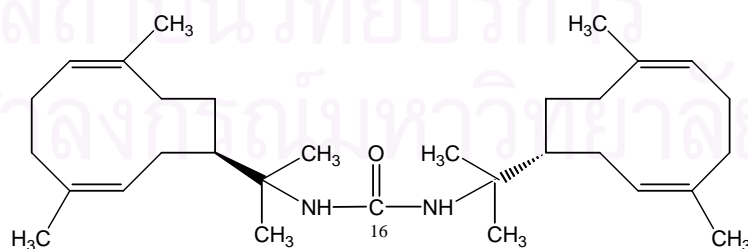
TR02

Table 2 ^{1}H (300 MHz) and ^{13}C (75 MHz) NMR, H,H-COSY, and HMBC Spectral

Data of **TR02** (*N,N′*-11-Bis-[(1Z,4Z)-7αH-germacra-1(10),4-dienyl]urea)

position	TR02 (in CDCl$_3$)			
	^{1}H (mult., *J* in Hz)	^{13}C (mult)	H,H COSY	HMBC (H-C long range correlation)
1, 1′	5.10 (br t, 6.2, 2 ×1H)	124.6 (d)	H$_2$-2 (2′)	C-15 (15′)
2, 2′	2.00 (m, 2 × 2H)	22.7 (t)	H-1 (1′), H$_2$-3 (3′)	
3, 3′	1.50 (m, 2 × 1H), 1.89 (m, 2 × 1H)	36.8 (t)	H$_2$-2 (2′)	C-1(1′)
4, 4′	-	133.7 d()		
5, 5′	5.33 (br s, 2 × 1H)	120.7 (d)	H$_2$-6 (6′)	C-7 (7′), C-8 (8′), C-11 (11′)
6, 6′	1.97 (m, 2 × 2H)	26.6 (t)	H-5 (5′), H-7 (7′)	
7, 7′	2.17 (br t, 12.3, 2× 1H)	41.2 (d)	H$_2$-6 (6′)	
8, 8′	1.17 (m, 2 × 2H)	24.6 (t)	H$_2$-9 (9′)	
9, 9′	1.87 (m, 2 × 2H)	31.5 (t)	H$_2$-8 (8′)	C-15 (15′)
10, 10′	-	131.1 (s)		
11, 11′	-	57.4 (s)		
12, 12′	1.05 (s, 2 × 3H)	21.4 (q)		C-7 (7′), C-11 (11′)
13, 13′	1.57 (s, 2 × 3H)	17.7 (q)		C-11 (11′)
14, 14′	1.59 (s, 2 × 3H)	23.4 (q)		C-4 (4′), C-5 (5′)
15, 15′	1.65 (s, 2 × 3H)	25.8 (q)		C-1 (1′), C-10 (10′)
16	-	155.9 (s)		
NH, N′H	3.84 (br s, 2× 1H)			

1.3 Structure Determination of TR03 (Axinysterol)

Compound **TR03** was isolated as colorless needles. The molecular formula of $C_{28}H_{42}O_3$ was determined by EIMS of **TR03** showing the $[M]^+$ peak at m/z 426 (Figure 24). The IR spectrum showed absorption band at 3314 cm^{-1} (Figure 26) due to a hydroxyl group.

The ^1H (Figures 27, 28) and ^{13}C (Figures 29, 30) NMR data were presented in Table 3. Twenty-eight carbon signals appeared in the ^{13}C NMR and DEPT spectra indicated the presence of five methyls, seven sp^3 methylenes, one sp^2 methylene, six sp^3 methines, four sp^2 methines, four sp^3 quaternary carbons, and one sp^2 quaternary carbon. The presence of a peroxy group was suggested by the mass fragment ion of m/z 394 from the molecular ion (m/z 426) by loss of an oxygen molecule, and was also supported by ^{13}C NMR signals [δ 78.9 (s, C-8) and 81.8 (s, C-5), in C_6D_6] due to the quaternary carbons each bearing an oxygen atom of the peroxy group. The presence of three double bonds was indicated by the ^1H and ^{13}C NMR spectra and the configuration of each double bond was elucidated by coupling constant values. The *E* configuration of one of the two disubstituted olefins was shown by the coupling constant (J = 15.3 Hz) between the olefinic protons at δ 5.16 and 5.33. The *Z* configuration of another disubstituted olefin was also shown by the coupling constant (J = 8.4 Hz) between the olefinic protons at δ 6.27 and 5.95 (in C_6D_6).

The ^1H-^1H COSY (Figure 31, 32) correlation spectrum of **TR03** showed the partial structures of the A, B, C, D ring and side chain as shown in Figure 3. The ^1H-^{13}C correlations of H_2-1/C-5, H-6/C-5, H-6/C-8, H-6/C-10, H-7/C-8, H-7/C-9, H_3-19/C-1, H_3-19/C-10, and H_3-19/C-11 confirmed the connectivity of A and B rings, containing a hydroxyl group at C-3 and a methyl group at C-10 (Figure 3, Table 4). Correlations of H-14/C-9, H_3-18/C-13, H_3-18/C-12, and H_3-18/C-17 indicated the fusion of ring B, C, and D. The HMBC correlations (Figure 35, 36) of H_3-21/C-23, H_3-21/C-20, H-20/C-24, H_2-26/C-24, H_2-26/C-27, H_3-27/C-25, H_3-28/C-25, and H_3-28/C-23 demonstrated the presence of a 2,3-dimethylhepta-1,4-dienyl group in the side chain.

Based on the above spectral evidence and by comparison of its ^1H and ^{13}C NMR data (Table 3) with the reported data (Igushi *et al.*, 1993), compound **TR03** was identified as a known 5α,8α-epidioxy sterols, axinysterol, which was previously isolated from the Okinawan marine sponge of the *Axinyssa* genus. However, some

carbon chemical shifts should be revised as C-11 (δ 28.7), C-14 (δ 56.2), C-16 (δ 20.6), and C-17 (δ 51.2). This assignment was supported by HMQC (Figure 33, 34) and HMBC (Figure 35, 36) experiments.

Figure 3 Selected ^{1}H-^{13}C Long-Range Correlations in the HMBC Data of **TR03** (Axinysterol)

The absolute configuration of axinysterol in the published data was determined by chemical transformation of axinysterol to ergost-7-ene-3β,5α-diol comparison with hydrogenation of ergosterol peroxide to the same compound ergost-7-ene-3β,5α-diol. In this study, the configuration of **TR03** was confirmed by NOESY analysis, focusing on the ring junction of the steroidal skeleton (Figure 4). The α-orientation of the epidioxy group was determined by the correlation between H$_3$-18 and olefinic proton H-7 (Figure 37). The relative configuration of the angular methyl group at C-10 was indicated by the correlation between olefinic H-6 and H$_3$-19. The stereochemistry of two chiral centers in the side chain and C-3 was assigned by comparison of the ^{13}C NMR data with those in the reference (Igushi *et al.*, 1993).

Figure 4 NOESY Correlations of **TR03** (Axinysterol)

Table 3 ^{1}H (300 MHz) and ^{13}C (75 MHz) NMR Spectral Data of **TR03** (Axinysterol)

^{1}H	δ_H (mult., *J* in Hz)			^{13}C	δ_C (mult.)		
	TR03 (in C$_6$D$_6$)	**TR03** (in CDCl$_3$)	Axinysterol* (in CDCl$_3$)		**TR03** (in C$_6$D$_6$)	**TR03** (in CDCl$_3$)	Axinysterol* (in CDCl$_3$)
1	1.51 (m), 2.04 (m)	1.77 (m), 1.93 (m)		1	35.2	34.8	34.8
2	1.48 (m), 1.76 (m)	1.30 (m), 1.50 (m)		2	30.6	30.2	30.2
3	3.93 (m, 5.6)	3.95 (m, 5.2)	3.95 (m)	3	66.3	66.5	66.6
4	1.78 (m), 2.18 (m)	1.89 (m), 2.68 (m)	2.11 (ddd, 1.9, 5.1, 13.7)	4	37.6	34.8	37.1
5			-	5	81.8	82.1	82.3
6	5.95 (d, 8.4)	6.22 (d, 8.5)	6.24 (d, 8.4)	6	135.8	135.2	135.4
7	6.27 (d, 8.4)	6.48 (d, 8.5)	6.50 (d, 84)	7	130.7	130.6	130.8
8				8	78.9	79.4	79.5
9		1.58 (m)		9	52.0	51.7	512
10				10	37.3	36.9	37.1
11	1.57 (m)	1.38 (m)		11	28.9	28.7	20.7^a
12	0.91 (m)	1.23 (m)		12	39.7	39.4	39.5
13				13	44.5	44.7	44.7
14	1.00 (m)	1.20 (m)		14	56.3	56.2	518
15	1.18 (m)	0.83 (m)		15	23.7	23.5	23.5^a
16	1.33 (m)	1.35 (m)		16	21.1	20.6	28.7^a
17	1.51 (m)	1.41 (m)		17	51.9	51.2	56.3
18	0.58 (s)	0.79 (s)	0.82 (s)	18	12.9	13.0	13.0
19	0.67 (s)	0.86 (s)	0.88 (s)	19	18.2	18.3	18.3
20	1.91 (m)	2.06 (m)		20	39.9	39.6	39.6
21	0.96 (d, 6.6)	0.98 (d, 6.6)	1.00 (d, 6.6)	21	20.8	20.4	20.7
22	5.16 (dd, 8.2, 15.3)	5.21 (m)	5.23 (dd, 7.2, 15.2)	22	135.9	135.3	135.5
23	5.33 (dd, 6.8, 15.3)	5.23 (m)	5.26 (dd, 6.3, 15.2)	23	132.1	131.8	132.0
24	2.73 (quin,, 6.8)	2.64 (m, 6.4)	2.71 (quin, 6.5)	24	44.1	43.7	43.7
25				25	149.0	149.7	149.8
26	4.86 (d, 13.9)	4.68 (br s)	4.69 (br s)	26	109.5	108.7	109.0
27	1.70 (s)	1.75 (s)	1.67 (br s)	27	20.9	20.5	20.7
28	1.13 (d, 6.8)	1.05 (d, 6.6)	1.08 (d, 6.9)	28	19.1	19.0	18.9

^{a,b} Values may be interchanges in each column

*Igushi *et al.*, 1993

Table 4 H,H-COSY and HMBC Spectral Data of **TR03** (Axinysterol)

position	TR03 in C_6D_6		TR03 in $CDCl_3$	
	H,H-COSY	HMBC	H,H-COSY	HMBC
1	H-2	C-5	H-2	
2	H-1, H-3	C-3		
3	H-2, H-4	C-2	H-2, H-4	
4	H-3	C-3		
5				
6	H-7	C-5, C-8, C-10	H-7	C-4, C-5, C-7, C-8
7	H-6	C-5, C-8, C-9	H-6	C-5, C-6, C-8, C-9
8				
9				
10				
11		C-8		
12		C-11		
13				
14	H-15		H-15	C-8
15	H-14	C-9	H-14	C-16
16				
17			H-18	
18		C-14, C-17	H-17	C-13, C-14
19		C-1, C-5, C-9, C-10		C-1, C-4, C-5, C-9
20	H-21, H-22	C-21	H-21	
21	H-20	C-20, C-22	H-20	C-22
22	H-20	C-24		
23	H-24	C-20, C-24	H-24	C-24
24	H-23, H-28	C-23, C-25	H-23, H-28	
25				
26		C-24, C-27		C-24, C-27
27		C-25, C-26		C-24, C-26
28	H-24	C-23, C-24, C-25	H-24	C-23, C-24, C-25

2. Antimicrobial Activity

The EtOAc extract from a Thai marine sponge *Axinyssa* n. sp. was found to possess strong antimicrobial activity. Bioassay-guided fractionation led to discovery of two new nitrogenous germacranes **TR01** and **TR02**, along with a known axinysterol (**TR03**). All isolated compounds were tested with antimicrobial activity. The results presented in Table 5 showed that only **TR01** exhibited significant antimicrobial activity.

Table 5 Antimicrobial Activity of **TR01** ((1*Z*,4*Z*)-7αH-11-Aminogermacra-1(10),4-diene), **TR02** (*N*,*N*′-11-Bis-[(1*Z*,4*Z*)-7αH-germacra-1(10),4-dienyl]urea), and **TR03** (Axinysterol)

Sample (mg/disc)	Inhibition zone (mm)		
	S. aureus	*B. subtilis*	*C. albicans*
EtOAc extract (1 mg)	22	13	8
TR01 (500 μg)	23	22	27
TR02 (1 mg)	-	-	-
TR03 (1 mg)	-	-	-

CHAPTER V

CONCLUSION

This present investigation aimed to search for bioactive substances from Thai marine sponges. The reddish brown sponge, which was collected from the Andaman Sea of Trang province and later identified as the new species of the genus *Axinyssa*, possessed antimicrobial activity. The bioassay-guided fractionation of the EtOAc extract of this sponge led to isolation of two new nitrogenous compounds, including (1Z,4Z)-7αH-11-aminogermacra-1(10),4-diene and *N,N'*-11-bis-[(1Z,4Z)-7αH-germacra-1(10),4-dienyl]urea, together with a known sterol, axinysterol. The structure elucidations of all isolated compounds were accomplished by means of 1D, 2D, NMR, MS, and IR spectroscopy.

(1Z,4Z)-7αH-11-Aminogermacra-1(10),4-diene exhibited strong antimicrobial activity against *Staphylococcus aureus, Bacillus subtilis,* and *Candida albicans* with the inhibition zones of 23, 22, and 27 mm, respectively (all at 500 μg/disc), while *N,N'*-11-bis-[(1Z,4Z)-7αH-germacra-1(10),4-dienyl]urea and axinysterol showed no antimicrobial activity at this level. Compound *N,N'*-11-bis-[(1Z,4Z)-7αH-germacra-1(10),4-dienyl]urea was directly detected from the EtOAc crude extract on a silica gel TLC plate. This observation ruled out that this compound was a urea artifact of (1Z,4Z)-7αH-11-aminogermacra-1(10),4-diene from chloroform decomposition during the purified process.
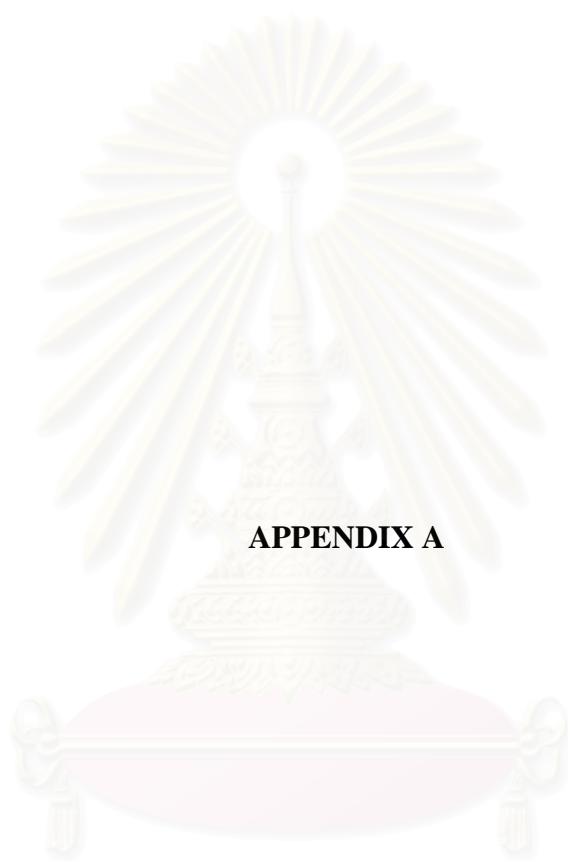
APPENDIX A
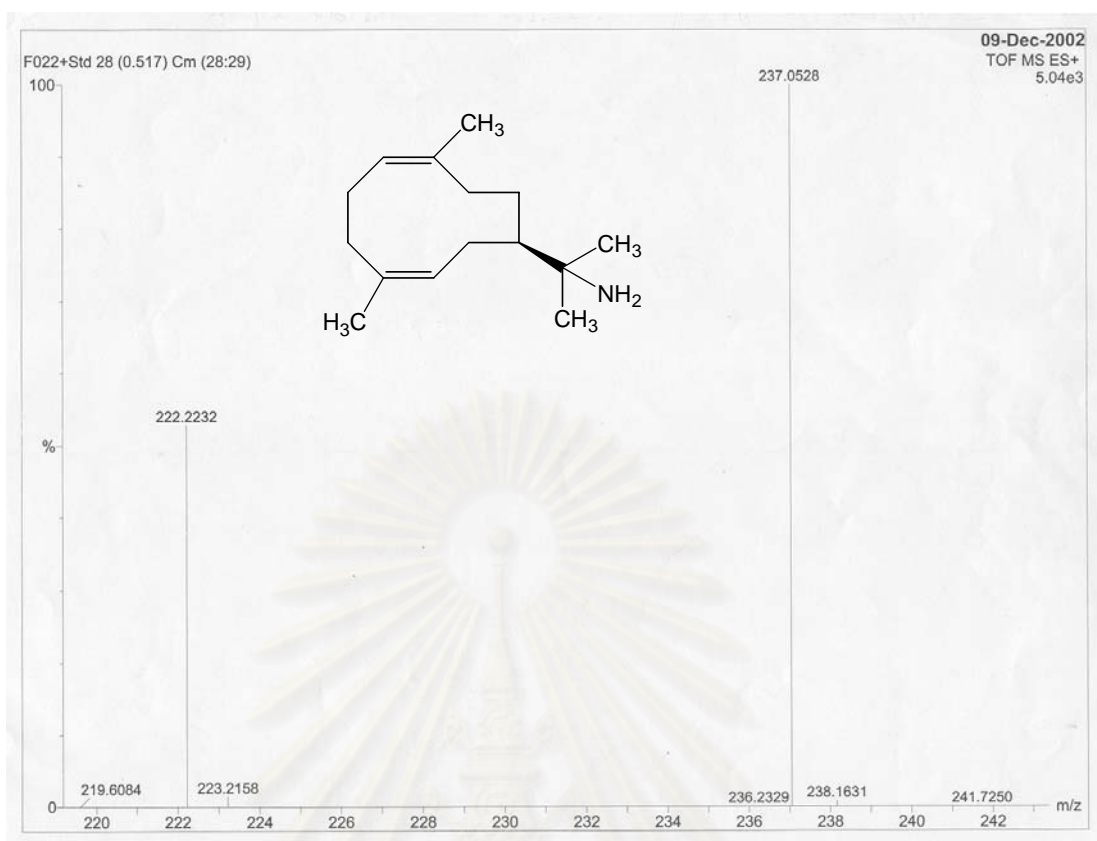
Figure 5 HR TOFMS Spectrum of **TR01** ((1*Z*,4*Z*)-7α*H*-11-Aminogermacra-
1(10),4-diene)
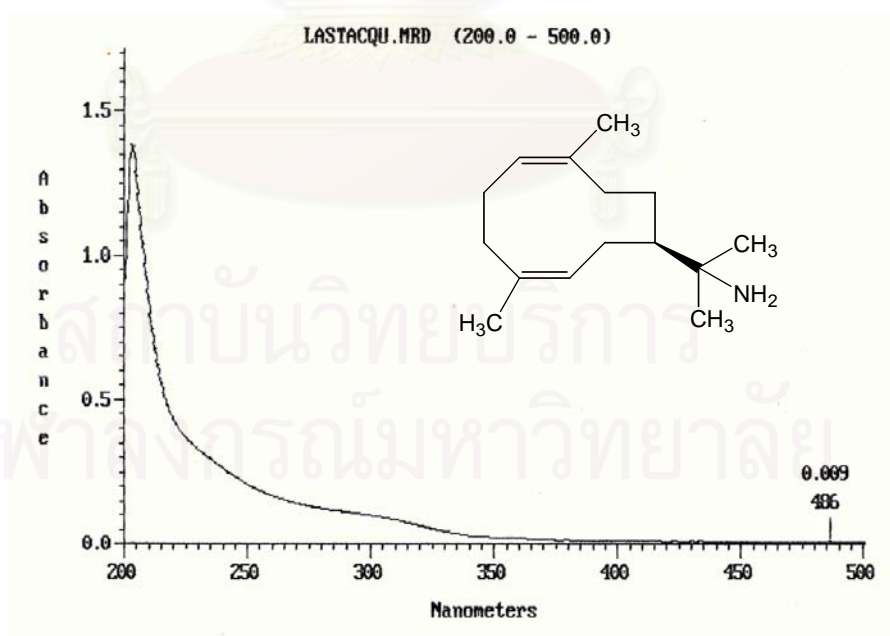
Figure 6 UV Spectrum of **TR01** ((1*Z*,4*Z*)-7α*H*-11-Aminogermacra-1(10),4-diene)
in MeOH
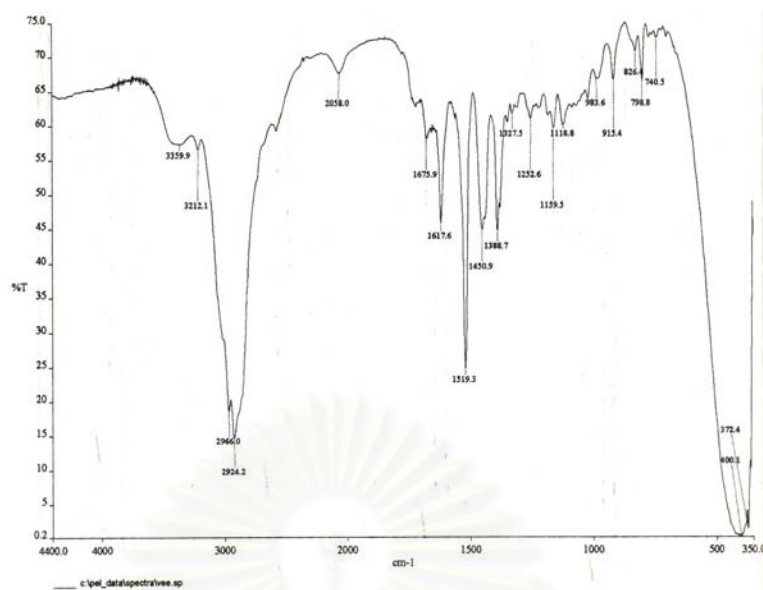
Figure 7 IR Spectrum (Film) of **TR01** ((1Z,4Z)-7αH-11-Aminogermacra-1(10),4-diene)
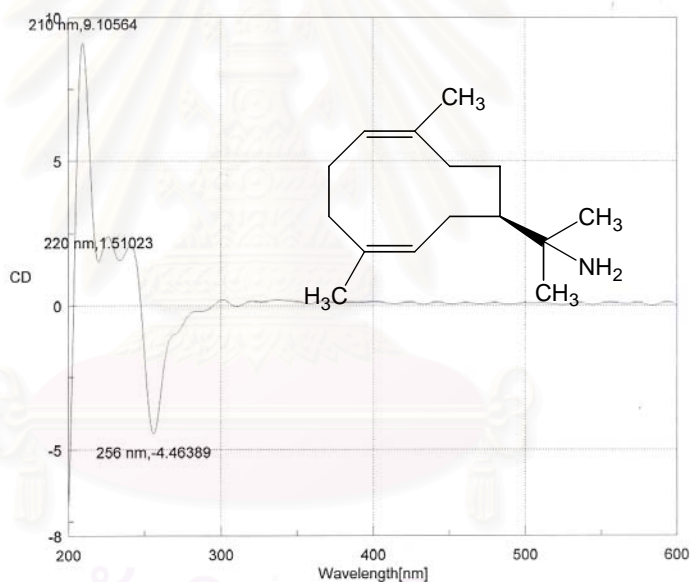
Figure 8 CD Spectrum of **TR01** ((1Z,4Z)-7αH-11-Aminogermacra-1(10),4-diene) in MeOH
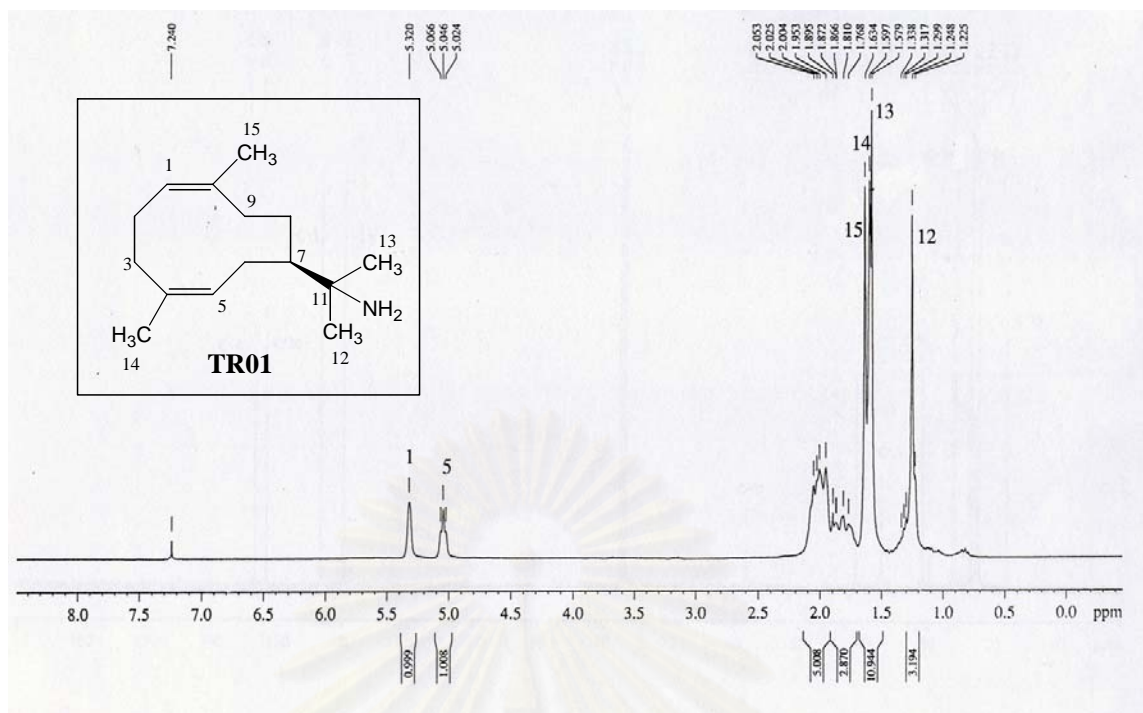
Figure 9 ^{1}H NMR (300 MHz) Spectrum of **TR01** ((1Z,4Z)-7αH-11-Aminogermacra-1(10),4-diene) in CDCl$_3$
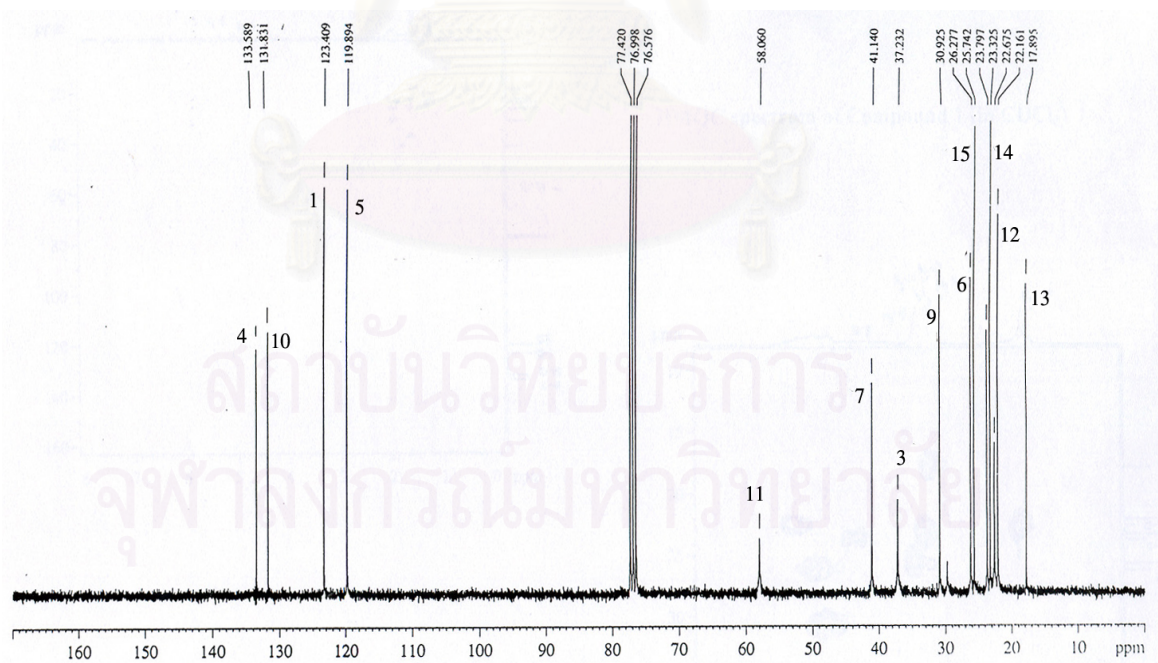
Figure 10 ^{13}C NMR (75 MHz) Spectrum of **TR01** ((1Z,4Z)-7αH-11-Aminogermacra-1(10),4-diene) in CDCl$_3$
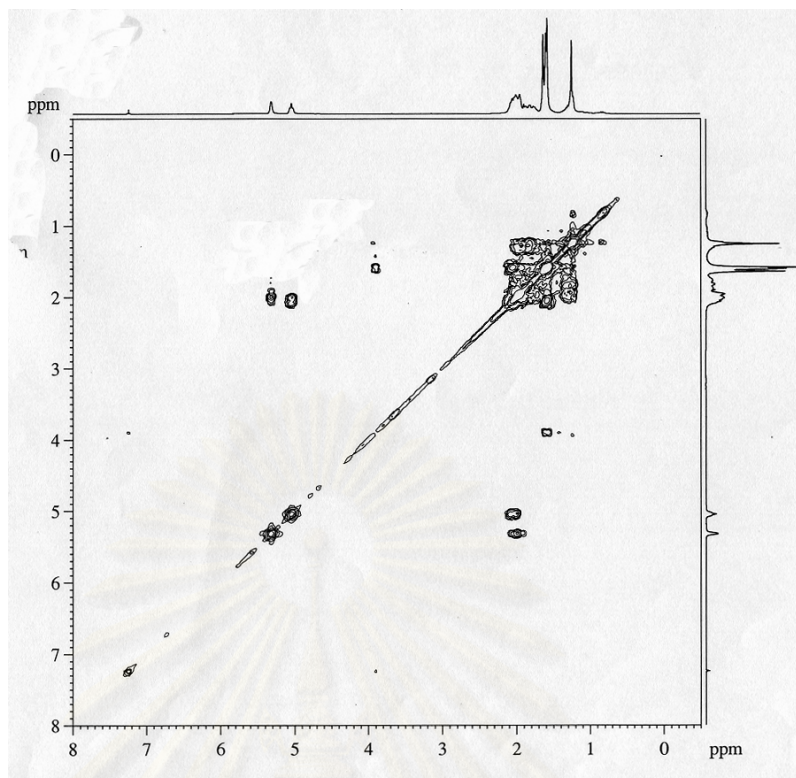
Figure 11 H,H-COSY Spectrum of **TR01** ((1Z,4Z)-7αH-11-Aminogermacra-1(10),4-diene) in CDCl$_3$
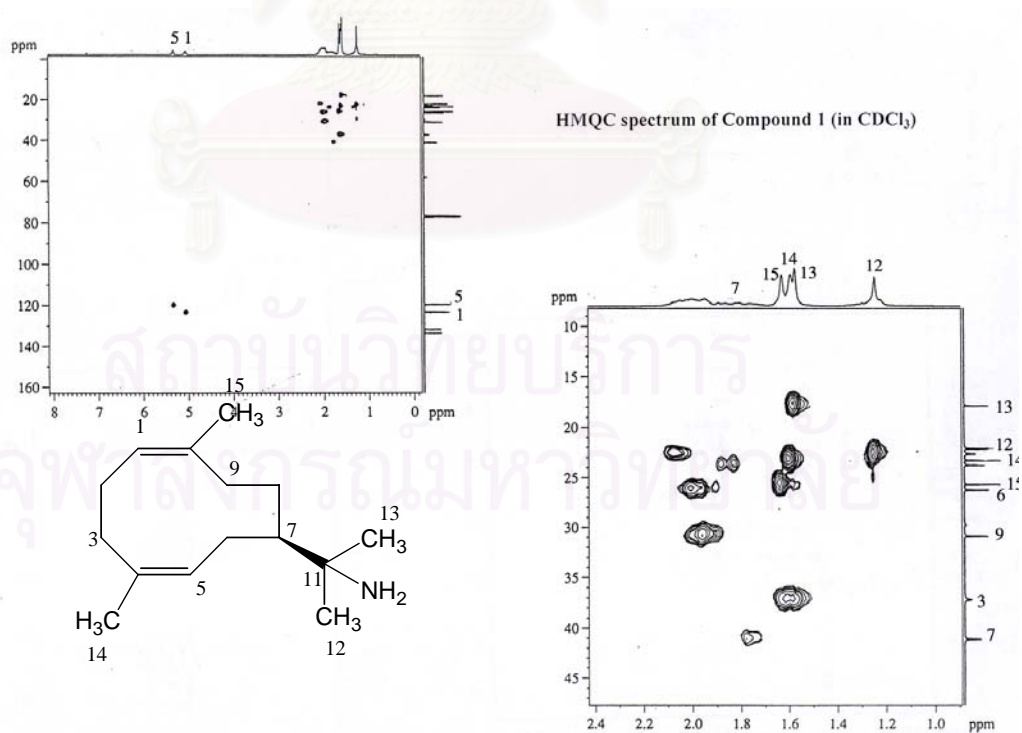
Figure 12 HMQC Spectrum of **TR01** ((1Z,4Z)-7αH-11-Aminogermacra-1(10),4-diene) in CDCl$_3$
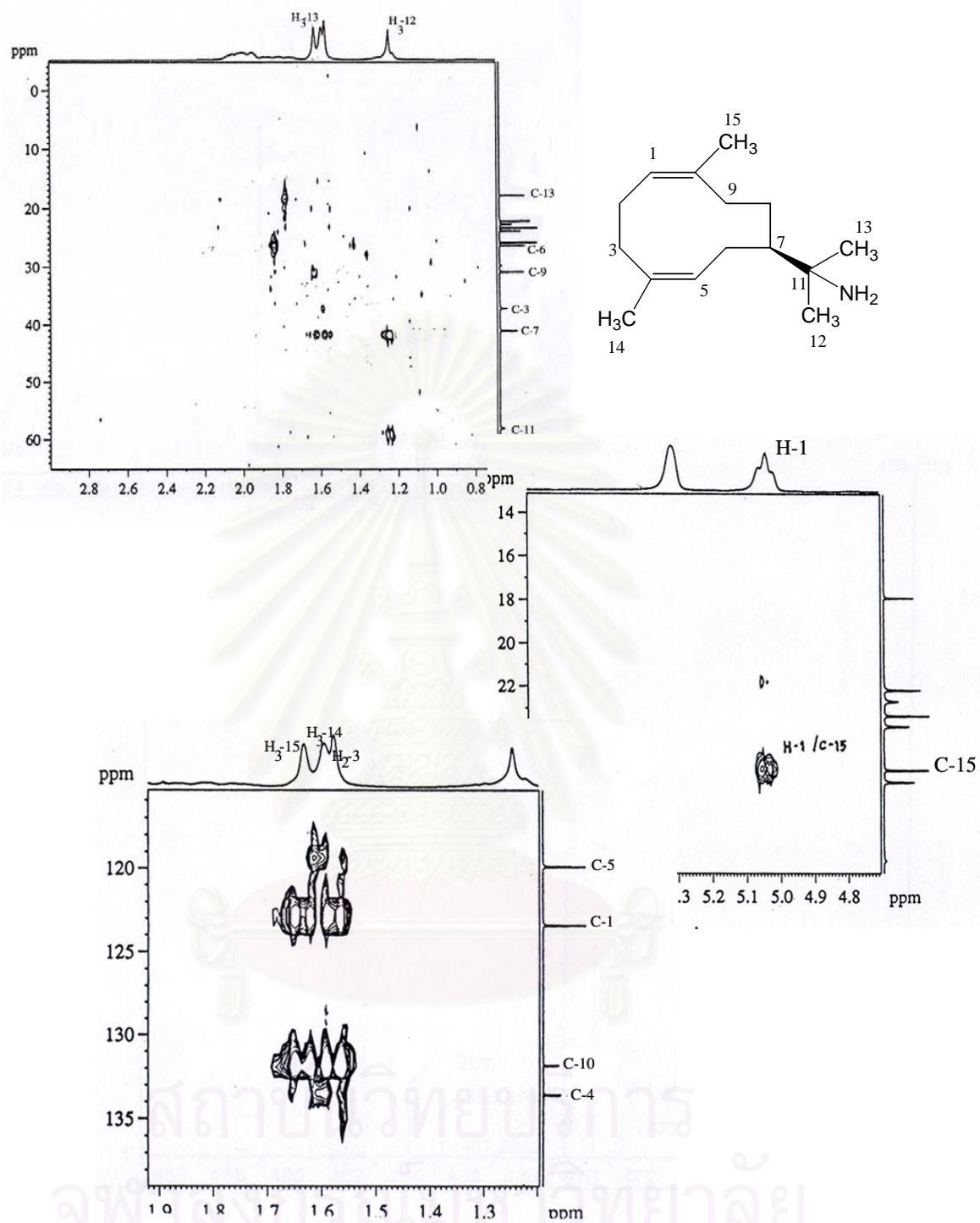
Figure 13 HMBC ($^n J_{HC}$ = 8 Hz) Spectrum of **TR01** ((1Z,4Z)-7αH-11-Aminogermacra-
1(10),4-diene) in CDCl$_3$
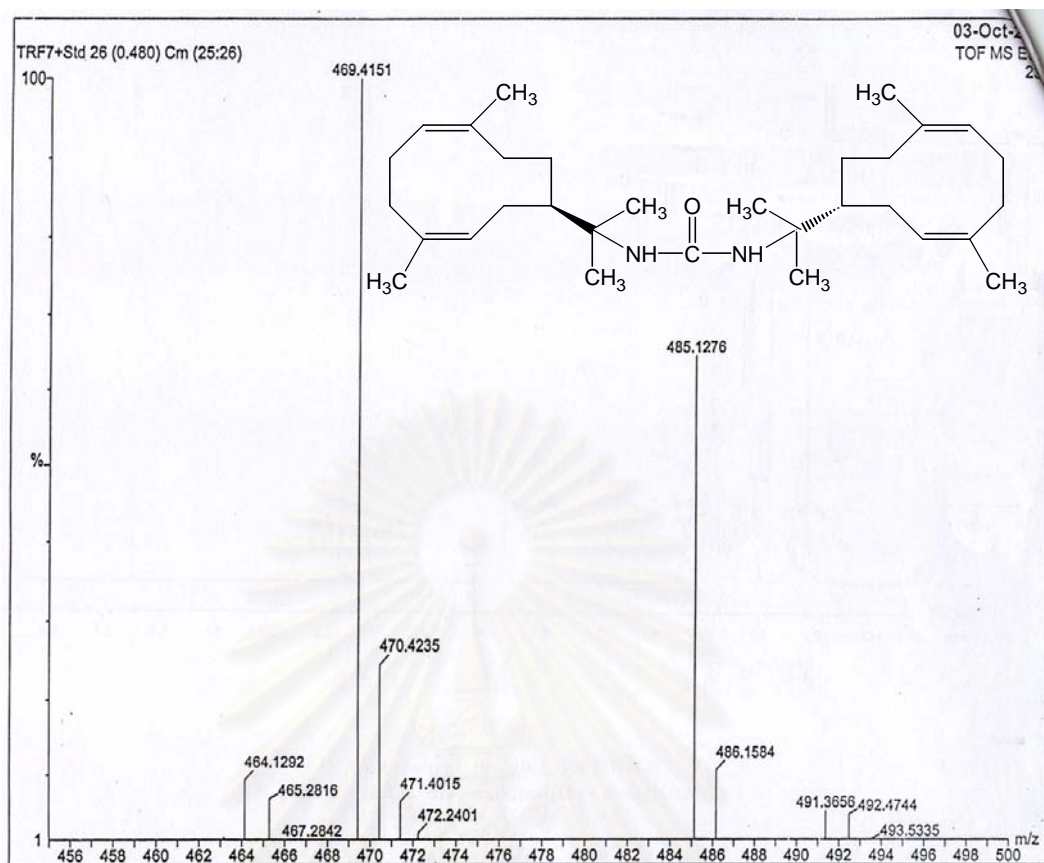
Figure 14 HR TOFMS Spectrum of **TR02** (*N*,*N′*-11-Bis[(1*Z*,4*Z*)-7α*H*-germacra-
1(10),4-dienyl]urea)
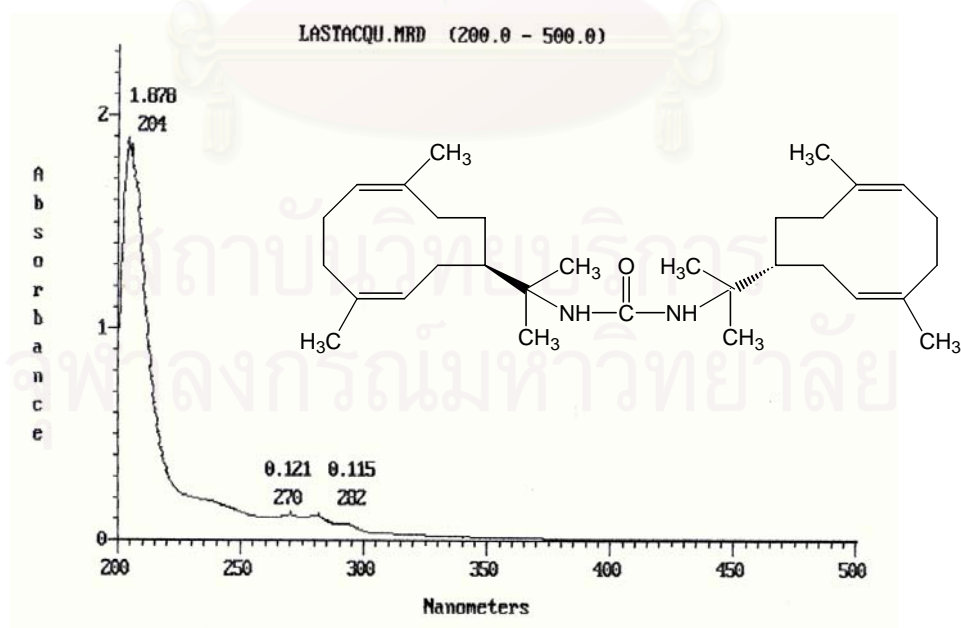
Figure 15 UV Spectrum of **TR02** (*N*,*N′*-11-Bis[(1*Z*,4*Z*)-7α*H*-germacra-1(10),4-
dienyl]urea) in MeOH
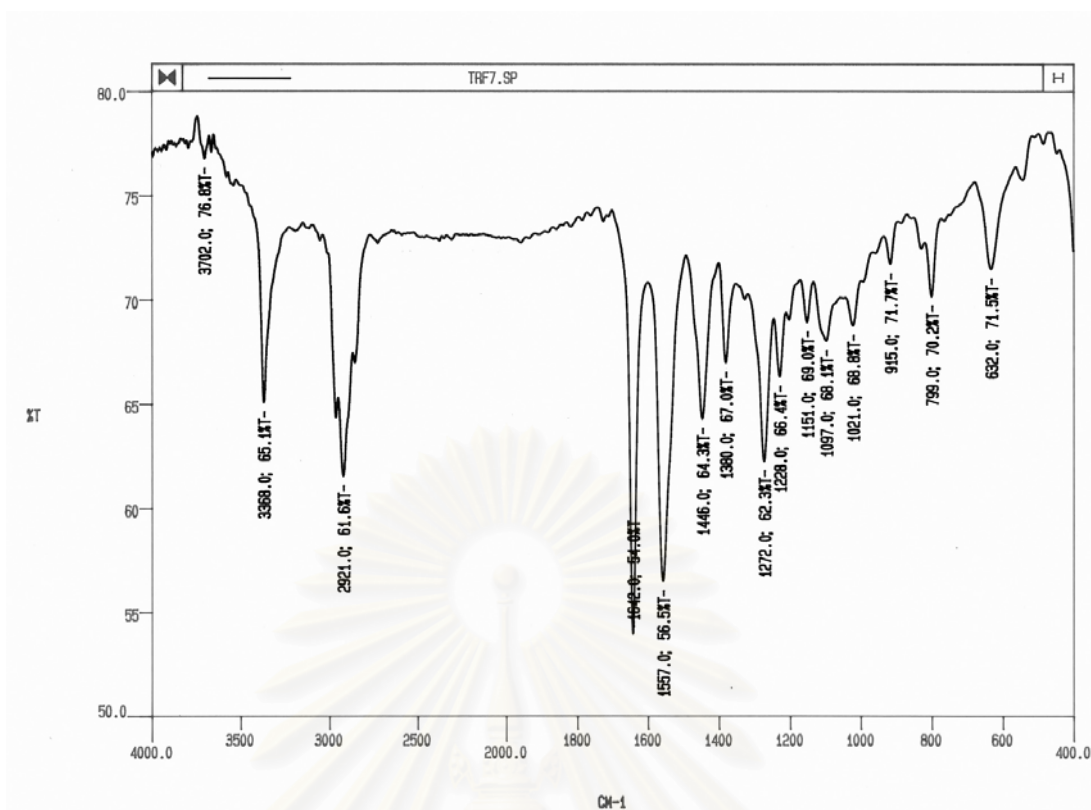
Figure 16 IR Spectrum (Film) of **TR02** (*N,N′*-11-Bis[(1Z,4Z)-7αH-germacra-1(10),4-
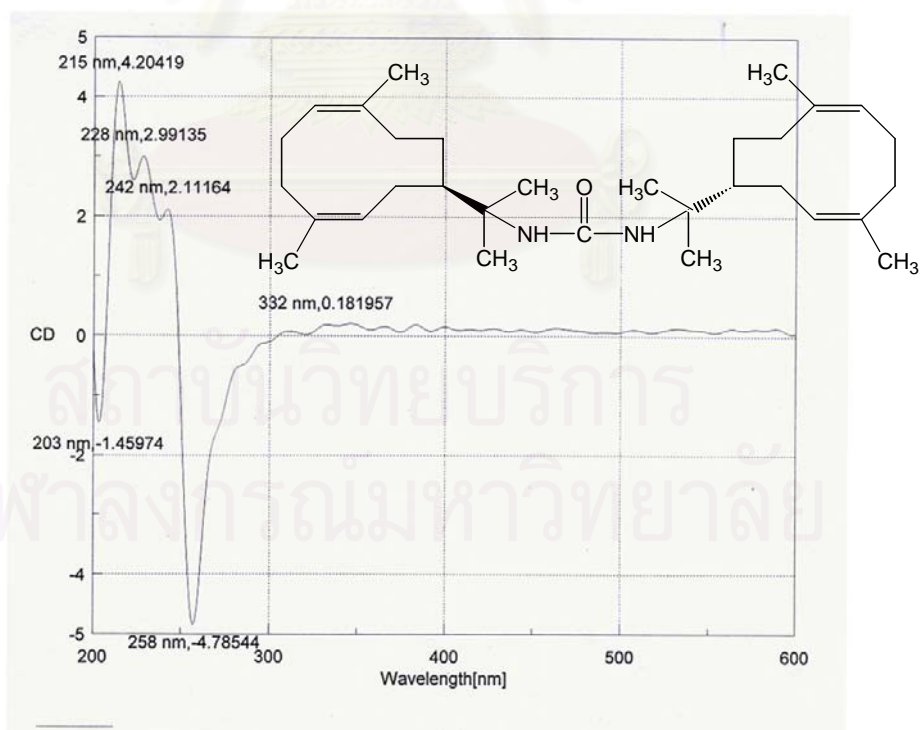
dienyl]urea)

Figure 17 CD Spectrum of **TR02** (*N,N′*-11-Bis[(1Z,4Z)-7αH-germacra-1(10),4-
dienyl]urea) in MeOH
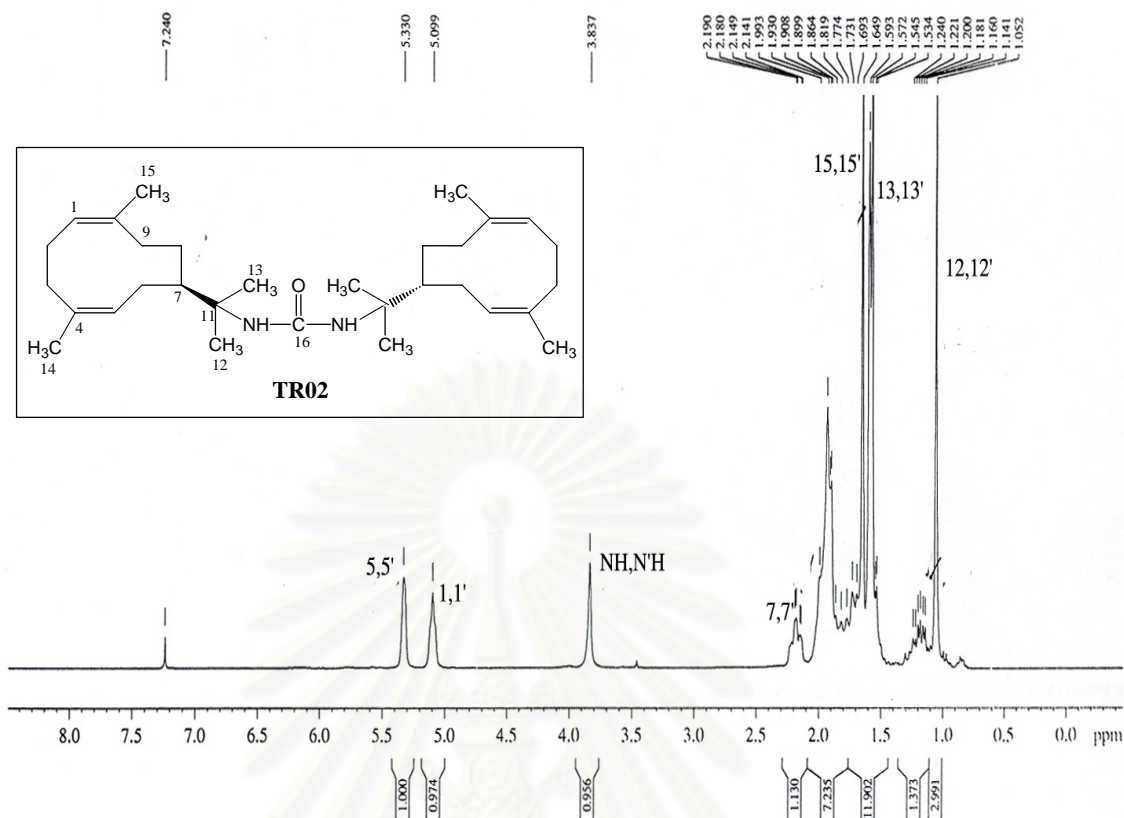
Figure 18 ^{1}H NMR (300 MHz) Spectrum of **TR02** (*N,N′*-11-Bis[(1Z,4Z)-7αH-germacra-1(10),4-dienyl]urea) in CDCl$_3$
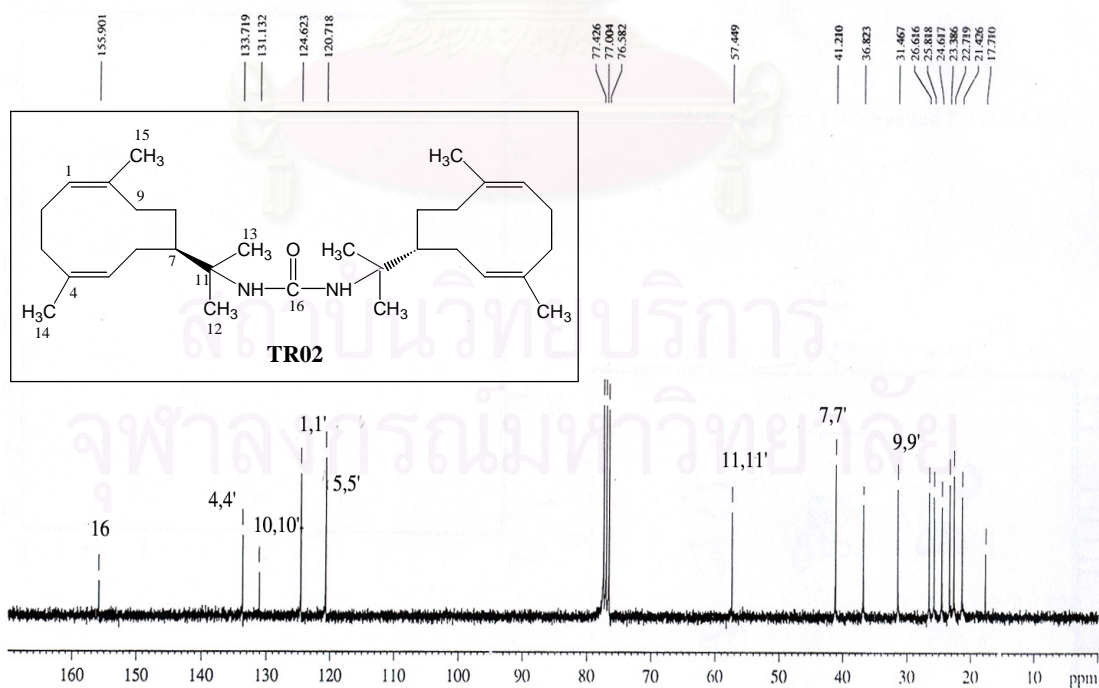
Figure 19 ^{13}C NMR (75 MHz) Spectrum of **TR02** (*N,N′*-11-Bis[(1Z,4Z)-7αH-germacra-1(10),4-dienyl]urea) in CDCl$_3$
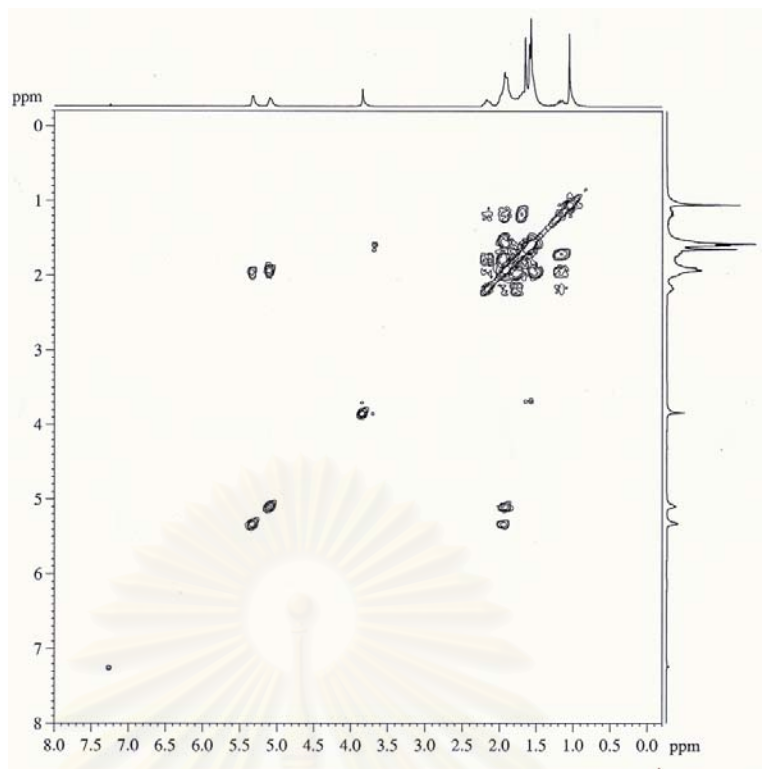
Figure 20 H,H-COSY spectrum of **TR02** (*N,N′*-11-Bis[(1*Z*,4*Z*)-7*αH*-germacra-1(10),4-

dienyl]urea) in CDCl₃
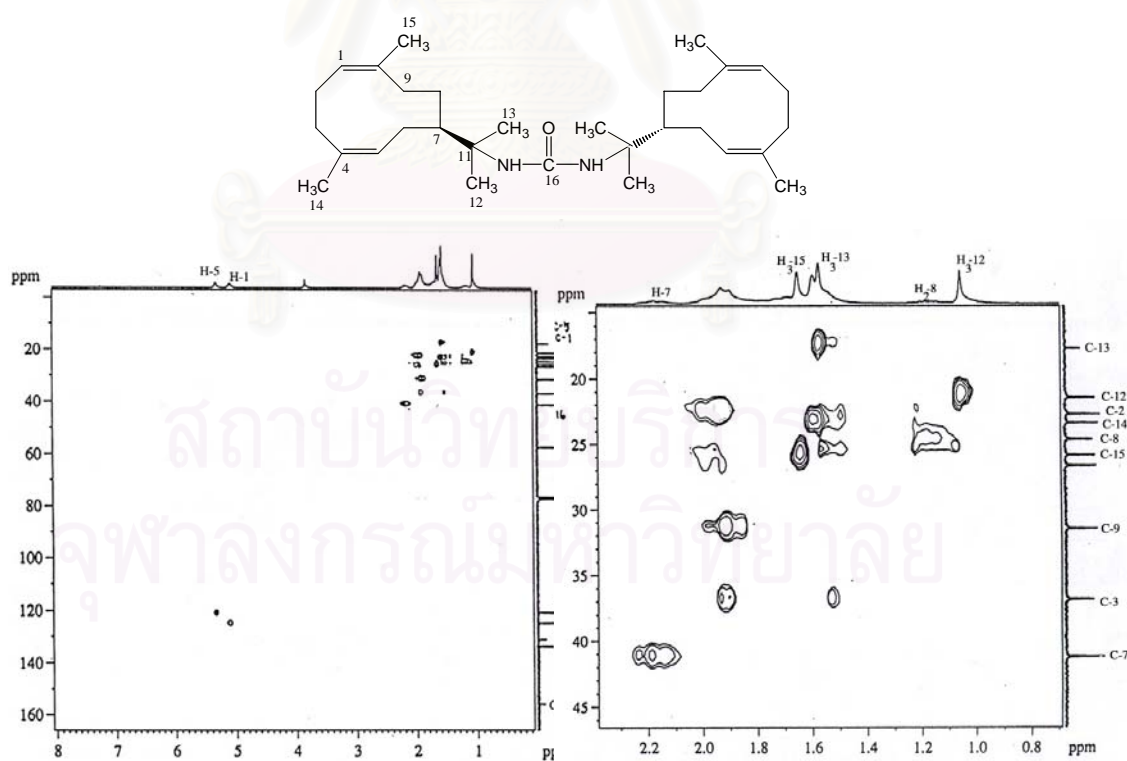
Figure 21 HMQC Spectrum of **TR02** (*N,N′*-11-Bis[(1*Z*,4*Z*)-7*αH*-germacra-1(10),4-
dienyl]urea) in CDCl₃
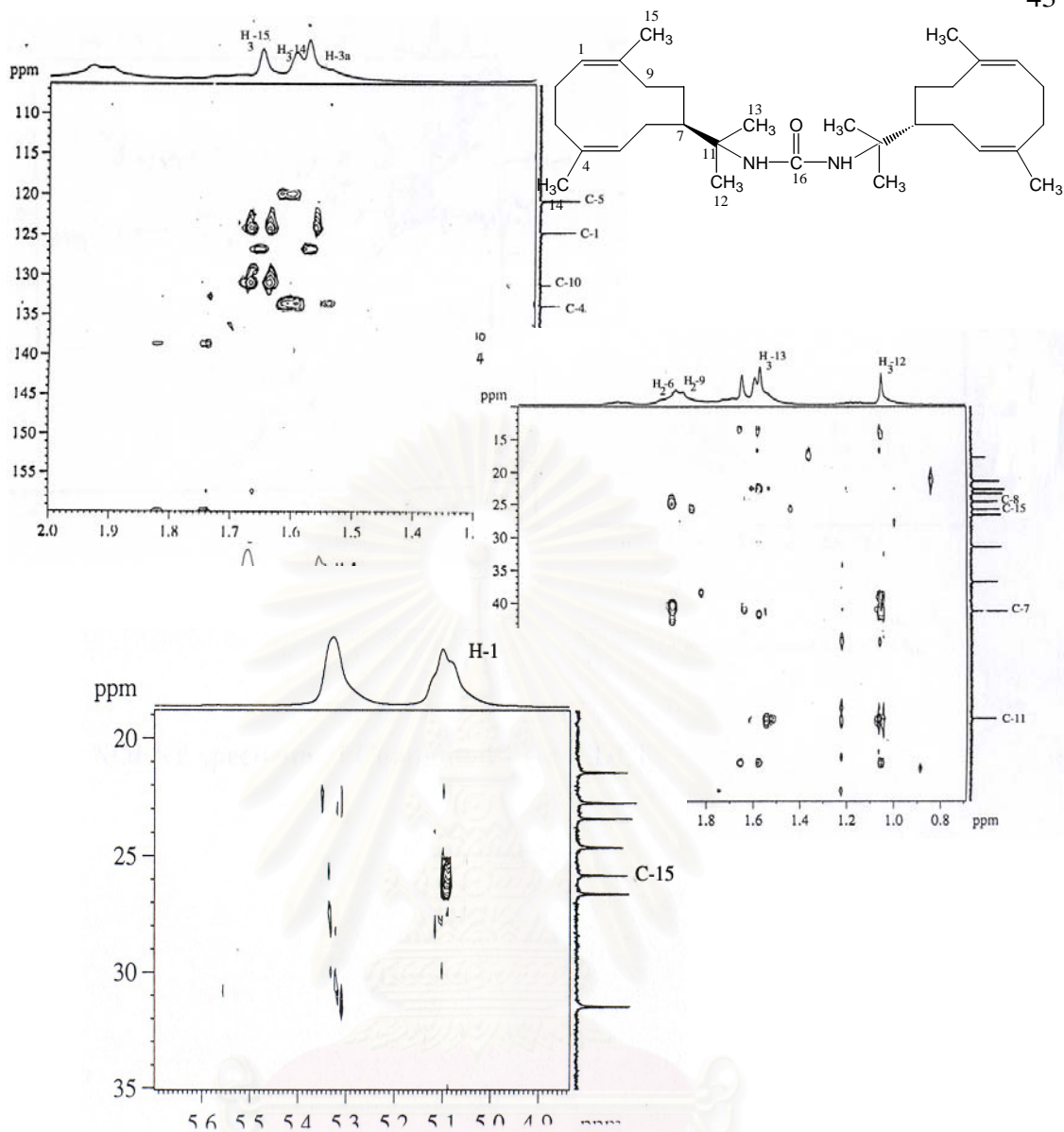
Figure 22 HMBC ($^n J_{HC}$ = 8 Hz) Spectrum of **TR02** (*N,N′*-11-Bis[(1Z,4Z)-7*αH*-germacra-1(10),4-dienyl]urea) in CDCl₃
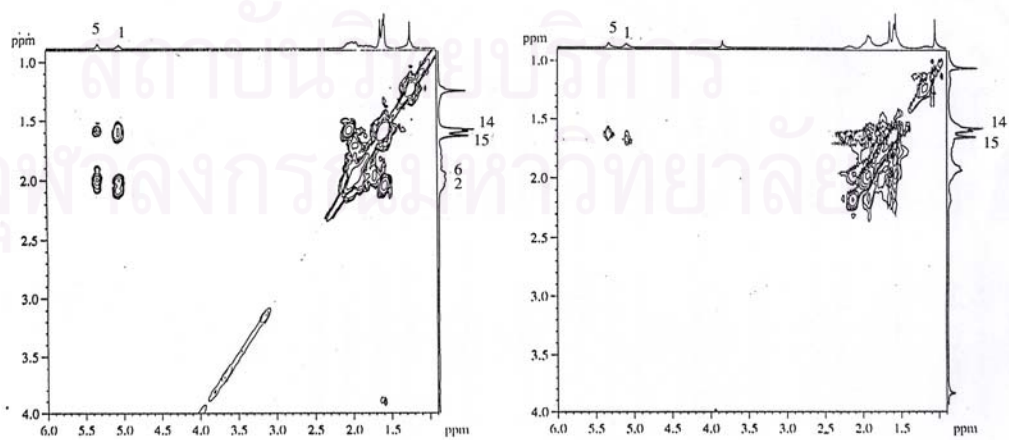
Figure 23 NOESY Spectra of **TR01** ((1Z,4Z)-7*αH*-11-aAminogermacra-1(10),4-diene) and **TR02** (*N,N′*-11-Bis[(1Z,4Z)-7*αH*-germacra-1(10),4-dienyl]urea) in CDCl₃
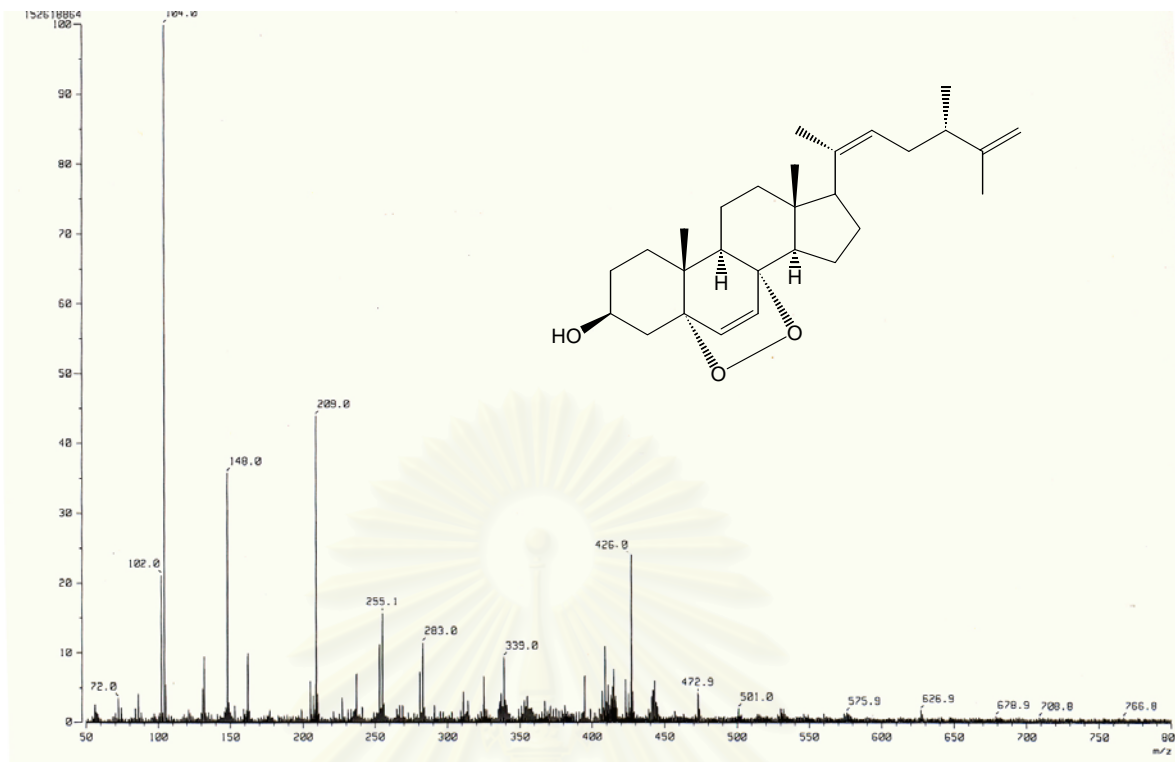
Figure 24 EIMS Spectrum of **TR03** (Axinysterol)
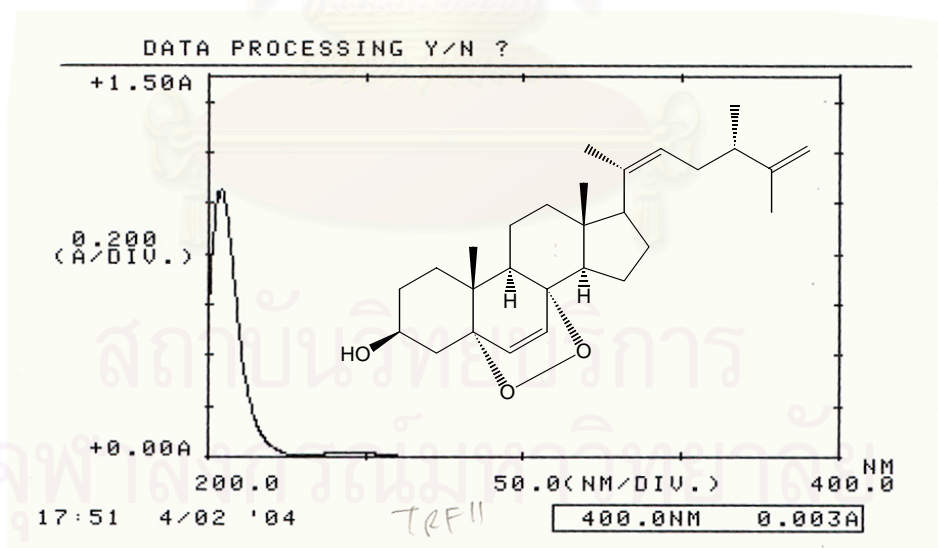
Figure 25 UV Spectrum of **TR03** (Axinysterol) in MeOH
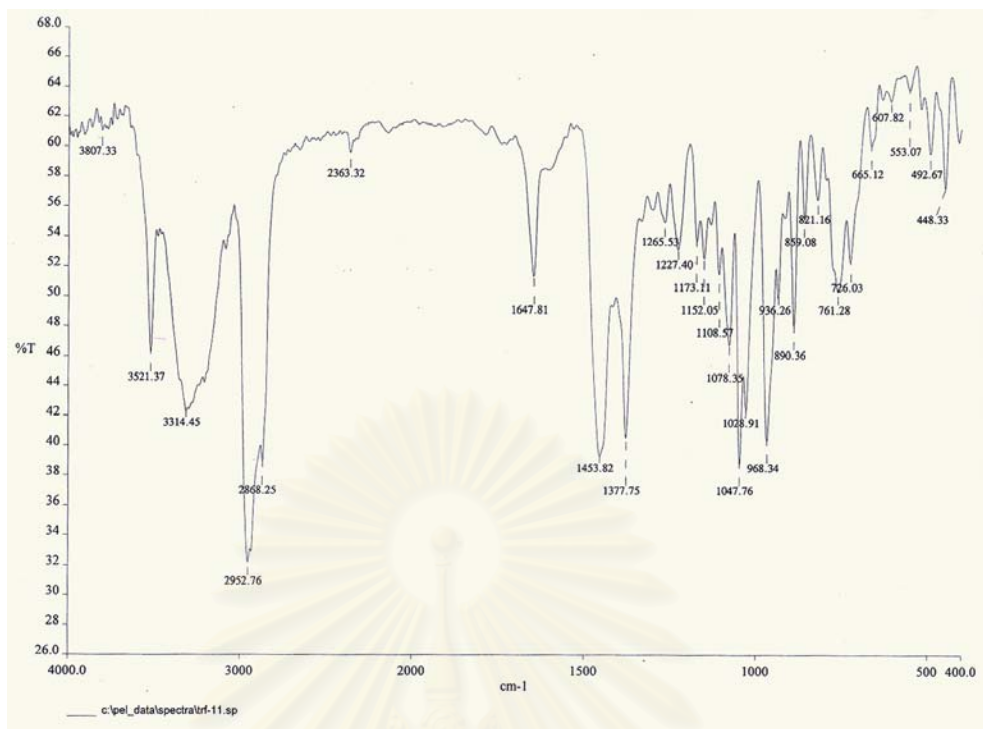
Figure 26 IR Spectrum (Film) of **TR03** (Axinysterol)
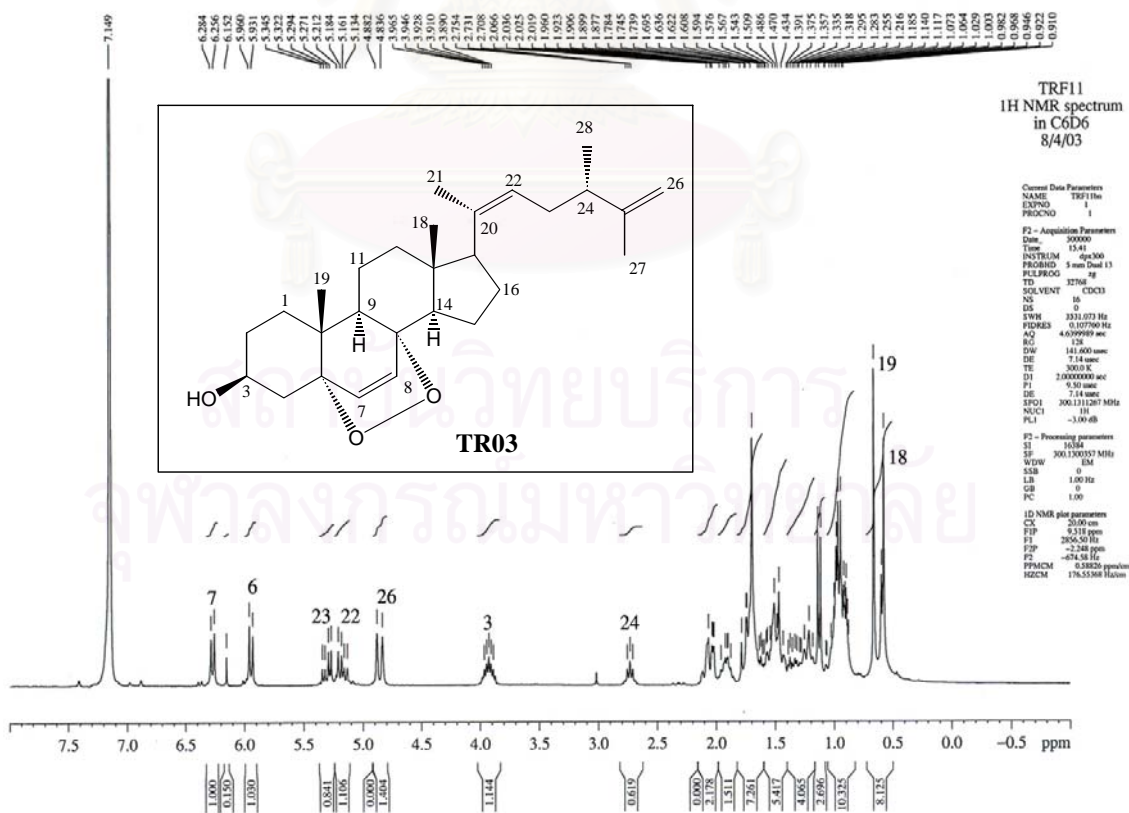
Figure 27 ¹H NMR (300 MHz) Spectrum of **TR03** (Axinysterol) in C_6D_6
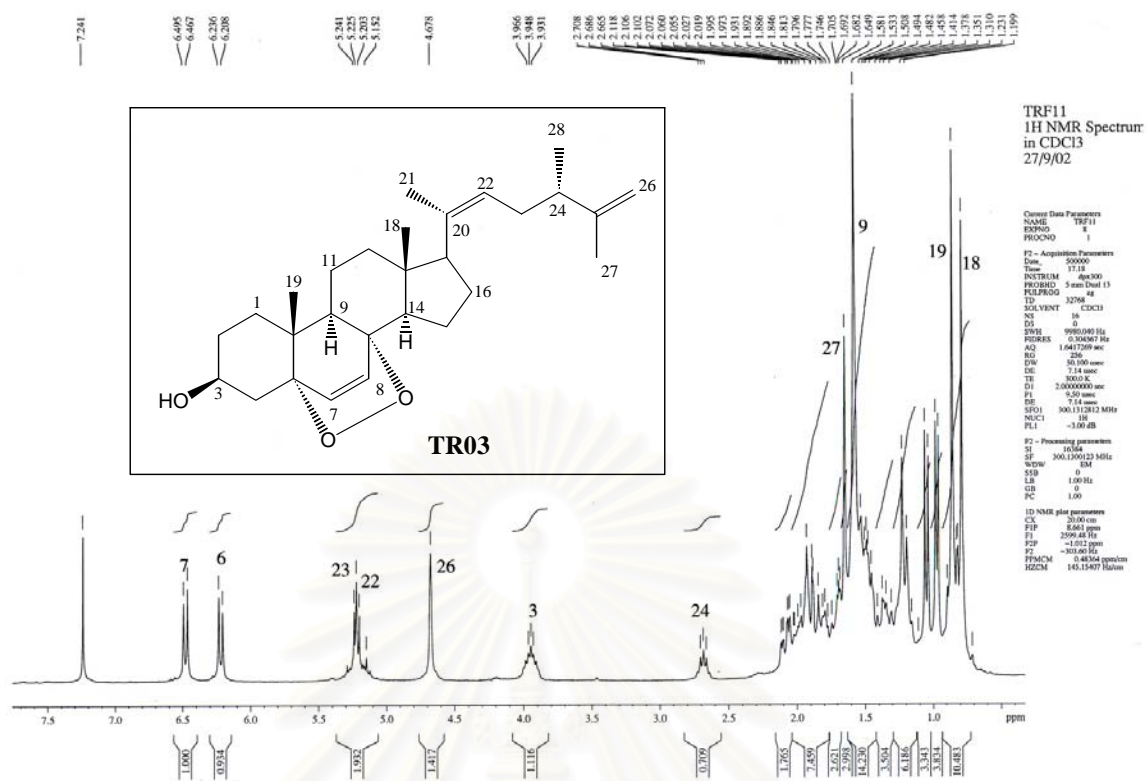
Figure 28 ^{1}H NMR (300 MHz) Spectrum of **TR03** (Axinysterol) in CDCl$_3$
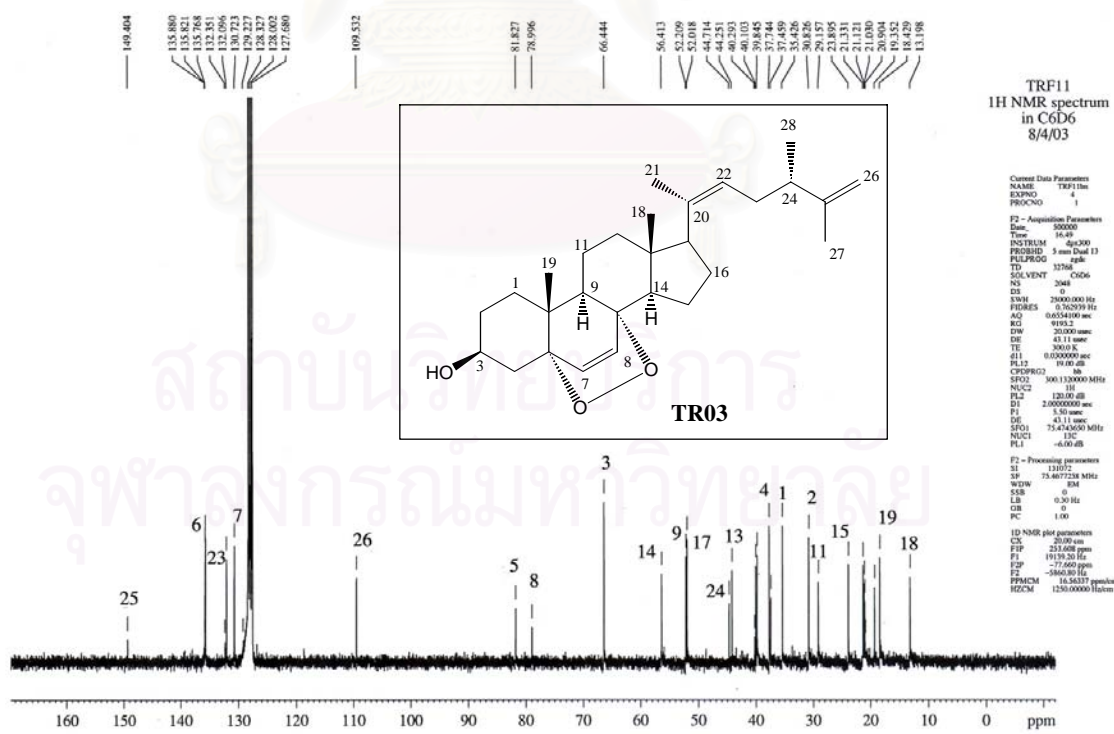
Figure 29 ^{13}C NMR (75 MHz) Spectrum of **TR03** (Axinysterol) in C$_6$D$_6$
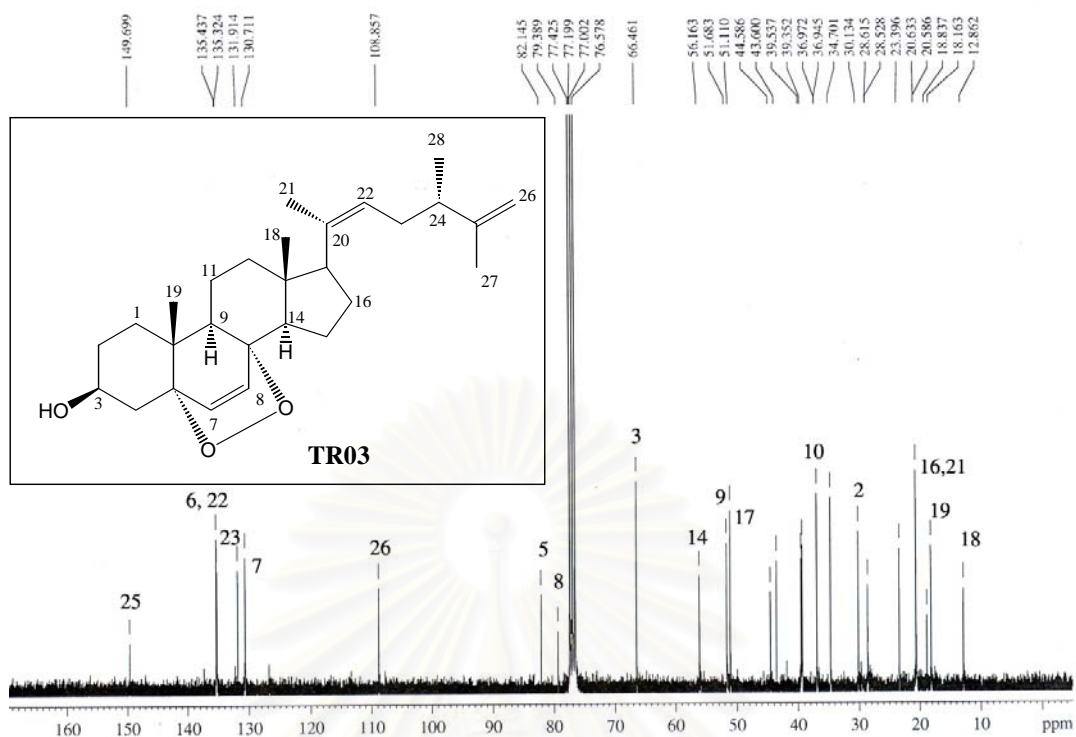
Figure 30 ^{13}C NMR (75 MHz) Spectrum of **TR03** (Axinysterol) in CDCl$_3$
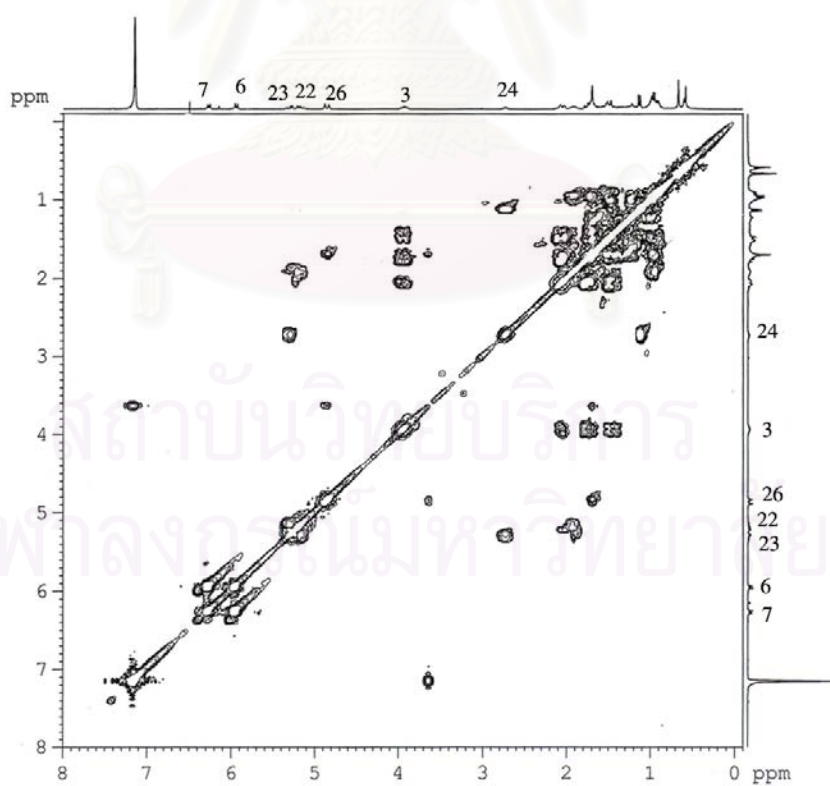
Figure 31 H,H-COSY Spectrum of **TR03** (Axinysterol) in C$_6$D$_6$
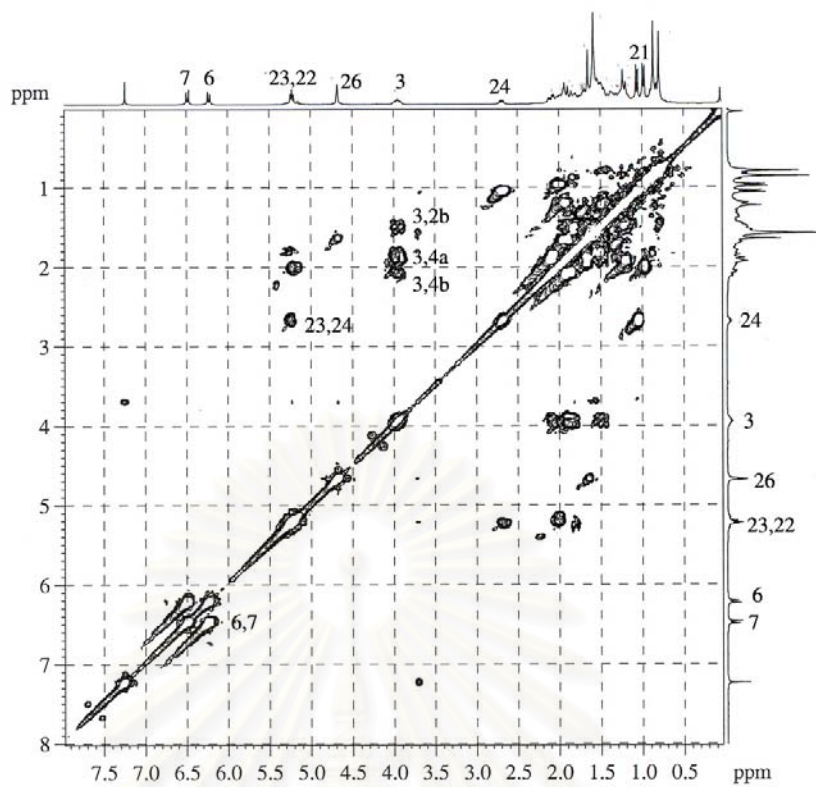
Figure 32 H,H-COSY Spectrum of **TR03** (Axinysterol) in CDCl₃
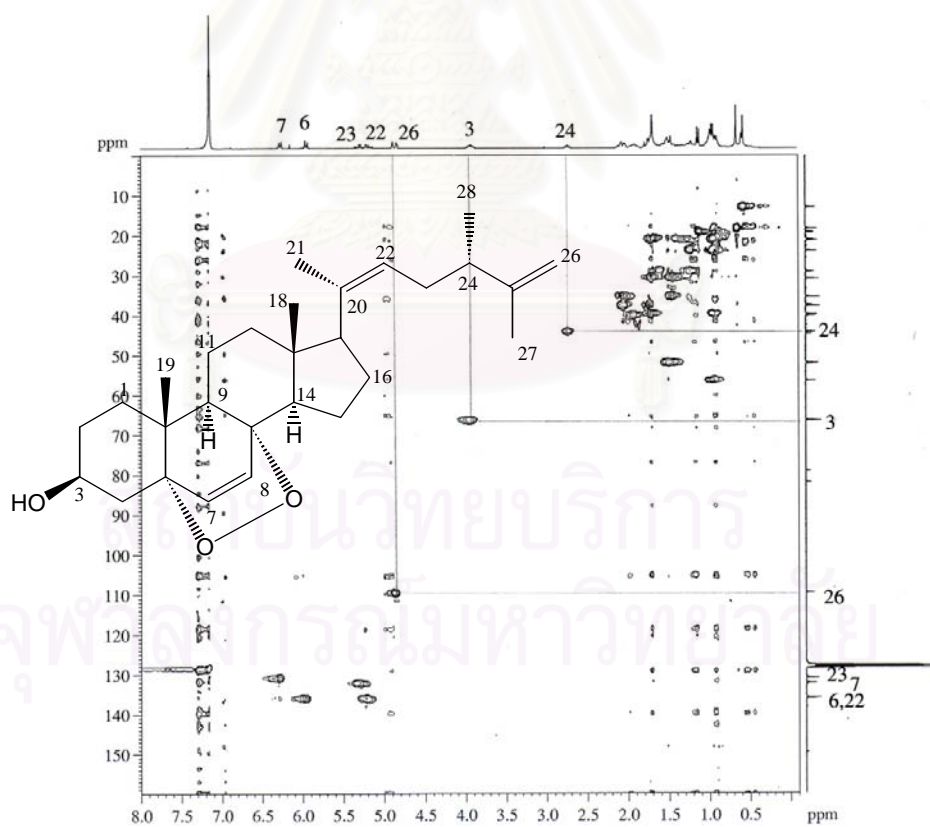
Figure 33 HMQC spectrum of **TR03** (Axinysterol) in C₆D₆
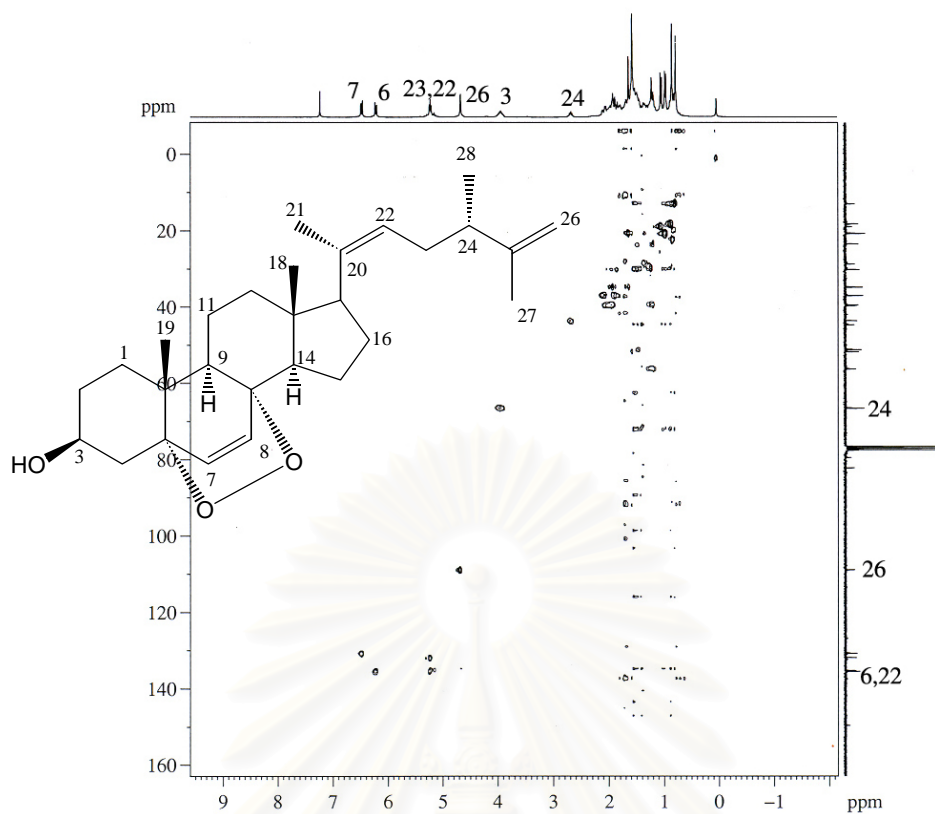
Figure 34 HMQC Spectrum of **TR03** (Axinysterol) in CDCl₃
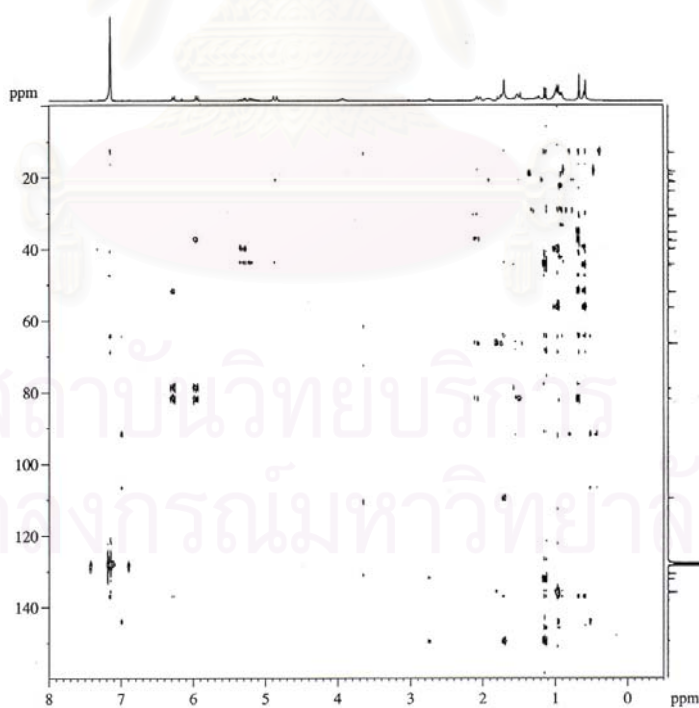
Figure 35 HMBC ($^n J_{HC}$ = 8 Hz) Spectrum of **TR03** (Axinysterol) in C₆D₆
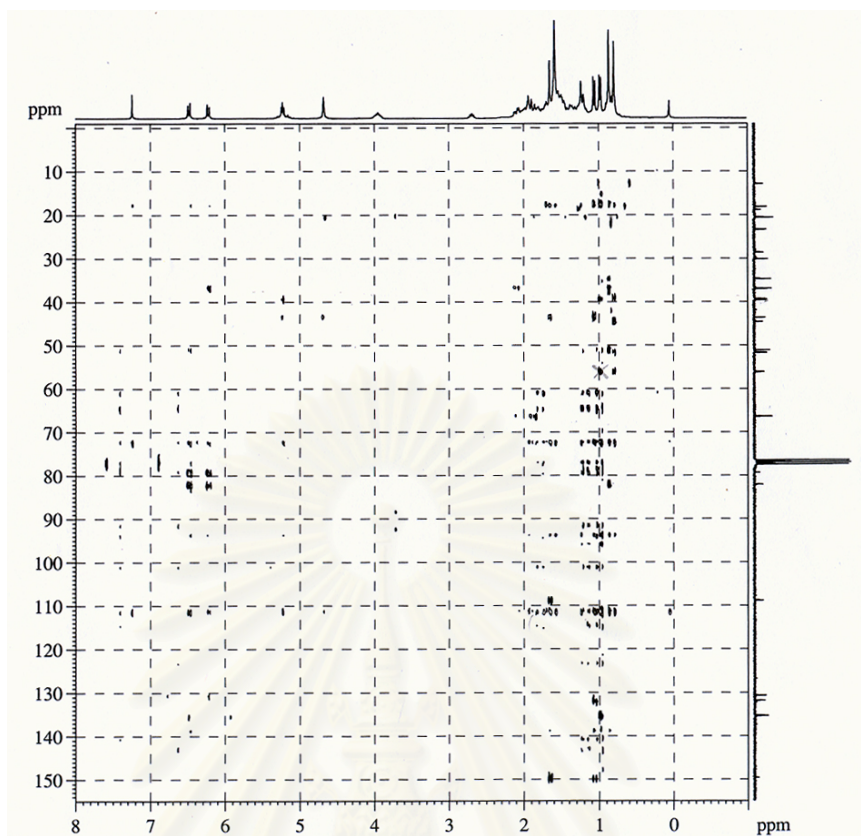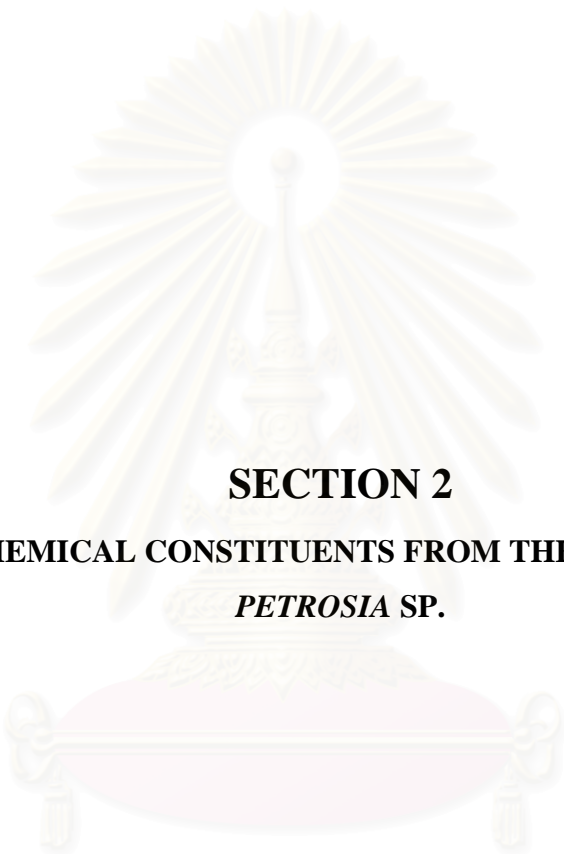
Figure 36 HMBC ($^nJ_{HC}$ = 8 Hz) Spectrum of **TR03** (Axinysterol) in CDCl$_3$
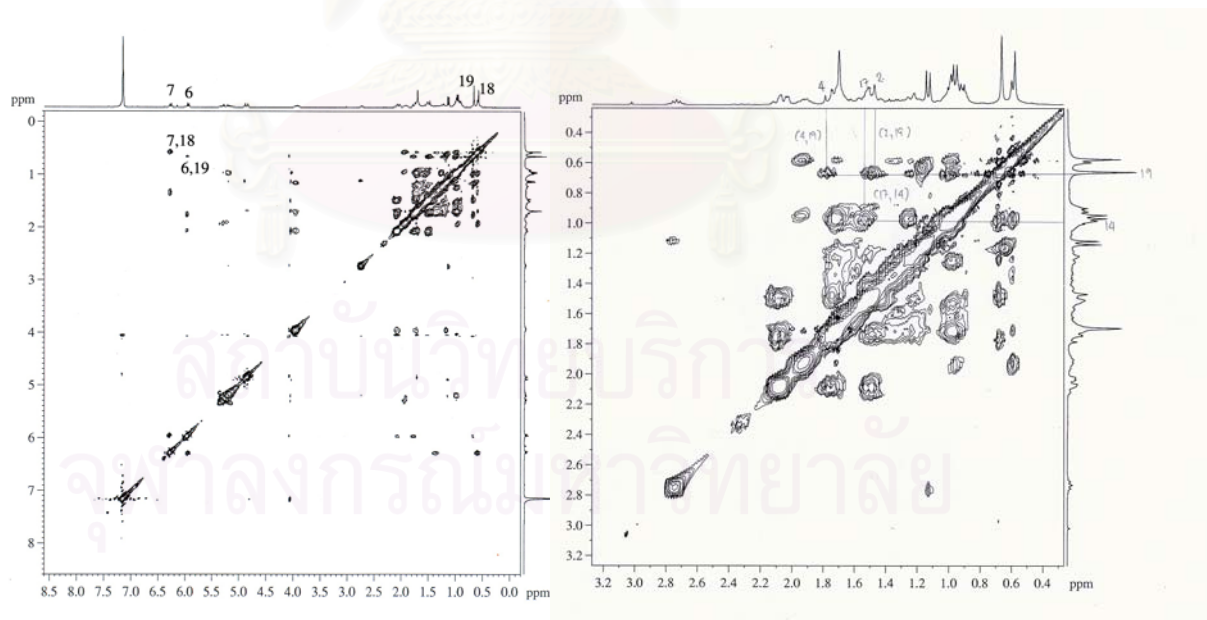
Figure 37 NOESY Spectrum of **TR03** (Axinysterol) in C$_6$D$_6$

SECTION 2

CHEMICAL CONSTITUENTS FROM THE SPONGE,
***PETROSIA* SP.**

CHAPTER I

INTRODUCTION

The pyridoacridines are a group of highly colored, polycyclic aromatic alkaloids isolated only from marine organisms. The structure of pyridoacridine alkaloids is based on the 11*H*-pyrido[4,3,2-*mn*]acridine skeleton [**1**]; however, the majority of this group are more accurately described as 'pyridoacridones' derivatives of the iminoquinone, 8*H*-pyrido[4,3,2-*mn*]acridone [**2**] (Molinski, 1993).

Pyridoacridine alkaloids have been found in several phylum of marine organisms, including sponge (phylum Porifera), tunicate (phylum Urochordata), anemone (phylum Cnidaria), and prosobranch (phylum Mollusca). It has been suggested that the unusual cross-phyletic distribution of the pyridoacridine natural products is due to symbiotic marine microorganisms. However, there does not appear to be solid evidence to support this conjecture. It seems just as likely that these compounds are *de novo* products of the host organisms, perhaps overexpressed secondary metabolites of aromatic amino acid secondary metabolic pathways common to many marine organisms.

[**1**] [**2**]

Also similar to the acridine compounds, most of pyridoacridine alkaloids are pH indicators, which correlate with the presence of at least two basic pyridine-like nitrogens and probably associate with electronic perturbations on extended chromophore with charge-transfer properties. This indicator property is absent in the less basic iminoquinones, such as cystodytin A [**3**] (Kobayashi *et al*., 1988) and diplamine [**4**] (Charyula, McKee, and Ireland, 1989). Alkaline solutions of free base

generally appear orange or red, while in acid solution they are green-blue to purple. Some quaternary ammonium alkaloids, like petrosamine [**5**], are deep blue or purple salts (Molinski *et al.*, 1988).

[**3**]   [**4**]
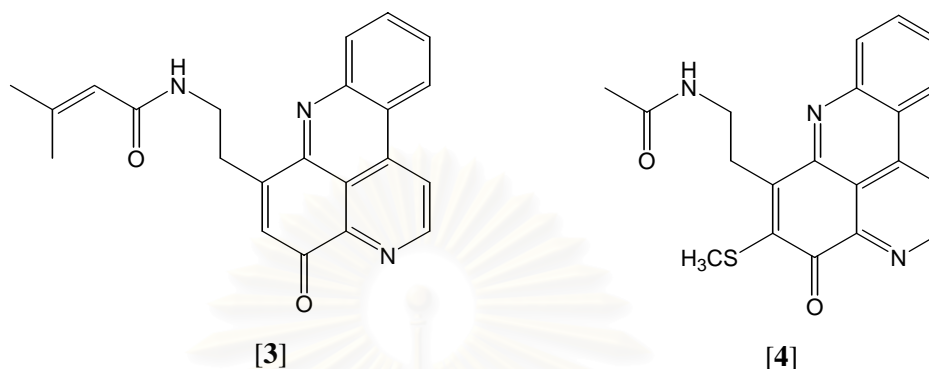
The ring system of the pyridoacridines highly conserved some general features in the appearance of the ^{1}H NMR spectra which are useful in identifying members of the pyridoacridine class. The disubstituted benzo ring A gives rise to a distinctive linear four protons coupled spin network (H1-H4, δ 7.0-9.0 ppm, *J* = 8-9 Hz) with H1 resonating at the lowest field due to the deshielding acridine nitrogen. The second AB spin system resonated at δ 8.5, 9.0 ppm with coupling constants of 5-6 Hz is assignable to H5-H6. This typical coupling constant value indicated the *ortho* and *meta* protons of a trisubstituted pyridine ring. Rings A and D make up the so-called "bay region" of the molecule. A strong nOe is always seen between the two "bay region" protons, H4-H5, therefore, linking these two nonscalar coupled substructures (Molinski, 1993).
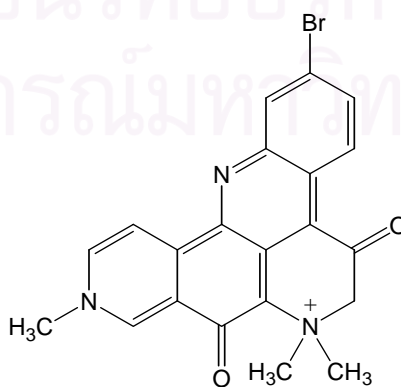
[**5**]

Although the common features in the ^{1}H NMR spectra of these polycyclic aromatic alkaloids facilitate their identification, structural studies of the pyridoacridines are not always easy, and indeed are often challenging to the natural product chemists. As highly unsaturated compounds, the alkaloids contain very few protons for the ^{1}H-^{1}H correlations, and the structure elucidation usually relies heavily on analyses of the ^{1}H-^{13}C long-range correlation experiments. In addition, some pyridoacridines were isolated as salts, such as the hydrochlorides, which cannot dissolve in most organic solvents completely. This solubility problem, also, provides additional challenges in the structure elucidation of the pyridoacridine alkaloids.

Pyridoacridine alkaloids have shown a wide range of biological activities. Almost all have been reported as having significant cytotoxicity; however, several specific biological properties have also emerged for different compounds, such as antifungal activity (McCarthy *et al.*, 1992), anti-HIV activity (Taraporewala *et al.*, 1992), antiviral activity, calcium release induction activity, immunosuppressant activity, and topoisomerase II inhibition through intercalation into DNA (McDonald *et al.*, 1994; Stanslas *et al.*, 2000).

As mentioned above, the combination of promising biological activities and challenging of complex structures have made pyridoacridine alkaloids one of the most interesting families of marine natural products. In an attempt to search for bioactive substances from Thai marine organisms, the greenish black sponge, later identified as *Petrosia* n. sp., was collected in intertidal zone, Phuket Island, Thailand in June 2000. Preliminary study of the methanol extract of this sponge showed significant antimicrobial and acetylcholinesterase (AChE) inhibitory activity. Furthermore, the typical pyridoacridine alkaloid signals were detected in the ^{1}H NMR spectrum of the crude methanol extract of the sponge *Petrosia* n. sp.

The following section will discuss the isolation, purification and structure determination of isolated compounds from the sponge *Petrosia* n. sp. The isolated compounds were tested for various biological activities, such as antimicrobial activity, cytotoxicity and acetylcholinesterase (AChE) inhibitory activity. In addition, a compound which possessed AChE inhibitory activity was further studied by molecular docking in order to identify its mode of action on AChE from *Torpedo californica* (*Tc*AChE).

CHAPTER II

HISTORICAL

1. Pyridoacridine Alkaloids

Since the discovery of the first pyridoacridine alkaloid, amphimedine [**6**] in 1983 (Schmitz, Agarwal, and Gunasekera 1983), more than 60 related alkaloids have been reported. The pyridoacridines vary in structure by appendage of different side chains or fusion of rings to ring C, and occasionally, to the acridine nitrogen. Halogenation is rarely seen, and when present, this is always bromine at C2 in ring A. The oxidation states of the rings vary, and sometimes partial saturation is seen in ring D, but more commonly, within additional rings appended to ring C. The extensive reviews on the chemical aspects of these alkaloids have already been reported (Molinski, 1993). Thus, to avoid redundancy, this review will focus on newly reported pyridoacridine alkaloids published in 1993 and after.
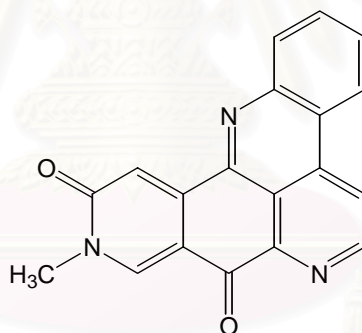
[**6**]

Tetracyclic pyridoacridine alkaloids are the archetypical members of this class of alkaloids. The cystodytins A-C [**3** and **7**-**8**] are the first pyridoacridine alkaloids isolated from a marine tunicate *Cystodytes dellechiajei* and the first tetracyclic of this class (Kobayashi *et al*., 1988). The common heterocyclic nucleus of cystodytins A-C is an iminoquinone-substituted at C10 with a 2-amindoethyl side chain. In 1994, the Ireland group discovered a new member of the cystodytin series, cystodytin J [**9**] isolated from a Fijian tunicate *Cystodytes* sp., along with other new pyridoacridine alkaloids, dehydrokuanoniamine B [**10**], shermilamine C [**11**], in addition to the known compounds cystodytin A [**3**], kuanoniamine D [**12**], shermilamine B [**13**], and eilatin [**14**] (McDonald *et al*., 1994). All compounds were found to inhibit the topoisomerase II-mediated decatenation of kinetoplast DNA in a dose-dependent

manner. Although, all isolated compounds were strong DNA intercalators, the mechanisms of DNA damage following intercalation were proposed to vary between individual alkaloids. Cystodytin J has also been isolated from the New Zealand ascidian *Lissoclinum notti* along with another new cystodytin, cystodytin K [**15**], as well as diplamine [**16**] and isodiplamine [**17**], and lissoclinidine [**18**] (Appleton *et al.*, 2002). These alkaloids possessed moderate to high activity towards P388 murine leukemia, HCT-116 human colon tumor and non-malignant African green monkey kidney (BSC-1) cells. Diplamine [**16**] was the most cytotoxic compound towards BSC-1 cells, although interestingly this potency was not so clear–cut for P388 or HCT-116 tumor cells. Movement of the thiomethyl group from C-9 (diplamine) to C-5 (isodiplamine) clearly reduced cytotoxicity.

[**7**]	$R_1 = H$	$R_2 =$ (2-methyl-1-propenyl)	$R_3 = H$
[**8**]	$R_1 = H$	$R_2 =$ (2-hydroxy-2-methylpropyl)	$R_3 = H$
[**9**]	$R_1 = H$	$R_2 = CH_3$	$R_3 = H$
[**15**]	$R_1 = H$	$R_2 = CH_3$	$R_3 = OCH_3$
[**16**]	$R_1 = SCH_3$	$R_2 = H$	$R_3 = H$
[**17**]	$R_1 = H$	$R_2 = SCH_3$	$R_3 = H$
[**19**]	$R_1 = SCH_3$	$R_2 =$ (isobutyl)	$R_3 = H$
[**20**]	$R_1 = SCH_3$	$R_2 =$ (2-methylbutyl)	$R_3 = H$
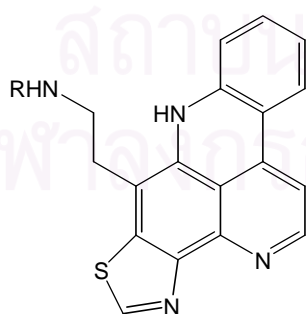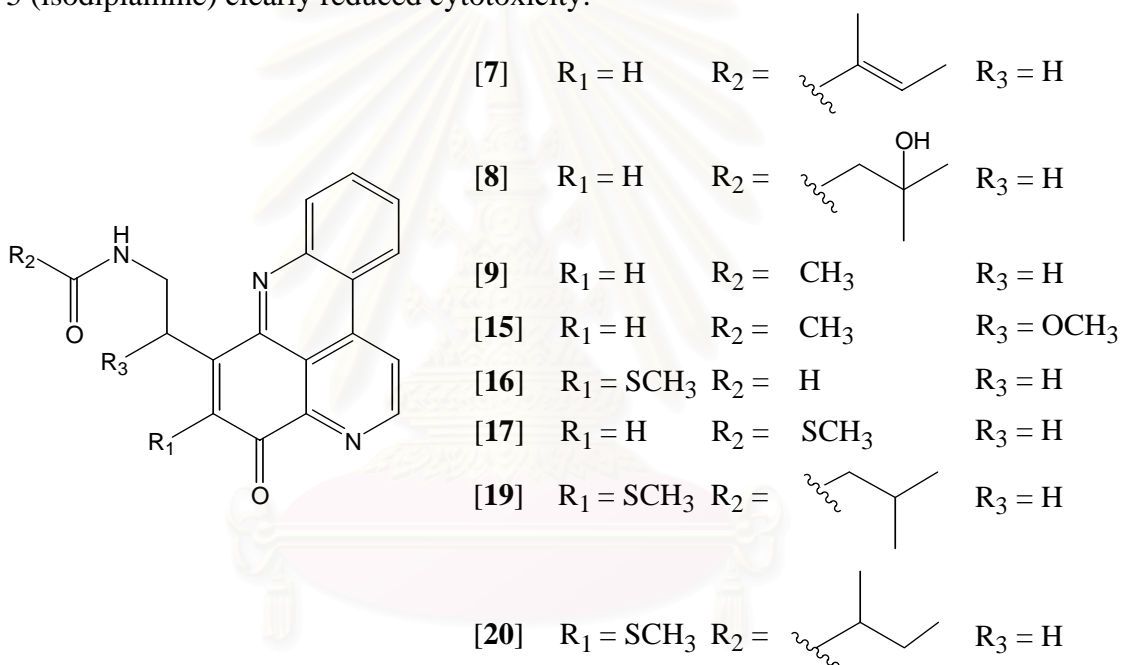
[**10**] $R = COCH=C(CH_3)_2$
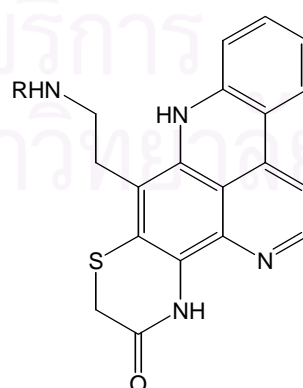
[**12**] $R = COCH_3$

[**11**] $R = COCH=C(CH_3)_2$

[**13**] $R = COCH_3$
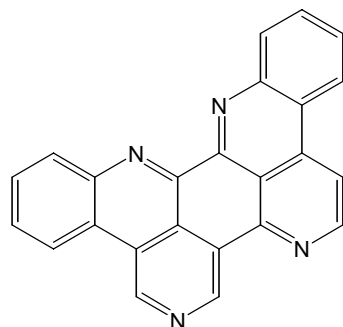
[**14**]
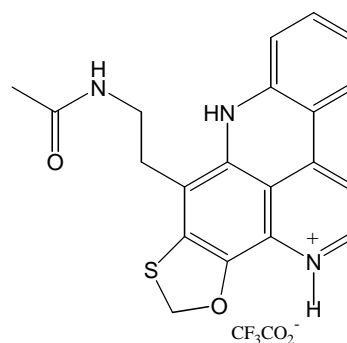
[**18**]

In 1994, the Molinski group reported five new alkaloids from the Austalian tunicate, *Lissoclinum* sp (Searle and Molinski, 1994). Derived from three distinct biosynthetic pathways, the compounds isolated included pyridoacridines lissoclin A [**19**] and lissoclin B [**20**], the indole alkaloid, lissoclin C [**21**], and the polysulfide alkaloids, lissoclinotoxin C [**22**], and the dimeric lissoclinotoxin D [**23**]. Compounds [**19**] and [**20**] were shown to be analog of diplamine [**16**], differed only in substitution of the acyl group on the ethylamino side chain. Although the crude extract of *Lissoclinum* sp. showed antifungal activity against *Candida albicans*, only lissoclinotoxin D exhibited significant antifungal activity.
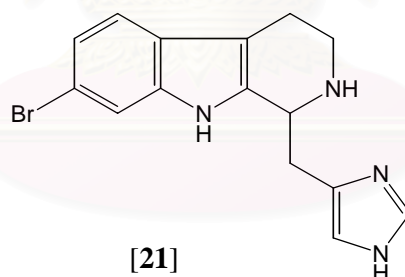
[**21**]
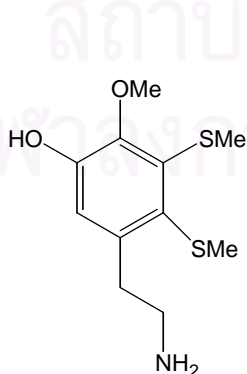
[**22**]
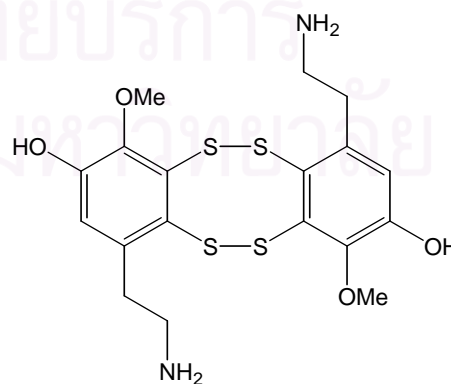
[**23**]

Another member of the tetracyclic pyridoacridines was pantheridine [**24**] which isolated from another Australian tunicate, *Aplidium pantherinum* (Kim *et al.*, 1993). This alkaloid contains the iminoquinone subunit similar to that of the cystodytins. However, it lacks the ethyl amino side chain and has an amino group at C-9 and a bromine substituent at C-3, which is different from the more typical C-2 bromine substitution. Pantheridine displayed mild cytotoxicity against P388 murine leukemia cells with $ED_{50} = 4.5$ μg/mL.
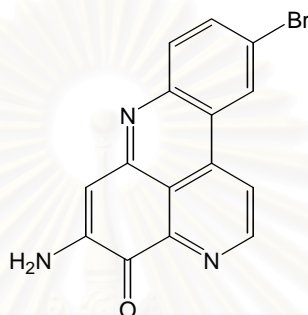
[**24**]

Recently, a new series of the tetracyclic pyridoacridine alkaloids, styelsamines A-D [**25-28**], was isolated as trifluoroacetate salts from the Indonesian tunicate *Eusynstyela latericius* (Copp *et al.*, 1998). The main skeleton of the styelsamines resembles, but different in oxidation state from that of the cystodytins. The iminoquinone subunit in the cystodytins is reduced to aminophenol in the styelsamines. However, after standing at room temperature for 2 months, styelsamine A was composed to a closely related new compound [**29**] containing the same oxidation state as the cystodytins. Styelsamines A, B, C and D exhibited mild cytoxicity toward the human colon tumor cell line HCT-116, with IC_{50} values of 33, 89, 2.6, and 16 μM, respectively.
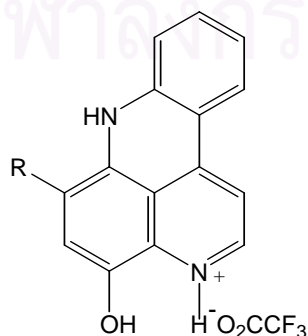
[**25**] $R = CH(OH)CH_2NH_3^+.O_2CCF_3$

[**26**] $R = CH_2CH_2NHCOCH_3$

[**27**] $R = CHO$ (free base)

[**28**] $R = CH_2CH_2NH_3^+.O_2CCF_3$

[**29**]   R = CH(OH)CH$_2$NH$_3^+$.O$_2$CCF$_3$
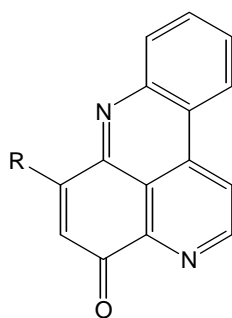
The pentacyclic pyridoacridines can be classified into two groups, first, those having one additional angular fused ring at C-9, C-10 of the acridine system at ring C, such as in meridine [**30**] (Schmitz *et al.*, 1991), and second, those having linear ring fusion at C-8, C-9 of ring C, such as in ascididemin [**31**] (Kobayashi *et al.*, 1988). Typical ring appendages include pyridine, tetradehydropyridine, thiazine, or even thiazole heterocycle. In addition, a substituted 2-ethylamino side chain can also be found attached to the acridine ring C.
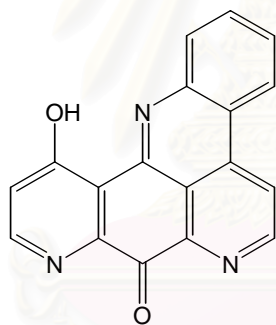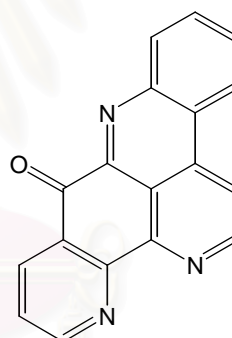
[**30**]   [**31**]

The sponge *Oceanapia sagittaria* from Palau contained the known dercitamide [**32**] and the new sagitol [**33**] (Salomon and Faulkner, 1996). Dercitamide was firstly reported from a sponge *Stelletta* sp. and a tunicate of the genus *Cystodytes* (Gunawardana *et al*., 1992). The structure of dercitamide was revised again as identical to kuanoniamide C, previously isolated from an unidentified tunicate and its mollusc predator *Chelynotus semperi* (Carroll and Scheuer, 1990).   Because the structure of sagitol showed structural similarity to dercitamide, it was suggested that sagitol could be an isolation artifact. Nevertheless, autoxidation of dercitamide with singlet oxygen provided sagitol, and the synthetic sample of sagitol was racemic, whereas the natural material was chiral, confirming a natural origin for sagitol.

Sagitol was the first pyridoacridine alkaloid which the aromatic system has been disrupted.
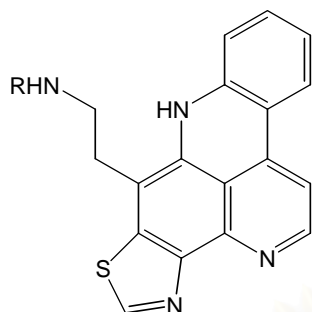
[32]   R = COC$_2$H$_5$

[34]   R = H

[35]   R = COCH$_3$
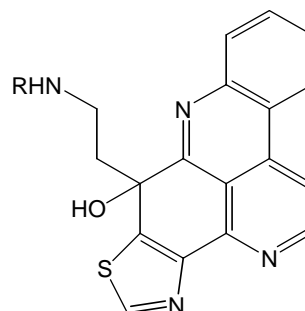
[33]   R = COC$_2$H$_5$

A new *N*-deacetyl derivative of the kuanoniamines [34] was isolated from the Micronesian sponge *Oceanapia* sp., along with the known kuanoniamine C [32] and kuanoniamine D [35].   The *N*-deacetyl derivative showed the same range of cytotoxicity as kuanoniamines C and D when tested against HeLa and MAC 6 cells (Eder *et al*., 1998).

The brownish-purple tunicate *Cystodytes* sp., collected in the vicinity of Arno Atoll, Republic of the Marshall Islands, contained two cytotoxic pyridoacridine alkaloids, arnoamines A [36] and B [37] (Plubrukan and Davidson, 1998).   The arnoniamines were proposed to be the first members of a new class of pentacyclic pyridoacridine alkaloids possessing a pyrrole ring fused to the pyridoacridine ring system.   Closely related compounds included the hexacyclic pyridoacridines cyclodercitin [38] (Gunawardana, Kohmoto, and Burres, 1989) and stelletamine [39] (Gunawardana *et al.*, 1992).   For each of these metabolites it can be proposed that pyrrole rings are formed through cyclization of the more common amidoethyl side chain observed in cystodytin A [3] and veramine A [40] (Molinski and Ireland, 1989).
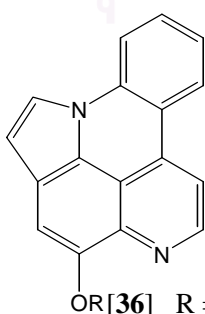
OR [36]   R = H
   [37]   R = CH$_3$
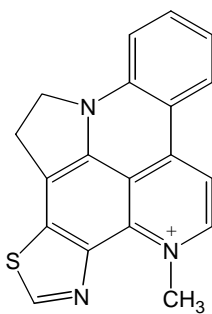
[38]
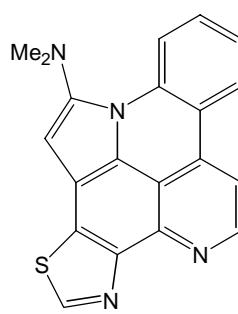
[39]
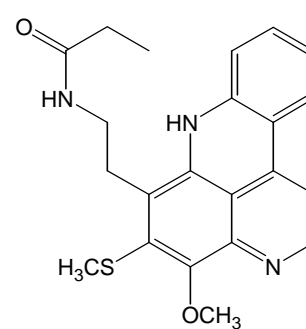
[40]

In addition to tintamine [**40**], a new alkaloid with a novel heterocyclic system, two new members of the shermilamines, shermilamines D [**41**] and E [**42**], were isolated from the Indian Ocean tunicate *Cystodytes violatinctus,* collected from the Comoros Islands (Koren-Goldshlager *et al*., 1998). Shermilamines D and E were deacetyl *N,N*-dimethyl derivatives of shermilamine B [**13**].
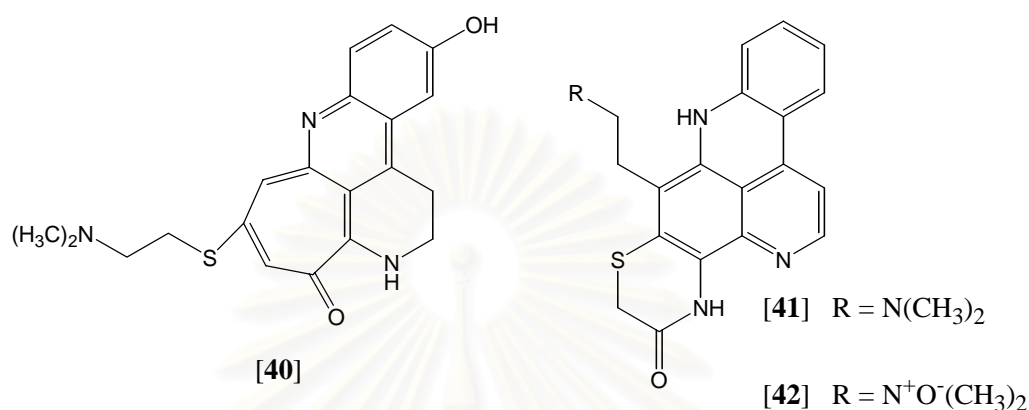
Tintamine possesses an unprecedented tropono-1,2-dihydro-phenanthroline skeleton, which has the C ring of the normal pyridoacridine structural unit expanded into a troponone ring. It was suggested that the biogenesis of tintamine, as shown in Figure 1, could be similar to that of the pyridoacridine, i.e. involving kynuramine [**43**], but with tropolone [**44**] replacing benzoquinone (Molinski, 1993).
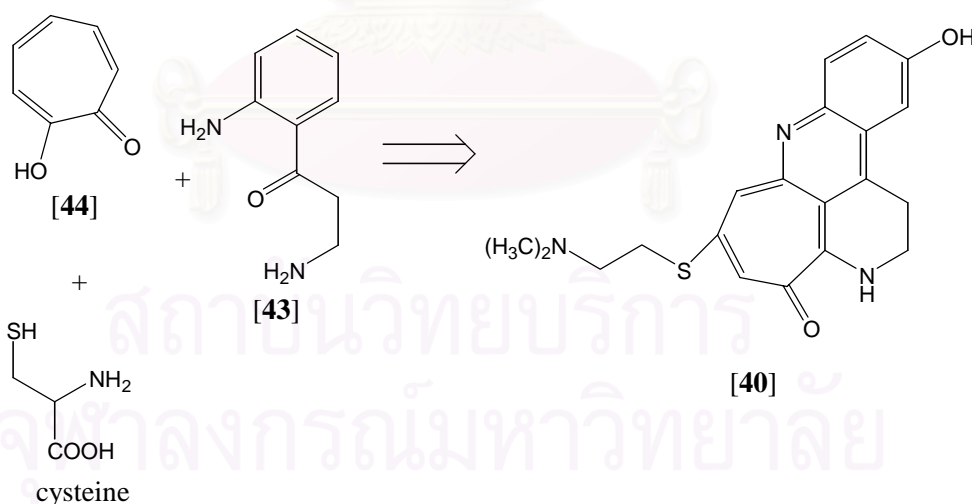
Figure 1 Proposed Biogenesis of Tintamine [**40**]

The Francisco group of France reported the isolation of cystodamine [**45**] from green morphs of the Mediterranean tunicate *Cystodytes dellechiajei* (Bontemps *et al.,* 1994). Interestingly, while cystodamine was the major alkaloid from tunicates whose colonies were found to harbor the green symbiotic alga (prochloron), the gray morphs

of the same species, which lack the symbiotic alga, yielded ascididemin [31]. Cystodamine exhibited cytotoxicity toward CEM human leukemic lymphoblasts with an IC_{50} of 1.0 μg/mL.
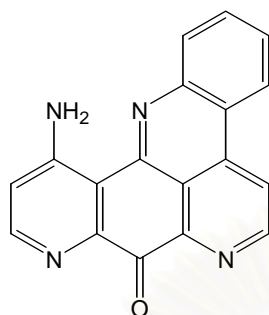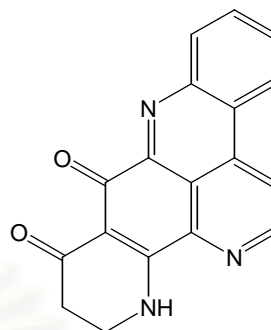
[45]   [46]

Another ascididemin derivative, 8,9-dihydro-11-hydroxyascididemin [46], was isolated from the Okinawan sponge *Biemna* sp., along with a new octacyclic pyridoacridine alkaloid biemnadin [47] (Zeng *et al*., 1993). Biemnadin, actually, is an isomer of the known alkaloid eudistone A [48] (He and Faulkner, 1991). Both biemnadin and 8,9-dihydro-11-hydroxyascididemin displayed cytoxicity against human epidermoid KB and murine lymphoma L1210 cells *in vitro*.
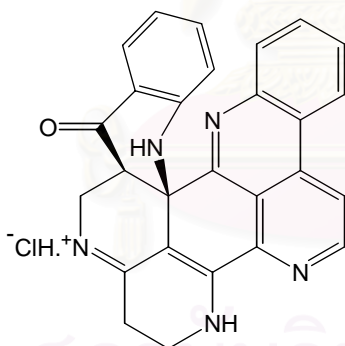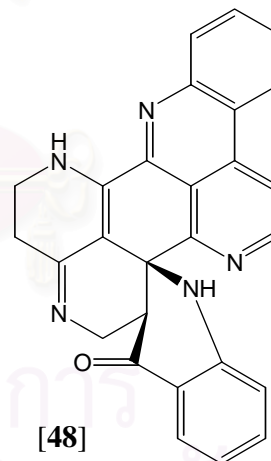
[47]   [48]

Deoxyamphimedine [49] was isolated along with neoamphimedine [50] and amphimedine [6] from two specimens of a *Xestospongia* sp. collected from the Philippines and Palau (Tasdemir *et al.*, 2001). Comparative bioactivity studies revealed that, unlike amphimedine and neoamphimedine, deoxyamphimedine appeared to damage DNA through the production of reactive oxygen species.

[**6**]   [**49**]   [**50**]

Petrosamine [**5**] is a natural product sharing the amphimedine skeleton isolated from a specimen of the sponge *Petrosia* sp. collected in Belize (Molinski *et al*., 1988). The structure of petrosamine contains a quaternary ammonium and bromine substituent at C-2. The color of a dilute solution of petrosamine varies according to the polarity of the solvent, such as purple in aqueous, blue in methanol, and green in dilute tetrahydrofuran. The correlation of the solvent-dependent changes in the UV and NMR spectra suggested that the remarkable color changes observed by varying solvent polarity were associated with shifts in the position of a keto-enol [**5a-5b**] equilibrium (Molinski, 1993).

[**5a**]   [**5b**]

Recently, the isolation of the crude methanol extract of the tunicate *Cystodytes dellechiajei* collected in Brazil yielded two novel alkaloids with unprecedented ring systems, sebastianine A [**51**] and sebastianine B [**52**] (Torres *et al*., 2002). The structure of sebastianine A comprised a pyridoacridine system fused with a pyrrole unit, whereas sebastianine B composed of a pyridoacridine system fused with pyrrolidine system condensed with α-hydroxyisovaleric acid. Both alkaloids

displayed a cytotoxic profile against a panel of HCT-116 colon carcinoma cells indicative of a p53 dependent mechanism.

[51] [52]
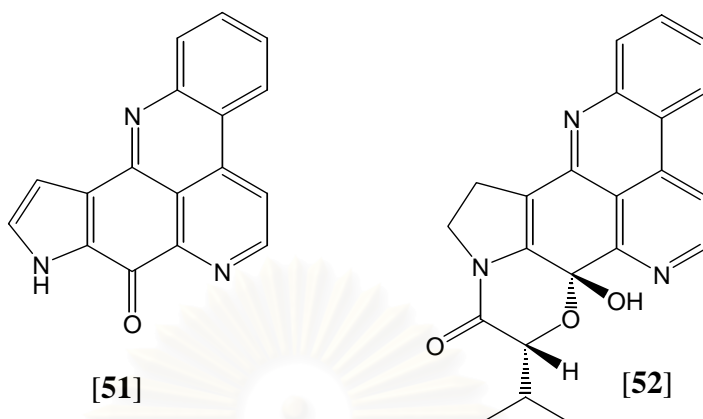
From an unidentified Singaporean tunicate, two new kuanoniamine series (kuanoniamines E and F [**53** and **54**]) were isolated, along with a new ring-opened pyridoacridine alkaloid, subarine [**55**] (Nilar *et al.*, 2002). The structure of submarine is interesting, as it could be a significant biosynthetic link in the biosynthesis of ascididemin [**31**] and other related pentacyclic pyridoacridines.

[**53**] R =

[**54**] R =

[**31**] [**55**]
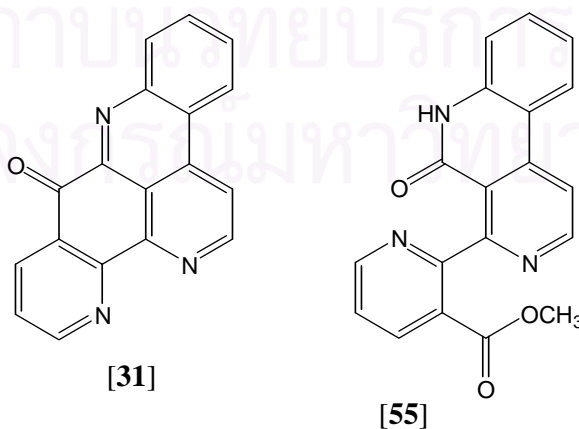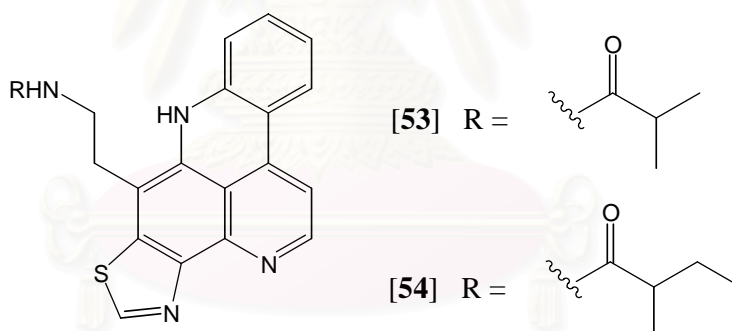
More recently, a new pyridoacridine alkaloid labuanine A [**55**] was obtained from the Indonesian marine sponge *Biemna fortis*, along with two regioisomer [**56** and

57] of known pyridoacridine alkaloids, meridine [**30**] and cystodamine [**45**], respectively (Aoki *et al*., 2003). Compounds [**56**] and [**57**] were the first case of isolation from natural source and compound [**56**] might be an artifact metabolite produced from labuanine A by air oxidation. These alkaloids induced multipolar neuritogenesis in more than 50% of cells at 0.03-3 μM concentration. Compound [**57**] showed the strongest neuritogenic activity, induced increase of acetylcholinesterase and arrested cell cycle at the G2/M phase.

[**55**] [**56**] [**57**]
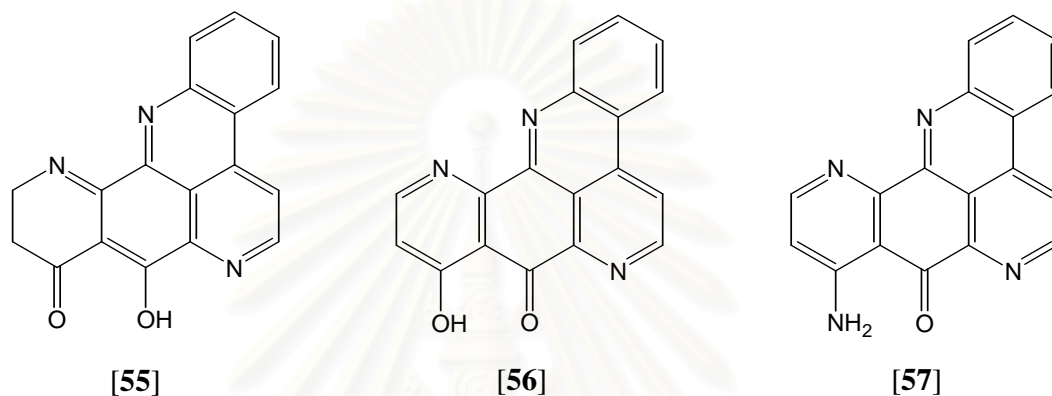
Like most heterocyclic alkaloids, the pyridoacridines are products of aromatic amino acid metabolism. Through feeding experiments *in situ* and with cell-free extracts of the Mediterranean tunicate *Cystodytes dellechiajei*, it has been shown that both L-[5-^{3}H] tryptophan and [7,8-[3]H$_2$] DOPA are precursors to shermilamine B [**13**] (Molinski, 1993). The author proposed a biosynthetic pathway to shermilamine B involving tryptophan, DOPA, and cysteine. The recent analysis of the "pyridoacridine family tree" by Skyler and Heathcock provided a comprehensive view of many potential biotransformations (Heathcock and Skyler, 2002). From this review, it is possible to devise a synthesis/possible biosynthesis and to predict the pyridoacridines natural products that may be as of yet undiscovered. In addition, recent report from Wenzel and Crews explored a possible biochemical pathway, from neoamphimedine [**50**] to 5-methoxyamphimedine (Wenzel and Crews, 2003). The results from semiempirical and ab initio methods could help understanding the relationships that favor the formation of 5-methoxyamphimedine and undiscovered bis-oxygenated pyridoacridine alkaloids.

2. Acetylcholinesterase

Acetylcholinesterase (AChE) functions in the central and peripheral nervous systems, along with the acetylcholine (ACh) [58] receptor, in the transmission of action potentials across nerve-nerve and neuromuscular synapses. The principal role of AChE is termination of impulse transmission at cholinergic synapses by rapid hydrolysis of ACh. Because of the pivotal role that AChE plays in the nervous system, the enzyme has long been attractive target for the rational design of mechanism-based inhibitors (Quinn, 1987).

[58]
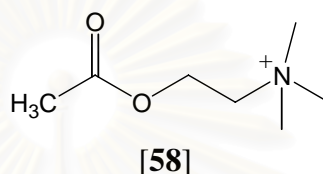
Alzheimer's disease (AD) is a neurodegenerative process associated with the deposition of amyloid plaques and fibrillary tangles, as well as with neurotransmitter alterations in the brain. One of the main functional deficits in AD involves cholinergic neurons, which provides the rationale for a potential therapeutic approach to treatment of AD (Bar-on *et al.*, 2002). It has been known that the density/activity of brain nicotinic ACh receptors (nAChR) is substantially reduced in AD patients compared with a control group of the same age.

Based on these well-established findings, the majority of current drug therapeutic approaches to AD follow the cholinergic hypothesis. These approaches are aimed at elevating the levels of ACh in the brain that may be achieved by inhibiting AChE with inhibitors (Siddiqui and Levey, 1999). Inhibition of AChE is considered one of the most promising strategies for the treatment of AD and related diseases, such as Parkinson's disease, aging, and myasthenia gravis.

Over the years, hundreds of compounds have been synthesized and tested for AChE activity, and several of them have found clinical applications. The chemical structures of these inhibitors are very different, ranging from bis-quaternary compounds such as decamethonium [59], to simple mono cationic compounds such as edrophonium [60], and formally neutral tricyclic compounds such as tarcine (THA) [61] (Harel *et al.*, 1993). In addition, donepezil [62], minaprine [63], huperzine [64] and galanthamine [65] (Figure 2) are also able to enhance memory in AD patients. The drugs approved by the US. Food and Drug Administration (FDA) so far include natural substances, such as galanthamine under its trade name Reminyl® (approved in

2003), which was isolated from Snowdrop (*Galanthus nivalis*) and Daffodil (*Narcissus pseudonarcissus*) (Greenblatt *et al.*, 1999), in addition to synthetic compounds, such as tarcine (Cognex®, approved in 1993), donepezil (Aricept®, approved in 1996) (Harel *et al.*, 1993; Sugimoto *et al.*, 1995), and rivastigmine (Exelon®, approved in 2000) (Kawakami *et al.*, 1996).
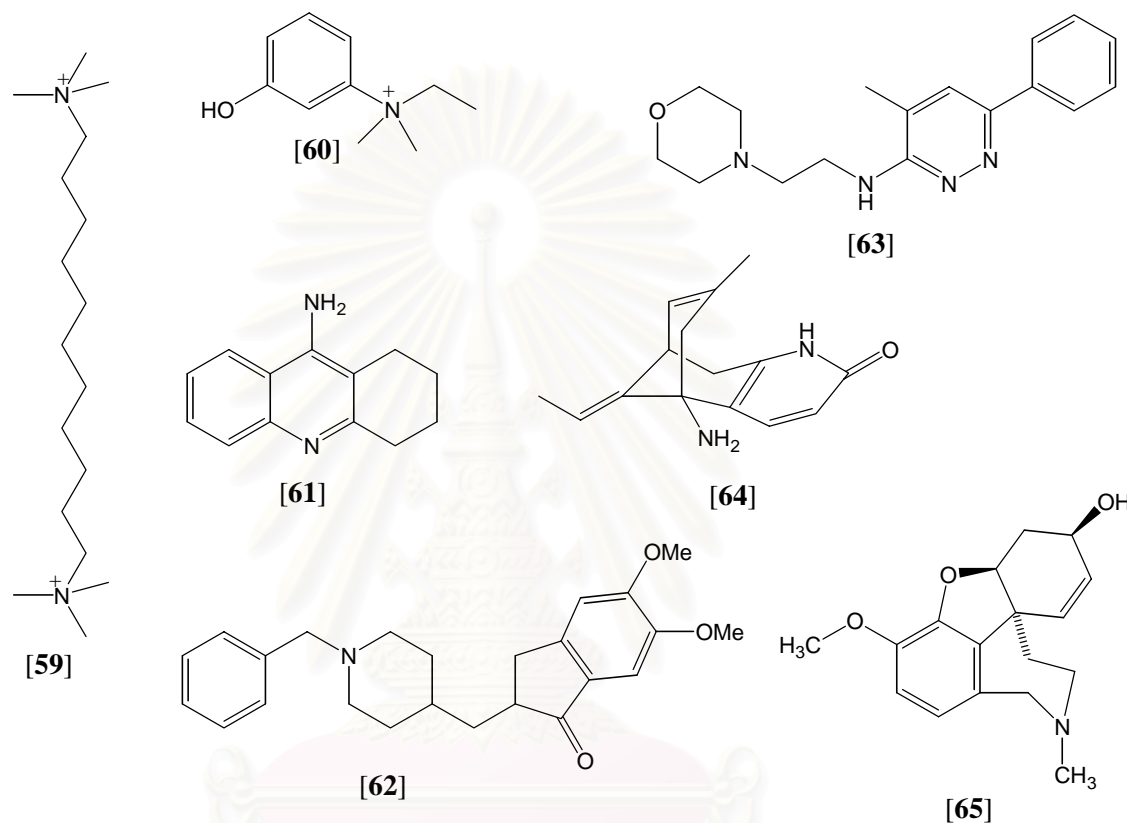
Figure 2 Molecular Structures of AChE Inhibitors

Among the different classes of AChE inhibitors reported to date, galanthamine [**65**] stands out as a very potent and promising drug treatment of the cholinergic deficit in AD patients due to its very low toxicity and side effects (Rhee *et al.*, 2001). The difficulty of isolating galanthamine from its natural source severely hindered its use as a commercial drug or even as a starting material for the synthesis of the derivatives. However, there are a number of total synthesis procedures presently available, of which those via (-)-narwedine are the most convenient and have been extensively employed for large-scale industrial preparation (Pilger *et al.*, 2001). However, to date, all the longer-term studies have shown clinical efficacy to decline with time as a result of either a loss of drug efficacy or the relentless progression of the disease. Since the

current AChE inhibitors lack perfection, the attempt to discover novel AChE inhibitors is, thus, continued

The AChE consists of globular catalytic subunits that have masses of 70-80 kDa. The catalytic subunits of this enzyme appear in two major classes of oligomers: globular forms and asymmetric forms. Each globular subunit contains a single active site, while asymmetric forms contain three major structural domains, including catalytic subunits, collagen-like tail, and non-collagenous tail. Polymorphic AChEs, including asymmetric forms, are found in fish electric organs, avian muscle, mammalian skeletal muscle, and in rat vagus nerve, smooth muscle, and heart muscle. Although AChE is polymorphic, activities of catalytic subunits in the asymmetric and globular forms of the enzyme are similar (Gordon, Carpenter, and Wilson, 1978).

Due to its important therapeutic role, the enzyme has been a subject of many recent experimental (Kozikowski *et al.*, 1991; Sugimoto *et al.*, 1995; Inoue *et al.*, 1996) and theoretical investigations (Gilson *et al.*, 1994; Cho *et al.*, 1996; Wlodek *et al.*, 1997). Early kinetic studies indicated that the active site of AChE contains two subsites, the "esteratic" and "anionic" subsites (Quinn, 1987). The esteratic subsite, comprised of the active serine, is believed to resemble the catalytic subsites of other serine hydrolases. The anionic site is ≥ 4.7 Å from the esteratic serine, where the quaternary ammonium pole of ACh and of various active site ligands binds. In addition to the two subsites of the catalytic center, AChE possesses one or more additional binding sites for ACh and other quaternary ligands (Figure 3). Such "peripheral" anionic sites, clearly distinct from the choline-binding pocket of the active site, have been proposed and firmly established by Taylor and Lappi (Taylor and Lappi, 1975), by use of the fluorescent probe propidium.

Recently, Sussman's group has described the three-dimensional structure of AChE from *Torpedo californica* electric organ as determined by X-ray analysis to 2.8 Å (Sussman *et al.*, 1991). Their result suggested that the enzyme monomer is an α/β protein that contains 537 amino acids. It consists of a 12-stranded mixed β-sheet surrounded by 14 α-helices and bears a striking resemblance to several hydrolase. The active site, like other serine hydrolase, contains a Ser-His-Glu catalytic triad.
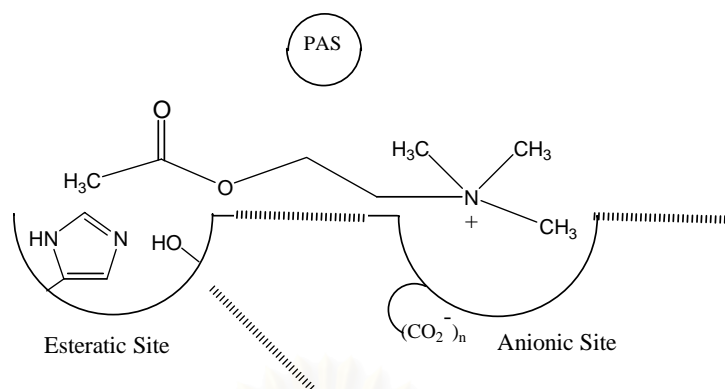
Figure 3 Representation of the Active site of AChE

(PAS, peripheral anionic binding site(s), the hatched areas represent putative hydrophobic binding regions)

This triad is located at the bottom of a deep and narrow cavity, named the 'aromatic gorge'', since ≈ 40% of its lining is composed of the rings of 14 conserved aromatic amino acids. A modeling study for ACh binding to the enzyme suggested that the quarternary ammonium ion is bound not to a negatively charged "anionic" site but rather to some of the 14 aromatic residues that line the cleft. From the x-ray analysis of AChE from *Torpedo californica* reported by Sussman (Sussman *et al.*, 1991), it was shown that the quaternary nitrogen of ACh binds strongly with the π electron of the aromatic ring of a conserved tryptophan, Trp84. According to this model, Chen's group hypothesized that carbonyl center of physostigmine and other carbamates interact with the enzyme via the Ser-His-Glu catalytic triad and the quaternary nitrogen interacts with neighboring aromatic residue (Chen *et al.*, 1994). One of these aromatic residues might correspond to the second hydrophobic binding site (HSB-2) proposed by Ishihara in 1991 (Ishihara, Kato, and Goto, 1991). The report from Sugimoto's group described two additional hydrophobic regions in the hypothetical binding site of donepezil on AChE. One hydrophobic region was thought to be closely adjacent to both the negative charge and the hydrogen-bonding sites while another was a defined distance away from the negative charge site (Sugimoto *et al.*, 1995).

. In the attempt toward understanding the inhibitor in the active site of AChE enzyme, molecular docking study was, thus, employed. The availability of several crystal structures of AChE complexing with the inhibitors provides the possibility to

apply docking protocol for the other protein-inhibitor complexes (Zaheer-ul-haq *et al.*, 2003).

Successful design of novel potent inhibitors of AChE could be greatly facilitated by rational analysis of experimental structure-activity relationships among the enzyme inhibitors and accurate prediction of their conformations in the enzyme bound form. Recent X-ray crystallographic analysis of AChE from *Torpedo californica* (EC 3.1.1.7) (Sussman *et al.*, 1991) followed by X-ray determination of the complexes of the enzyme with several structurally diverse inhibitors, such as tarcine (Harel *et al.*, 1993), edrophonium (Ravelli *et al.*, 1998), donepezil (Kryger, Schalk, and Sussman, 1998), and decamethonium (Harel *et al.*, 1993), provided crucial information with respect to the orientation of these inhibitors in the active site of the enzyme. More recently, the structure of *Tc*AChE galanthamine complex was also elucidated by X-ray crystallography to 2.5 Å resolution (Pilger *et al.*, 2001). The major difference in these complexes is the orientation of Phe330. This side chain controls the access to the bottom of the gorge and was identified as adopting three major conformations: an open, a close, and an intermediate access position (Pilger *et al.*, 2001). These results of the structural analysis of AChE-ligand complexes provide an excellent basis for the application of the described docking procedures to a large number of de novo designed and synthesized AChE inhibitors.

CHAPTER III

EXPERIMENTAL

1. Sample Collection

The greenish black sponges (Figure 4) were collected at the intertidal zone, Panwa Bay, Phuket Island, Thailand in June 2000 and again in May 2002. This sponge was frozen on site, and preserved at -20 ^{o}C before extraction. The sponge was later identified as *Petrosia* n. sp. (Class Demonspongiae, Order Haploslerida, Family Petrosiidae) by Dr. John N.A. Hooper of Queensland Museum, South Brisbane, Australia. A voucher specimen of this sponge (No. QM G320225) has been deposited at Queensland Museum and also at Bioactive Marine Natural Products Chemistry Research Unit, Department of Pharmacognosy, Faculty of Pharmaceutical Sciences, Chulalongkorn University under code number of PK00-01.

1.1 Identification and Characterization of the Sponge *Petrosia* n. sp.

The sponge was identified and characterized by Dr. John N. A. Hooper from Queensland Museum, South Brisbane, Australia. The identification and characterization of this sponge were conducted as follows:

Name	: *Petrosia* new species [QM species file number # 113]
Phylum	: Porifera
Class	: Demospongiae
Order	: Haploscleida
Family	: Petrosiidae
Known Distribution	: Thailand (Andaman Sea, Gulf of Thailand), northern Australia (Timor and Arafura Seas), Indonesia (Bali, Sulawesi)
Habitat	: Growing on rocks and dead coral, shallow subtidal and intertidal
Grown form	: Massive, bulbous encrusting, with lobate bulbous nodes arising from a convoluted base

Color   **:** Variable depending on habitat, commonly light or dark blue alive, occasionally violet or blackish blue, or rarely black internally and externally; color probably due to the presence of a microalgal symbiont; produces mucus exudates, bluish, blackish or greenish in color

Oscules   **:** Large, on apex of surface bulbs

Texture   **:** Hard, brittle, friable

Surface ornamentation: Even, porous microscopically

Ectosomal skeleton **:** Tangential paucispicular tracts, with choanosomal spicules protruding a short way through the surface

Choanosomal skeleton: Irregularly reticulate, multispicular tracts producing oval meshes, wider meshes at core of skeleton becoming smaller towards periphery; no fibres, sparse mesohyl collagen

Megascleres   **:** Oxeas, single size category 180-(232)-250 × 5-(12)-18 μm, slightly curved, robust, the larger abruptly pointed

Microscleres   **:** Absent

Figure 4 The sponge *Petrosia* n. sp.

2. General Techniques

2.1 Solvents

Throughout this work, all organic solvents were of commercial grade and were redistilled prior to use.

2.2 Analytical Thin-Layer Chromatography (TLC)

Technique   :   One dimension, ascending

Adsorbent   :   Silica gel 60 F_{254} (E. Merck) pre-coated plate

Layer thickness   :   250 μm

Distance   :   5.0 cm

Temperature   :   Laboratory temperature (25-30 $^{\circ}$C)

Detection   :   1. Visual detection under daylight

                       2. Visual detection under ultraviolet light (254 and 365 nm)

                       3. Anisaldehyde reagent and heating at 105 $^{\circ}$C for 10 min.

                       4. Dragendorff's reagent

2.3 Column Chromatography

2.3.1 Flash Column Chromatography

Adsorbent   :   Silica gel 60 (No. 7734) particle size 0.063-0.200 nm (70-230 mesh ASTM) (E. Merck)

Packing method   :   Wet packing: the adsorbent was slurried in the eluent, poured into a column and then allowed to settle.

Sample loading   :   The sample was dissolved in a small amount of eluent, and then applied gently on top of the column.

Detection   :   Fractions were examined by TLC technique in the same manner as described in section 2.2

2.3.2 Gel Filtration Chromatography

Gel Filter   :   Sephadex LH-20 (Pharmacia Biotech AB)

Packing method	:	Gel filter was suspended in the eluent and left standing to swell for 24 hours prior to use. It was then poured into the column and allowed to set tightly.
Sample loading	:	The sample was dissolved in a small amount of eluent and then applied gently on top of the column.
Detection	:	Fractions were examined by TLC technique in the same manner as described in section 2.2

2.3.3 High Speed Countercurrent Chromatography (HSCCC)

Instrument	:	High speed countercurrent chromatograph P.C. Inc. model MKII, equipped with a polytetrafluoroethylene (PTFE) multilayer coil with diameter of 2 mm and a total capacity of 320 mL.
Solvent system	:	The two –phase solvent systems were composed of chloroform-methanol-water at various ratios. After thoroughly equilibrated the mixture, the two phases were separated shortly before use. The aqueous phase was used as the stationary phase and the organic phase as the mobile phase.
Sample loading	:	The sample was dissolved in equal volume of upper phase and lower phase and filtered before injection.
Detection	:	Fractions were examined by TLC technique in the same manner as described in section 2.2

2.4 Crystallzation Technique

Compound **PK01** was crystallized by dissolving in CHCl$_3$ until saturated, and then MeOH was added. The solution was left standing at room temperature until yellowish amorphous solid was formed.

Compound **PK02** was crystallized by dissolving in MeOH until saturated, and then CHCl$_3$ was added. The solution was left standing at room temperature until dark blue needle was formed.

Compound **PK03** was crystallized from MeOH. The compound was dissolved in MeOH until saturated, and left standing at room temperature until white powder was formed.

2.5 Spectroscopy

2.5.1 Ultraviolet (UV) Spectra

UV spectra were obtained on a Milton Roy Spectronic 3000 Array spectrophotometer (Pharmaceutical Research Instrument Center, Faculty of Pharmaceutical Sciences, Chulalongkorn University).

2.5.2 Infrared (IR) Spectra

IR spectra were recorded on a Perkin Elmer FT-IR 1760X spectrometer (Pharmaceutical Research Instrument Center, Faculty of Pharmaceutical Sciences, Chulalongkorn University).

2.5.3 Mass Spectra

Mass spectra were obtained by an Electrospray Ionization Time of Flight mass spectra (ESITOFMS) made on a Micromass LCT mass spectrometer (The National Center for Genetic Engineering and Biotechnology, BIOTEC, Thailand), and the lock mass calibration was applied for the determination of accurate mass, Electron Impact mass spectrometry (EIMS) on a JEOL JMS-700 (Meiji University, Japan), and high resolution fast atom bombardment mass spectrometry (HRFABMS) on a VG70E-HF (University of Minnesota, USA).

2.5.4 Proton and Carbon-13 Nuclear Magnetic Resonance (^{1}H and ^{13}C NMR) Spectra

^{1}H (300 MHz) and ^{13}C (75 MHz) NMR Spectra were measured on a Bruker DPX-300 FT-NMR spectrometer (Pharmaceutical Research Instrument Center, Faculty of Pharmaceutical Sciences, Chulalongkorn University).

^{1}H (500 MHz) and ^{13}C (125 MHz) NMR Spectra were obtained with a JEOL JMN-A 500 NMR spectrometer (Scientific and Technological Research Equipment Center, Chulalongkorn University).

The solvents for NMR spectra were deuterated dimethysulfoxide (DMSO-d_6), deuterated chloroform (CDCl$_3$), deuterated trifluoroacetic acid (TFA-d). The chemical shifts were reported in ppm scale using the chemical shift of residual undeuterated solvents as the reference signals at δ 7.24 ppm (^{1}H) and 77.0 ppm (^{13}C) for CDCl$_3$, 2.49 ppm (^{1}H) and 39.7 ppm (^{13}C) for DMSO-d_6.

2.6 Melting Points

Melting points were obtained on a Fisher-John Melting Point Apparatus (Department of Pharmaceutical Botany, Faculty of Pharmaceutical Sciences, Chulalongkorn University).

2.7 Molecular Docking Study Equipments

All programs and computer resource were supported from the Computational Chemistry Unit Cell, Department of Chemistry, Faculty of Science, Chulalongkorn University.

3. Extraction and Isolation of Compounds from *Petrosia* n. sp.

3.1 Extraction

The frozen brittle sponge *Petrosia* n. sp. (10 kg wet wt) was crushed into small pieces and macerated with methanol (4 × 8 L). The combined extracts were evaporated under reduced pressure to yield 10 g of the methanol extract (**BS01**).

The methanol extract was dissolved in 10% methanol in water and then partitioned with ethyl acetate and n-butanol, respectively. Each extract was concentrated *in vacuo* to obtain 2 g of the ethyl acetate extract (**BS02**) and 8 g of the butanol extract (**BS03**) (Scheme 1).

Sponge *Petrosia* n. sp. (10 kg wet wt)

Macerated with methanol

Aqueous methanol extract (**BS01**)

Partitioned with EtOAc/H$_2$O

Aqueous layer   EtOAc extract (**BS02**) (2 g)

Partitioned with n-BuOH

n-BuOH extract (**BS03**)* (8 g)   Aqueous extract

* positive antimicrobial activity
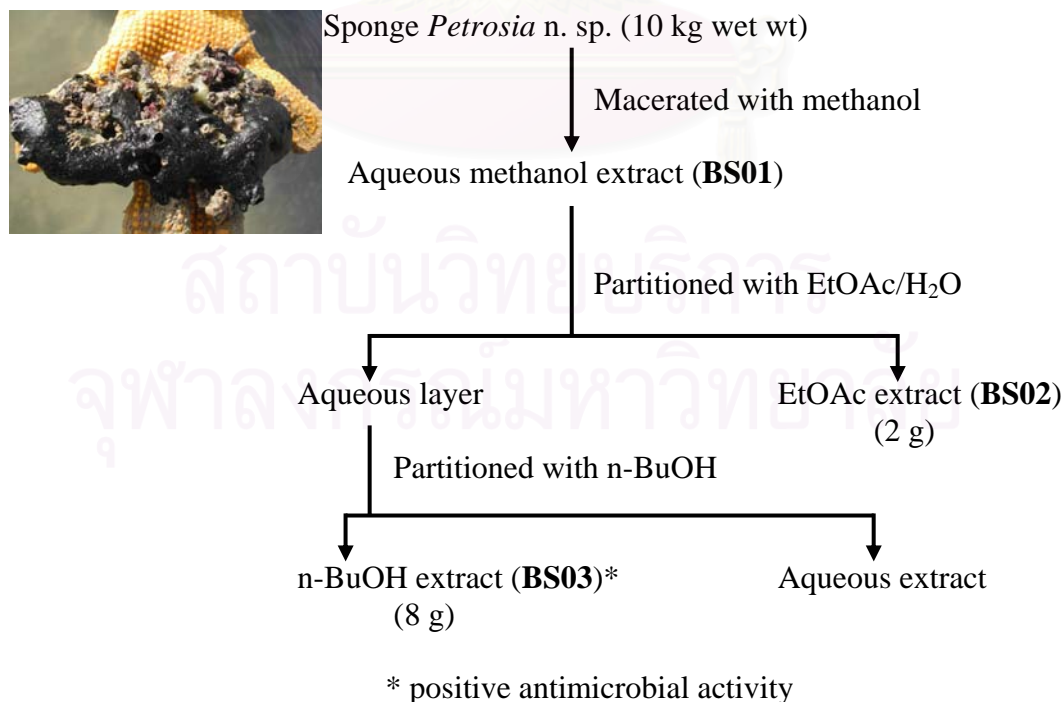
Scheme 1 Extraction of the Greenish Black Sponge *Petrosia* n. sp.

3.2 Isolation

The isolation of the extracts from *Petrosia* n. sp. was followed by bioassay-guided fractionation using antimicrobial activity and acetylcholinesterase (AChE) inhibitory activity. The antimicrobial activity was tested on *Bacillus subtilis, Staphylococcus aureus,* and *Escherichia coli* by the agar disc diffusion method (Lorian, 1980). The inhibitory effect on AChE was evaluated by using silica gel TLC combining with AChE microplate assay as described by Rhee *et al*. (Rhee *et al*., 2001). Only the n-butanol extract exhibited the antimicrobial activity against *B. subtilis* and the potent AChE inhibitory activity. Therefore, this extract was further purified by chromatographic techniques.

The n-butanol extract (**BS03**, 8 g) was equally divided into four portions. Each was fractionated by gel filtration chromatography using a Sephadex LH-20 column (500 g, 3.5 × 80 cm) with methanol as the eluent. Each 30 mL fraction was collected and fractions with similar TLC (silica gel, organic phase of CHCl$_3$:MeOH:0.5% aqueous acetic acid, 5:5:3) pattern and color were combined and evaporated to dryness, to give six fractions, **BS04**-**BS09** (Scheme 2, Table 1).

Table 1 Fractions Obtained from the Fractionation of **BS03**

Fraction	Band Color	No. of eluate	Total weight (g)
BS04	Pale brown	1-4	0.13
BS05	Yellow-brown	5-17	0.91
BS06	Green	18-28	0.64
BS07	Blue	29-40	4.90
BS08	Pale brown	41-49	0.43
BS09	Brown	50-60	0.59

After being examined by AChE TLC assay and antimicrobial activity, the active, dark blue fraction **BS07** (4.9 g) was further purified. Since this fraction consisted of both non-polar and very polar compounds, the suitable technique to isolate these compounds without irreversible adsorption on solid support is high speed countercurrent chromatography (HSCCC), which is liquid-liquid chromatography.

Fraction **BS07** was further purified by HSCCC using the conditions below.

Sample	:	Each 500 mg of fraction **BS07** was dissolved in equal volume (5 mL) of the aqueous and organic phase and filtered before injection.
Solvent system	:	Chloroform-methanol-water (5:10:6, v/v), isocratic
Stationary phase	:	Aqueous phase (upper phase)
Mobile phase	:	Organic phase (lower phase)
Mode	:	Normal phase; lower phase (organic phase), (H) $\rightarrow$ T Reversed phase; upper phase (aqueous phase), (T) $\rightarrow$ H
Rotational speed	:	800 r.p.m.
Flow rate	:	2 mL/min
Fraction (S_F)	:	0.74
Fraction volume	:	30 mL/fraction
Pressure	:	80-95 psi

Fractions were examined by TLC using the mobile phase of HSCCC as the developing solvent. After fraction combination according to their TLC behavior, nine fractions were collected (**BS10**-**BS17**).

Table 2 Fractions Obtained from the Fractionation of **BS07**

Fraction	Color	No. of eluate	Total weight (g)
BS10	Pink	1-4	0.12
BS11	Orange-red	5-13	0.10
BS12	Yellow-green	14-26	0.62
BS13	Green	28-47	0.38
BS14 (reversed)	Brown	48-65	1.02
BS15	Green-brown	66-72	0.54
BS16	Blue	73-88	1.18
BS17	Blue-green	89-100	0.92

Sequential chromatography of the less polar fraction BS11 with a silica gel column using CHCl$_3$:EtOAc (1:4) as an eluent gave four fractions (**BS18**-**BS21**). Fraction **BS20** was repeatedly separated on a silica gel column, eluted with the isocratic mixture of the lower phase of CHCl$_3$:MeOH:H$_2$O (5:10:6) and CHCl$_3$ in the

ratio 1:8 to afford 3 mg of compound **PK01** as a yellowish solid (R_f 0.40, Si gel TLC, in solvent system; CHCl$_3$:EtOAc, 1:4). This compound was later identified as a new pyridoacridine alkaloid, namely 2-bromoamphimedine.
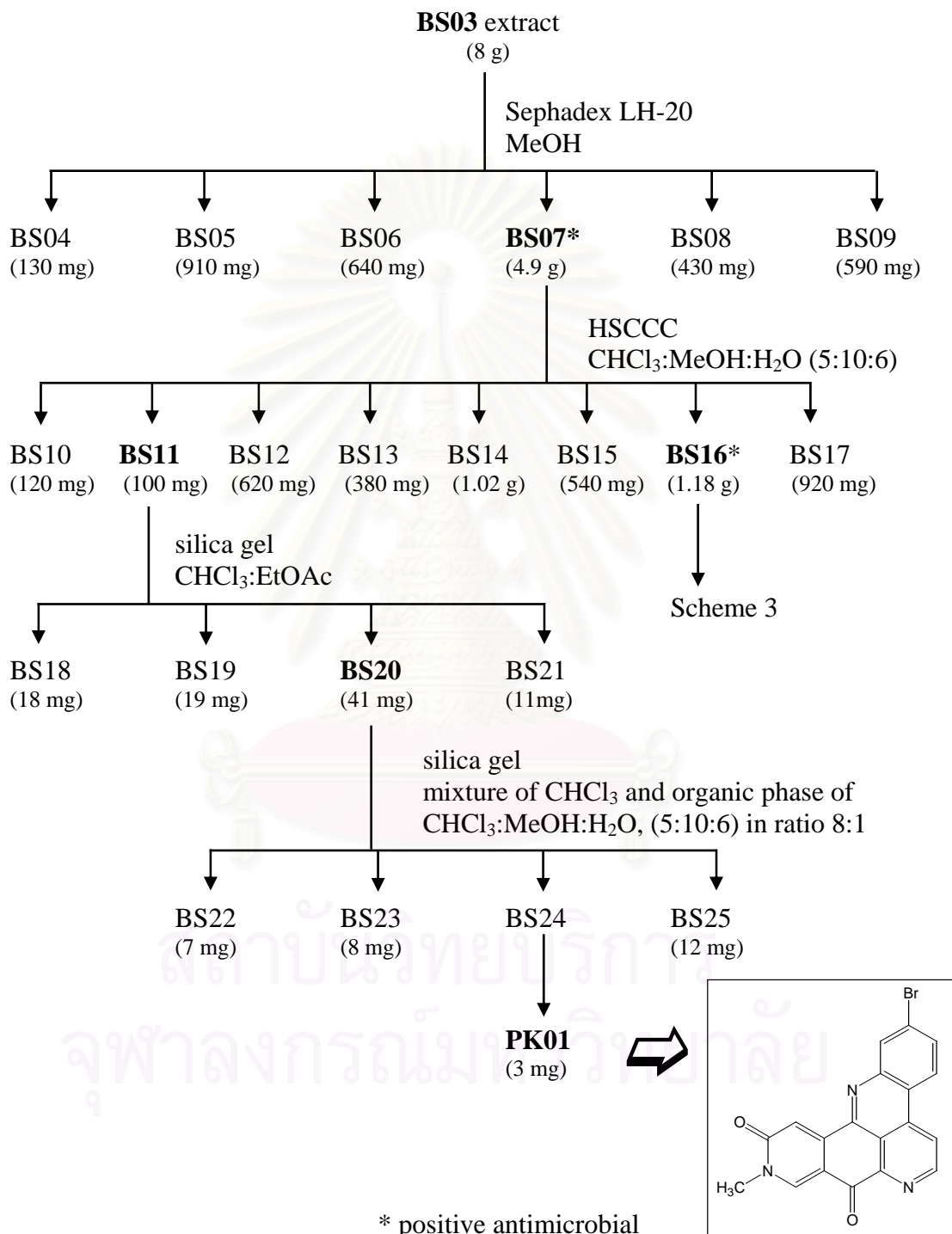
Scheme 2 Isolation of the n-Butanol Extract from the Sponge *Petrosia* n. sp.

The more polar blue fraction (**BS16**) was successively purified by Sephadex LH-20 columns (MeOH) to yield five fractions (**BS26**-**BS30**) (Scheme 3). Fraction **BS28** showing the potent antimicrobial and AChE inhibitory activity was subjected to another Sephadex LH-20 column (MeOH-EtOAc, 1:4) resulting in 120 mg of the active dark blue needle compound **PK02** (R_f 0.27, Si gel TLC, organic phase of $CHCl_3$:MeOH:H_2O in ratio 5:10:6) which was later identified as petrosamine. In addition, **PK02** was changed to an enolate form with dropping of NaOD and the structure was checked by NMR data.
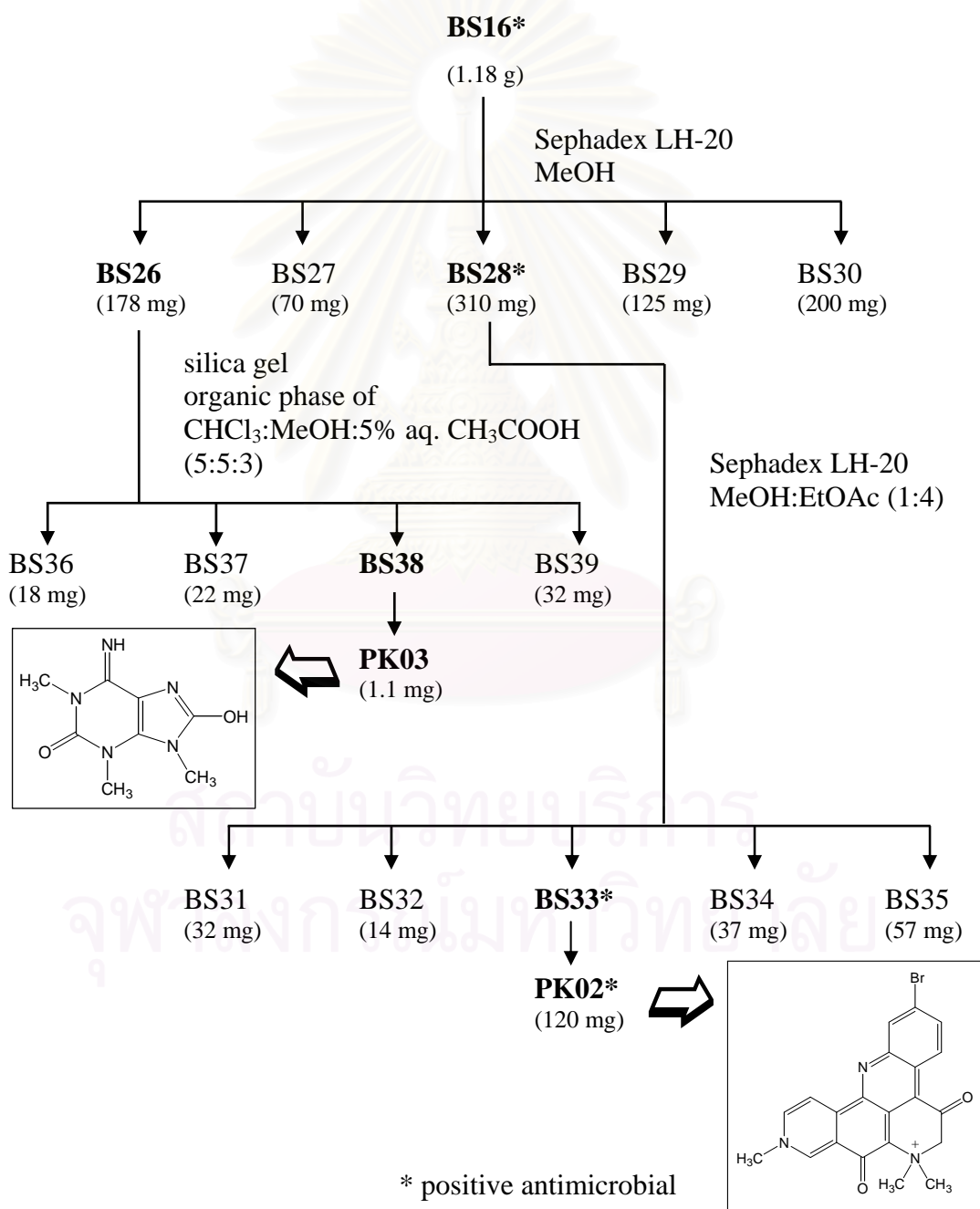
Scheme 3 Isolation of **BS16** from the Sponge *Petrosia* n. sp.

The remaining fraction **BS26** was further purified by flash column chromatography (silica gel, organic phase of CHCl$_3$:MeOH:5% aq. CH$_3$COOH, 5:5:3) which resulted in the isolation of a white powder compound **PK03** in 1.1 mg (R_f 0.30, Si gel TLC, in solvent system; organic phase of CHCl$_3$:MeOH:H$_2$O in ratio 5:10:6). However, **PK03** was obtained in small amount due to its high polarity and the difficulty to separate from other compounds. Therefore, the benzylation was performed with the fraction containing highest amount of **PK03**. Coupling fraction containing **PK03** with benzyl bromide and small amount of potassium carbonate at room temperature overnight yielded the product which was then cleaned up by a silica gel column using hexane:CHCl$_3$ (3:2) as an eluent to yield a yellow oil **PK04** (5 mg). The complete structure of **PK04** was established by NMR and MS techniques. The new compound **PK03** was identified as a new isoguanine derivative, and given the name 1,3,9-trimethyl-8-hydroxyisoguanine.

4. Physical and Chemical Properties of the Isolated Compounds

4.1 Compound PK01 (2-Bromoamphimedine)

Compound **PK01** was obtained as a yellowish amorphous solid, slightly soluble in common organic solvent, soluble clearly in mixed solvent such as CHCl$_3$ and trifluoroacetic acid.

HR ESI-TOF MS	: [M+H]$^+$ *m/z* 392.0035 (calcd for C$_{19}$H$_{11}$N$_3$O$_2$Br 392.0034); Figure 17
UV	: λ_{max} nm (ε), in methanol; Figure 18
	236 (23,225), 278 (8,680), 309 (8,797), 371 (4,653)
IR	: ν_{max} cm^{-1}, Film; Figure 19
	1680, 1640, 1593
^{1}H NMR	: δ ppm, 300 MHz, in CDCl$_3$; Table 3; Figure 20
	500 MHz in CDCl$_3$/TFA-*d*; Table 3; Figure 21
^{13}C NMR	: δ ppm, 125 MHz, in CDCl$_3$/TFA-*d*; Table 3; Figure 22

4.2 Compound PK02 (Petrosamine)

Compound **PK02** was obtained as dark blue needles, soluble in DMSO, MeOH, H$_2$O. The color of solution varies according to the solvent such as purple in aqueous solution, blue in methanol, and green in DMSO and tetrahydrofuran solution.

HR FABMS	**:** [M]$^+$ m/z 422.0505 (calcd for C$_{21}$H$_{17}$N$_3$ O$_2$Br 422.0504);
	Figure 26
UV	**:** λ_{max} nm (ε), in methanol; Figure 27
	286 (36,418), 346 (11,732), 369 (11,183), 414 (6,161)
IR	**:** ν_{max} cm^{-1}, Film; Figure 28
	3403 (br), 1644, 1583, 1531
^{1}H NMR	**:** δ ppm, 300 MHz, in DMSO-d_6; Table 4; Figure 29
^{13}C NMR	**:** δ ppm, 75 MHz, in DMSO-d_6; Table 4; Figure 30

4.3 Compound PK02+ NaOD

| **^{1}H NMR** | **:** δ ppm, 300 MHz, in DMSO-d_6; Figure 34 |
| **^{13}C NMR** | **:** δ ppm, 75 MHz, in DMSO-d_6; Figure 35 |

4.4 Compound PK03 (1,3,9-Trimethyl-8-hydroxyisoguanine)

Compound **PK03** was obtained as a white powder, soluble in DMSO, MeOH.

HR ESI-TOF MS	**:** [M+H]$^+$ m/z 210.0992 (calcd for C$_8$H$_{12}$ N$_5$O$_2$ 210.0991);
	Figure 37
EIMS	**:** m/z (% relative intensity); Figure 36
	209 (M$^+$, 100), 180 (39), 152 (9), 151 (23), 137 (17), 124 (5),
	83 (6), 42 (8)
UV	**:** λ_{max} nm (ε), in methanol; Figure 38
	210 (24,000), 268 (3,175), 324 (6,300)
IR	**:** ν_{max} cm^{-1}, Film; Figure 39
	3302, 1753, 1673, 1544
^{1}H NMR	**:** δ ppm, 300 MHz, in DMSO-d_6; Table 5, Figure 40
^{13}C NMR	**:** δ ppm, 75 MHz, in DMSO-d_6; Table 5, Figure 41

4.5 Compound PK04 (1,3,9-Trimethyl-8-*O*-benzylisoguanine)

Compound **PK04** was obtained as yellow oil, soluble in CHCl$_3$.

TOF MS	**:** [M+H]$^+$ m/z 300.07; Figure 43
EIMS	**:** m/z (% relative intensity); 299 (M$^+$, 100), 208 (77), 151 (29),
	91 (45), 71 (36), 57 (45), 43 (20); Figure 42

UV	**:** λ_{max} nm (ε), in methanol; Figure 44
	208 (21,700), 296 (6,910)
IR	**:** ν_{max} cm^{-1}, Film; Figure 45
	3346, 1760, 1673, 1535, 1455
^{1}H NMR	**:** δ ppm, 300 MHz, in CDCl$_3$; Table 5, Figure 46
^{13}C NMR	**:** δ ppm, 75 MHz, in CDCl$_3$; Table 5, Figure 47

5. Biological Activities

5.1 Determination of Antimicrobial Activity

Antimicrobial activity of the fractions and pure compounds were tested by using agar disc diffusion method (Lorian, 1980). Activity was tested against *Escherichia coli* ATCC 25922, *Staphylococcus aureus* ATCC 25923, *Bacillus subtilis* ATCC 6633 and *Candida albicans* ATCC 10231. All tested bacteria were cultivated on tryptic soy agar slant, TSA (Difco®), and the yeast *Candida albicans* ATCC 10231 was cultivated on Sabouraud dextrose agar slant, SDA (Difco®) at 37 °C for 24 hours. The cell cultures were washed from the agar surface and suspended in the steriled normal saline solution (NSS), and standardized to match a 0.5 turbidity standard of MacFarland No. 1, provided approximately 1×10^8 CFU (colony forming unit/mL). Each 20 mL of molten TSA and SDA was separated and poured into 9 cm diameter petri dish and allowed to solidify to form base layer. A loopful of each tested microorganisms was swabbed on the surface of TSA and SDA plates. All tested samples were dissolved in the suitable solvent and then applied on sterile paper disc for disc diffusion assay. These paper discs were left in steriled petri dish until the solvent was completely dried. The dried paper discs were placed on the surface of the swabbed plates and incubated at 37 °C for 24 hours. The diameters of inhibition zones were measured. Fractions which exhibited good antimicrobial activity were subsequently selected for further study.

5.2 Determination of Acetylcholinesterase Inhibitory Activity

In order to search for new AChE inhibitors from the extract of the sponge *Petrosia* n. sp., two techniques were used for the determination of the inhibitory activity: the TLC combining with bioassay for AChE inhibitors and the microplate assay using Ellman's colorimetric method.

Chemicals

Acetylthiocholine iodide (ATCI), *Tc*AChE, bovine serum albumin (BSA), 5,5´ dithiobis[2-nitrobenzoic acid] (DTNB), and the reference galanthamine were obtained from Sigma (St. Louis, MO). All organic solvents (analytical-reagent grade) were purchased from Merck (Darmstadt, Germany). 50 mM Tris-HCl pH 8.0 was used as a buffer throughout the experiment unless otherwise stated. *Tc*AChE used in the assay was from electric eel, *Torpedo californica* (type VI-S lyophilized powder, 480 U/mg solid, 530 U/mg protein). The lyophilized enzyme was prepared in the buffer to obtain 1,130 U/mL stock solution. The enzyme stock solution was kept at –80 ºC. The further enzyme-dilution was dissolved in 0.1% BSA in buffer. DTNB was dissolved in the buffer containing 0.1 M NaCl and 0.02 M $MgCl_2$. ATCI was dissolved in deionized water**.**

5.2.1 TLC Assay

The TLC combining with bioassay for AChE inhibitors was modified from the method of Rhee *et al.* (Rhee *et al.*, 2001). The sample extracts were dissolved and spotted on the silica gel TLC plate. After being developed in the appropiate solvent system, the TLC plate was dried at room temperature and then sprayed with 30 mM ATCI followed by 20 mM DTNB. The plate was dried at room temperature for 45 min and then sprayed with 10.17 U/mL *Tc*AChE. After 20 min, the plate was observed under visible light. The TLC plate appeared as a yellow background with white spots of AChE inhibitory compounds.

$$\text{Acetylthiocholine} + H_2O \xrightarrow{\text{AChE}} \text{acetate} + \text{thiocholine}$$

$$\text{Thiocholine} + \text{DTNB} \longrightarrow \text{5-thio-2-nitrobenzoate (yellow color)} +$$
$$\text{2-nitrobenzoate-5-mercaptothiocholine}$$
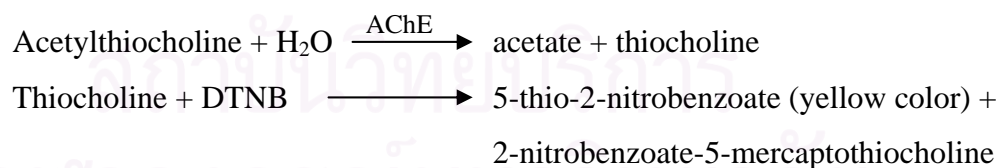
5.2.2 Microplate Assay

The assay for AChE inhibitory activity was performed according to the methods developed by Ellman *et al.* (Ellman *et al.*, 1961) and Ingkaninan *et al.* (Ingkaninan *et al.*, 2000). Briefly, 125 μL of 3 mM DTNB, 25 μL of 15 mM ATCI, 50 μL of Tris-buffer, and 25 μL of sample solution were added to the wells followed by 25 μL of 0.28 U/ml *Tc*AChE. The microplate was then read at 405 nm every

second for 2 min by a CERES UV 900C microplate reader (Bio-Tek instrument, USA). The velocities of the reactions were measured. Enzyme activity was calculated as a percentage of the velocities of the samples compared to that of the blank. Inhibitory activity was calculated from one hundred percentage subtracted by the percentage of enzyme activity. Each experiment was done in triplicate. The IC_{50} value, corresponding to the inhibitor concentration that caused 50% inhibitory activity, was determined with the software package Prism (Graph Pad Inc, San Diego, USA) using 8-10 different concentrations of the inhibitors.

5.3 Cytotoxic Acitvity

Cytotoxic activity against a breast cancer cell line (BC), a human epidermoid carcinoma cell line of the nasopharynx (KB), and a vero cell line (African monkey kidney cell line) was performed by sulforhodamine B (SRB) colorimetric method (Skehan *et al.*, 1990).

6. Molecular Docking Experiment

6.1 Receptor AChE Models

Since galanthamine was used as the reference in the AChE inhibitory assay, therefore, the X-ray structure of AChE-galanthamine complex was chosen in this docking study. Recently, the structure of *Tc*AChE-galanthamine complex (Greenblatt *et al.*, 1999) was elucidated by X-ray crystallography to 2.3 Å resolusion as deposited in the Brookhaven Protein Data Bank (PDB entry code 1DX6) (Figure 5). Thus, this present docking study was carried out on this enzyme structure. Initially, galanthamine was taken out of the *Tc*AChE complex structure and then docked back to its binding gorge of the enzyme to validate the procedure of docking. Both polar and non-polar hydrogen atoms were added by the program PDBFIL after deleting the crystalline water molecules present in the X-ray structure. The Kollman all-atom charges and atomic solvation parameters were then assigned.

6.2 Ligand Models

The coordinate of galanthamine was extracted directly from the X-ray structure of the *Tc*AChE complex (PDB 1DX6), while the atomic coordinate of **PK02** keto-form [**5a**] was taken from its crystal structure from NCI database, and the other two compounds, **PK02** enol-form [**5b**] and **PK01**, were modeled from [**5a**]. The

hydrogen atoms were added and then optimized with the PM3 semiempirical method on Gaussian98 (Frisch *et al.*, 1998). Atomic charges were assigned using the Gasteiger-Marsili formalism (Gasteiger and Marsili, 1980). The compounds were setup for docking with the help of AutoTor.

6.3 Ligand-Receptor Docking

Docking studies were performed using the AutoDock version 3.0 (Morris *et al.*, 1998) to deduce conformations and orientations of ligands in the *Tc*AChE-binding site. The grid maps representing the protein were calculated with AutoGrid. The grids (one for each atom type in the ligand, plus one for the electrostatic interactions) were chosen to be sufficiently large to include not only the binding gorge but also significant portions of the surrounding surface. The dimensions of the grid were 60 Å × 60 Å × 60 Å, with a spacing of 0.375 Å between the grid points and the center on the ligand, galanthamine. The docking search for the orientations of ligand binding to the gorge of *Tc*AChE was carried out using the new empirical free energy function and the Lamarckian genetic algorithm.

Figure 5 Structure of *Tc*AChE-Galanthamine Complex (Greenblatt *et al*, 1999)

CHAPTER IV

RESULTS AND DISCUSSION

The n-butanol extract from the Thai sponge *Petrosia* n. sp. collected from Phuket Island, Thailand was separated based on antimicrobial and AChE inhibitory activities-guided fractionation. Several chromatographic techniques were used to afford two pentacyclic pyridoacridine alkaloids, petrosamine [**PK02**] and 2-bromoamphimedine [**PK01**], and one isoguanine derivative, 1,3,9-trimethyl-8-hydroxyisoguanine [**PK03**]. Their structures were determined based on their UV, IR, MS, NMR data, and comparison with the literature values. The structure of compound [**PK03**] was comfirmed by comparison to that of its benzyl derivative [**PK04**].

These compounds were evaluated for their biological activities, including antimicrobial activity, cytotoxicity, and acetylcholinesterase inhibitory activity. The molecular docking study of two pyridoacridine alkaloids to assess their possible binding mode in the active site of *Tc*AChE has been employed.
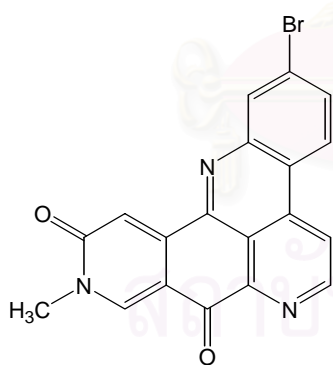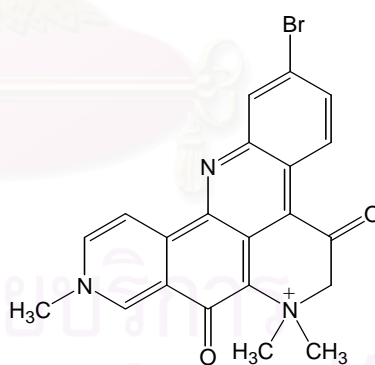
[**PK01**]   [**PK02**]
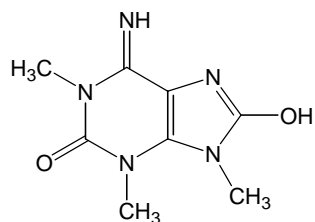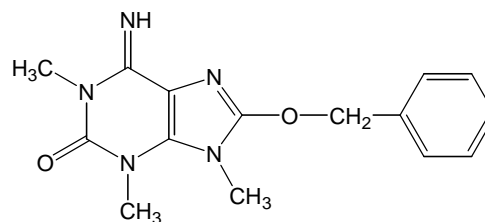
[**PK03**]   [**PK04**]

1. Structure Determination of the Isolated Compounds

1.1 Structure Determination of PK01 (2-Bromoamphimedine)

Compound **PK01** was obtained as a yellowish amorphous solid. The structure of **PK01** was elucidated by interpretation of NMR and MS data and comparison to the NMR data of amphimedine (Schmitz *et al*, 1983). The TOFMS (Figure 16) showed the intensity of the pseudomolecular ion $[M + H]^+$ and the isotopic peaks at *m/z* 392 and 394 with the ratio 1:1, indicating the presence of one bromine atom in the molecule. The molecular formula of $C_{19}H_{10}N_3O_2Br$ was deduced from the accurate mass obtained from ESITOFMS (Figure 17) showing the $[M + H]^+$ peak at *m/z* 392.0035 (calcd for $C_{19}H_{11}N_3O_2Br$ 392.0034). The UV spectrum (Figure 18) showed maximal absorptions at λ_{max} (MeOH) 236, 278, 309, and 371 nm characterizing a polyheteroaromatic system. In addition, the absorption band at 1680 cm^{-1} in the IR spectrum (Figure 19) and the carbon signal at δ 174.7 in the ^{13}C NMR spectrum (Figure 22) revealed the presence of an α,β-unsaturated ketone. Furthermore, the amide functionality was readily assigned by the IR absorption at 1640 cm^{-1} and the amide carbonyl carbon at δ 164.2 in the ^{13}C NMR spectrum.

The ^{1}H NMR spectrum (Figure 20) in CDCl$_3$ of **PK01** showed seven aromatic protons and one singlet of N-methyl protons. Due to the solubility limitation of **PK01** in common organic solvent, **PK01** was dissolved in CDCl$_3$/TFA-*d* in order to obtain the better S/N signals in the ^{13}C NMR spectrum (Figure 22). In addition to the above two carbonyl carbons, the ^{13}C NMR spectrum revealed one N-methyl carbon, seven aromatic methine carbons, and nine quaternary carbons. Interestingly, the proton signals of H-5 and H-6 appeared as the well-defined doublets with *J* = 5.5 Hz in CDCl$_3$ and these signals became broad singlets and moved downfield in CDCl$_3$/TFA-*d* (Figure 21). The ^{1}H and ^{13}C NMR data for **PK01** was summarized in Table 3.

Analyses of the ^{1}H NMR and H-H COSY (Figure 23) spectra in CDCl$_3$ indicated the presences of three spin systems. The first system consisted of three coupled protons [δ 8.74 (1H, d, 1.9 Hz, H-1), 8.21 (1H, d, 8.7 Hz, H-4), and 8.04 (1H, dd, 8.7, 1.9 Hz, H-3)] which were assigned to the 1,2,4-trisubstituted aromatic ring (ring A) due to the coupling constant values. The second spin system comprised two *ortho*-coupled protons in a pyridine ring (ring D) with characteristic chemical shifts and coupling constants at δ 9.30 (1H, d, 5.5 Hz, H-6) and 8.55 (1H, d, 5.5 Hz, H-5).

The last system consisted of three singlet protons of the N-methyl at δ 3.78 (3H, s, H_3-14) and two olefinic protons at δ 8.78 (1H, s, H-9), and 8.00 (1H, s, H-12) in ring E.

The adjacency of these partial structures was assured by the HMBC experiment in CDCl$_3$/TFA-d. Long-range H-C correlations observed in the HMBC spectrum (Figure 6) from H-4 to C-4a and C-4b supported the connection between ring A and ring B. Correlations from H-9 to C-12a and H-12 to C-12b ensured the connection between ring C and ring E. Moreover, correlations from N-methyl protons to C-9 and C-11 confirmed the presence of the amide functionality in ring E. The quaternary aromatic carbon (δ_C 126.2) and the carbonyl carbon (δ_C 174.7) were assigned to the remaining position C-7a and C-8, respectively. Interestingly, the non-splitting broad signals of H-5 and H-6 in CDCl$_3$/TFA-d showed no correlations in the HMBC spectrum (Figure 25), but the correlation between H-4 to C-5 confirmed the structure of **PK01**. The structure of **PK01**, thus, was established as a new pyridoacridine alkaloid, namely 2-bromoamphimedine.
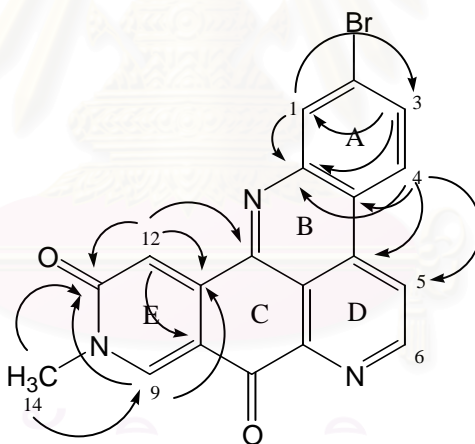
Figure 6 Important ^{1}H-^{13}C Long Range Correlations in the HMBC Data of **PK01** (2-Bromoamphimedine) in CDCl$_3$/TFA-d

Table 3 ^{1}H and ^{13}C NMR Spectral Data of **PK01** (2-Bromoamphimedine)

No.	PK01			
	δ_C(mult)^a	δ_H (mult, J, Hz)^b	δ_H (mult, J, Hz)^c	HMBC^a
1	126.9 (d)	8.74 (d, 1.9)	8.84 (d, 1.9)	C-3, C-13a
2	117.9 (s)			
3	138.1 (d)	8.04 (dd, 1.9, 8.7)	8.22 (dd, 1.9, 8.8)	C-1, C-13a
4	133.7 (d)	8.21 (d, 8.7)	8.35 (d, 8.8)	C-4a, C-4b, C-5, C-13a
4a	114.4 (s)			
4b	122.0 (s)			
5	122.7 (d)	8.55 (d, 5.5)	8.95 (br s)	
6	146.0 (d)	9.30 (d, 5.5)	9.43 (br s)	
7a	126.2 (s)			
8	174.7 (s)			
8a	113.4 (s)			
9	145.7 (d)	8.78 (s)	8.90 (s)	C-11, C-12a, C-14
11	164.2 (s)			
12	115.6 (d)	8.00 (s)	8.17 (s)	C-8a, C-9, C-11, C-12a, C-12b
12a	142.8 (s)^d			
12b	142.8 (s)^d			
12c	111.1 (s)			
13a	144.9 (s)			
14	39.7 (q)	3.78 (s)	3.80 (s)	C-9, C-11

^{a} ^{13}C NMR (125 MHz), CDCl$_3$/TFA-d; ^{b} ^{1}H NMR (300 MHz), CDCl$_3$;

^{c} ^{1}H NMR (500 MHz), CDCl$_3$/TFA-d, ^{d} overlapping signal

1.2 Structure Determination of PK02 (Petrosamine)

Compound **PK02** was obtained as dark blue needles. The HRFABMS spectrum (Figure 26) showed a pseudomolecular ion [M$^+$] and isotopic peak at *m/z* 422.0505 and 422.0503 with the ratio 1:1, corresponding to molecular formula of $C_{21}H_{17}N_3O_2Br$. The IR spectrum (Figure 28) exhibited absorption bands for carbonyl (1644 cm^{-1}) functionality.

The ^{1}H NMR signals in DMSO-d_6 (Table 4 and Figure 29) revealed the presence of three singlet methyl (δ 3.83, 4.60, and 4.75) and six aromatic protons (δ 7.92, 8.37, 9.16, 9.17, 9.29, and 9.88). The ^{13}C NMR spectrum (Figure 29) in DMSO-d_6 showed three singlet methyl carbons, seven methine carbons, one methylene carbon and ten quaternary carbons.

PK02 was identified as the known petrosamine by extensive analysis of spectral data, including 1D and 2D NMR, MS and IR, and comparison with the previous reported data (Molinski *et al.*, 1988). Surprisingly, the ^{1}H and ^{13}C NMR data of **PK02** in DMSO-d_6 showed some different signals from the reported data. **PK02** in DMSO-d_6 existed as a keto-form showing the methylene signal (C-6) at δ_H 4.75 (2H, s) and δ_C 69.8, while previous study reported as an enol-form showing an olefinic proton signal at δ_H 7.70 (1H, s). To prove the above data, **PK02** in DMSO-d_6 was changed to an enolate-form by adding NaOD and the ^{13}C NMR data was reacquired (Figure 35). The co-appearance of the olefinic carbon at δ_C 126.5 and the oxygenated olefinic carbon at δ_C 142.0 with the broad methylene carbon at δ_C 69.2 and the carbonyl carbon at δ_C 186.8 confirmed the co-occurrence of the enolate-keto forms of **PK02**. However, **PK02** also existed as the enol form in D$_2$O or CD$_3$OD.

PK02-keto form   **PK02-enol form**
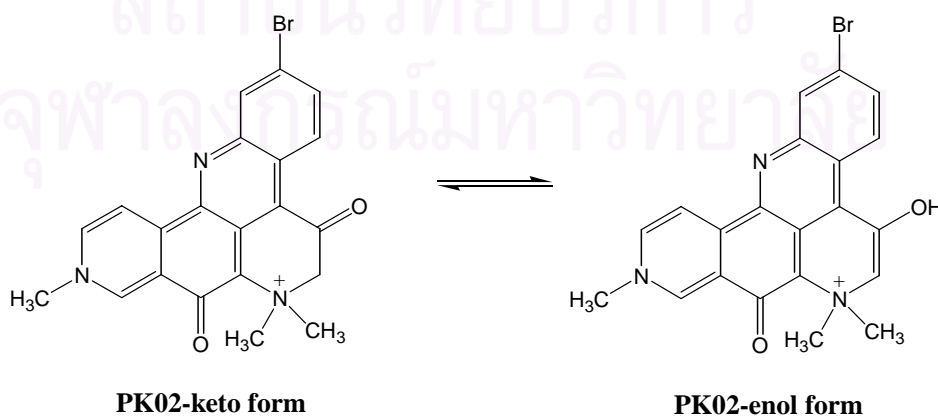
Interestingly, the color of **PK02** in diluted solution varies according to the polarity of solvent. Aqueous solution of **PK02** is purple, methanolic solution is blue, and solution in DMSO or tetrahydrofuran is green.

In the previous publication (Molinski *et al*., 1988), the NMR assignments of the **PK02** have not been reported, therefore, in this present work, the complete NMR assignment data of **PK02** is reported for the first time. The assignment was confirmed by correlations in the HMQC (Figure 32) and HMBC spectra (Figures 7, 33).

Key amino acids (shown in Figure 13) are given in bold letter.
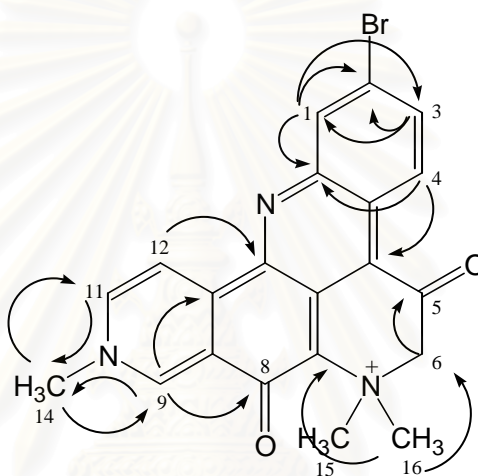
Figure 7 Selected ^{1}H-^{13}C Long Range Correlations in the HMBC Data of **PK02** (Petrosamine)

Table 4. [1]H (300 MHz) and ^{13}C (75 MHz) NMR Spectral Data for **PK02**

(Petrosamine)

No.	PK02 (in DMSO-d_6)		
	δ_C (mult)	δ_H (mult, J, Hz)	HMBC (H-C)
1	131.8 (d)	8.37 (d, 2.0)	C-2, C-3, C-4a
2	122.9 (s)		
3	135.1 (d)	7.92 (dd, 2.0, 9.2)	C-1, C-2
4	126.3 (d)	9.16 (d, 9.2)	C4b, C-13a
4a	120.0 (s)		
4b	128.8 (s)		
5	187.2 (s)		
6	69.8 (t)	4.75 (s)	C-5, C-7a,C-15, C-16
7a	114.2 (s)		
8	161.3 (s)		
8a	139.9 (s)		
9	145.6 (d)	9.88 (s)	C-11, C-12a, C-12b, C-14
11	142.5 (d)	9.17 (d, 5.6)	C-9, C-12, C-12b
12	121.7 (d)	9.29 (d, 5.6)	C-8a, C-11,C-12a
12a	131.5 (s)		
12b	141.4 (s)		
12c	114.3 (s)		
13a	142.1 (s)		
14	48.3 (s)	4.60 (s)	C-9, C-11
15, 16	53.1 (s)	3.83 (s)	C-6, C-7a

1.3 Structure Determination of PK03 (1,3,9-Trimethyl-8-hydroxyisoguanine)

Compound **PK03** was obtained as a white powder. The molecular formula of $C_8H_{11}N_5O_2$ was deduced by an accurate mass from the ESI TOF-MS (Figure 36) showing the $[M+H]^+$ peak at *m/z* 210.0992 (cald for 210.0991), indicating the presence of six unsaturations in the molecule. The IR spectrum (Figure 38) showed characteristic band of urea carbonyl at 1673 cm^{-1}.

The ^{1}H NMR spectrum of **PK03** (Figure 40) revealed that it contained three *N*-methyl singlets at δ 3.41, 3.54, and 3.71. The ^{13}C NMR spectrum of **PK03** (Figure 41) showed signals for five quaternary carbons (δ 93.5, 140.3, 145.4, 148.7, and 151.3) as well as three methyl carbons (δ 30.1, 31.9, and 32.5). These typical carbon chemical shifts suggested that **PK03** would have a purine skeleton. The ^{1}H and ^{13}C NMR data of **PK03** were summarized in Table 5.

The EIMS of **PK03** (Figure 37) displayed an abundant ion of *m/z* 151, corresponding to $[M-CH_3NCO-H]^+$ fragment peak which was deduced via a retro-Diel-Alder reaction involving the N_1 and C_2 atoms (Figure 8) (Rice and Dudek, 1967). This above data proved that purine heterocycle was an *N*-methyl substituted isoguanine. Elucidation of the 2D NMR data would give complete the structure of **PK03.** Nevertheless, **PK03** was obtained in small amount (1.1 mg) due to its high polarity and the difficulty of its separation. Benzylation of the fraction containing the highest amount of **PK03** was, thus, designed in order to get its benzyl derivative of which its NMR data could be comparable to that of **PK03.** The benzyl derivative of **PK03** (**PK04**) was much easier isolated and given in larger amount (5.4 mg) than the original compound.

After overnight reaction, the benzyl derivative **PK04** was isolated as a yellow oil and its ESI TOF-MS spectrum (Figure 42) displayed $[M+H]^+$ at *m/z* 300.07, corresponding to the molecular formula of $C_{15}H_{17}N_5O_2$, accounting for ten.

The ^{1}H (Figure 46) and ^{13}C (Figure 47) NMR spectra of **PK04** were similar to that of **PK03** except for the presence of the benzyl group signals at δ$_H$ 5.41/ δ$_C$ 46.0 and δ$_H$ 7.28-7.39/ δ$_C$ 127.3-128.8. The fragment peaks at *m/z* 208 and 151 in the EIMS spectrum of **PK04** (Figure 43) generated from the benzylic cleavage and the retro-Diel-Alder fragmentation, respectively. The location of three *N*-methyl groups was assigned by the HMBC experiments (Table 5, Figure 9), with correlations observed from 1-NCH$_3$ (δ 3.48) to C-2 (δ 149.6) and C-6 (δ 147.3), from 3-NCH$_3$ (δ

3.41) to C-2 (δ 149.6) and C-4 (δ 136.4), and from 9-NCH$_3$ (δ 3.67) to C-4 (δ 136.4) and C-8 (δ 152.4). The chemical shift of the methylene signal (δ$_H$ 5.41/ δ$_C$ 46.0) of benzyl group and ^{1}H-^{13}C long range correlation between methylene protons (δ$_H$ 5.41) to C-8 (δ 152.4) confirmed the presence of *O*-substitution at C-8.

Through analyses of the above spectra data, compound **PK04** was identified as 1,3,9-trimethyl-8-*O*-benzylisoguanine. Therefore, **PK03** can be unambiguously assigned as a new natural isoguanine compound 1,3,9-trimethyl-8-hydroxyisoguanine. To date, several groups have reported the isolation of methylated guanine base analogs from sponges and tunicates, including 1,3-dimethylguanine (Lindsay, Battershill, and Copp, 1999), 1,7,9-trimethylguanine (Yogi, Matsunaga, and Fusetani, 1994), 1,3,7-trimehylguanine (Perry, Blunt, and Munro, 1987), doridosine:1-methylisoguanine (Kim *et al*., 1981), 1,3-dimethylisoguanine (Chehade *et al*., 1997; Mitchell *et al.,* 1997), 3,7-dimethylisoguanine (Cafieri *et al*., 1995), and 1,3,7-trimethylisoguanine (Copp *et al*., 2000). Unfortunately, no significant physiological role for these methylated guanine analogs from sponges and tunicates are apparent.
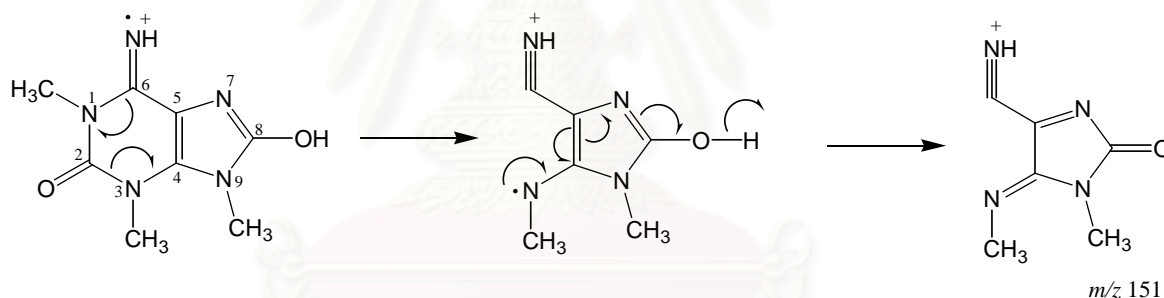
Figure 8 Mass Fragmentation of **PK03** (1,3,9-Trimethyl-8-hydroxyisoguanine)
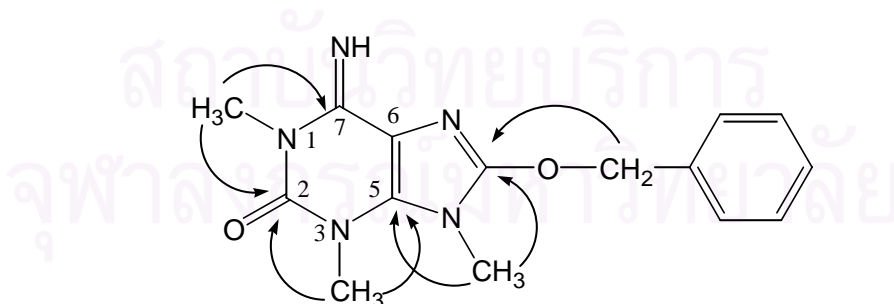
Figure 9 Important ^{1}H-^{13}C Long Range Correlations in the HMBC Data of **PK04**
(1,3,9-Trimethyl-8-*O*-benzylisoguanine) in CDCl$_3$

Table 5 [1]H (300 MHz) and ^{13}C (75 MHz) NMR Spectral Data of **PK03**

(1,3,9-Trimethyl-8-hydroxyisoguanine) and **PK04** (1,3,9-Trimethyl-8-*O*-

benzylisoguanine)

Position	**PK03** (in DMSO-d_6)		**PK04** (in CDCl$_3$)		
	δ_H (mult., J in Hz)	δ_C (mult.)	δ_H (mult., J in Hz)	δ_C (mult.)	HMBC H-C correlation
N$_1$-Me	3.41 (s, 3H))	30.1 (q)	3.48 (s)	30.5 (q)	C-2, C-6
2		148.7 (s)		149.6 (s)	
N$_3$-Me	3.71 (s, 3H)	32.5 (q)	3.71 (s)	32.3 (q)	C-2, C-4
4		140.3 (s)		136.4 (s)	
5		93.5 (s)		97.2 (s)	
6		145.4 (s)		147.3 (s)	
7					
8		151.3 (s)		152.4 (s)	
N$_9$-Me	3.54 (s, 3H)	31.9 (q)	3.67 (s)	30.9 (q)	C-4, C-8
Bn			5.41 (s, 2H) 7.28-7.40 (m, 5 H)	46.0 (t) 128.8 (d), 127.9(d), 127.3(d)	C-8

2. Biological Activities

2.1 Antimicrobial Activity

All isolated compounds were evaluated for antimicrobial activity. Only **PK02** showed significant activity against *B. subtilis* with an inhibition zone diameter of 22 mm at 200 μg/disc.

2.2 Cytotoxicity

Compounds **PK01**, **PK02** and **PK04** had no detectable activity toward tumor cell lines (tested at 100 μM concentration against NCI-H187 human, small cell lung carcinoma, KB human epidermal carcinoma, and BC breast carcinoma) as well as the Vero cell line (African monkey kidney cell line).

2.3 Acetylcholinesterase Inhibitory Activity

In the preliminary examination, the blue colored crude MeOH extract of the Thai marine sponge, *Petrosia* n. sp. showed strong inhibitory effect on AChE. The MeOH extract was further partitioned to give the EtOAc, n-BuOH, and aqueous extracts. All extracts were evaluated for their bioactivity using Si gel TLC combining with AChE inhibitory bioassay as described by Rhee *et al*. Only the n-BuOH extract exhibited the activity by showing a clear active zone as the blue spot (R_f 0.25; solvent system: organic phase of $CHCl_3$:MeOH:H_2O, 5:10:6). The n-BuOH, therefore, was further purified by several chromatographic techniques to obtain **PK01**, **PK02** and **PK03**.

To investigate the potential inhibitory effects on AChE of **PK01**, **PK02**, and **PK03**, the *Tc*AChE inhibitory activity of each compound was measured using a microplate reader based on the modified Ellman method (Ingkaninun *et al*, 2000). **PK02** showed the IC_{50} value of 0.091 μM while the reference galanthamine showed the IC_{50} value of 0.590 μM (Figure 10 and Table 5). The result showed that **PK02** displayed potent AChE inhibitory activity about six times the potency of the reference galanthamine, whereas **PK01** and **PK03** showed very weak potency with IC_{50} higher than 300 μM. This encouraging result led us to study molecular docking of the pyridoacridine alkaloids **PK01** and **PK02** in order to assess their probable binding mode in the active site of *Tc*AChE.
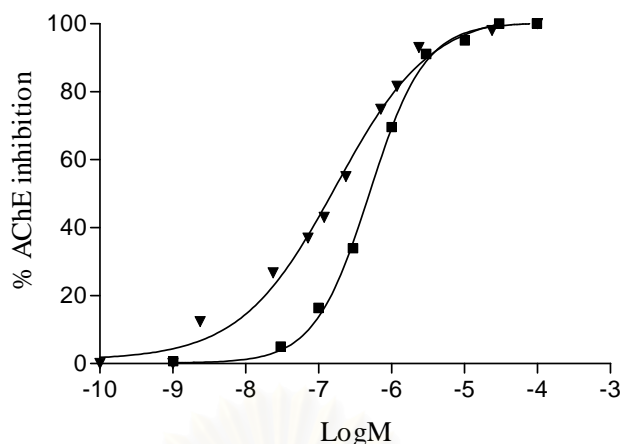
Figure 10 Inhibition Effects of **PK02** (Petrosamine) (▼) and Galanthamine (■) on
 TcAChE.

(Percentage inhibitions were assayed by the procedure described in the text.   The
points are averages of one typical experiment done in triplicate.)

3. Molecular Docking Study of PK01 and PK02 for AChE Binding.

Compound **PK02** possessed strong AChE inhibitory activity, making this
molecule attractive for further study with molecular docking experiment.
Interestingly, **PK01**, of which its structure is related to **PK02**, displayed very weak
activity.   To investigate the binding mode of both compounds to TcAChE, the
molecular docking was carried out using the AutoDock version 3.0.

To verify the method used, molecular docking of the reference compound,
galanthamine, was examined.   The result showed that the docked conformation of
galanthamine (Figure 11) reproduced its originally bound conformation in TcAChE
gorge with the root-mean-square deviation (rmsd) of 0.782 Å.   This indicated the
reliability of the docking procedure which was used to predict the binding mode of the
new TcAChE inhibitors, **PK01** and **PK02**.
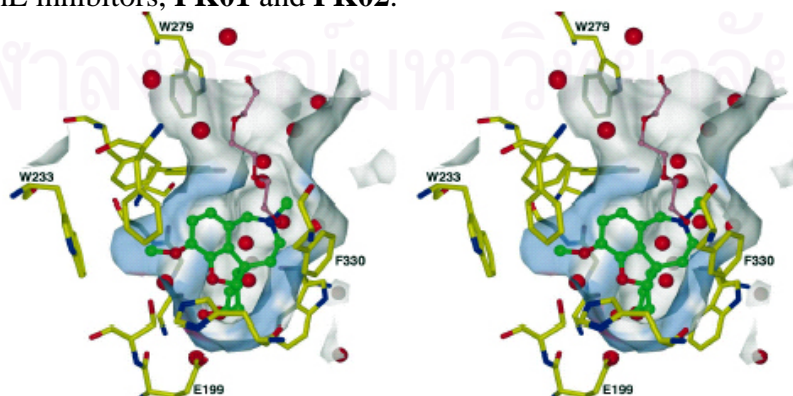
Figure 11 Binding Mode of Galanthamine in the Active site Gorge of TcAChE

The X-ray structure of **PK02** in keto-form (Figure 12) was obtained from the NCI database and then modified to generate the structure of the new alkaloid **PK01**. Refer to the above experimental result which observed two possible tautomers of petrosamine, keto-form (**PK02a**) and enol-form (**PK02b**). Therefore, both of them were, then, taken into consideration. The docking resulted for galanthamine, **PK01**, **PK02a** (Figure 13) and **PK02b** in the vicinity of *Tc*AChE, were compared in term of molecular orientation and estimated free energy of binding as given in Figure 14 and Table 6, respectively. In addition, the amino acid residues located around the active site of *Tc*AChE within the radius of 6 Å from the inhibitor were analyzed and summarized in Table 7.
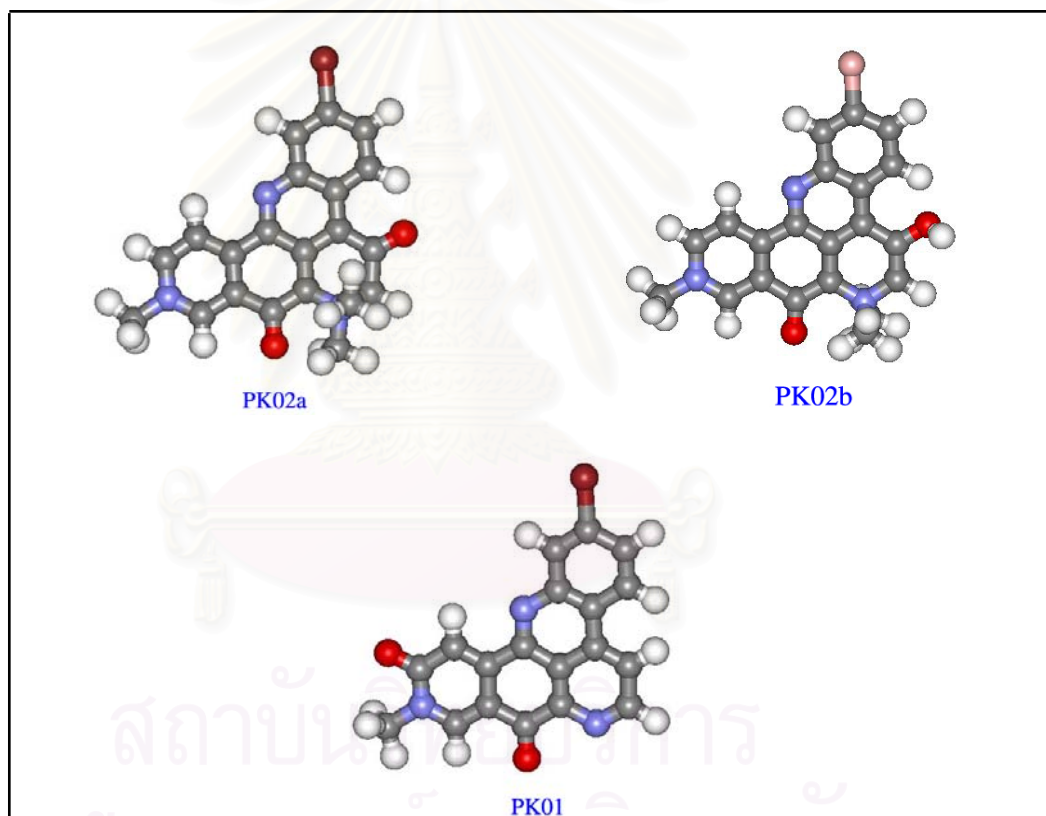
Figure 12 Three-Dimensional Structures of **PK02a**, **PK02b**, and **PK01**

As shown in Table 6, the obtained free energy of binding (–21.62 kcal/mol) of **PK02a** and **PK02b** (–20.32 kcal/mol) are significantly lower than that of galanthamine (–17.13 kcal/mol), indicating higher potency of the newly discovered compound in comparison to that of galanthamine. An order of the obtained free

energy of binding for all compounds is in good agreement with their IC_{50} for inhibitory activity against *Tc*AChE in which **PK02a** ≈ **PK02b** < galanthamine << **PK01**.
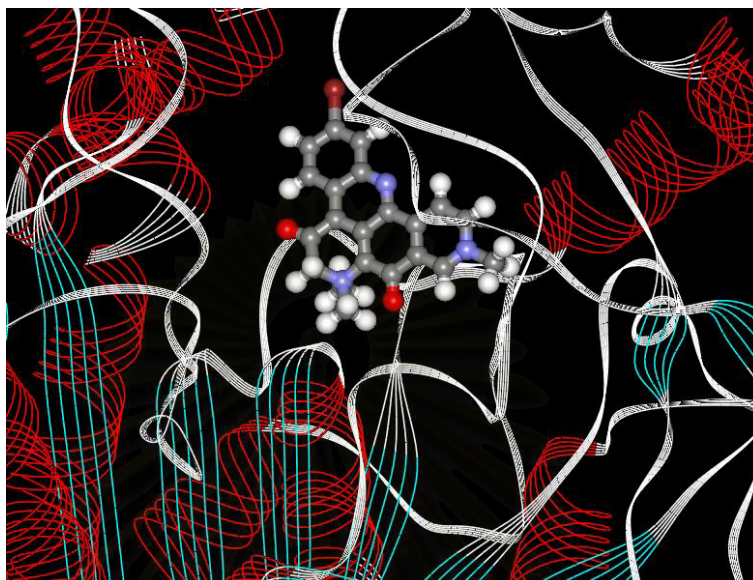
Figure 13 PK02 (Petrosamine) in the 'Aromatic Gorge' Active Site of *Tc*AChE

Table 6. Estimated Free Energy of Binding and IC_{50} Values of the AChE Inhibitors.

Compound	Estimated free energy of binding (kcal/mol)	IC_{50}* (μM)
galanthamine	-17.13	0.590 ± 0.099
PK02a	-21.62	0.091 ± 0.034
PK02b	-20.32	
PK01	-11.84	> 300

* The IC_{50} values are expressed as mean ± standard deviations (n = 3) from individual determinations performed in triplicate.

Insight into the binding of these compounds to *Tc*AChE is given in Table 7. It was shown that almost 26 amino acid residues were observed as locating within 6 Å far from the investigated inhibitors. Note that among the catalytic triad, including Ser200, His440, and Glu327 (Pilger *et al.*, 2001; Zaheer-ul-haq *et al*., 2003), only the

first two residues were detected within this distance. Interest is centered on Glu327 which lies farther than 6 Å away from all four inhibitors. This catalytic residue binds indirectly to the inhibitors via the strong hydrogen bond network among the catalytic triad where the hydrogen bond distances are 2.62 Å from Glu327 to His440 and 2.68 Å from His440 to Ser200 (Figures 14A-14D). Another remarkable interaction is the direct interactions between the inhibitors and the two catalytic residues, Ser200 and His440. These are observed only for inhibitors galanthamine, **PK02a** and **PK02b** with distances between heavy atoms in the range of 3.5 – 4.0 Å (Table 7 and Figures 14A-14C). Lack of these important interactions for **PK01** (Table 7 and Figure14D) could be one of the reasons for the lower *Tc*AChE inhibitory activity of **PK01** in comparison to other compounds. Additionally, the strong interactions to the charge residue of Glu199 were also observed only for galanthamine, **PK02a** and **PK02b**. The formation of a strong hydrogen bond between galanthamine and Glu199 with the distance of 2.62 Å agrees well with the data derived from X-ray crystallography of 2.70 Å (Greenblatt *et al*., 1999).

Table 7. Amino Acid Residues of *Tc*AChE within 6 Å from the Inhibitors (marked as ×).

Compound	Gln69	Tyr70	Val71	Asp72	**Trp84**	Asn85	Pro86	Tyr116	Gly117	Gly118	Gly119	Tyr121	Ser122	Gly123	Ser124	Leu127	Tyr130	**Glu199**	**Ser200**	Ala201	Trp233	**Phe330**	Phe331	Tyr334	**His440**	Gly441
Ref*				×	×				×	×	×	×						×	×	×	×	×		×	×	×
PK02a	×			×	×	×	×	×	×	×			×	×	×			×	×	×		×	×	×	×	×
PK02b				×	×	×			×	×	×		×	×	×	×	×	×	×					×	×	×
PK01	×	×	×	×	×	×	×	×	×	×	×		×	×	×	×	×					×	×	×		

*Galanthamine

(Key amino acids (shown in Figure 13) are given in bold letter)

Relative to galanthamine and **PK01**, the docking data shown both **PK02a** and **PK02b** bind more tightly and locate more closely to the catalytic triad of the binding gorge. Major interaction arises from the quaternary ammonium on ring D of **PK02**. Strong electrostatic interaction between N^+ and Glu199 is indicated by the distances between N^+ to O1 and O2 of 4.53 Å and 3.23 Å for **PK02a** and 4.06 Å and 4.02 Å for

PK02b, respectively. Note that these distances for **PK01** are longer than 10.00 Å. In addition, non-conventional hydrogen bond, via its N$^+$-methyl group, to O1 and O2 of Glu199 were also observed at the docked configuration with distances of 2.98 Å and 4.34 Å for **PK02a** and 3.16 Å and 3.03 Å for **PK02b**, respectively. Moreover, this quaternary ammonium interacts directly with Trp84 known as the choline-binding site, arises the cation-π interaction. The closest distance for this interaction of 3.77 Å for **PK02a** is significantly larger than that of 4.63 Å of **PK02b**.
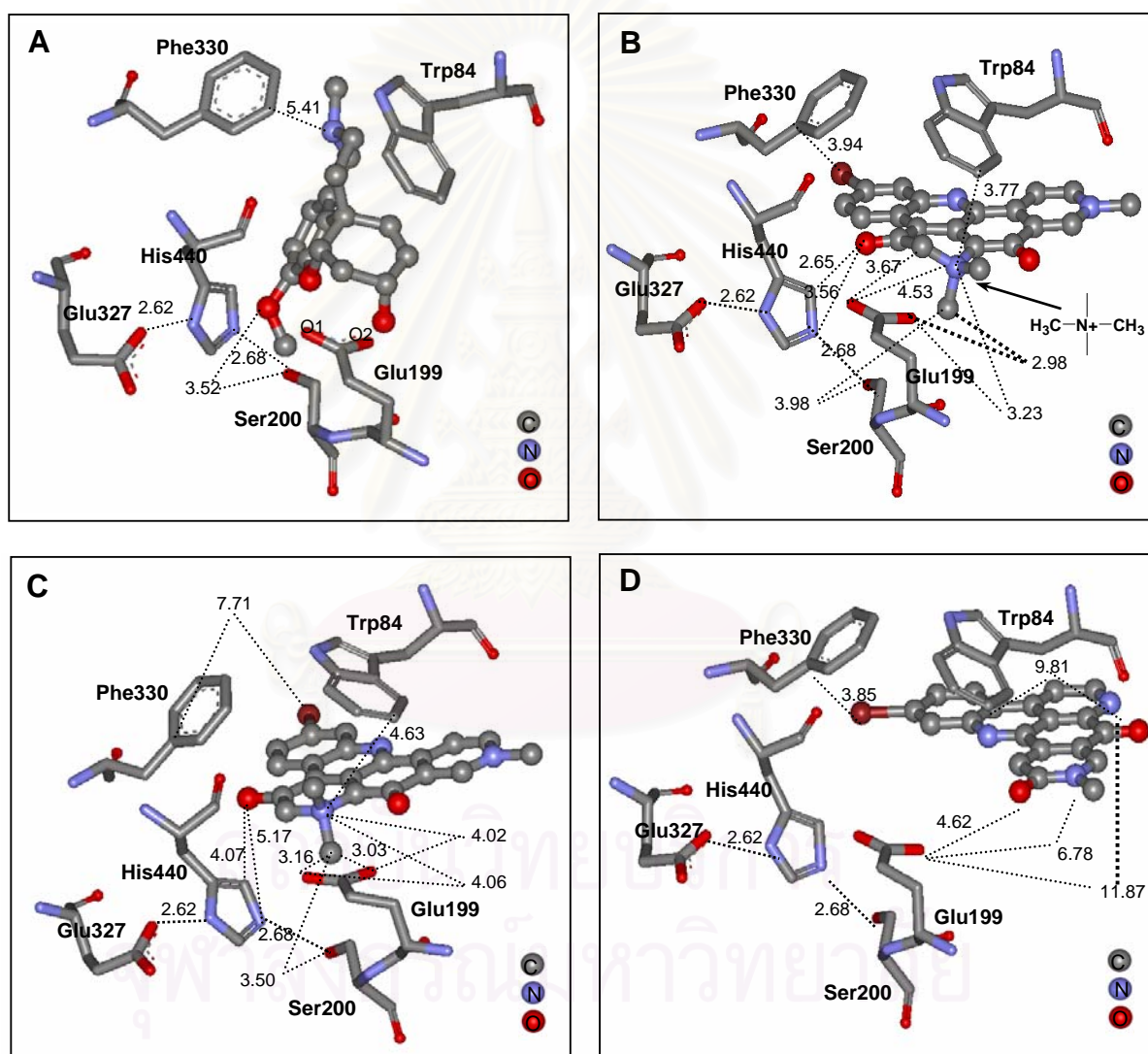
Figure 14 Predicted Docking Conformations of Galanthamine (**A**), **PK02a** (**B**), **PK02b** (**C**) and **PK01** (**D**) in the Catalytic Triad Binding Gorge of *Tc*AChE.

Although Trp84 was detected within 6 Å around galanthamine and **PK01** (Table 7), the measurement centered on all atoms of the inhibitors to all atoms of *Tc*AChE- but the closest cation- π distances for galanthamine and **PK01** are larger

than 4.46 Å and 6.54 Å, respectively. It clearly indicates that the quaternary dimethyl ammonium on ring D of **PK02** mainly and strongly interacts with the key amino acid residues located at the binding site (Glu199 and Ser200). These observations could explain why binding free energy of **PK02a** in the vicinity of *Tc*AChE is slightly lower than that of **PK02b** (Table 6).

Owing to our docking conformation, the obtained Phe330-inhibitor distances, defined in Figures 14A-14D, are 5.41 Å, 3.94 Å, 7.71 Å and 3.80 Å for galanthamine, **PK02a**, **PK02b** and **PK01**, respectively. No correlation has been found between these distances which might relate directly to their interactions, and the IC$_{50}$ of AChE inhibitory activity shown in Table 6. This data clearly indicates that Phe330 may not play any roles in the catalytic ability of the AChE.

In Figure 15, the electrostatic potential surfaces for the above mentioned residues, lying at the catalytic region, were calculated for **PK02a** and **PK01**. Both plots show mainly the negative (red) regions that are implied to fit well to the positive charge substrate such as acetyl-choline or the positive charge inhibitors, such as **PK02**. It is clearly demonstrated by the electrostatic potential surfaces that **PK02** is more preferable than **PK01** in term of electrostatic interaction. Moreover, the tighter binding of **PK02** to *Tc*AChE in comparison to **PK01** appears to arise from a number of different degrees of interactions with the enzyme.
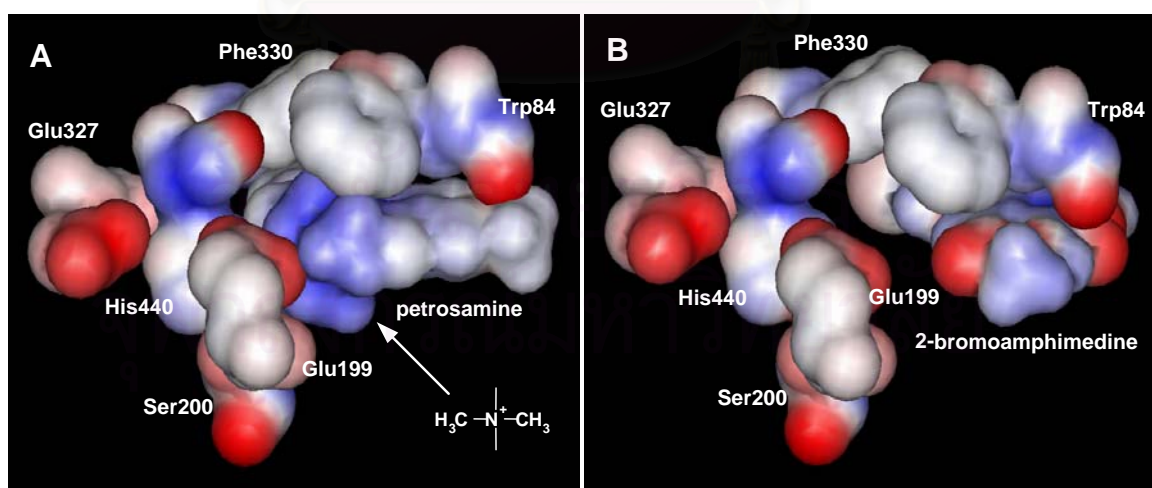
Figure 15 Electrostatic Potential Surfaces of the Amino Acid Residues Located at the
Catalytic Binding Gorge of *Tc*AChE with **PK02a** (**A**) and **PK01** (**B**)
(negative regions are in red and positive regions are in blue)

CHAPTER V

CONCLUSION

As part of our continuing investigation on bioactive substances from Thai marine sponges, the sponge code named PK00-01 was collected from Phuket Island and later identified as a new species of the genus *Petrosia*. The antimicrobial activity and acetylcholinesterase inhibitory activity screening of the n-butanol extract of this sponge showed significant activity. The bioassay-guided fractionation along with several chromatographic techniques, including high speed countercurrent, flash column, and gel filtration chromatography, led to isolation of two pentacyclic pyridoacridine alkaloids; a known petrosamine and a new 2-bromoamphimedine, together with a new isoguanine derivative, 1,3,9-trimethyl-8-hydroxyisoguanine in 1.5, 0.04, and 0.01 % w/w based on the n-butanol extract, respectively. Only petrosamine exhibited antimicrobial activity against *Bacillus subtilis* with 22.0 mm diameter of the zone of inhibition at the concentration of 200 μg/disc and showed potent AChE inhibitory activity. This biological result identified petrosamine as a prototype of the new class of potent AChE inhibitors, presenting an IC_{50} (0.091 μM) about six times lower than galanthamine (IC_{50} of 0.590 μM).

The attempt toward understanding of the pyridoacridines; petrosamine and 2-bromoamphimedine, at the active site of AChE enzyme from *Torpedo californica* was performed by preliminary molecular docking study in comparison to galanthamine. According to the molecular docking study, the order of free energy of binding was in good agreement with that of the experimental IC_{50} of the activity. The docked conformations demonstrated the binding mode of these compounds to their binding gorge of *Tc*AChE. One major observation found from computational docking was that the quaternary ammonium of petrosamine donated the mainlyr and strongly interacted with the key amino acid residues, Glu199 and Trp84.
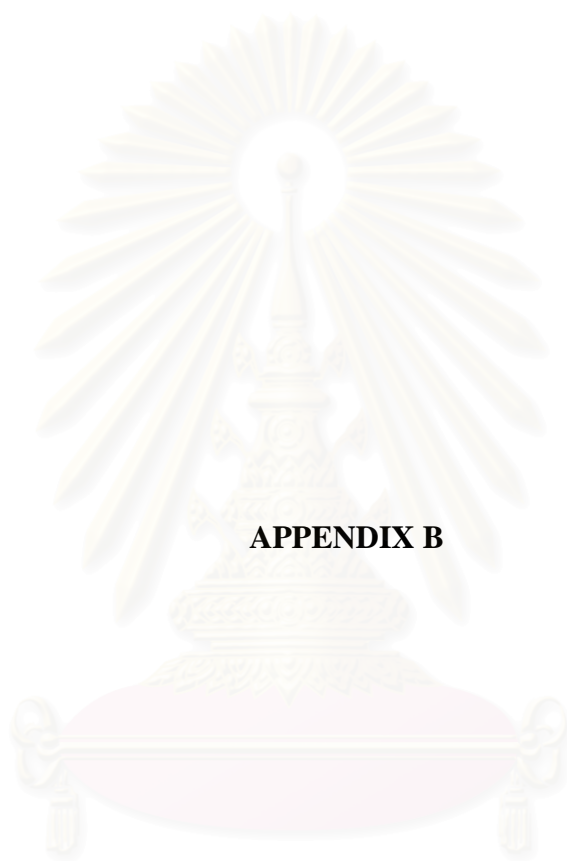
APPENDIX B
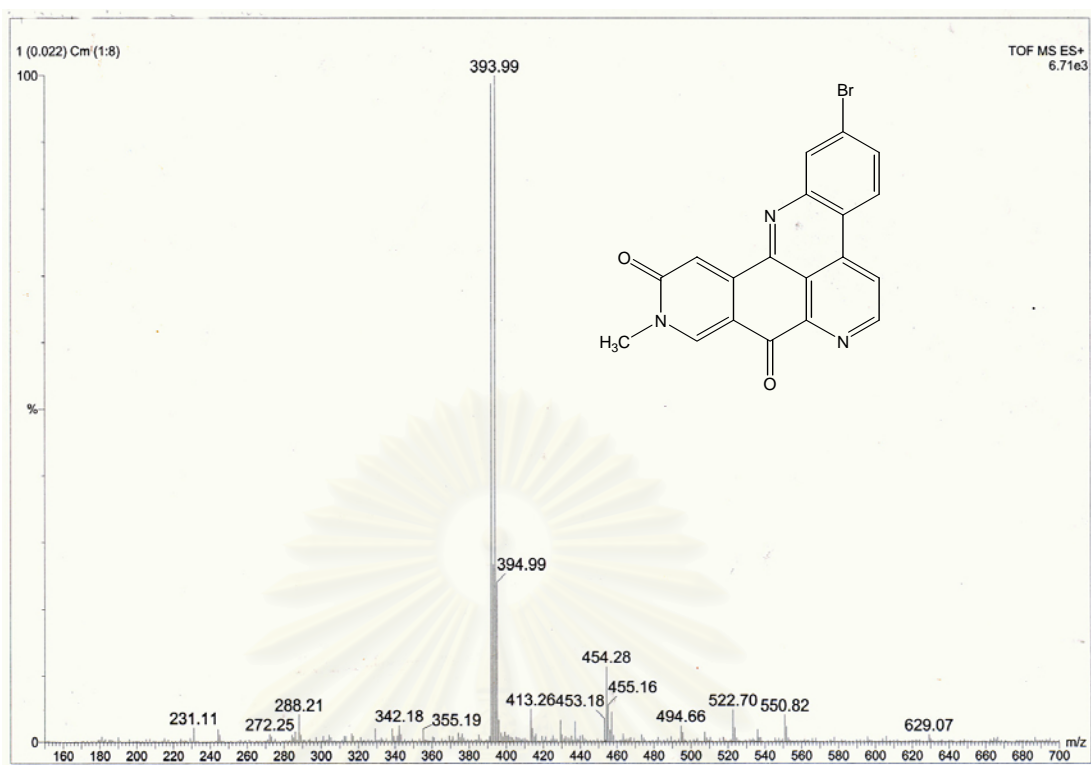
Figure 16 TOF MS Spectrum of **PK01** (2-Bromoamphimedine)
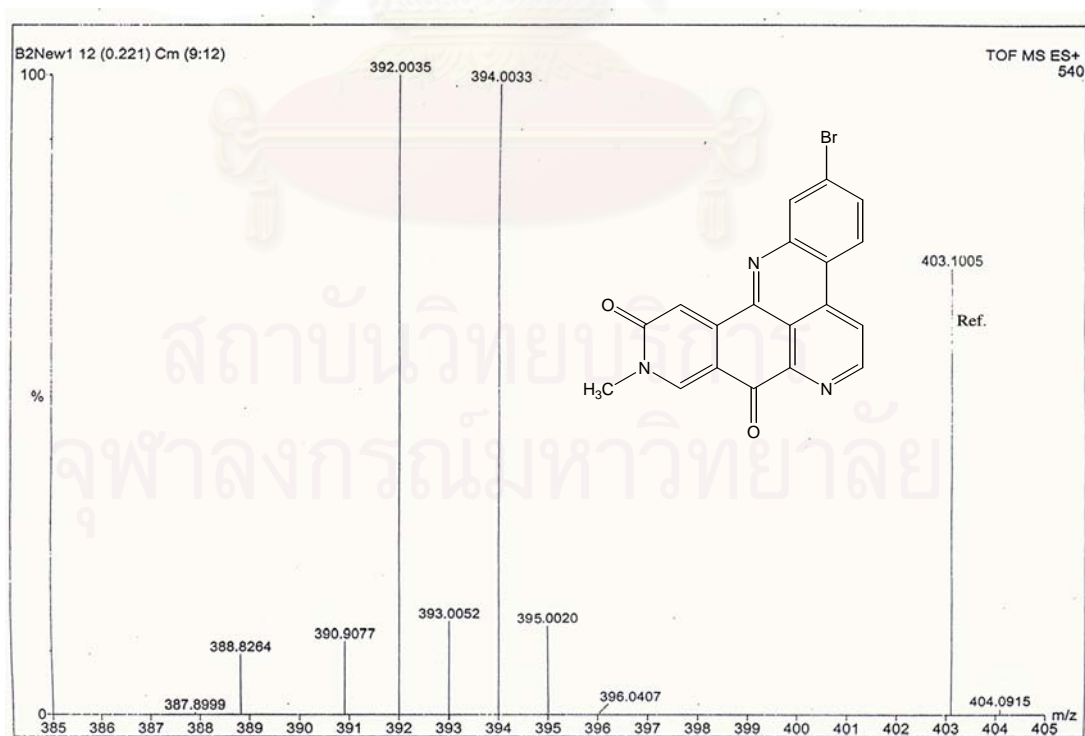
Figure 17 HR TOFMS Spectrum of **PK01** (2-Bromoamphimedine)
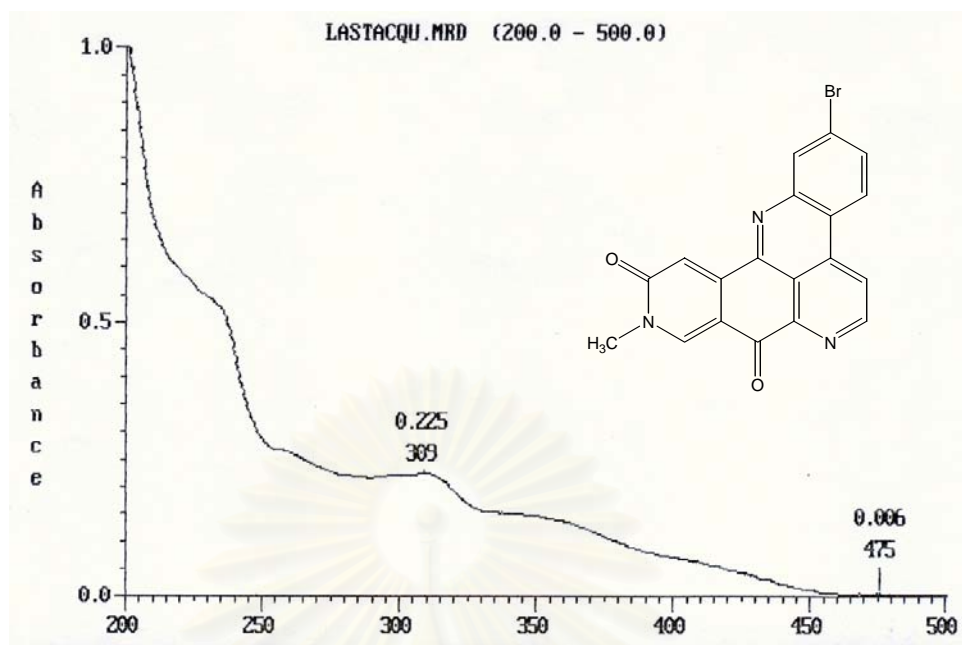
Figure 18 UV Spectrum of **PK01** (2-Bromoamphimedine) in MeOH
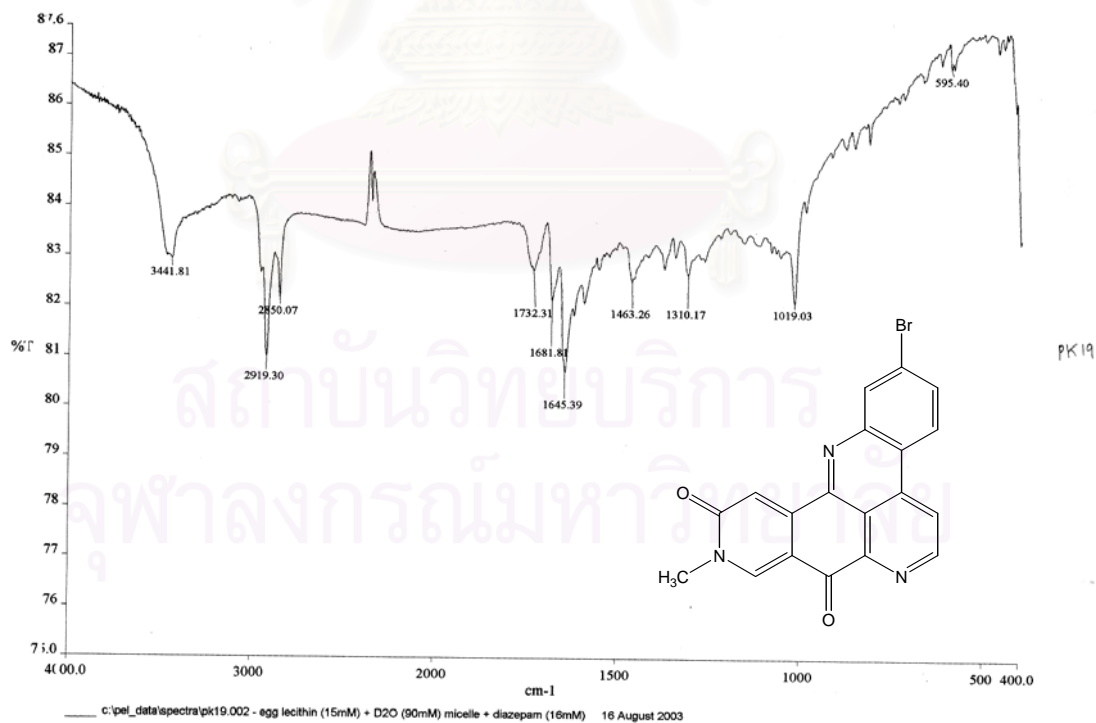
Figure 19 IR Spectrum (Film) of **PK01** (2-Bromoamphimedine)
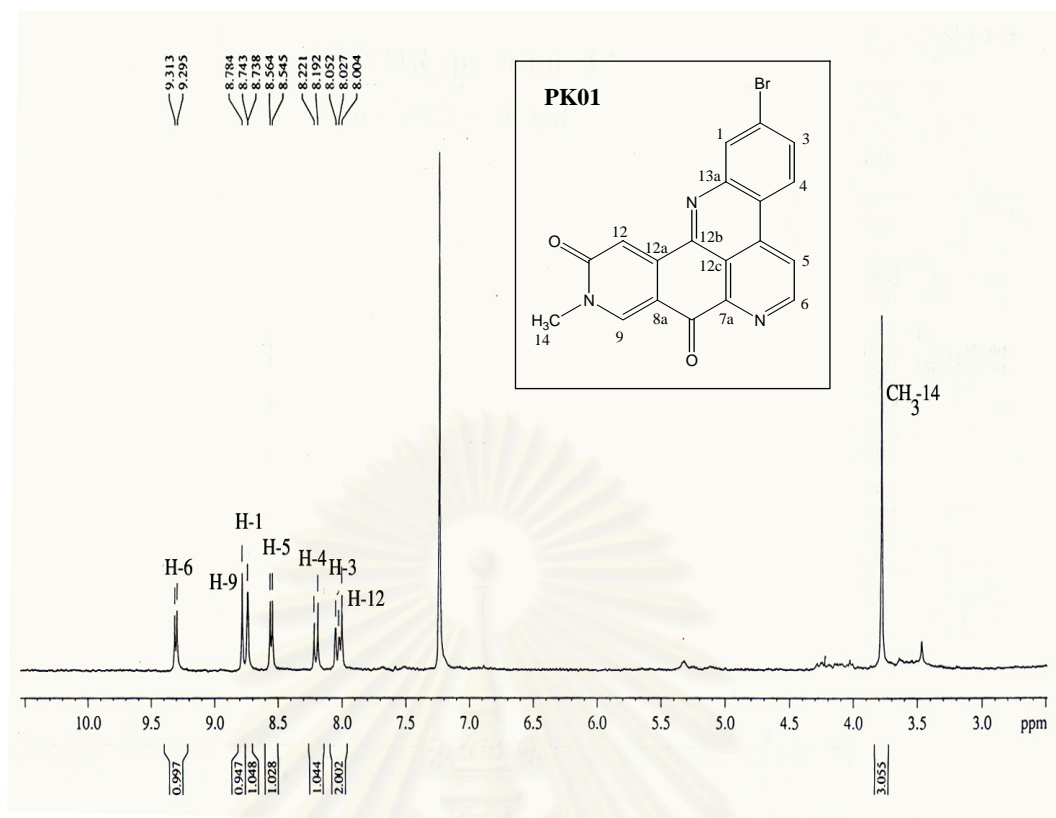
Figure 20 ^{1}H NMR (300 MHz) Spectrum of **PK01** (2-Bromoamphimedine)
in CDCl$_3$
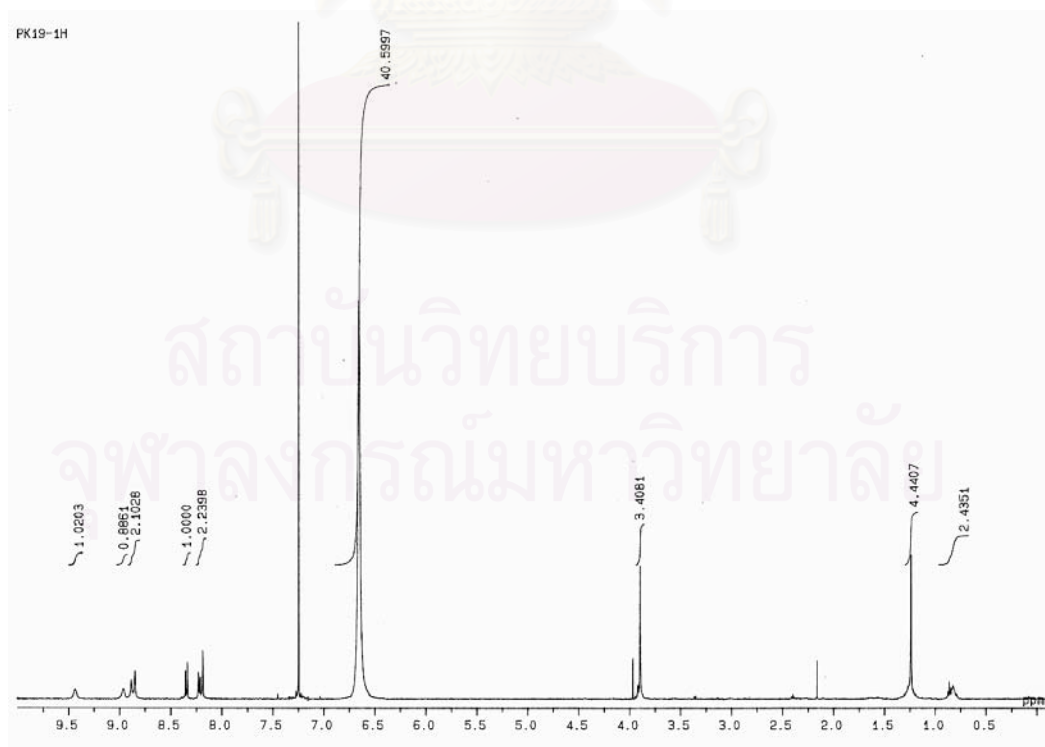
Figure 21 ^{1}H NMR (500 MHz) Spectrum of **PK01** (2-Bromoamphimedine)
in CDCl$_3$/TFA-d

Figure 22 ^{13}C NMR (125 MHz) Spectrum of **PK01** (2-Bromoamphimedine)
in CDCl$_3$/TFA-*d*

Figure 23 H,H-COSY Spectrum of **PK01** (2-Bromoamphimedine) in CDCl$_3$
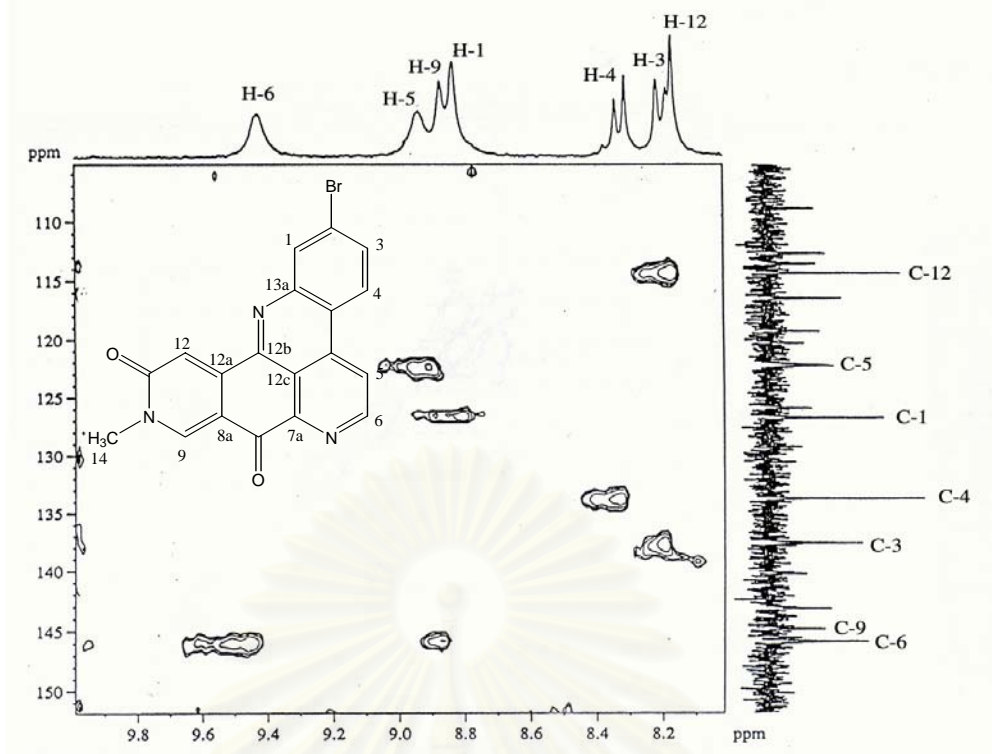
Figure 24 HMQC Spectrum of **PK01** (2-Bromoamphimedine) in CDCl$_3$/TFA-*d*
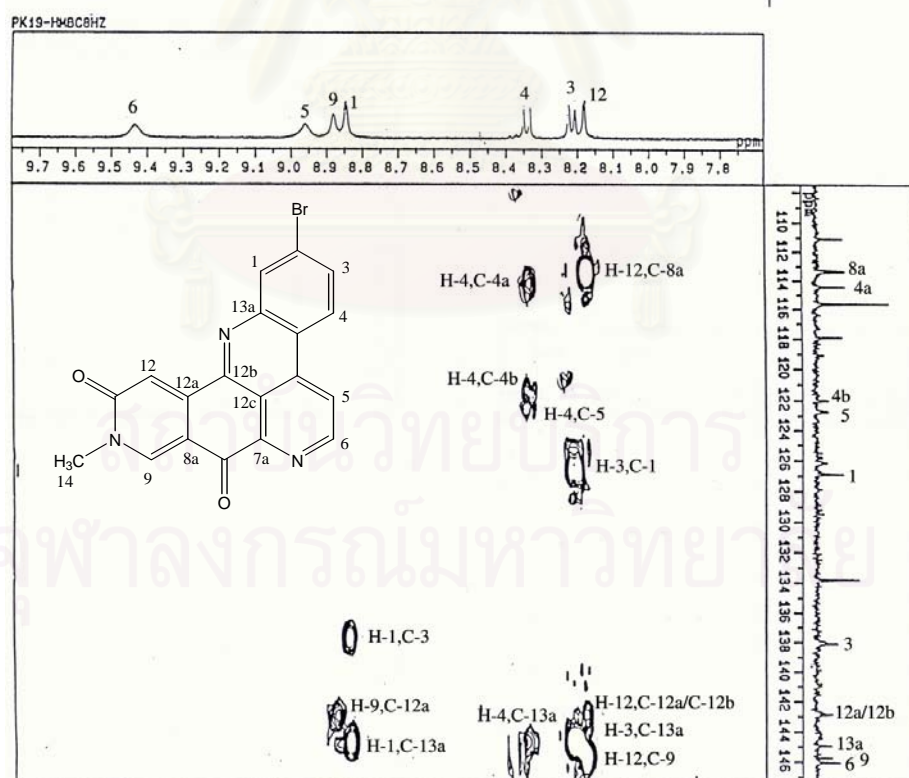
Figure 25 HMBC ($^nJ_{HC}$ = 8 Hz) Spectrum of **PK01** (2-Bromoamphimedine)
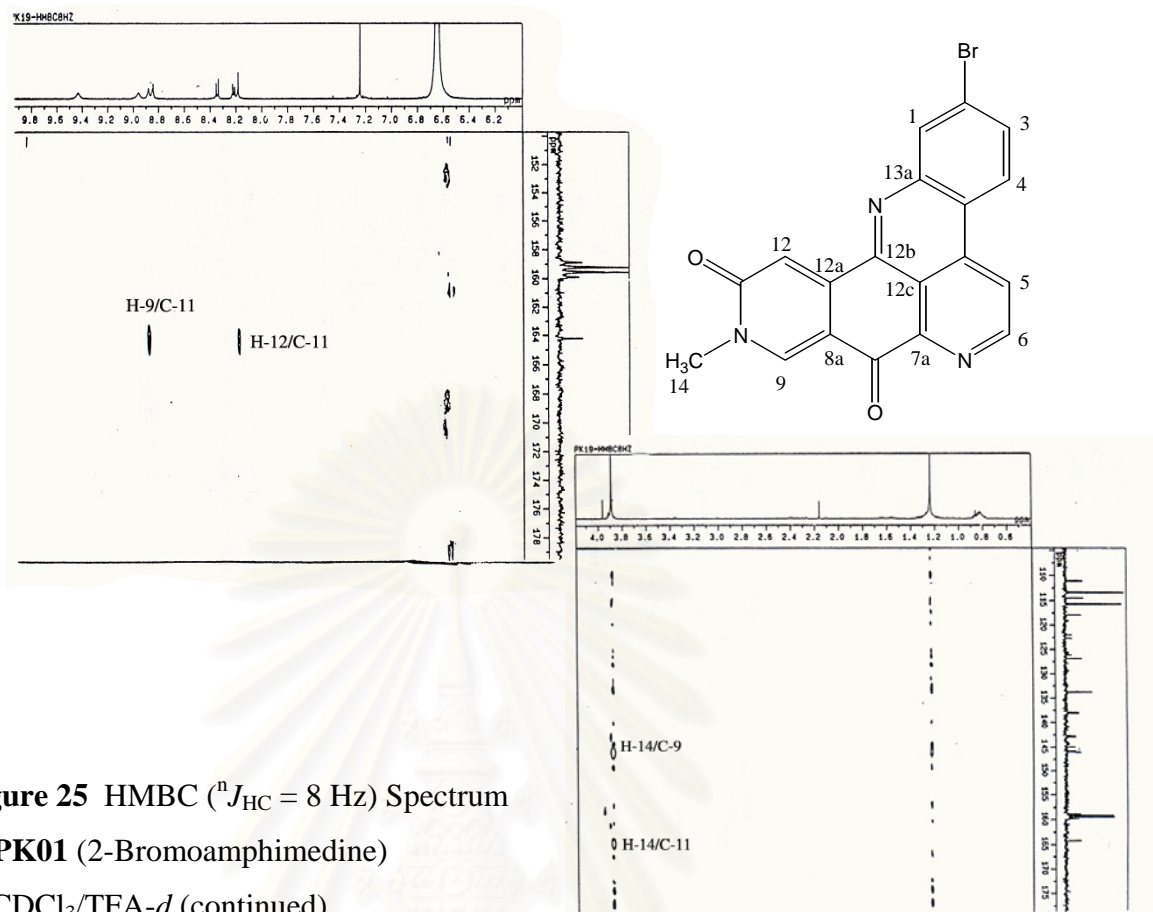
in CDCl$_3$/TFA-*d*

Figure 25 HMBC ($^{n}J_{HC}$ = 8 Hz) Spectrum of **PK01** (2-Bromoamphimedine) in CDCl$_3$/TFA-*d* (continued)
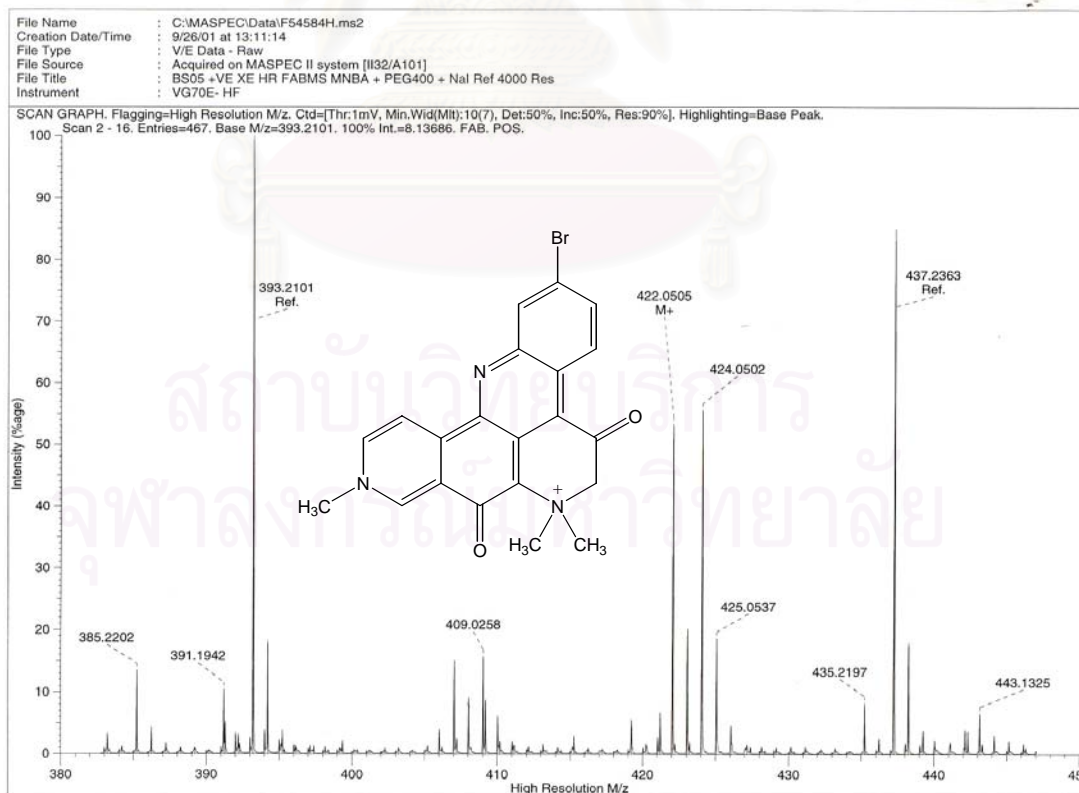
Figure 26 HR FABMS Spectrum of **PK02** (Petrosamine)
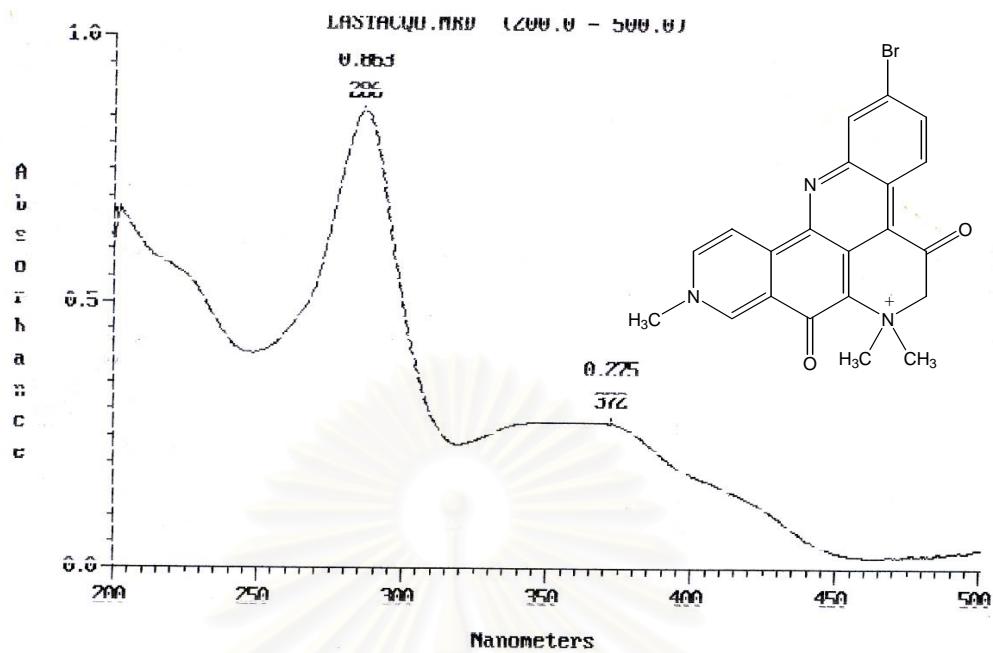
Figure 27 UV Spectrum of **PK02** (Petrosamine) in MeOH
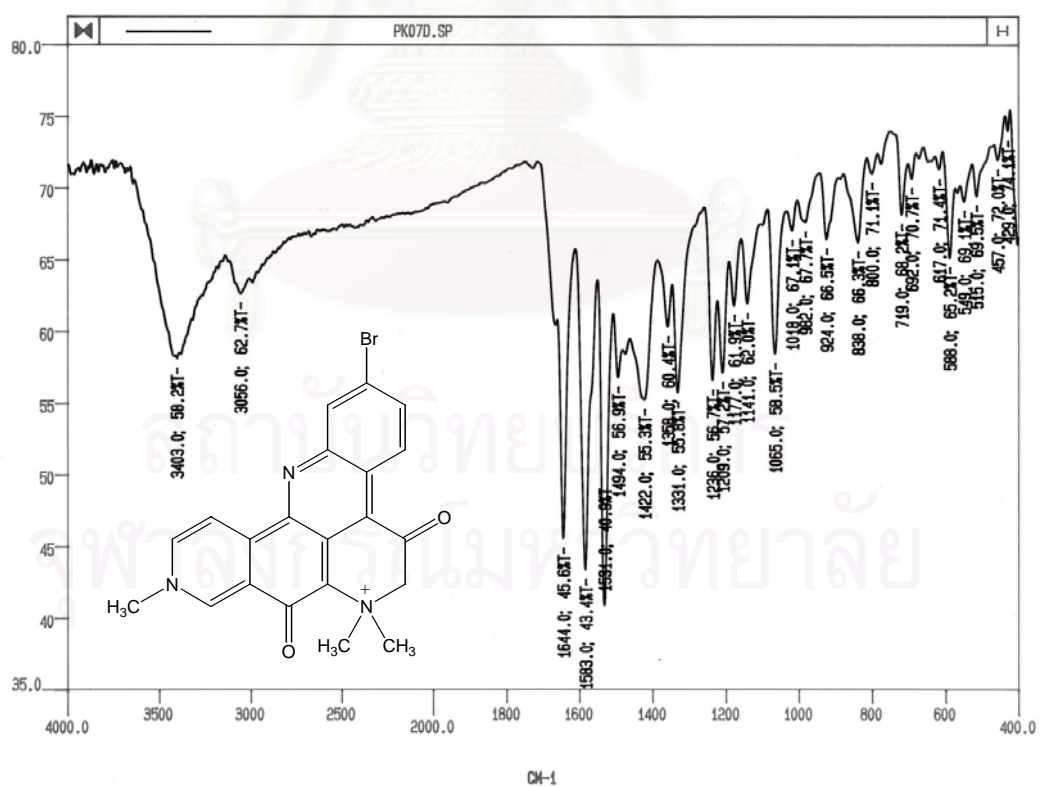
Figure 28 IR Spectrum (Film) of **PK02** (Petrosamine)

Figure 29 ^{1}H NMR (300 MHz) Spectrum of **PK02** (Petrosamine) in DMSO-d_6

Figure 30 ^{13}C NMR (75 MHz) Spectrum of **PK02** (Petrosamine) in DMSO-d_6
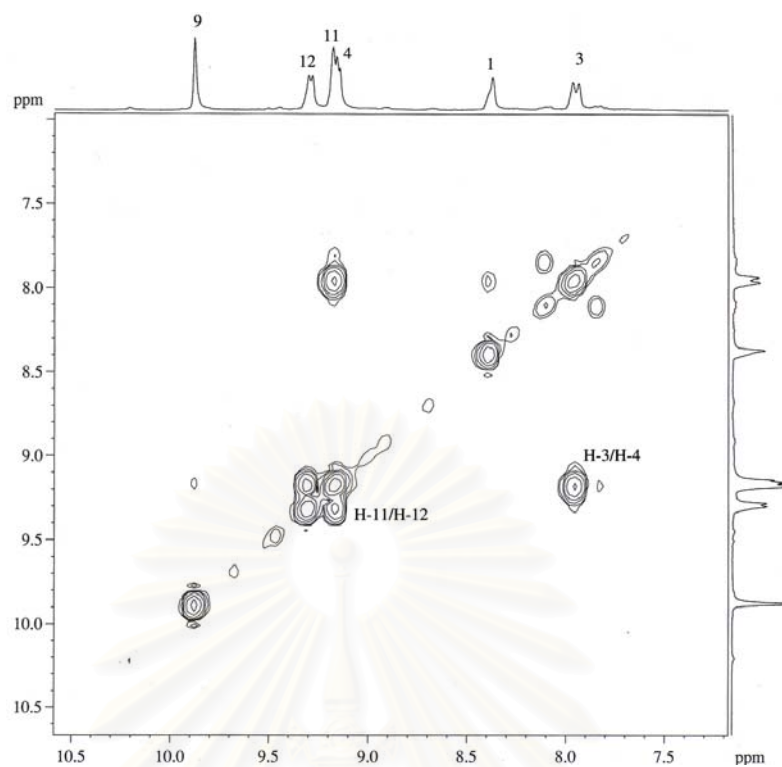
Figure 31 H,H-COSY Spectrum of **PK02** (Petrosamine) in DMSO-d_6
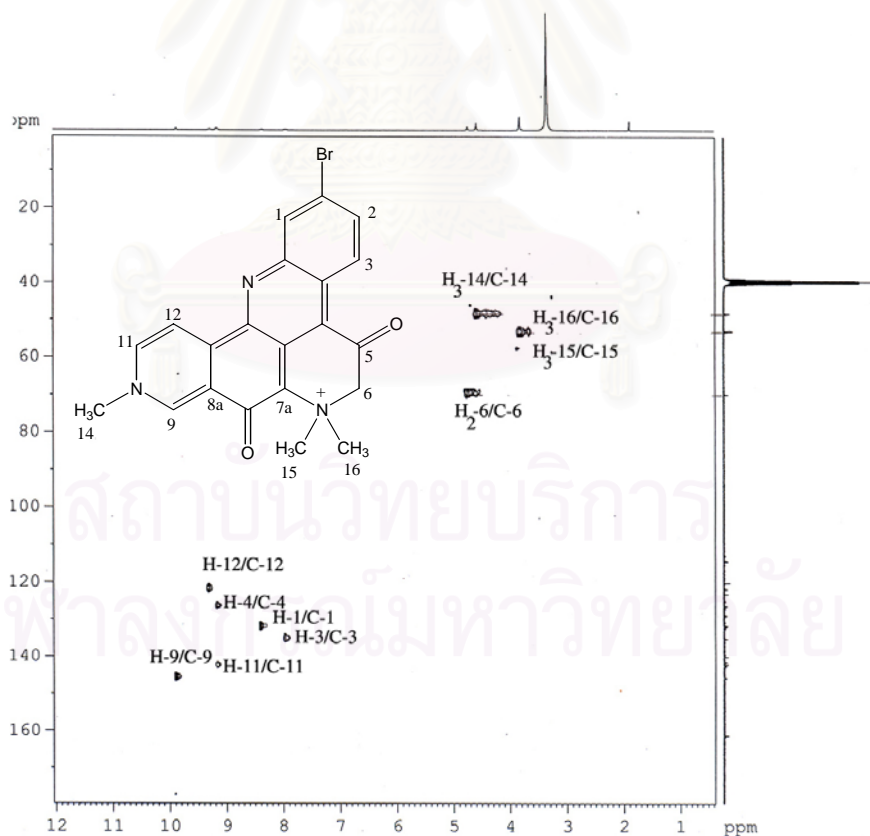
Figure 32 HMQC Spectrum of **PK02** (Petrosamine) in DMSO-d_6
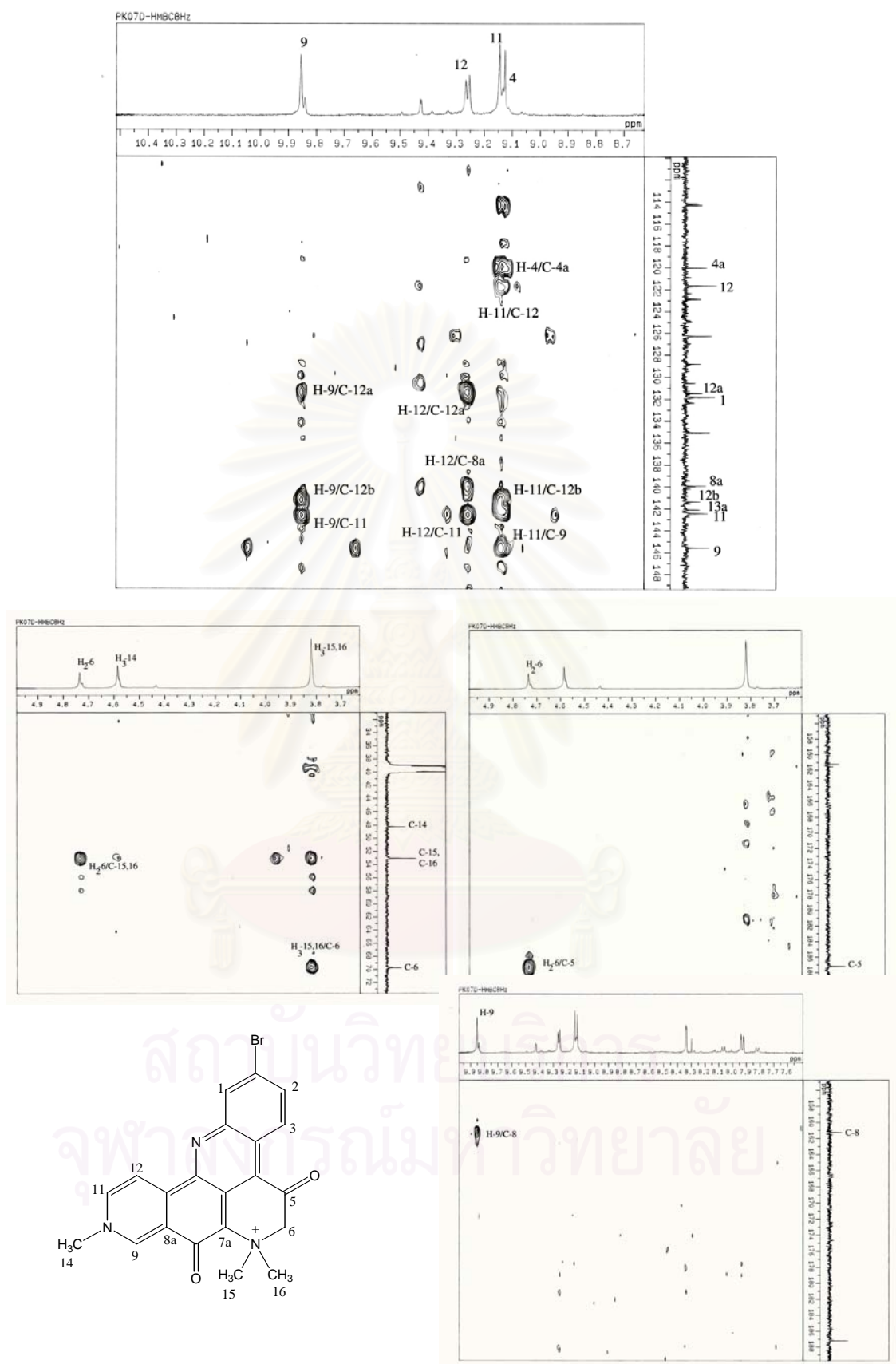
Figure 33 HMBC ($^{n}J_{HC}$ = 8 Hz) Spectrum of **PK02** (Petrosamine) in DMSO-d_6
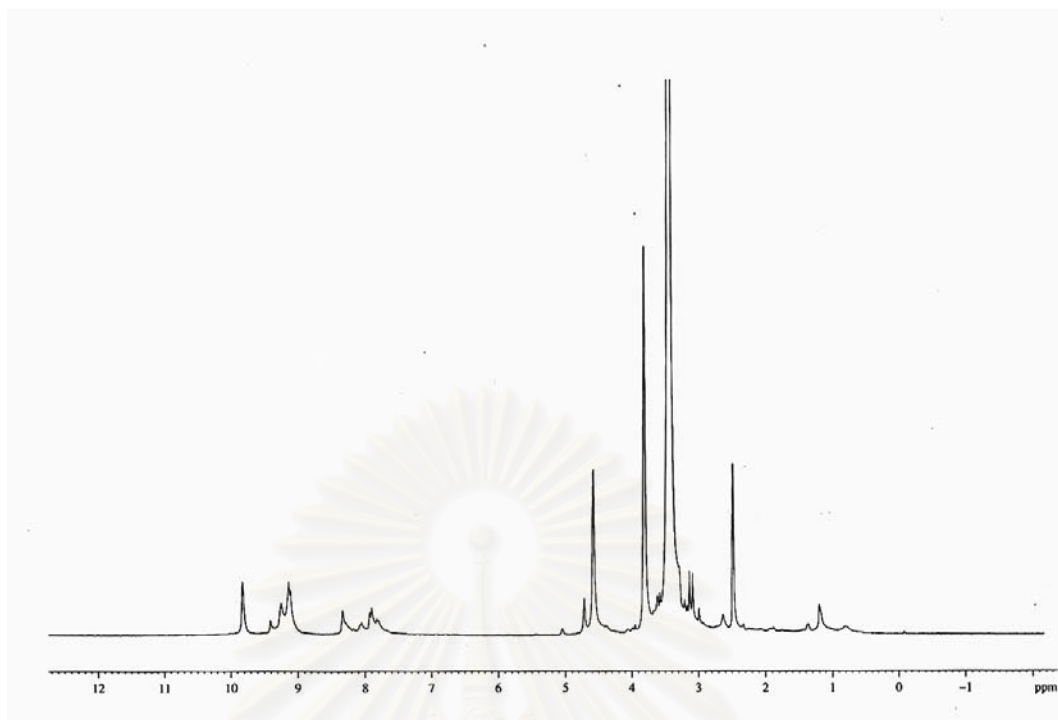
Figure 34 ^{1}H NMR (300 MHz) Spectrum of **PK02**+NaOD in DMSO-d_6
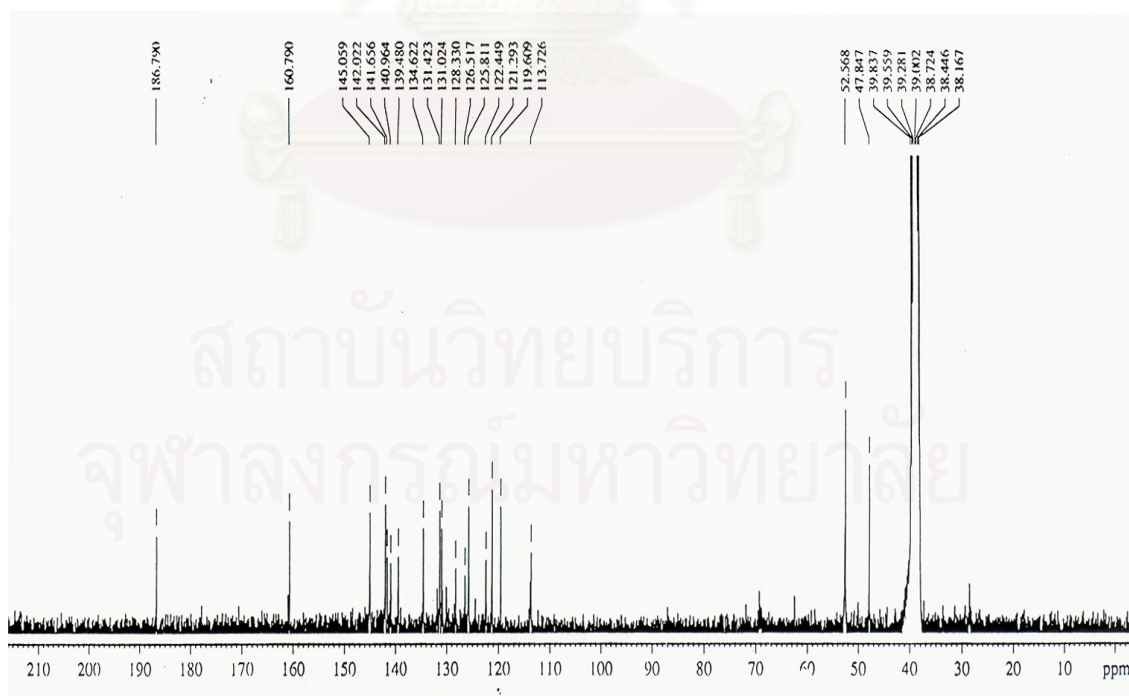
Figure 35 ^{13}C NMR (75 MHz) Spectrum of **PK02**+NaOD in DMSO-d_6
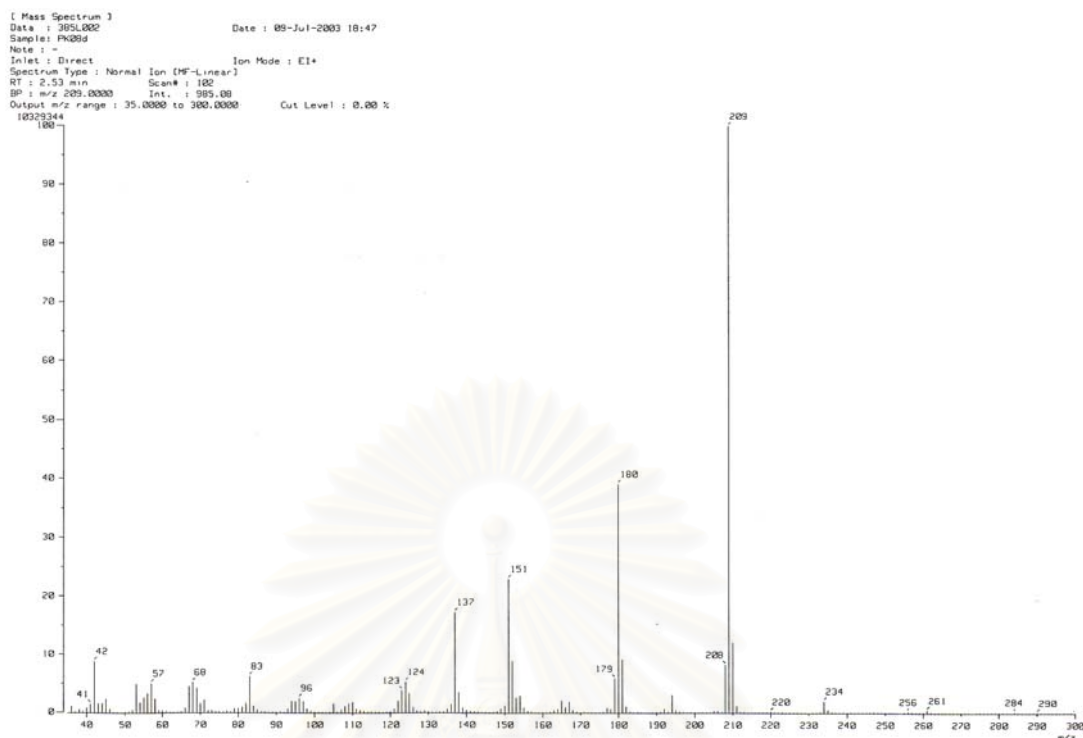
Figure 36 EIMS Spectrum of **PK03** (1,3,9-Trimethyl-8-hydroxyisoguanine)
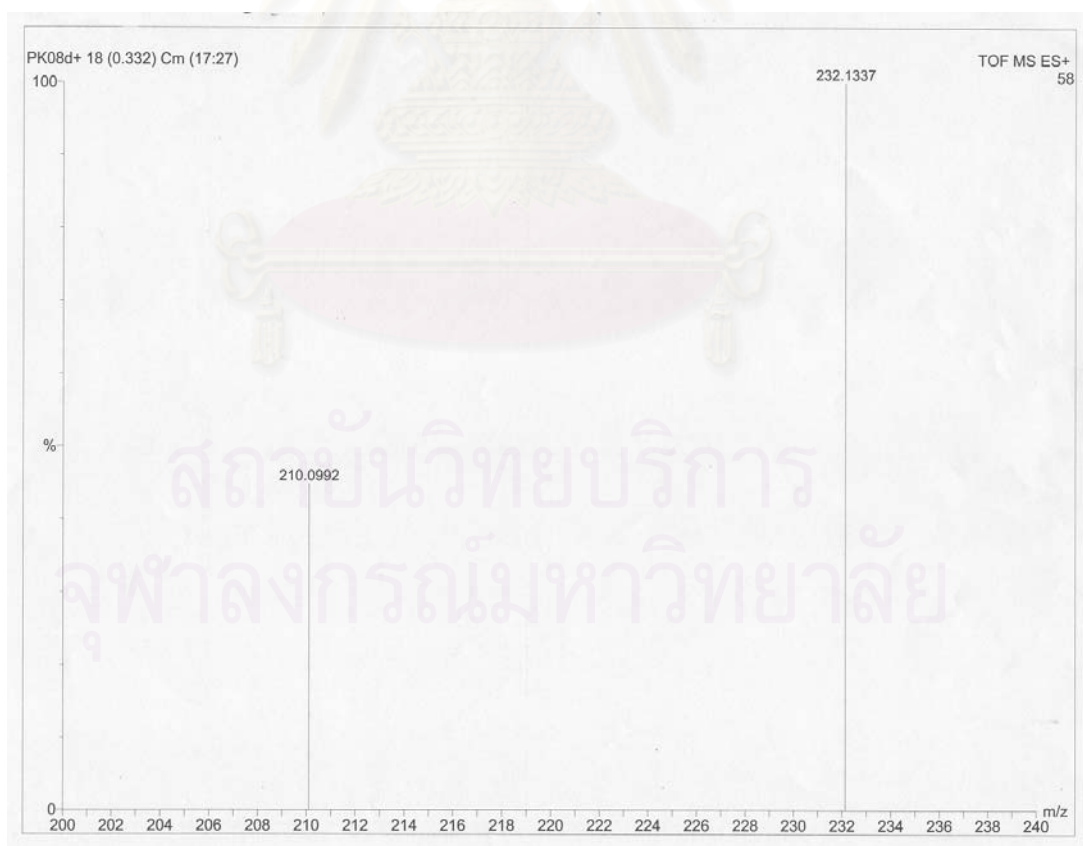
Figure 37 HR TOFMS Spectrum of **PK03** (1,3,9-Trimethyl-8-hydroxyisoguanine)
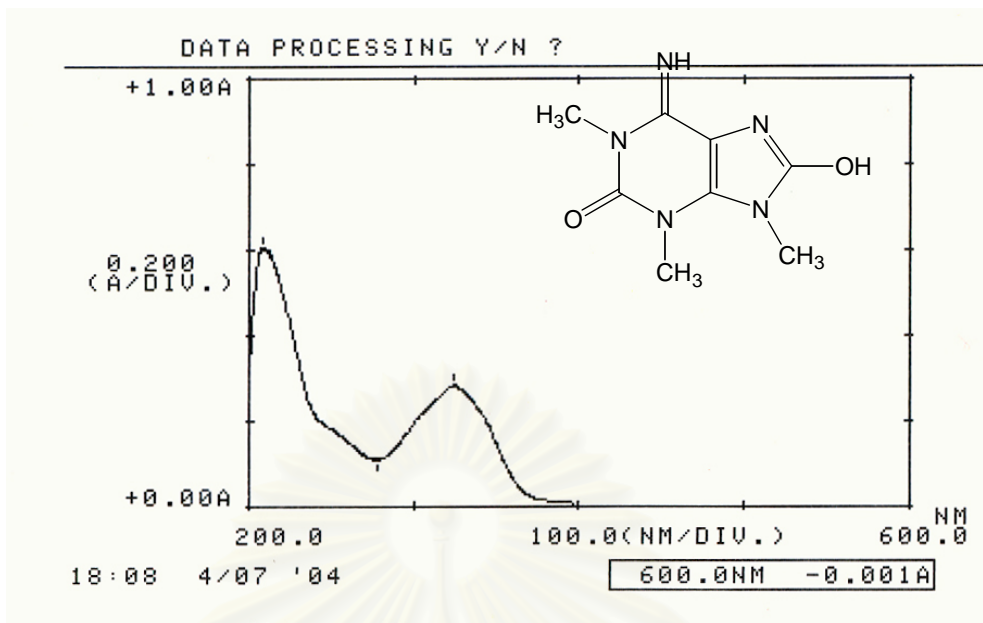
Figure 38 UV Spectrum of **PK03** (1,3,9-Trimethyl-8-hydroxyisoguanine) in MeOH
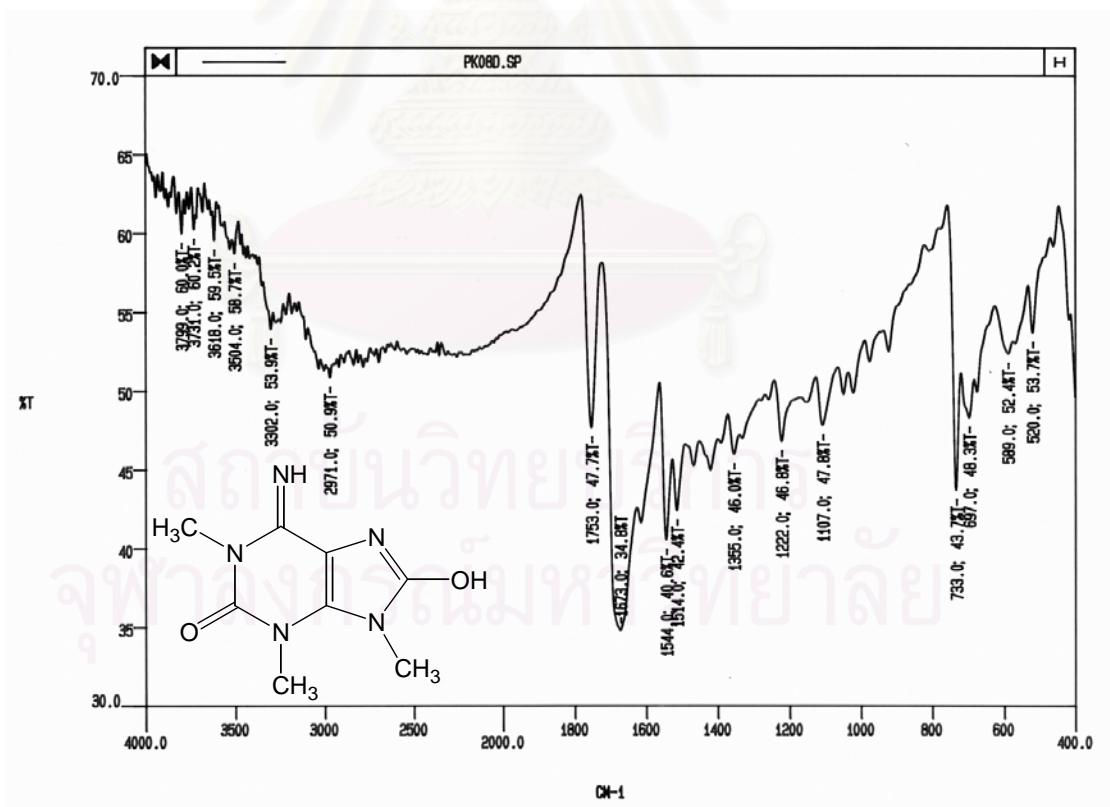
Figure 39 IR Spectrum (Film) of **PK03** (1,3,9-Trimethyl-8-hydroxyisoguanine)
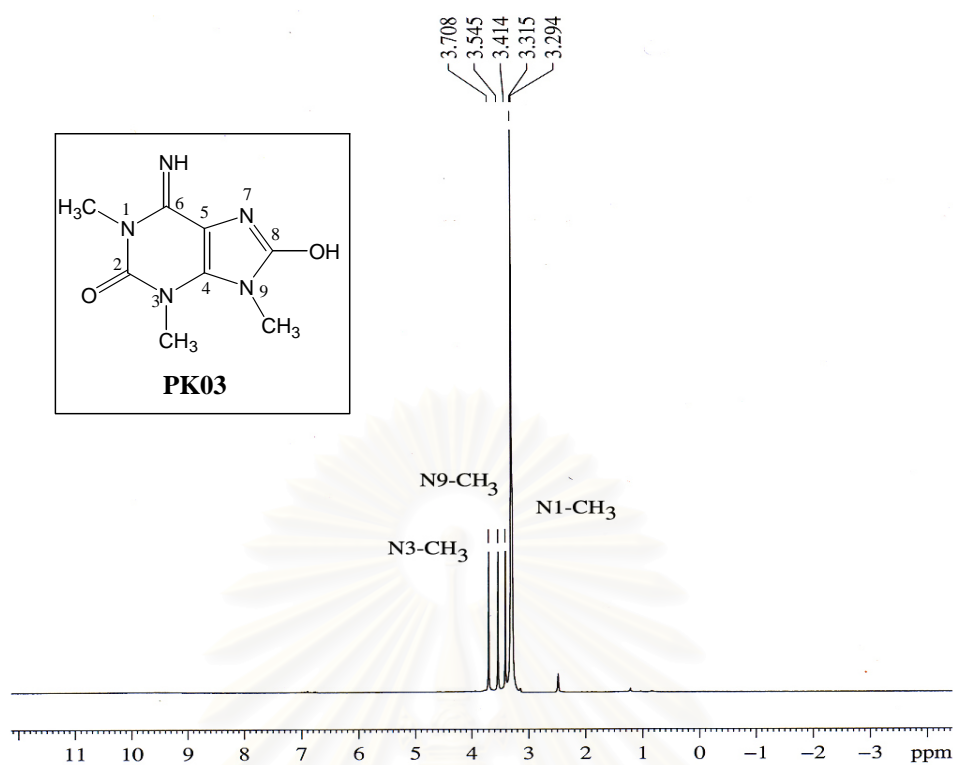
Figure 40 ^{1}H NMR (300 MHz) Spectrum of **PK03** (1,3,9-Trimethyl-8-hydroxyisoguanine) in DMSO-d_6
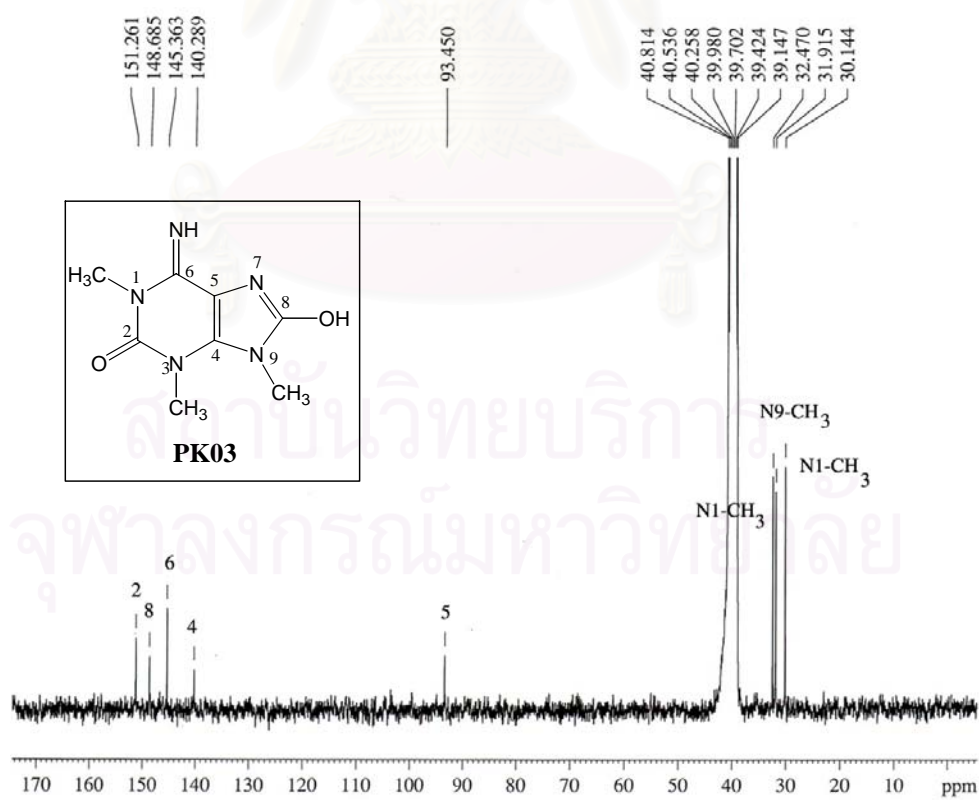
Figure 41 ^{13}C NMR (75 MHz) Spectrum of **PK03** (1,3,9-Trimethyl-8-hydroxyisoguanine) in DMSO-d_6
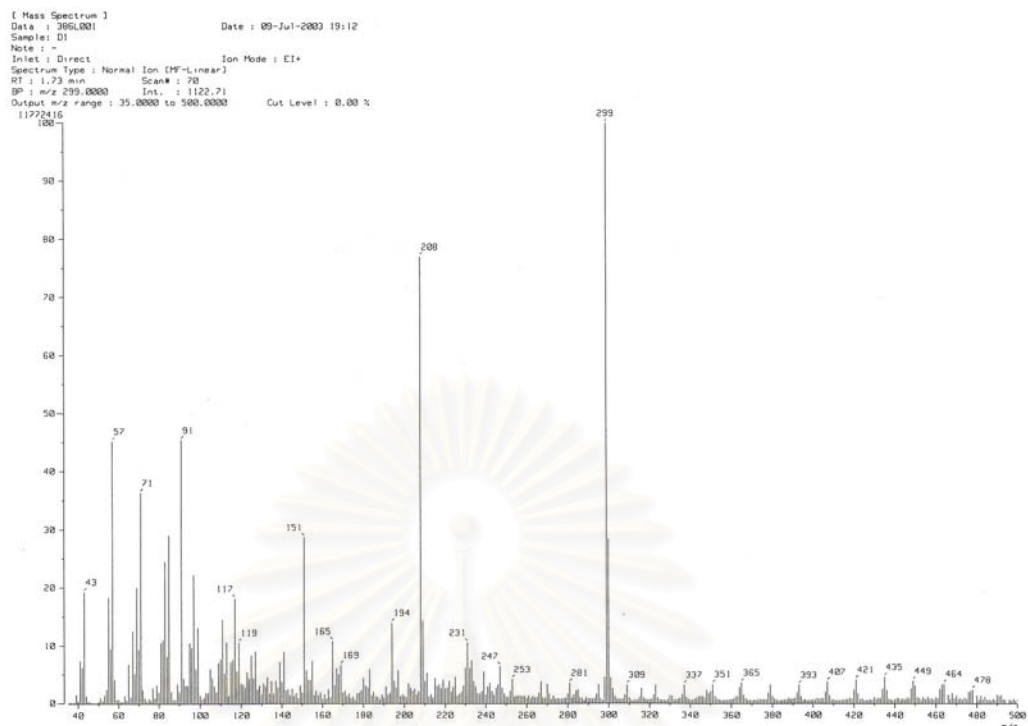
Figure 42 EIMS Spectrum of **PK04** (1,3,9-Trimethyl-8-*O*-benzylisoguanine)
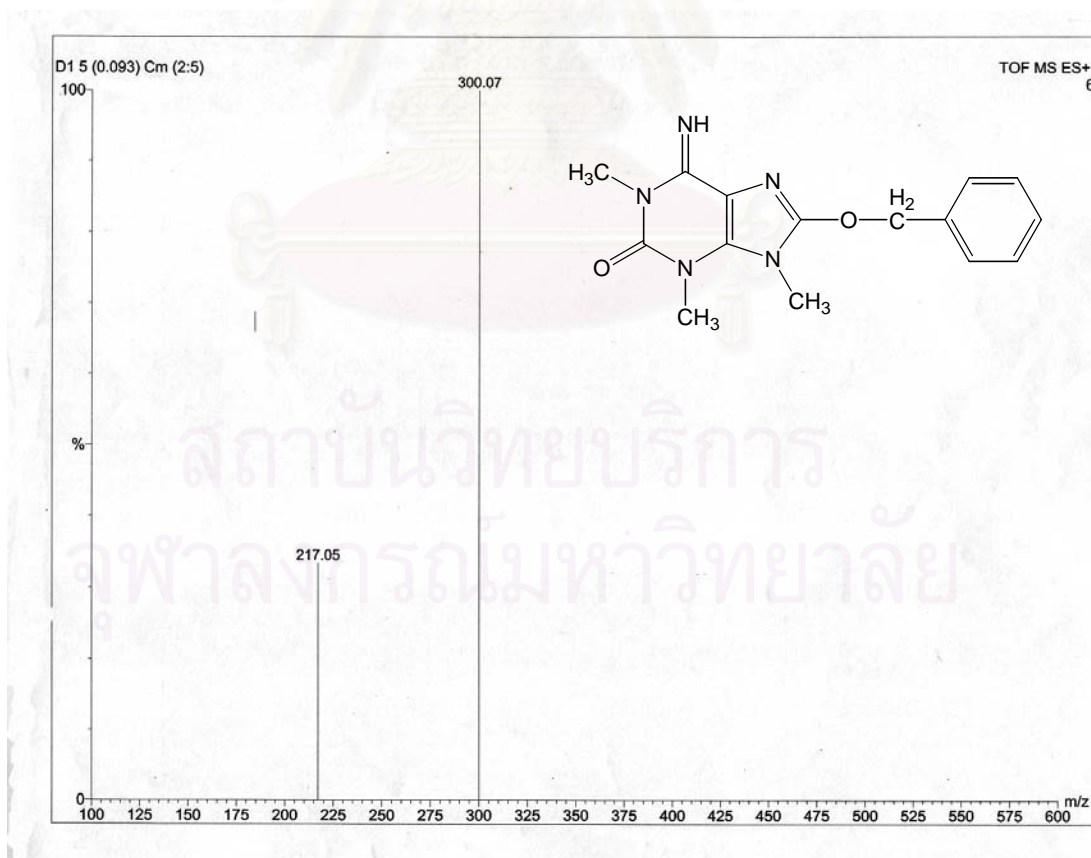
Figure 43 TOF MS Spectrum of **PK04** (1,3,9-Trimethyl-8-*O*-benzylisoguanine)
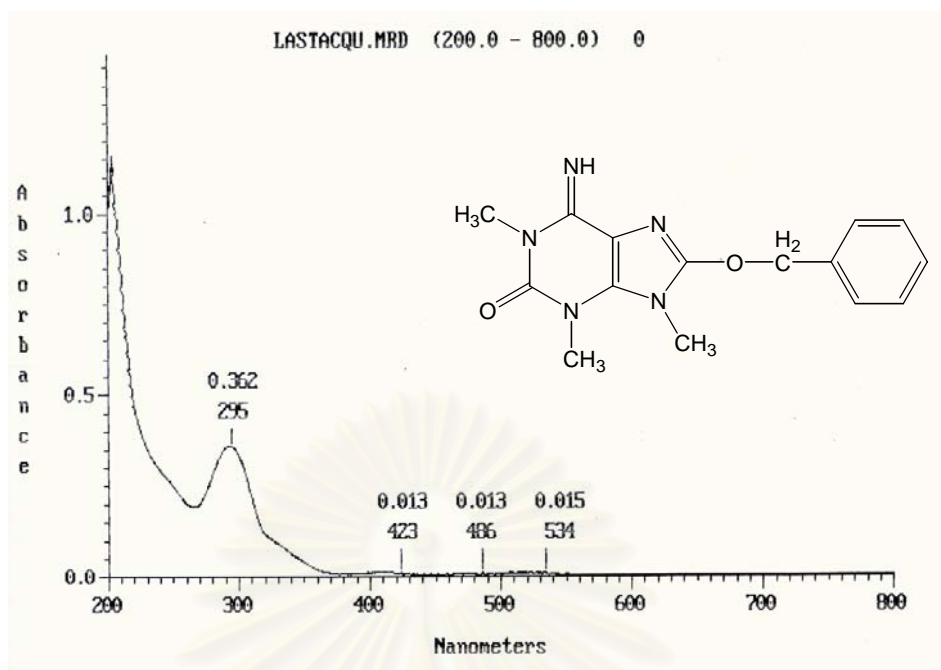
Figure 44 UV Spectrum of **PK04** (1,3,9-Trimethyl-8-*O*-benzylisoguanine) in MeOH
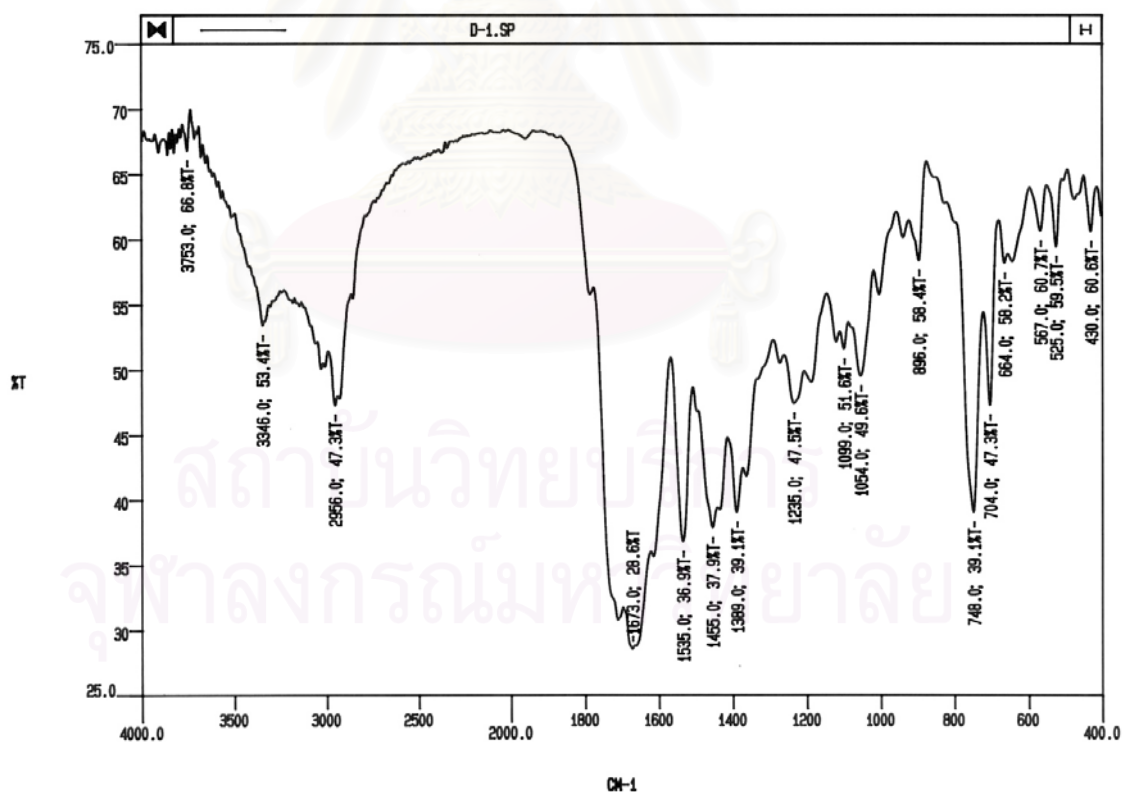
Figure 45 IR Spectrum (Film) of **PK04** (1,3,9-Trimethyl-8-*O*-benzylisoguanine)
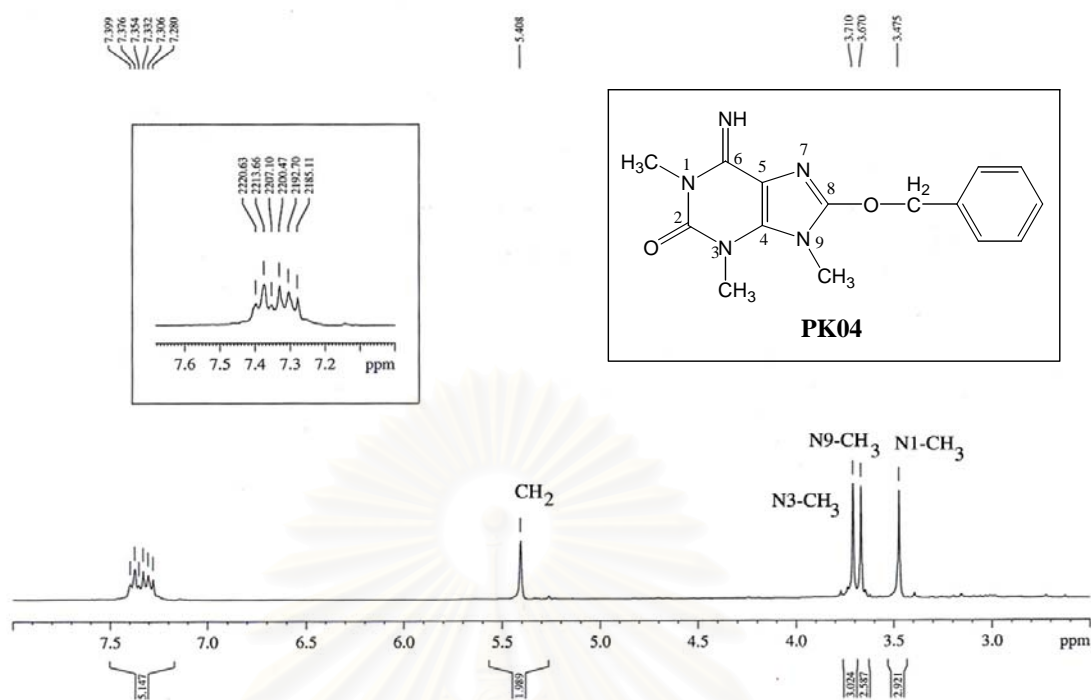
Figure 46 ^{1}H NMR (300 MHz) Spectrum of **PK04** (1,3,9-Trimethyl-8-*O*-
benzylisoguanine) in CDCl$_3$
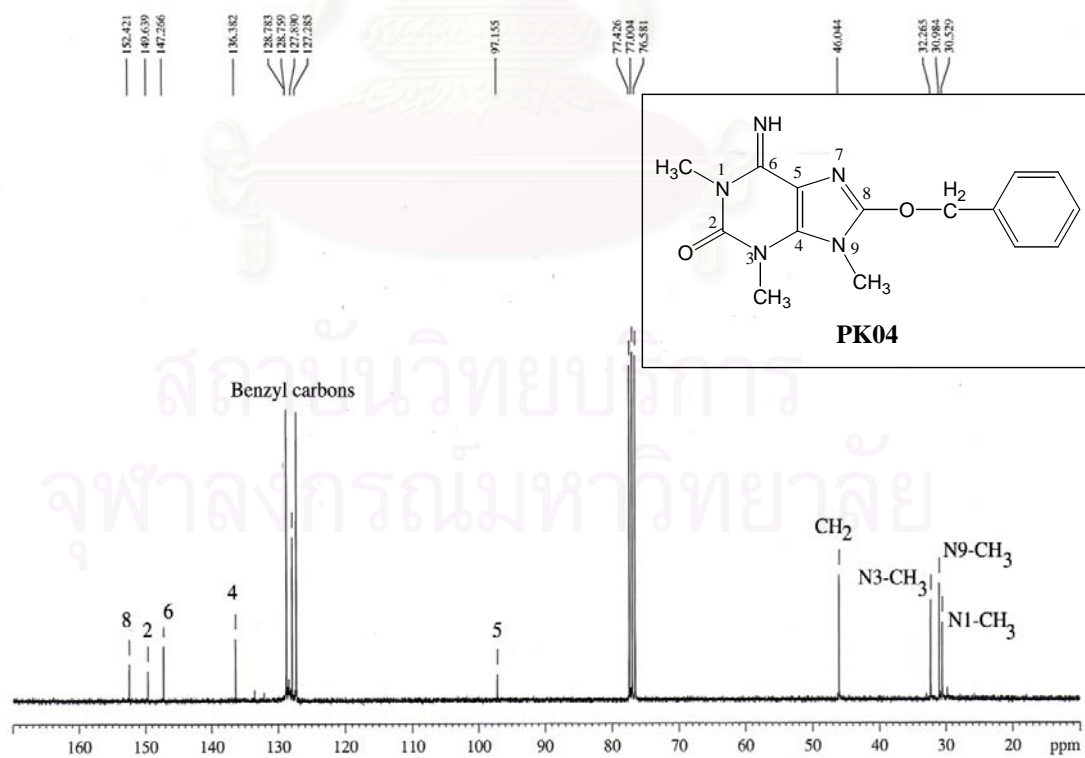
Figure 47 ^{13}C NMR (75 MHz) Spectrum of **PK04** (1,3,9-Trimethyl-8-*O*-
benzylisoguanine) in CDCl$_3$
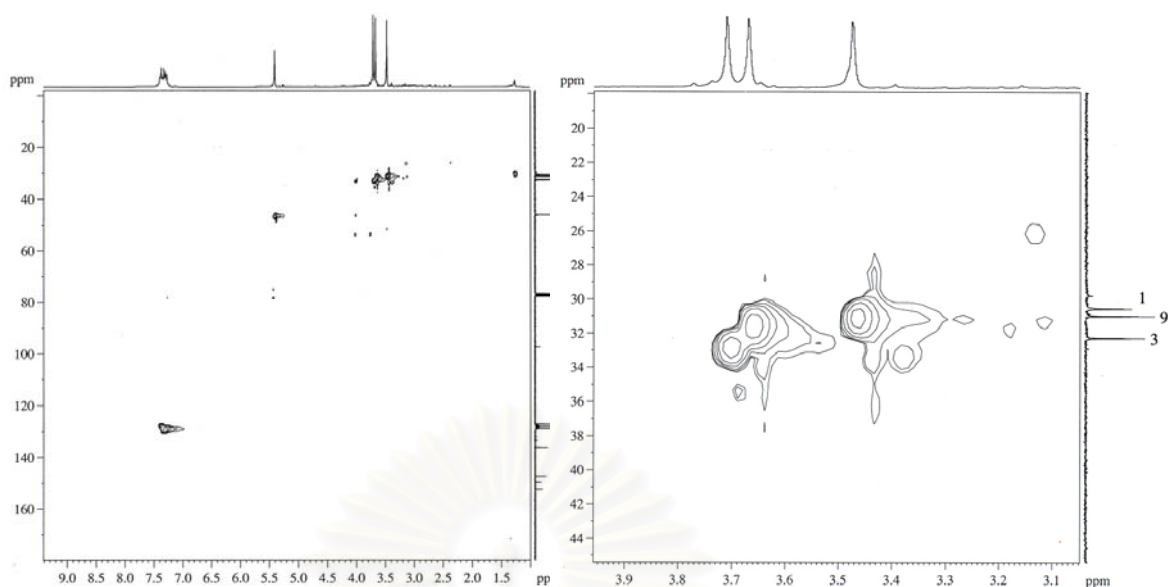
Figure 48 HMQC Spectrum of **PK04** (1,3,9-Trimethyl-8-*O*-benzylisoguanine) in CDCl₃
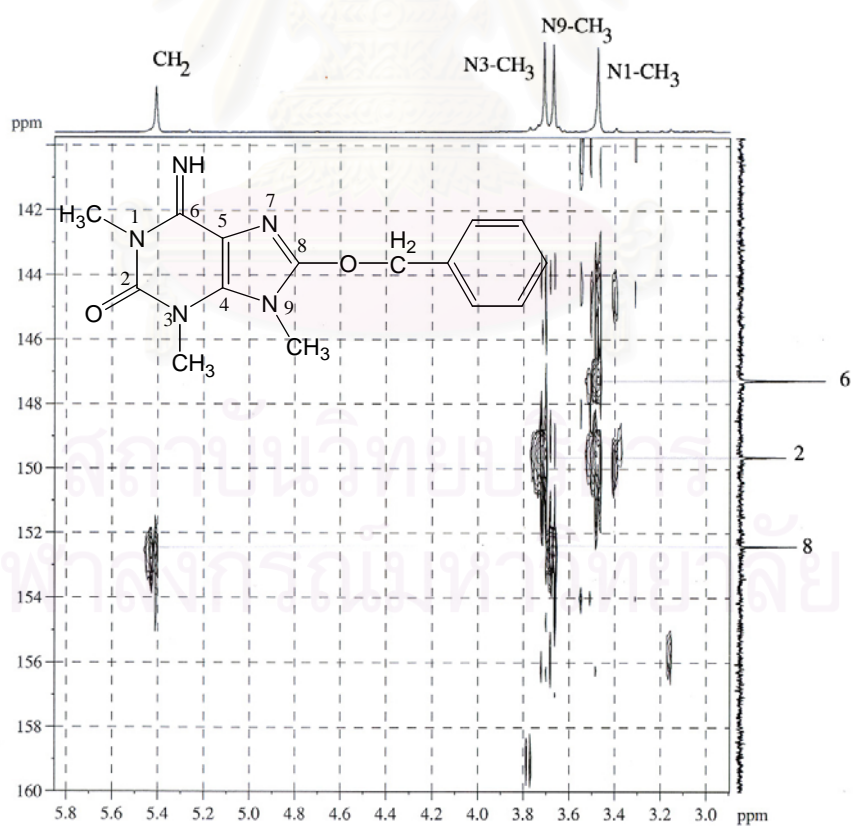
Figure 49 HMBC (ⁿ*J*HC = 8 Hz) Spectrum of **PK04** (1,3,9-Trimethyl-8-*O*-benzylisoguanine) in CDCl₃

SECTION 3

CHEMICAL CONSTITUENTS FROM THE SPONGE, *CACOSPONGIA MYCOFIJIENSIS*

CHAPTER I

INTRODUCTION

Microtubules play key roles in many cellular processes including intracellular transport, motility, architecture, and cell division. Microtubules are long, straight cylinders with a diameter of 180-250 A^o and a hollow core approximately 150 A^o in diameter. Typically, the walls of microtubules are composed of 13 protofilaments of the subunit protein called tubulin, aligned longitudinally along the axis of the cylinder. Tubulin, a 100-kDa protein, consists of two almost identical protein subunits known as α- and β-tubulins. The tubulin α-β heterodimer contains two guanosine triphosphate (GTP) binding sites. One of these sites is exchangeable with free GTP (E site) located at the β-subunit, and the other is non-exchangeable (N site) and thought to be on the α-subunit (Nicolaou, Dai, and Guy, 1994; Nicolaou, Roschanger, and Vourloumis, 1998; Nogales, Wolf, and Downing, 1998)

Microtubules are often grouped into two broad classes on the basis of their sensitivity to antimitotic agents, temperature, pressure, or the presence of other microtubule-associated proteins (MAPs). Easily disrupted microtubules, called labile microtubules, include those that form the mitotic spindle required for cell division. Stable microtubules are the usual component of cilia, flagella, centrioles, and related structures. Once microtubules are formed, the assembly and disassembly of microtubules, which are regulated by cellular activities, take place through the polymerization and depolymerization of the tubulin units. Apart from many other critical functions, they are of particular importance for the formation of the mitotic spindle, which provides the structural framework for the physical segregation of sister chromatids during cell division. Therefore, interruption of microtubule dynamics has proven to be an effective target for cancer chemotherapy.

Chemotherapeutic agents that target tubulin are important in the treatment of cancer. The success of these drugs is related to their mechanism of action that leads to disruption of cell division and induction of apoptosis. Unfortunately, the clinical usefulness of these agents is limited by the emergence of drug-resistant tumor cells, and in some patients, unacceptably high levels of neurological and bone marrow

toxicity (Gottesman and Pastan, 1993). To overcome these obstacles and to improve therapy, identifying and developing new agents that target tubulin have been focused.

As part of a program aimed at the discovery of new microtubule-stabilizing antitumor agents (MSAA) from marine organisms by Dr. Bradley S. Davidson's group, extracts from marine invertebrates collected from the Marshall Islands were screened for antimicrotubule activity. The extract of a brownish-gray sponge (BD95-102-17), which was later identified as *Cacospongia mycofijiensis*, showed particularly promising activity, exhibiting potent cytotoxicity toward A-10 smooth muscle cells and striking paclitaxel-like microtubule-stabilizing activity. The initial chemical investigation indicated that the extract contained one major and several minor compounds. The major compound was identified as latrunculin A [**1**], initially isolated from the branching, red sea sponge *Latrunculia magnifica* as an ichthyotoxic compound (Kashman, Groweiss, and Shmueli, 1980; Groweiss, Shmueli, and Kashman, 1983) but later also found in a sponge of the family Thorectidae (Gulavita, Gunasekera, and Pompani, 1992) and in nudibranchs of the genera *Chromodoris* (Okuda Scheuer, 1985; Kakou, Crews, and Bacus, 1987).

Interestingly, while latrunculin A had been reported to cause profound changes in the organization of microfilaments by inhibiting the polymerization of actin, it does not cause changes in the microtubule (Spector *et al.*, 1983).

[**1**]
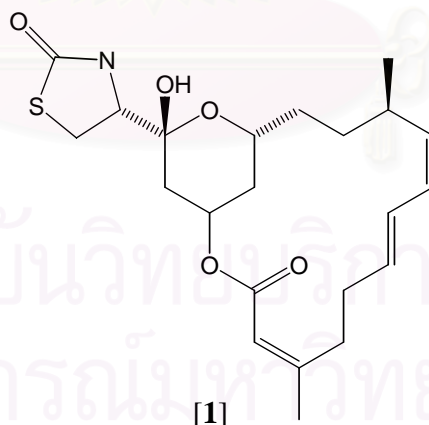
Guided by a mechanism-based assay for antimicrotubule activity, the active compounds were isolated and identified as the known macrolides, laulimalide [**2**] and isolaulimalide [**3**]. Through collaboration with Dr. Susan L. Mooberry of the Cancer Research Center of Hawaii, University of Hawaii, initial biological testing and mechanism of action studies of laulimalide and isolaulimalide have been performed.

Testing of pure laulimalide and isolaulimalide confirmed that both compounds stabilize microtubules in a paclitaxel-like manner (Moobery *et al.*, 1999).

[**2**]
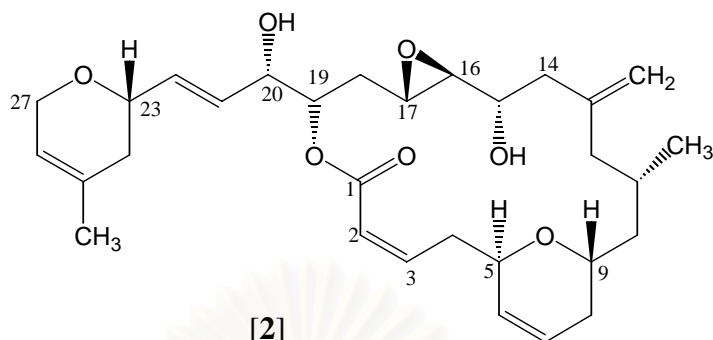
Although paclitaxel (Taxol®), a microtubule-stabilizing agent is already in the clinic and other compounds with similar mechanisms of action have recently been discovered, it is highly likely that further research will result in the development of improved therapeutic agents. As mentioned above, laulimalide could represent an important anticancer drug lead.

[**3**]
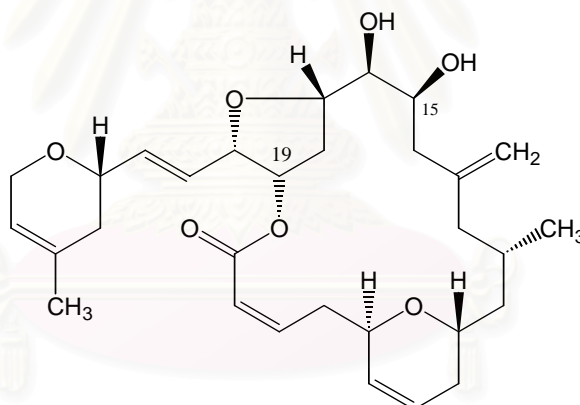
Apart from the significant clinical potential of laulimalide, the restriction of natural supply as well as the unique and complex molecular architecture, the synthesis of laulimalide and analogs, therefore, has been attractive to the chemists.

This project has been focused on the re-isolation of laulimalide from the natural sources for initial *in vivo* evaluation and on the synthesis of structural analogs of the C1-C14 fragment of laulimalide (Figure 1) to serve as intermediates toward syntheses of laulimalide analogs with the goals of improving stability and obtaining structure-activity relationship data. In the following, it will be described the isolation, purification, structure elucidation of isolated compounds from the sponge

Cacospongia mycofijiensis, and the synthesis of three C1-C14 fragment analogs of laulimalide.
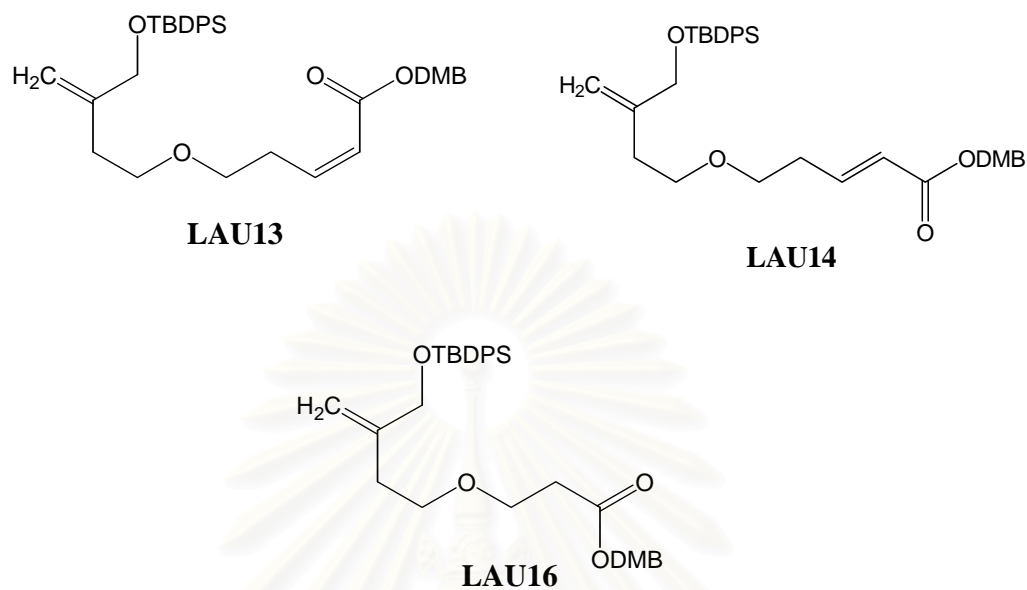
Figure 1 Three C1-C14 Fragment Analogs of Laulimalide

CHAPTER II

HISTORICAL

To date, the most clinically useful classes of antimitotic drugs can be divided into two classes: the *vinca* alkaloids and the taxanes (Figure 2). Both are from natural products and are used extensively in the treatment of a number of human cancers (Kovallaris, Verrills, and Hill, 2001). The *vinca* alkaloids (e.g. vincristine, vinblastine and vinorelbine) are cell-cycle specific, blocking cells at the metaphase/anaphase junction of mitosis, and in common with other antimitotic drugs such as colchicine and podophyllotoxin, destabilize microtubules. Drugs in the *vinca* alkaloids class bind to monomeric tubulin, preventing its polymerization into microtubules, leading to a rapid loss of cellular microtubules (Nicolaou *et al.*, 1998). Vincristine and vinblastine were introduced into clinical practice in the 1960s and remain in use as important components of curative combination chemotherapy regimens for diseases such as testicular cancer, Hodgkin's disease and acute lymphocytic leukemia.

The other group, taxanes, consists of paclitaxel and paclitaxel-like agents. They have an opposite effect on the cell in that they promote tubulin polymerization and stabilize microtubules, thereby altering normal microtubule dynamics leading to the formation of abnormal mitotic spindles, mitotic arrest, and the initiation of apoptosis (Jordan *et al*., 1996). At high concentrations, paclitaxel causes the formation of thick microtubule bundles, whereas the *vinca* alkaloids bring about complete loss of the microtubules (Schiff and Horwitz, 1980).

Paclitaxel, a complex diterpenoid, was originally isolated from the bark of the Pacific yew, *Taxus brevifolia* (Wani *et al.*, 1971). Its activity as a microtubule assembly promoter and microtubule stabilizer was first reported in 1979 (Schiff, Fant, and Horwitz, 1979). Tubulin is the primary target responsible for the cytotoxic properties of paclitaxel, as reflected by its ability to arrest cells in mitosis and to induce the assembly of tubulin into microtubules *in vitro*. Paclitaxel induces microtubule assembly by shifting the equilibrium between tubulin dimers and microtubules by lowering the critical concentration of tubulin required for polymerization. The most visible effect of paclitaxel on cells is the formation of

microtubule bundles in interphase cells and spindle asters in mitotic cells. However, low concentrations (3 and 10 nM) of paclitaxel are capable of inducing the formation of multiple micronuclei in HCT116 human colon carcinoma cells as a result of the inhibition of mitotic spindle assembly or function without causing mitotic arrest or microtubule bundling. These observations have led to the concept that paclitaxel can cause cell death by different mechanism, depending on the drug concentration. Paclitaxel is a powerful resource in cancer chemotherapy and has been established as one of the most active antineoplastic agent against a wide spectrum of malignancies, including ovarian, breast, lung and head and neck cancers and Kaposi's sarcoma. Paclitaxel was approved by the Food and Drug Administration in the United States for the treatment of advanced ovarian cancer in 1992 and metastatic breast cancer in 1994 (Ojima *et al*., 1999). Clinical studies on the treatment of other combination protocols are being pursued. The success of paclitaxel for the clinical treatment of ovarian, breast, and lung carcinomas has generated much interest in this drug.

Vinblastine ; R = CH$_3$
Vincristine ; R = CHO

	R$_1$	R$_2$
Paclitaxel;	Ph	Ac
Docetaxel;	*t*-BuO	H
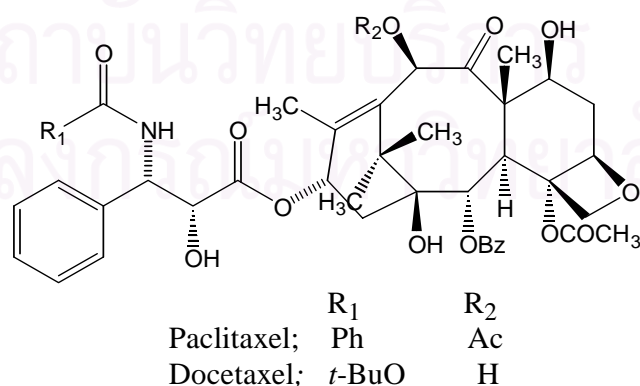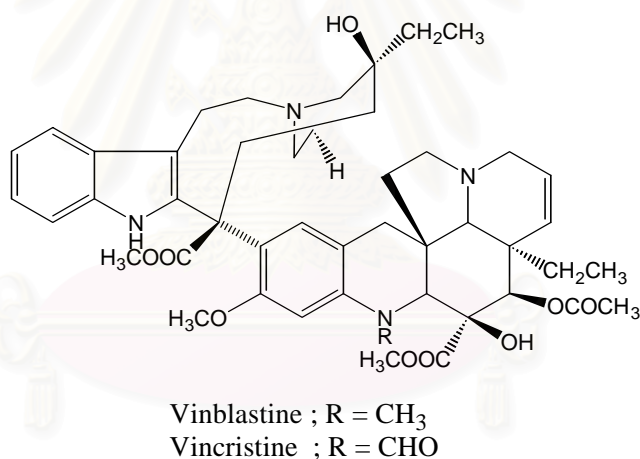
Figure 2 Antimitotic Drugs

Although paclitaxel has demonstrated its usefulness as an effective anticancer drug, there are limitations to its extended administration. The small amount of the natural compound from the yew tree bark cannot provide sufficient supply of this drug. Besides, the low aqueous solubility of paclitaxel and the development of clinical drug resistance have led to a search for new compounds that may have a greater or comparable efficacy relative to paclitaxel. Ideally, the new agents would be more soluble in aqueous solvents and would be poor substrates for P-glycoprotein, a known mediator of paclitaxel resistance (Cowden and Peterson, 1997).

Since the property of paclitaxel which causes massive reorganization of intracellular microtubule and promote biochemical assembly reactions of both microtubule protein and purified tubulin was first recognized in 1979 by Horwitz and co-workers, paclitaxel and its analogs (including the clinical anticancer drug docetaxel or Taxotere®) for more than 15 years were the only class of compounds known to act as microtubule stabilizers. However, after 1995 a diverse set of other natural products have been established to share the taxanes' ability to inhibit the polymerization of microtubule, and these discoveries have opened new perspectives for the development of next generation of Taxol-like clinical anticancer agents (Altmann, 2001).

Microtubule-stabilizing antitumor agents (MSAA) (Figure 3) include epothilones A and B, discodermolide, eleutherobin, sarcodictyins A and B, laulimalide, FR182877 (also known as wS9885B), and peloruside A. The epothilones represent a family of 16-membered ring macrolides that were originally isolated by Hofle and Reichenbach in 1992 from the fermentation broth of myxobacterium *Sorangium cellulosum* (Hofle *et al.*, 1996). The macrocyclic core of these polyketide molecules is formed by the successive decarboxylative condensations of acetate and propiaonate units. Epothilones A and B differ by a single methyl group at C-12 position of their carbon skeleton. This structural variance results from the incorporation of an acetate in the assembly of epothilone A and a propionate in that of epothilone B. Interest in the potential use of an epothilone as an anticancer agent, which had a mode of action similar to paclitaxel, was kindled after the report by Bollag *et al* in 1995 (Bollag *et al.*, 1995). This report was the result of a large scale screening effort of almost 8,000 natural product extracts for compounds that would polymerize protein. Epothilone B was reported to be more potent than paclitaxel and epothilone A in promoting microtubule assembly *in vitro*. The epothilones are 30 times more water-soluble than paclitaxel. In addition, the epothilones retain

sensitivity in P-glycoprotein expressing cells that were resistant to paclitaxel (Kavallaris *et al.*, 2001). Their improved solubility characteristics as well as their better activity profiles against drug-resistant cell lines have generated enormous excitement, leading to publication of nearly 30 papers within two years describing biological testing and synthetic approaches for their preparation as well as for the preparation of structural analogs (Altmann, Wartmann, and O'Reilly, 2000). For example, from the effort of Bristol-Myers Squibb Pharmaceutical Research Institute, BMS-24550, a semisynthetic lactam analog of the natural product epothilone B, emerged as the most efficacious epothilone in phase I clinical trial (Lee *et al.*, 2001).

Discodermolide, a linear polypropionate backbone punctuated by (*Z*)-olefinic linkages at C-8/C-9, C-13/C-14, and C-21/C-22, isolated from the deep-water marine sponge *Discodermia dissoluta*, was initially investigated as an immunosuppressant, but later was screened for antimitotic activity on the basis of a predictive structure-activity relationship with other tubulin-interacting drugs (ter Haar *et al.*, 1996). Studies with purified tubulin confirmed that discodermolide was significantly more potent than paclitaxel in inducing polymerization under a variety of reaction conditions (Kowalski *et al.*, 1997).

Discodermolide has been predicted to be 100-fold more soluble than paclitaxel and to have a reduced affinity for P-glycoprotein. It displays potent activity against multidrug-resistant (MDR) carcinoma cell lines, including paclitaxel-resistant lines. Discodermolide has received less attention, because of a lack of available material. However, discovery of its paclitaxel-like activity has heightened interest and recent syntheses would supply compounds for further testing and analogs for structure-activity relationship (SAR) studies (Smith *et al.*, 2000; Gunasekera, Longley, and Isbrucker, 2001).

Eleutherobin, another marine natural product, was isolated from an Australian marine soft coral *Eleutherobia* sp. collected in the waters off Western Australia. Eleutherobin is a glycosylated diterpene and shown to have activity comparable to that of paclitaxel (Long *et al.*, 1998). The first synthesis of this compound was reported by Nicolaou and co-workers just two months after its reported isolation (Nicolaou *et al.*, 1998.). Shortly thereafter, a second synthesis was reported by the Danishefsky group (Chen *et al.*, 1998), resulting in a total of five published papers from both efforts. However, eleutherobin displayed cross-resistance in multidrug resistant cell lines, an

effect that was reversible by verapamil, suggesting that eleutherobin is a substrate of P-glycoprotein (Hamel *et al.*, 1999).

	R₁	R₂	R₃	Urocanoyl residue

Sarcodictyin   A   H   COOCH₃   H   *E*
                       B   H   COOCH₂CH₃   H   *E*
                       C   H   COOCH₃   OH   *E*
                       D   H   COOCH₃   OH   *Z*

Eleutherobin   CH₃   H   *E*

Discodermolide

Epothilone A : R = H
Epothilone B : R = CH₃
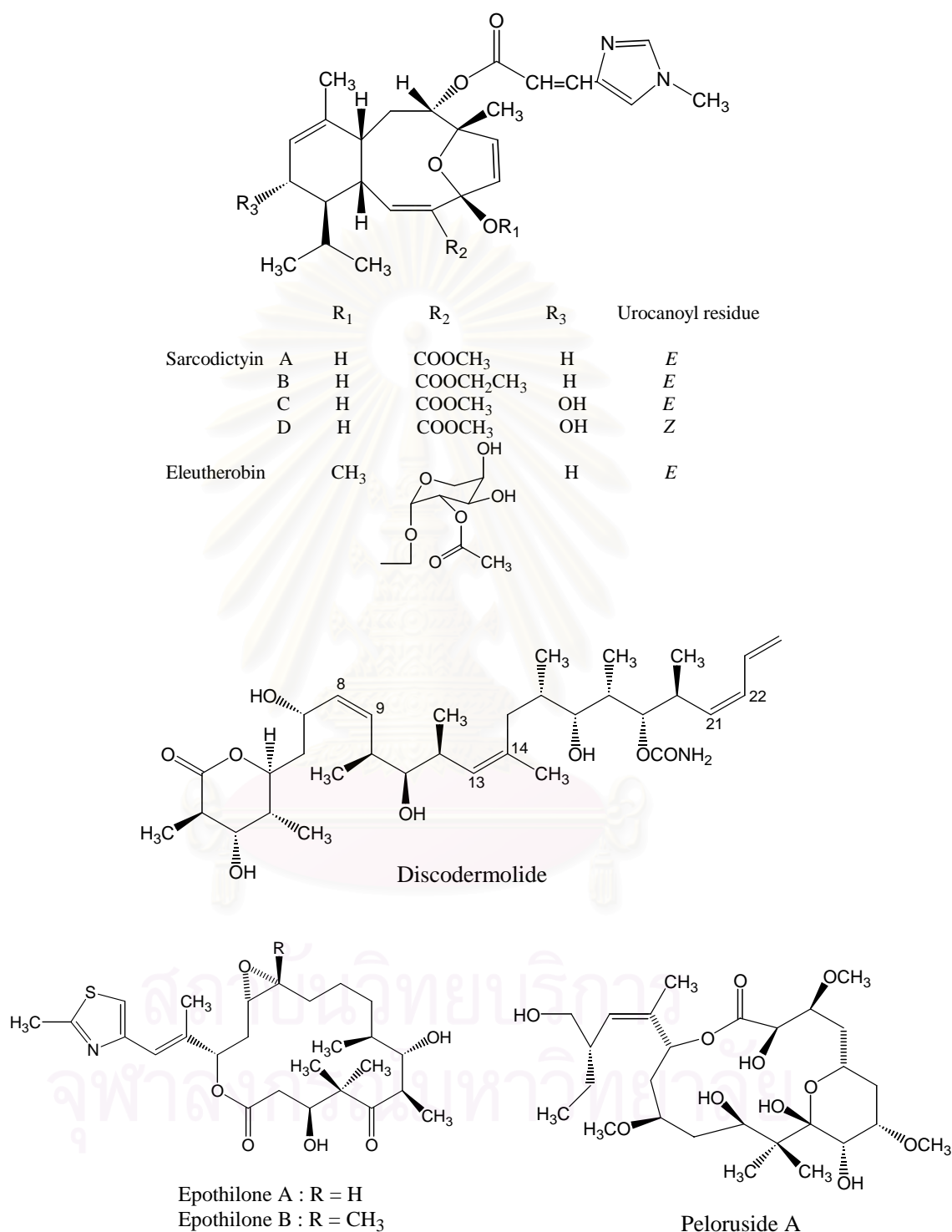
Peloruside A

Figure 3 Microtubule-Stabilizing Agents

Most recently, peloruside A is a new antimitotic agent with paclitaxel-like microtubule-stabilizing activity. Peloruside A was isolated from a New Zealand marine sponge, *Mycale hentscheli*. Its 16-membered macrolide ring is similar to that of epothilones. Like paclitaxel, peloruside A arrests cells in the G2-M phase of the cell cycle and induces apoptosis (Hood *et al.*, 2002).

In 1988, a chocolate sponge, *Cacospongia mycofijiensis*, collected from Vanuatu was attracted to the Crew's group because the liquid squeezed from freshly collected material killed tropical fish held in an aquarium within 10 min. This primary effort to protect the sponge against predators originates from two cytotoxic macrolides, fijianolide B [**2**] and its tetrahydrofuran-containing isomer fijianolide A [**3**] (Quinoa, Kakou, and Crews, 1988). Independently, the same compounds were isolated by Hawaiian scientists from an Indonesian sponge *Hyatella* sp. and given the now commonly used names laulimalide [**2**] and isolaulimalide [**3**], the names being derived from Hawaiian language ("laulima" = people working together), due to the cooperating research group (Corley *et al.*, 1988). Laulimalide and isolaulimalide were also obtained from an Okinawan sponge *Fasciospongia rimosa* (Tanaka *et al.*, 1996), and very recently also from a sponge in the genus *Dactylospongia* (Cutignano *et al.*, 2001). Interestingly, both compounds were also isolated from a predator nudibranch, *Chromodoris lochi*, that was found grazing on the sponge. The structure of laulimalide was initially established mostly by NMR analysis. Subsequently, its absolute configuration was established by X-ray analysis by Higa and co-workers in 1996 (Jefford *et al.*, 1996). Higa's group also isolated a ring-expanded regioisomer of laulimalide, neolaulimalide [**4**] (Tanaka *et al.*, 1996).
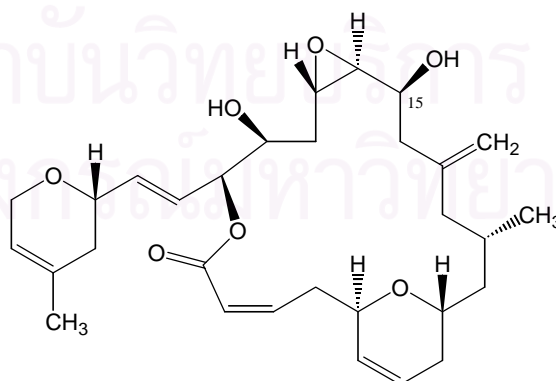
[**4**]

Laulimalide, in original report identified as a potent inhibitor of cellular proliferation towards several cell lines with the IC_{50} values in the low nanomolar range (Corley *et al.*, 1988; Quinoa *et al.*, 1988), is an 18-membered macrolide (within

the inner perimeter) that contains nine chiral carbons ($5R$, $9S$, $11S$, $15S$, $16S$, $17S$, $19S$, $20S$, $23S$) and two dihydropyran rings, one (C-5 to C-9) annulated to the macrocycle in 2,6-trans fashion and the second on (C-23 to C-27) connected to the macrolide core via an E-allylic alcohol. In addition, laulimalide contains a trans-disubstituted epoxide at C-16 and C-17 and a 2,3-Z-enolate.

Isolaulimalide is a laulimalide rearrangement product, whose tetrahydrofuran ring is formed through an S_N2-type attack of the side chain C-20 hydroxyl group on the C-17 position of the epoxide ring, the acid catalyzed isomerization being complete within a few hours. Isolaulimalide exhibits significantly reduced activity with the IC_{50} values in the low micromolar range.

Neolaulimalide is the ring-enlarged regioisomer of laulimalide with an intact epoxide moiety and was reported to exhibit high cytotoxicity in the same range as laulimalide. It is distinctly more stable than laulimalide, and the acid-catalyzed rearrangement to isolaulimalide being complete only after 2 days.

In February 1999, laulimalide and isolaulimalide were recognized as new members of the MSAA family of compounds, which share the same or a similar mechanism of action as the frontline anticancer drugs the taxol group (Mooberry *et al.*, 1999). One of the intriguing properties of laulimalide is that it inhibits the P-glycoprotein that is responsible for multidrug resistance in tumor cells. Laulimalide is as much as 100-fold more potent than paclitaxel against SKVLB-1 cells, a P-glycoprotein overexpressing multidrug-resistant cell line. Recently, the high therapeutic potential of laulimalide was further underlined by Hamel, who found that laulimalide also kills human ovarian carcinoma cells which, due to taxoid site mutations in the M40 human β-tubulin gene, which is resistant to paclitaxel (PTX10, PTX22), epothilone A (A8), and epothilone B (B1) (Pryor *et al.*, 2002). Interestingly, microtubules formed by the induction of laulimalide and isolaulimalide were morphologically different from those formed in the presence of paclitaxel (Mooberry *et al.*, 1999).

Several synthetic endeavors toward laulimalide have been described since 1996 when the absolute configuration of laulimalide was first determined (Jefford *et al.*, 1996). These early efforts resulted in three reports on fragment syntheses by the group of Ghosh (Ghosh, Mathivanan, and Cappiello, 1997) and Nishiyama (Shimizu and Nishiyama, 1997a; Shimizu and Nishiyama, 1997b). However, these primary approaches were not successfully brought to completion. In 1999 after laulimalide

was identified as a new member of the MSAA family, Mulzer's group reported the synthesis of the "lower" C1-C12 moiety, utilizing ring-closing olefin metathesis (RCM) for the construction of the dihydropyran subunit (Mulzer and Hanbauer, 2000). This communication was followed in close succession by an independent report of Ghosh and Wang, concerning the synthesis of an extended C2-C16 fragment which used a slightly different RCM methodology for elaboration of the dihydropyran moiety (Ghosh and Wang, 2000b).

Since these early fragment syntheses, an impressive number of sixteen approaches to key fragments of laulimalide have been contributed by different groups, and seven teams have completed as many as 10 total syntheses (Mulzer and Ohler, 2003). The first total synthesis of laulimalide was accomplished in 2000 by Ghosh and Wang (Ghosh and Wang, 2000a), who later refined their first approach by a stereoselective introduction of the 2,3-*cis*-enoate. Lately, the series of total syntheses of laulimalide has been complemented by two closely related approaches from the Crimmins' (Crimmins, Stanton, and Allwein, 2002) and Williams' (Williams *et al.*, 2002) groups which both focus on a diastereoselective allylic transfer of a C1-C14 allylstannane (or silane) to a C15-C27 α,β-epoxyaldehyde. A very recent synthesis by Nelson (Nelson *et al.*, 2002) is characterized by extensive use of asymmetric acyl halide aldehyde cyclocondensation methodology for the construction of main fragments. Although, there are many publications dealing with the synthesis of laulimalide, to date, only a few studies exist concerning the synthesis of laulimalide derivatives (Pryor *et al.*, 2002; Ahmed *et al.*, 2003).

CHAPTER III

EXPERIMENTAL

1. Sample Collection

The brownish-gray sponge was collected at the depths of 10-30 meters on the exposed ocean reef-slopes of Majuro and Arno Atolls, Republic of the Marshall Islands in November 1995 and again in December 1996. This sponge was identified as *Cacospongia mycofijiensis* Bakus (Order Dictyoceratida, Family Thorectidae) by Dr. Michelle Kelly-Borges, the Museum of Natural History, London, although the species has previously been known as *Spongia mycofijiensis*. The specimens were preserved at -20° C before extraction.

2. General Techniques

2.1 Solvents

Unless stated otherwise, all reagents and chromatographic solvents were reagent grade and were used as purchased. THF was freshly distilled prior to use from sodium-benzophenone. CH_2Cl_2 was freshly distilled prior to use from calcium hydride. Hexane, DMSO, and benzene were distilled from calcium hydride and stored over Linde type $4A^{\circ}$ molecular sieves. Et_3N was distilled from calcium hydride and stored over potassium hydroxide. All reactions requiring anhydrous conditions were conducted under an atmosphere of dry nitrogen in oven-dried, flame-dried reaction vessels.

2.2 Analytical Thin-Layer Chromatography (TLC)

Technique	:	One dimension, ascending
Adsorbent	:	Silica gel 60 F_{254} (E. Merck) pre-coated plate
Layer thickness	:	250 μm
Distance	:	5.0 cm
Temperature	:	Laboratory temperature (25-30 $^{\circ}$C)
Detection	:	1. Visual detection under daylight
		2. Ultraviolet light (254 and 365 nm)

3. Phosphomolybdic acid (10% solution in ethanol) and heated 5 min at 110 ^{o}C until blue green spots appear on yellow background.

2.3 Column Chromatography

2.3.1 Flash Column Chromatography

Adsorbent	:	Silica gel 60 (No. 9385) particle size 0.400-0.630 nm (70-230 mesh ASTM) (E. Merck)
Packing method	:	Wet packing: the adsorbent was slurried in the eluent, poured into a column and then allowed to settle.
Sample loading	:	The sample was dissolved in a small amount of eluent and then applied gently on top of the column.
Detection	:	Fractions were examined by TLC technique in the same manner as described in section 2.2

2.3.2 Gel Filtration Chromatography

Gel Filter	:	Sephadex LH20 (Pharmacia)
Packing method	:	Gel filter was suspended in the eluent and left standing to swell for 24 hours prior to use. It was then poured into the column and allowed to set tightly.
Sample loading	:	The sample was dissolved in a small amount of eluent and then applied gently on top of the column.
Detection	:	Fractions were examined in the same manner as described in section 2.2

2.3.3 High Pressure Liquid Chromatography (HPLC)

Column	:	1. Hamilton PRP-1 semi-preparative (5 μm, 10 mm x 25 cm) C-18 polymer-based column
		2. Dynamx-60A semi-preparative (5 μm, 10 mm x 25 cm) silica gel column
Flow rate	:	1. 1.5 mL/min for PRP-1 semi-preparative column
		2. 3 mL/min for silica gel semi-preparative column

Mobile phase	:	1. Gradient Acetonitrile-H_2O for PRP-1 semipreparative column
		2. Isocratic 5% MeOH in CH_2Cl_2 for silica gel analytical column
Sample preparation	:	The sample was dissolved in a small amount of eluent and filtered through Millipore filter paper before injection
Injection volume	:	200 μL
Pump	:	Waters model 515
Detector	:	Waters model 486 variable wavelength
Temperature	:	Room temperature

2.4 Spectroscopy

2.4.1 Ultraviolet (UV) Spectra

UV spectra were obtained on a Milton Roy Spectronic 3000 Array spectrophotometer (Pharmaceutical Research Instrument Center, Faculty of Pharmaceutical Sciences, Chulalongkorn University).

2.4.2 Infrared (IR) Spectra

IR spectra were recorded on a Perkin Elmer FT-IR 1760X spectrometer (Pharmaceutical Research Instrument Center, Faculty of Pharmaceutical Sciences, Chulalongkorn University).

2.4.3 Mass Spectra

Mass spectra were obtained by an Electrospray Ionization Time of Flight (ESI-TOF) Micromass LCT mass spectrometer (The National Center for Genetic Engineering and Biotechnology, BIOTEC, Thailand), and the lock mass calibration was applied for the determination of accurate mass.

2.4.4 Proton and Carbon-13 Nuclear Magnetic Resonance (^{1}H and ^{13}C NMR) Spectra

^{1}H (400 MHz) and ^{13}C (100 MHz) NMR Spectra were measured on a Bruker ARX 400 spectrometer (Utah State University, Utah, USA)

^{1}H (300 MHz) and ^{13}C (75 MHz) NMR spectra were measured on a Bruker DPX-300 FT-NMR spectrometer (Pharmaceutical Research Instrument Center, Faculty of Pharmaceutical Sciences, Chulalongkorn University).

The chemical shifts were reported on the δ-scale relative to solvent signals. The operating NMR solvents used in this section were chloroform-*d* (7.24 ppm of residual CHCl$_3$ for ^{1}H NMR and 77.0 ppm for ^{13}C NMR) and benzene-*d$_6$* (7.15 ppm of residual C$_6$HD$_5$ for ^{1}H NMR and 128.0 ppm for ^{13}C NMR).

2.5 Chemicals

1,4-Butanediol	(Aldrich)
Cerium(III) chloride heptahydrate (CeCl$_3$.7H$_2$O)	(Merck)
18-Crown-6	(Aldrich)
Dicyclohexylcarbodiimide (DCC)	(Fluka)
2,4-Dimethoxy benzoic acid	(Aldrich)
4-Dimethylaminopyridine (4-DMAP)	(Fluka)
Diisobutylammonium hydride (DIBAH)	(Aldrich)
Hydrogen peroxide (H$_2$O$_2$)	(Fluka)
Imidazole	(Merck)
KN(TMS)$_2$	(Aldrich)
Lithium Aluminium Hydride (LAH)	(Fluka)
N,N,N′,N′-Tetramethyldiaminomethane	(Aldrich)
Oxalyl chloride (COCl)$_2$	(Aldrich)
1,3-Propanediol	(Aldrich)
Pyridinium-*p*-toluenesulfonate (PPTS)	(Aldrich)
Sodium borohydride (NaBH$_4$)	(Fluka)
Sodium hydride (NaH)	(Fluka)
Sodium bicarbonate (NaHCO$_3$)	(Aldrich)
Sodium chlorite (NaClO$_2$)	(Merck)
Sodium sulfite (Na$_2$SO$_3$)	(Merck)
tert-Butyldiphenylsilyl chloride (TBDPS Cl)	(Aldrich)
Tetrabutylammonium fluoride (TBAF)	(Fluka)
Trimethylsilylchloride (TMSCl)	(Aldrich)
Zinc chloride (ZnCl)	(Merck)

3. Extraction and Isolation of Compounds from *Cacospongia mycofijiensis*

The lyophilized tissues of *Cacospongia mycofijiensis* were extracted with methanol. The methanol extract (5.0 g) was subjected to a solvent partition scheme to yield fractions of hexane (**BD01**, 2.3 g), dichloromethane (**BD02**, 1.9 g), and n-butanol (**BD03**, 0.6 g) soluble materials. All extracts were purified based on bioassay-guided fractionation using antimicrotubule activity as shown in Scheme 1-3.

From the bioassay-guided fractionation, the dichloromethane and hexane extract (**BD01** and **BD02**) showed microtubule bundling activity. Thus, these extracts were then separately chromatographed over Sephadex LH-20 columns using 20% methanol in dichloromethane as an eluent to yield five fractions (**BD04-BD08**) (Scheme 1) and six fractions (**BD13-BD19**) (Scheme 2), respectively. Fractions **BD17** and **BD18** showing antimicrofilament activity were combined and further purified on Sephadex LH-20 using dichloromethane-hexane-methanol (75:20:5) to furnish **BD20** (latrunculin A) as a major compound (27 mg).

The active antimicrotubule fractions, **BD05** and **BD14**, were subjected to semi-preparative PRP-1 C18 polymer-based HPLC columns using gradient aqueous acetonitrile as eluting solvents (from 20% acetonitrile to 65% acetonitrile, with convex curve profile, in 12 min, then from 65% to 100% acetonitrile in 8 min, then flushing with 100% acetonitrile for additional 5 min, all at a constant flow rate of 1.5 mL/min), yielded the active fractions, **BD12** and **BD23**. Both active fractions were combined based on the same retention time at 15.7 min, similar TLC, and ^{1}H NMR patterns. The combined fraction was further purified using a semi-preparative silica gel HPLC column with isocratic 5% methanol in dichloromethane (flow rate 3 mL/min). The pure compound was obtained (**BD27**, 1.4 mg) and later identified as an active compound, laulimalide.

BD01 extract
(2.3 g)

Sephadex LH-20
20% MeOH in CH$_2$Cl$_2$

BD04	**BD05**	BD06	BD07	BD08
(280 mg)	(320 mg)	(470 mg)	(510 mg)	(600 mg)

PRP-1, C18 HPLC
Gradient H$_2$O : MeCN

BD09	BD10	BD11	**BD12**
(55 mg)	(48 mg)	(110 mg)	(70 mg)
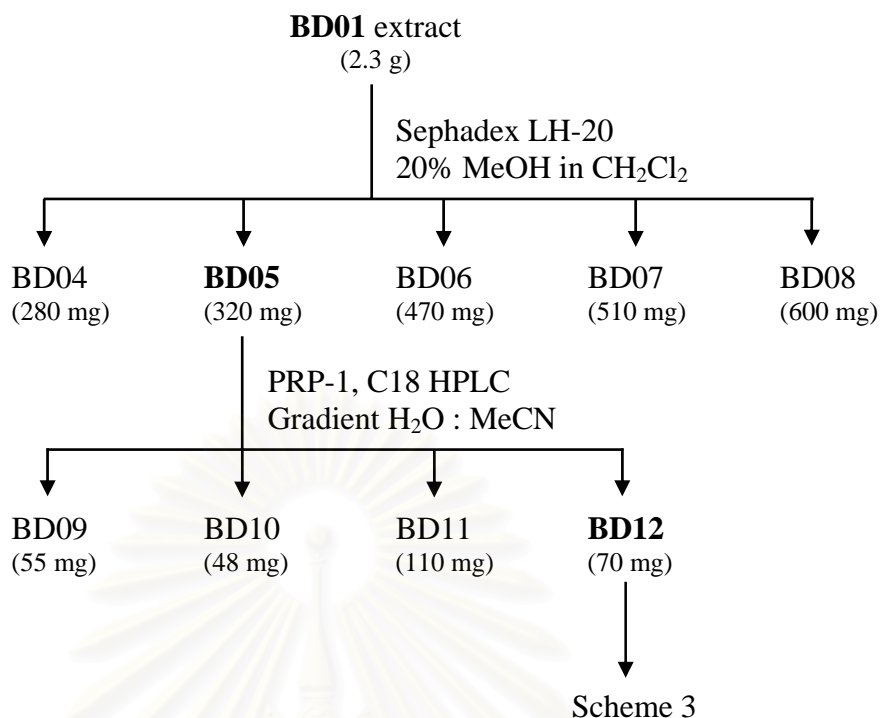
Scheme 3

Scheme 1   Isolation of the Hexane Extract from the Sponge *Cacospongia mycofijiensis*

BD02 extract
(1.9 g)

Sephadex LH-20
20% MeOH in CH$_2$Cl$_2$

BD13	**BD14**	BD15	BD16	**BD17**	**BD18**	BD19
(260 mg)	(150 mg)	(370 mg)	(360 mg)	(120 mg)	(175 mg)	(340 mg)

PRP-1, C18 HPLC
Gradient H$_2$O:MeCN

Sephadex LH-20
CH$_2$Cl$_2$:Hexane:MeOH
(75:20:5)

BD21	BD22	**BD23**	BD24
(20 mg)	(35 mg)	(32 mg)	(40 mg)

BD20
(latrunculin A)
(27 mg)
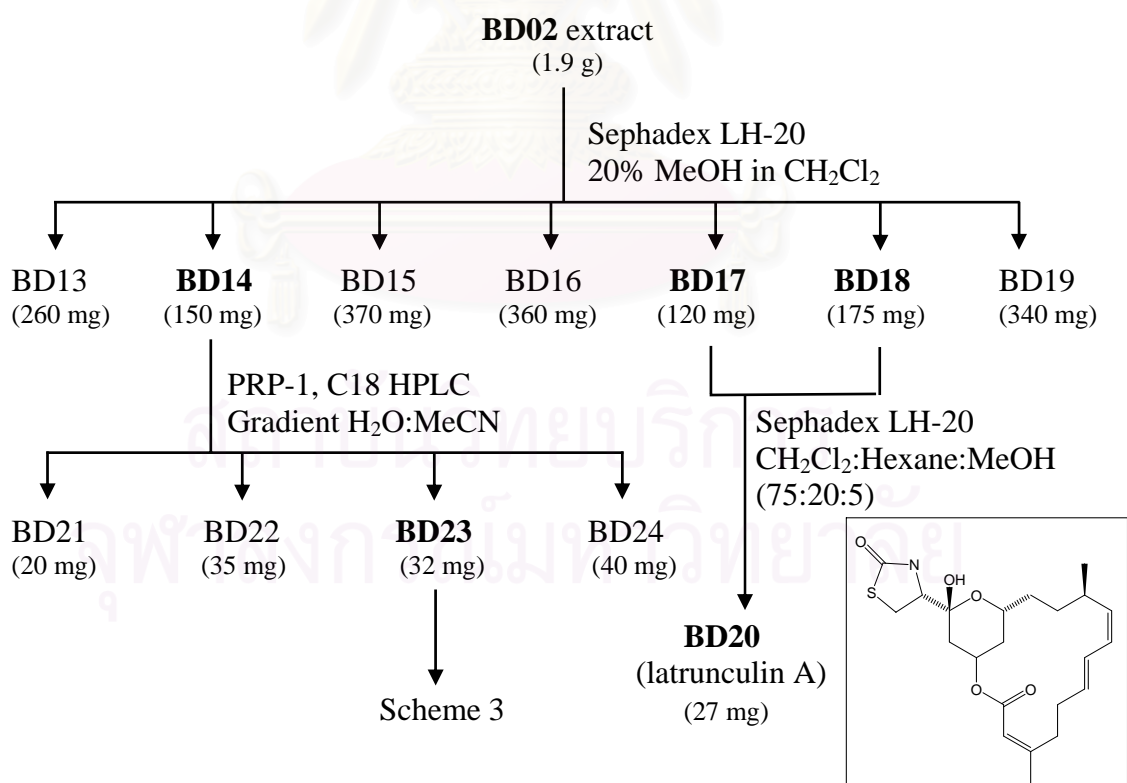
Scheme 3

Scheme 2   Isolation of the CH$_2$Cl$_2$ Extract from the Sponge *Cacospongia mycofijiensis*
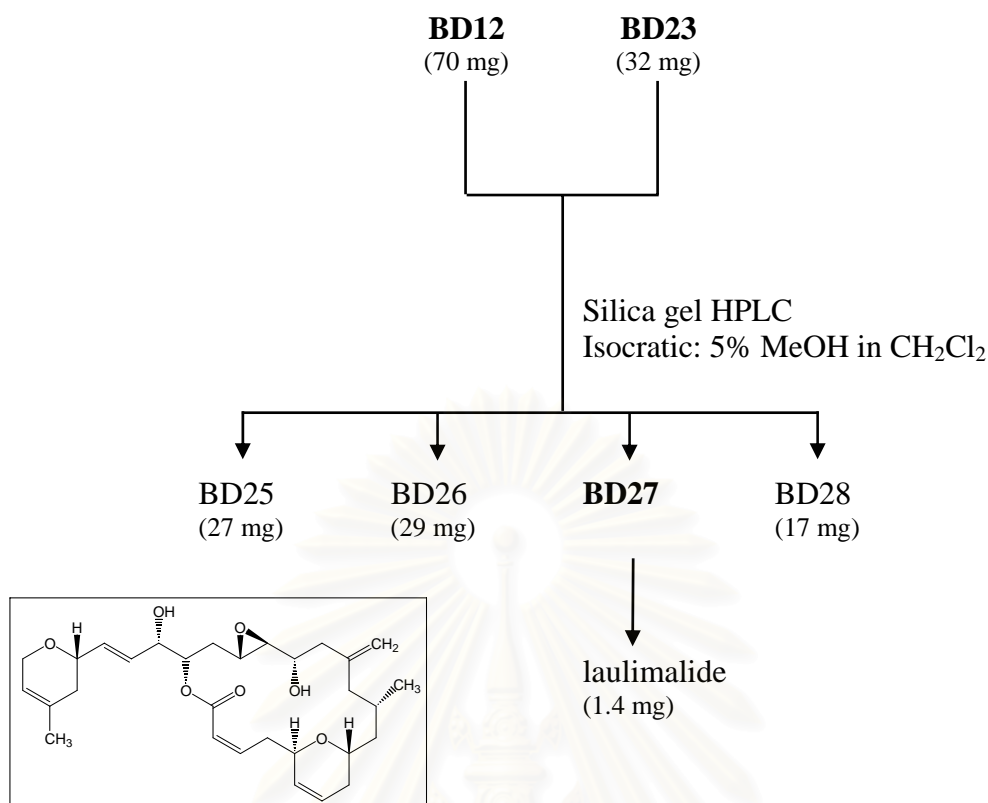
Scheme 3 Isolation of the Active Fractions from the Sponge *Cacospongia mycofijiensis*

Compound BD20 was obtained as a white foam (27 mg, 0.54% w/w based on the MeOH extract), soluble in CHCl$_3$.

TOFMS : [M+H]$^+$ *m/z* 422.03; Figure 16

UV : λ_{max} nm (ε), in MeOH; Figure 17

216 (23000), 318 (1307), 339 (1684)

IR : ν_{max} cm^{-1}, Film; Figure 18

3410 (br), 2922, 1693, 1441, 757

^{1}H NMR : δ ppm, 400 MHz, in CDCl$_3$; Table 1, Figure 13

^{13}C NMR : δ ppm, 100 MHz, in CDCl$_3$; Table 1, Figure 14

Compound BD27 was obtained as yellow oil (1.4 mg, 0.028% w/w based on the MeOH extract).

^{1}H NMR : δ ppm, 400 MHz, in CDCl$_3$; Table 2, Figure 19

4. Synthesis of the C$_1$-C$_{14}$ Fragment Analogs of Laulimalide

4-(*tert*-Butyldiphenylsilanyloxy)butan-1-ol (LAU01)

NaH (2.22 g of 60% dispersion in mineral oil, 55.5 mmol) was washed with 50 mL of dry hexane, dried under an atmosphere of nitrogen, and suspended in dry THF (100 ml). The 1,4-butanediol (5.0 g, 55.5 mmol) was added dropwise and the mixture was stirred at room temperature for 45 min, during which time white-opaque precipitate gradually developed. After that, *tert*-TBDPS Cl (9.15 g, 33.3 mmol) was added. After being stirred at room temperature for 1 hour, the mixture was diluted with diethyl ether, washed with saturated sodium bicarbonate and water, and dried over anhydrous sodium sulfate. After solvent removal, the resulting oil was chromatographed on a silica gel column using 30% diethyl ether in petroleum ether to yield 4-(*tert*-Butyldiphenylsilanyloxy)butan-1-ol (**LAU01**) as clear oil (17.3 g, 95%). ^{1}H NMR (CDCl$_3$, 400 MHz), Figure 20, δ (mult., *J* in Hz): 0.88 (s; 9H), 1.49 (m; 4H), 3.46 (br t, 3.2; 2H), 3.53 (br t, 5.2; 2H), 7.20 (m; 6H), 7.49 (m; 4H).

4-(*tert*-Butyldiphenylsilanyloxy)butyraldehyde (LAU02)

A slurry of oxalyl chloride (7 mL, 78.7 mmol) in dry CH$_2$Cl$_2$ (87 mL) was stirred at -78 ^{o}C for 15 min, and then DMSO (7 mL, 104.9 mmol) in dry CH$_2$Cl$_2$ (80 mL) was added dropwise. The mixture was stirred at -78 ^{o}C for 15 min, and the cooled **LAU01** (17.2 g, 52.4 mmol) in dry CH$_2$Cl$_2$ (126 mL) was then added quickly dropwise. The mixture was stirred at -78 ^{o}C for 30 min, and triethylamine (37 mL, 262.2 mmol) was added. After stirring at -78 ^{o}C for 15 min, the mixture was allowed to warm to room temperature, and stirred for one additional hour. Diethyl ether was then added and the mixture was washed with saturated ammonium chloride solution and brine, and dried over anhydrous sodium sulfate. The solvent was removed and the crude product was purified by a silica gel column using 10% diethyl ether in petroleum ether as eluent to furnish **LAU02** as yellow oil (16.6 g, 97% yield). ^{1}H NMR (CDCl$_3$, 400 MHz), Figure 21, δ (mult., *J* in Hz): 0.88 (s; 9H), 1.70 (quin, 7.0; 2H), 2.35 (td, 7.0, 1.6; 2H), 3.52 (t, 7.5; 2H), 7.20 (m; 6H), 7.47 (m; 4H), 9.60 (t, 1.6; 1H).

(3-[1,3]Dioxan-2-yl-propoxy)-*tert*-butyldiphenylsilane (LAU03)

To a solution of the aldehyde **LAU02** (16.5 g, 50.6 mmol) in dry benzene (327 mL), 1,3-propanediol (11 mL, 151.8 mmol) and pyridinium-*p*-toluenesulfonate (2.54 g, 10.1 mmol) were added and the mixture was refluxed in benzene at 91 $^{\circ}$C with water separation by a Dean-Stark trap apparatus until the starting aldehyde was completely used (overnight). The reaction was checked by measuring ^{1}H NMR to observe the disappeared aldehyde proton peak. After the reaction finished, the mixture was diluted with diethyl ether, washed with saturated sodium bicarbonate and water, dried over anhydrous sulfate, and evaporated to dryness. The residue was chromatographed on a silica gel column eluting with 10% diethyl ether in petroleum ether to give the pure product, **LAU03** (18.78 g, 97.0%). ^{1}H NMR (CDCl$_3$, 400 MHz), Figure 22, δ (mult., *J* in Hz): 0.88 (s; 9H), 1.31 (m; 1H), 1.66 (m; 4H), 2.04 (m; 1H), 3.63 (m; 4H), 4.05 (dt; 4.9, 6.8, 2H), 4.49 (t, 4.7; 1 H), 7.33 (m; 6H), 7.52 (m; 4H).

0.15 M Zinc borohydride (ZnBH$_4$)

Dissolved zinc chloride (60 g, 0.4 mol) in diethyl ether (75 mL) was added dropwise into stirred suspension of sodium borohydride (4.16 g, 0.1 mol) in anhydrous diethyl ether (225 mL). The mixture was stirred at room temperature for 16 hours. After salt setting, the supernatant solution was decanted through cotton plug and kept under nitrogen.

3-[(4-*tert*-Butyldiphenylsilanyloxy)-butoxy]-propan-1-ol (LAU04)

To a diethyl ether solution (10 mL) of the acetal **LAU03** (18.7 g, 48.7 mmol) at -20 $^{\circ}$C was added successively ZnBH$_4$ (187 mL of 0.15 M in diethyl ether solution; 28.0 mmol) and TMSCl (7 mL, 58.4 mmol). When TMSCl was added, a small amount of gas evolution was observed. The mixture was stirred at -20 $^{\circ}$C for 5.5 hours. During the reaction, the solution gradually turned cloudy white. The reaction was quenched with ammonium chloride and extracted with diethyl ether (3 × 30 mL). The combined extracts were dried and evaporated to afford pale yellow oil **LAU04** (18.31 g, 97.4%). ^{1}H NMR (CDCl$_3$, 400 MHz), Figure 23, δ (mult., *J* in Hz): δ (mult., *J* in Hz) 0.92 (s; 9H), 1.49 (m; 4H), 1.66 (m; 2H), 3.28 (t, 6.4; 2H), 3.42 (t, 5.8; 2H), 3.55 (t, 5.8; 2H), 3.60 (t, 5.6; 2H), 7.21 (m; 6H), 7.54 (m; 4H).

3-[4-(*tert*-Butyldiphenylsilanyloxy)-butoxy]-propyl benzoate (LAU05)

The alcohol **LAU04** (18.1 g, 46.9 mmol) in CH_2Cl_2 (500 mL) was cooled down to 0 °C. Subsequently, pyridine (19 mL, 234.5 mmol) and benzoyl chloride (11 mL, 93.8 mmol) was added. The mixture was stirred at 0 °C for 4 hours and quenched with ammonium chloride. The solution was extracted with diethyl ether (3 × 30 mL), washed with sodium bicarbonate and brine, and dried over anhydrous ammonium sulfate. After solvent removal, the resulting product was purified by a silica gel column with 10% ethyl ether in petroleum ether to yield **LAU05** as tan oil (21.28 g, 92.6%). ^{1}H NMR ($CDCl_3$, 400 MHz), Figure 24, δ (mult., *J* in Hz): 0.97 (s; 9H), 1.60 (m; 4H), 2.00 (m; 2H), 3.40 (t, 6.1; 2H), 3.52 (t, 6.3; 2H), 3.65 (t, 6.1; 2H), 4.39 (t, 6.4; 2H), 7.35 (m; 8H), 7.50 (m; 5H), 8.00 (m; 2H).

3-(4-Hydroxy-butoxy)-propyl benzoate (LAU06)

The starting material **LAU05** (21.1 g, 43.1 mmol) was dissolved in dry THF (27 mL) and a solution of tetra-n-butylammonium fluoride in THF (86 mL of 1.0 M solution, 86.1 mmol) was added with stirring at room temperature overnight. The mixture was partitioned between CH_2Cl_2 and water, washed with brine, and dried over anhydrous sodium sulfate. After solvent removal, the crude product was subjected to chromatography over a silica gel column using 30% petroleum ether in diethyl ether as an eluent generating **LAU06** as yellow oil (10.19 g, 94%). ^{1}H NMR ($CDCl_3$, 400 MHz), Figure 25, δ (mult., *J* in Hz): 1.46 (m; 4H), 1.84 (m; 2H), 3.28 (t, 5.6; 2H), 3.41 (t, 6.0; 2H), 3.92 (t, 7.0; 2H), 4.22 (t, 6.4; 2H), 7.19-7.86 (m; 5H).

3-(4-Oxo-butoxy)-propyl benzoate (LAU07)

To a slurry of oxalyl chloride (5 mL, 60.1 mmol) in dry CH_2Cl_2 (67 mL) at -78 °C was added dropwise DMSO (6 mL, 80.2 mmol). The mixture was stirred at -78 °C for 15 min and the alcohol **LAU06** (10.1 g, 40.1 mmol) was added. The mixture was further stirred for 30 min at -78 °C and triethylamine (28 mL, 200.4 mmol) was added. After stirring at -78 °C for 15 min, the mixture was allowed to warm to room temperature where it was stirred for one additional hour, at which time diethyl ether was added. The mixture was washed with saturated ammonium chloride solution and brine, dried over anhydrous sodium sulfate, and the solvent was removed. Chromatography of the crude product over a silica gel column with petroleum

ether/ethyl acetate (15:1) afforded the aldehyde **LAU07** as yellow oil (8.0 g, 80%). ^{1}H NMR (CDCl$_3$, 400 MHz) , Figure 26, δ (mult., J in Hz): 1.86 (quin, 6.1; 2H), 1.99 (quin, 6.3; 2H), 2.49 (td; 5.2, 1.6, 2H), 3.44 (t, 6.0; 2H), 3.53 (t, 6.4; 2H), 4.38 (t, 6.4; 2H), 7.41 (m; 2H), 7.51 (m; 1H), 8.01 (m; 2H), 9.74 (t, 1.6; 1H).

Eschenmoser's salt

To a solution of *N,N,N′,N′*-tetramethyldiaminomethane (22 mL, 161.3 mmol) in 125 mL dry diethyl ether, the solution of acetyl chloride (13 mL, 177.4 mmol) in diethyl ether was added. The mixture was stirred until crystals precipitating. Filtered crystals in Buchner funnel, and then washed with diethyl ether 3-5 times until the filtrate was colorless. After drying briefly on funnel, the product (14.7 g, 97.4%) was transferred to a bottle quickly and flushed with nitrogen before sealed.

3-(3-Formyl-but-3-enyloxy)-propyl benzoate (LAU08)

Eschenmoser's salt (11.2 g, 119.1 mmol) was added to a slurry of the aldehyde **LAU07** (7.8 g, 29.8 mmol) in dry CH$_2$Cl$_2$. The mixture was stirred at room temperature for 2 days and then checked the reaction with ^{1}H NMR. After the aldehyde proton signal in ^{1}H NMR showed coupling pattern in doublet instead of triplet peak, the reaction was chilled to 0 ^{o}C and added triethylamine (25 mL, 178.6 mmol) dropwise. The mixture was allowed to warm to room temperature and stirred until the adehyde proton showed singlet peak in ^{1}H NMR. The mixture was partitioned with diethyl ether and water, and the organic layer was washed with ammonium chloride, and dried over anhydrous sodium sulfate. After solvent removal, unsaturated aldehyde **LAU08** (6.4 g, 82%) was obtained. The compound was carried through to the next step immediately without further purification. ^{1}H NMR (CDCl$_3$, 400 MHz) , Figure 27, δ (mult., J in Hz): 1.18 (t, 6.4, 2H), 1.98 (m; 2H), 3.44 (t, 6.8; 2H), 3.53 (t, 6.4; 2H), 4.37 (t, 6.4; 2H), 6.03 (s; 1H), 6.34 (s; 1H), 7.41 (m; 2H), 7.53 (m; 1H), 8.00 (m; 2H), 9.45 (s; 1H).

3-(3-Hydroxymethyl-but-3-enyloxy)-propyl benzoate (LAU09)

The unsaturated aldehyde **LAU08** (6.1 g, 23.1 mmol) was dissolved in absolute ethanol (400 mL) and a solution of cerium (III) chloride heptahydrate (9.5 g, 25.4 mmol) in absolute ethanol (200 mL) was added. The solution was cooled to -78

^{o}C and added sodium borohydride (1.9 g, 32.3 mmol) slowly. After stirring at -78 ^{o}C until the reaction done, the mixture was allowed to warm to room temperature and excess ammonium solution was added until a white colloidal suspension developed. The mixture was partitioned between diethyl ether and saturated sodium bicarbonate and the organic layer was washed with brine, and then dried over anhydrous sodium sulfate. The unsaturated alcohol **LAU09** (5.8 g, 95%) that was obtained after solvent removal was carried through to the next step immediately without further purification. ^{1}H NMR (CDCl$_3$, 400 MHz), Figure 28, δ (mult., J in Hz): 2.03 (quin, 6.3; 2H), 2.36 (t, 6.2; 2H), 3.56 (m; 2H), 3.70 (m; 2H), 4.06 (s; 2H), 4.40 (t, 6.4; 2H), 4.90 (s; 1H), 5.04 (s; 1H), 7.42 (m; 2H), 7.53 (m; 1H), 8.01 (m; 2H).

3-[3-(*tert*-Butyldiphenylsilanyloxymethyl)-but-3-enyloxy]-propyl benzoate (LAU10)

To a solution of the unsaturated alcohol **LAU09** (5.2 g, 19.7 mmol) in CH$_2$Cl$_2$ (35 mL), imidazole (5.36 g, 78.8 mmol) and *tert*-butylchlorodiphenylsilane (7 mL, 24.6 mmol) were added and stirred at room temperature overnight. The mixture was partitioned between diethyl ether and water, washed with ammonium chloride and brine, and dried over anhydrous sodium sulfate. After the solvent was removed, the crude product was chromatographed over a silica gel column using petroleum ether/diethyl ether (15:1) as solvent to afford **LAU10** in yellow oil (8.31 g, 84%). ^{1}H NMR (CDCl$_3$, 400 MHz), Figure 29, δ (mult., J in Hz): 1.06 (s; 9H), 1.96 (quin, 6.3; 2H), 2.27 (br t, 6.9; 2H), 3.48 (t, 6.9; 2H), 3.50 (t, 6.3; 2H), 4.11 (s; 2H), 4.35 (t, 6.4; 2H), 4.90 (d, 1.2; 1H), 5.19 (d, 1.2; 1H), 7.33-8.10 (m; 15H).

3-[3-(*tert*-Butyldiphenylsilanyloxymethyl)-but-3-enyloxy]-propan-1-ol (LAU11)

To cleave the benzoyl group, **LAU10** (8.2 g, 16.3 mmol) in CH$_2$Cl$_2$ (250 mL) was cooled down to -78 ^{o}C and then added dropwise of DIBAH (40 mL, 40.8 mmol, 1.0 M in cyclohexane). The mixture was stirred at -78 ^{o}C. After the TLC was done, the mixture was quenched with water and warmed to room temperature. Then solid NaHCO$_3$ and EtOAc were added and continuously stirred for 30 min. The mixture was diluted with CH$_2$Cl$_2$ and then filtered. After the filtrate was concentrated under reduced pressure, the resulting oil was purified by a silica gel column using petroleum ether/diethyl ether (2:1) as eluent to afford **LAU11** (6.25 g, 96%). ^{1}H NMR (CDCl$_3$,

400 MHz), Figure 30, δ (mult., *J* in Hz): 1.05 (s; 9H), 1.76 (quin, 5.6; 2H), 2.28 (br t, 6.8; 2H), 3.48 (t, 6.8; 2H), 3.54 (t, 6.0; 2H), 3.69 (t, 5.6; 2H), 4.11 (s; 2H), 4.90 (d, 1.2; 1H), 5.18 (d, 1.2; 1H), 7.36 (m; 6H), 7.66 (m; 4H).

3-[3-(*tert*-Butyldiphenylsilanyloxymethyl)-but-3-enyloxy]-propionaldehyde (LAU12)

To a slurry of oxalyl chloride (2 mL, 23.0 mmol) in dry CH_2Cl_2 (206 mL) at -78°C was added dropwise DMSO (2 mL, 30.7 mmol). The mixture was stirred at -78 °C for 15 min and the alcohol **LAU11** (6.1 g, 15.3 mmol) was added. The mixture was further stirred for 30 min at -78 °C and triethylamine (11 mL, 76.7 mmol) was added. After stirring at -78 °C for 15 min, the mixture was allowed to warm to room temperature where it was stirred for one additional hour, at which time diethyl ether was added. The mixture was washed with saturated ammonium chloride solution and brine, dried over anhydrous sodium sulfate, and the solvent was removed. **LAU12** was then obtained in 95% yield (5.76 g). ^{1}H NMR ($CDCl_3$, 400 MHz), Figure 31, δ (mult., *J* in Hz): 1.04 (s; 9H), 2.26 (br t, 6.7; 2H), 2.56 (td, 1.8, 6.2; 2H), 3.48 (t, 6.8; 2H), 3.68 (t, 6.2; 2H), 4.10 (s; 2H), 4.88 (d, 1.6; 1H), 5.18 (d, 1.6; 1H), 7.37 (m; 6H), 7.65 (m; 4H), 9.71 (t, 1.6; 1H).

2,4-Dimethoxybenzyl (DMB) alcohol

The solution of 2,4-dimethylbenzoic acid (15 g, 82.3 mmol) in THF (170 mL) was added to the solution of LAH (2.63 g, 82.3 mmol) in THF (315 mL). The mixture was stirred at room temperature for 30 min to 1 hour (until the TLC was done) and then cooled to 0°C. Then water (10 mL) and 10% NaOH (3 mL) were added and stirred for 30 min. After precipitate was removed through celite, the mixture was washed with diethyl ether, dried and concentrated to furnish **DMB alcohol** (11.63 g, 84%). ^{1}H NMR ($CDCl_3$, 400 MHz), Figure 32, δ (mult., *J* in Hz): 3.78 (s; 3H), 3.83 (s; 3H), 4.59 (s; 2H), 6.43 (m; 2H), 7.14 (d, 8.0; 1H).
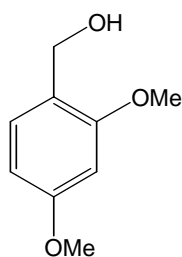
DMB alcohol

2,4-Dimethoxybenzyl (DMB) bis(diethylphosphono)acetate

The bis(diethylphosphono)acetic acid (12.24 g, 62.4 mmol) in THF (587 mL) was added to DMB alcohol (7 g, 41.6 mmol). The solution was cooled to 0 ^{o}C and then added DCC (12.88 g, 62.4 mmol). The solution was stirred at room temperature for 1.5 hours. The mixture was partitioned between diethyl ether and water, washed with brine, and dried over anhydrous sodium sulfate. After the solvent was removed, the crude product was chromatographed over a silica gel column using petroleum ether/diethyl ether (1:2.5) as solvent to afford 2,4-dimethoxybenzyl (DMB) bis(diethylphosphono) acetate (14.0 g, 97%)
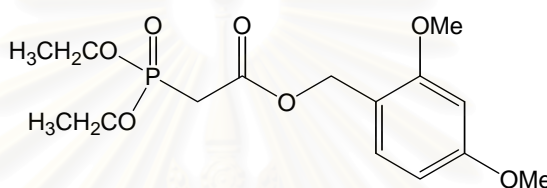
**2,4-dimethoxybenzyl (DMB)
bis(diethylphosphono)acetate**

5-[3-(tert-Butyldiphenylsilanyloxymethyl)-but-3-enyloxy]-pent-2Z-ene-1-(2,4-dimethoxy)benzyl ester (LAU13)

A solution of 2,4-dimethoxybenzyl (DMB) bis(2,2,2-trifluoroethylphosphono) acetate (2.18 g, 4.8 mmol), 18-crown-6 (6.34 g, 24.0 mmol) in 163 mL anhydrous THF was cooled to -78 ^{o}C under nitrogen and treated with (10 mL, 4.8 mmol) of KN(TMS)$_2$. The aldehyde **LAU12** (1.9 g, 4.8 mmol) in anhydrous THF 16 mL was then added and the resulting mixture was stirred for 30 min to 1 hour at -78 ^{o}C. Saturated NH$_4$Cl was added and the product was extracted into diethyl ether (3 × 50 mL). The extract was dried and evaporated, and the product was isolated by flash column chromatography using petroleum ether/diethyl ether (3:1) as mobile phase to furnish **LAU13** (2.6 g) in 92% yield.

TOFMS : [M+ Na]$^+$ *m/z* 611; Figure 33

UV : λ_{max} nm (ε), in methanol; Figure 34

207 (21000), 394 (106)

IR : ν_{max} cm^{-1}, Film; Figure 35

2931, 2858, 1697, 1430, 1111, 704, 505

^{1}H NMR : (CDCl$_3$, 300 MHz), Figure 36

δ (mult., *J* in Hz): 0.90 (s; 9H), 2.12 (t, 6.9; 2H), 2.74 (dq, 1.4, 6.2; 2H), 3.30 (t, 6.2; 2H), 3.31 (t, 7.0; 2H), 3.64 (s; 3H), 3.65 (s; 3H), 3.96 (s; 2H), 4.76 (br d, 1.0; 1H), 4.97 (s; 2H), 5.06 (br d, 1.0; 1H), 5.66 (dt, 1.8, 11.5; 1H), 6.09 (dt, 6.2, 11.5; 1H), 6.30 (m; 2H), 7.09 (m; 1H), 7.25 (m; 6H), 7.52 (m; 4H)

¹³C NMR : (CDCl₃, 75 MHz), Figure 37

δ: 19.4, 26.9, 29.7, 33.1, 55.4, 55.5, 61.2, 66.6, 69.5, 69.6, 98.5, 103.9, 110.1, 116.6, 120.8, 127.5, 129.5, 131.2, 133.5, 135.4, 145.2, 146.7, 158.7, 161.0, 166.1

5-[3-(tert-Butyldiphenylsilanyloxymethyl)-but-3-enyloxy]-pent-2*E*-ene-1-(2,4-dimethoxy)benzyl ester (LAU14)

To a stirring suspension of NaH (126.7 mg, 5.3 mmol) in 35 mL of THF, was added dropwise a solution of 2,4-dimethoxybenzyl (DMB) bis(diethylphosphono) acetate (1.99 g, 5.8 mmol). After stirring for 10 min at room temperature, the aldehyde **LAU12** (1.9 g, 4.8 mmol) was added dropwise. After being stirred for 2 hours, the mixture was quenched by the addition of 5 mL of water. The mixture was diluted with 10 mL of diethyl ether, and the organic layer was washed with saturated brine, dried, and filtered. The solvent was removed with a rotary evaporator to afford the product **LAU14** (2.42 g) as colorless oil in 86% yield.

TOFMS : [M+ Na]⁺ *m/z* 611; Figure 41

UV : λ_{max} nm (ε), in methanol; Figure 42

207 (22100), 256 (867), 265 (1071)

IR : ν_{max} cm⁻¹, Film; Figure 43

2932, 2858, 1698, 1111, 705, 506

¹H NMR : (CDCl₃, 300 MHz), Figure 44

δ (mult., *J* in Hz): 0.87 (s; 9H), 2.10 (t, 6.9; 2H), 2.22 (dq, 1.5, 6.7; 2H), 3.30 (t, 6.8; 2H), 3.27 (t, 6.0; 2H), 3.62 (s; 6H), 3.93 (s; 2H), 4.75 (br d, 1.6; 1H), 4.99 (s; 2H), 5.05 (br d, 1.6; 1H), 5.72 (dt, 1.5, 15.7; 1H), 6.30 (m; 2H), 6.78 (dt, 6.8, 15.7; 1H), 7.09 (m; 1H), 7.25 (m; 6H), 7.52 (m; 4H)

¹³C NMR : (CDCl₃, 75 MHz), Figure 45

δ: 19.4, 26.9, 32.7, 33.1, 55.4, 55.5, 61.4, 66.6, 68.8, 69.9, 98.5, 104.0, 110.3, 116.8, 122.7, 127.6, 129.5, 131.1, 133.5, 135.3, 145.0, 145.4, 158.7, 160.9, 166.3

3-[3-(tert-Butyldiphenylsilanyloxymethyl)-but-3-enyloxy]-propionic acid (LAU15)

A solution of 8 mL (5.8 mmol) of stock solution 0.762 M NaClO₂ was added dropwise to a 10 min stirred mixture of 1.9 g (4.8 mmol) of the aldehyde **LAU12** in AcCN 46 mL and NaH₂PO₄ (2 mL of stock solution 0.580 M, 1.1 mmol) and 5 mL (0.6 mmol) of 30% H₂O₂, keeping the temperature at 10 °C with water cooling. The solution turned to yellow and then was stirred at 10-18 °C until the color of solution vanished. A small amount (48.4 mg, 0.4 mmol) of Na₂SO₃ was added to destroy the unreacted HOCl and H₂O₂. The mixture was diluted with EtOAC, acidified with 2% aqueous HCl, and washed organic layer with water (3 × 30 mL). The resulting product **LAU15** (1.58 g) was obtained in 80% yield after solvent removal.

UV : λ_{max} nm (ε), in methanol; Figure 49

203 (18760)

IR : ν_{max} cm⁻¹, Film; Figure 50

3071, 2932, 2859, 1718, 1428, 1112, 705, 506

¹H NMR : (CDCl₃, 300 MHz), Figure 51

δ (mult., *J* in Hz): 1.05 (s; 9H), 2.28 (t, 6.9; 2H), 2.55 (t, 6.3; 2H), 3.52 (t, 6.9; 2H), 3.65 (t, 6.3; 2H), 4.10 (s; 2H), 4.90 (br d, 0.9; 1H), 5.19 (br d, 0.9; 1H), 6.00 (br s; 1H), 7.38 (m; 6H), 7.66 (m; 4H)

¹³C NMR : (CDCl₃, 75 MHz), Figure 52

δ: 19.4, 26.9, 33.0, 34.7, 65.7, 66.9, 69.9, 110.4, 127.6, 129.7, 134.6, 135.4, 144.8, 175.7

3-[3-(tert-Butyldiphenylsilanyloxymethyl)-but-3-enyloxy]-propionic acid-(2,4-dimethoxy) benzyl ester (LAU16)

To a stirred solution of the carboxylic acid **LAU15** (1.5 g, 3.6 mmol) in 16 mL of anhydrous CH₂Cl₂ was added 1.13 g (5.5 mmol) of DCC, and 918 mg (5.5 mmol) of DMB alcohol. Then 4-DMAP (133.4 mg, 1.1 mmol) was added to the reaction

mixture and allowed to stand at room temperature until esterification was completed. The reaction mixture was cooled down with ice, and then filtered out the *N,N*-dicyclohexyl urea. The filtrate was diluted with CH_2Cl_2, washed with water and NH_4Cl, dried, and evaporated to remove the solvent. The crude product was purified by a flash column chromatography using the mobile phase as petroleum ether/diethyl ether (3:1) to give the ester **LAU16** (1.37 g) in 67% yield.

TOFMS : $[M+ Na]^+$ *m/z* 585; Figure 53

UV : λ_{max} nm (ε), in methanol; Figure 54

207 (31000), 260 (1448), 265 (1502), 271 (1341)

IR : ν_{max} cm^{-1}, Film; Figure 55

2932, 2859, 1716, 1508, 1297, 1112, 705, 506

^{1}H NMR : (CDCl$_3$, 300 MHz), Figure 56

δ (mult., *J* in Hz): 0.90 (s; 9H), 2.11 (t, 7.0; 2H), 2.36 (t, 6.6; 2H), 3.32 (t, 7.0; 2H), 3.48 (t, 6.6; 2H), 3.62 (s; 3H), 3.63 (s; 3H), 3.95 (s; 2H), 4.75 (br d, 1.2; 1H), 4.95 (s; 2H), 5.05 (br d, 1.2; 1H), 6.29 (m; 2H), 7.05 (m; 1H), 7.23 (m; 6H), 7.51 (m; 4H)

^{13}C NMR : (CDCl$_3$, 75 MHz), Figure 57

δ: 19.4, 26.9, 33.0, 35.2, 55.4, 55.5, 61.7, 66.1, 66.6, 69.8, 98.5, 104.0, 110.1, 116.6, 127.5, 129.5, 131.1, 133.4, 135.3, 145.0, 158.7, 161.0, 171.4

5. Determination of Antimicrotubule Activity

The morphological effects on microtubule were examined by indirect immunofluorescence techniques (Mooberry *et al.*, 1999).

A-10 (aortic smooth muscle) cells were plated onto glass cover-slips and growth until 70-85% confluent, and then treated with tested compounds. The cells were fixed with ice-cold methanol for 5 min, blocked for 20 min with 10% calf serum in PBS (phosphate buffer saline), and incubated for 90 min with monoclonal β-tubulin antibody (T-4026; Sigma Chemical Co., St. Louis, MO). After a series of washes, the cells were incubated with FITC-conjugated sheep antimouse IgG (F-3008; Sigma Chemical Co.) for 1 hour. The cover-slips were washed, stained with 0.1 μg/mL DAPI (4,6-diamino-2-phenylindole) for 10 min, and mounted. Cellular microtubules and chromatin were visualized and photographed using a Zeiss Axioplan fluorescence microscope with optics for fluorescein and DAPI.

CHAPTER IV

RESULTS AND DISCUSSION

A solvent partition scheme yielded fractions of hexane, dichloromethane, and n-butanol soluble materials. The antimicrotubule active hexane and dichloromethane fractions were then separately chromatographed over Sephadex LH-20 columns, allowing the majority of latrunculin A to be removed. The active fractions, as monitored by the antimicrotubule assay, were purified by semi-preparative RP-18 HPLC followed by a semi-preparative HPLC silica gel column, yielding the active antimicrotubule compound, laulimalide. The syntheses of three structural analogs of the C1-C14 fragment of laulimalide, including **LAU13, LAU14**, and **LAU16**, were achieved by using 1,4-butanediol as a starting material. The fragment analogs **LAU13** and **LAU14** were synthesized in 13 steps while **LAU16** in 14 steps.

1. Structure Determination of the Isolated Compounds

1.1 Structure Determination of BD20 (Latrunculin A)

Previous research indicated that the sponge *Cacospongia mycofijiensis* from Marshall Island contained latrunculin A as a major component. The chemical shift assignments (Groweiss, Shmueli, and Kashman, 1983) and the absolute configurations (Jefford and Bernardinelli, 1996) of this compound have been reported. Bioassay-guided fractionation of the CH_2Cl_2 extract led to isolation of **BD20** as white foam in 27 mg (0.54% w/w based on the MeOH extract). The molecular formula of $C_{22}H_{31}NO_5S$ was confirmed by TOFMS at $[M+H]^+$ m/z 422. The ^1H (Figure 13) and ^{13}C NMR spectra (Figure 14) were determined by using $CDCl_3$ as a solvent. The identification of **BD20** was mainly through comparison of its NMR data with the reported data (Groweiss *et al.*, 1983) as summarized in Table 1 and Figure 15. Compound **BD20** was unambiguous identified as latrunculin A.
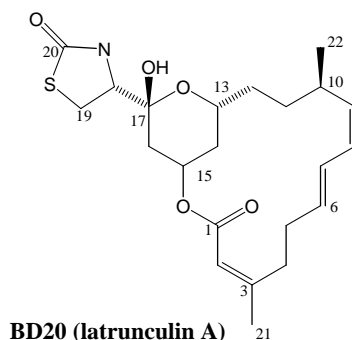
BD20 (latrunculin A)

Table 1 ¹H (400 MHz) and ¹³C (100 MHz) NMR Spectral Data of **BD20** (Latrunculin A)

position	δ_C (mult.) in CDCl₃		δ_H (mult., J in Hz) in CDCl₃	
	Latrunculin A*	**BD20**	Latrunculin A*	**BD20**
1	166.0 (s)	166.3		-
2	117.6 (d)	118.0	5.69 (d, 1.3; 1H)	5.68 (br s; 1H)
3	158.3 (s)	159.2		-
4	32.7 (t)	33.0	3.00 (dt, 13.0, 8.0; 1H)	2.90 (m; 1H)
			2.60 (dt, 13.0, 8.0; 1H)	2.60 (m; 1H)
5	30.6 (t)	30.8	2.26 (m; 2H)	2.27 (m; 2H)
6	131.8 (d)	132.5	5.74 (dt, 15.0, 4.5; 1H)	5.74 (dt, 14.9, 4.9; 1H)
7	126.3 (d)	126.7	6.41 (dd, 15.0, 10.5; 1H)	6.38 (dt, 14.9, 10.7; 1H)
8	127.3 (d)	127.8	5.98 (t, 10.5; 1H)	5.95 (t, 10.7; 1H)
9	136.5 (d)	137.2	5.02 (t, 10.5; 1H)	4.90 (t, 10.7; 1H)
10	29.2 (d)	29.5	2.83 (m; 2H)	2.74 (m; 1H)
11	31.8 (t)	31.9		
12	31.2 (t)	31.4		
13	62.3 (d)	62.7	4.29 (m; 1H)	4.25 (m; 1H)
14	35.1 (t)	35.3		
15	68.1 (d)	68.6	5.43 (br t, 3.0; 1H)	5.38 (br t, 2.6; 1H)
16	32.1 (t)	32.1		
17	96.9 (s)	97.8		-
18	62.1 (d)	61.9	3.87 (dd, 8.0, 7.0; 1H)	3.84 (dd, 7.5, 7.3; 1H)
19	28.7 (t)	29.0	3.51 (dd, 11.5, 7.0; 1H)	3.49 (dd, 11.4, 7.5; 1H)
			3.48 (dd, 11.5, 8.0; 1H)	3.43 (dd, 11.4, 7.3; 1H)
20	175.5 (s)	175.8		-
21	24.7 (q)	24.8	1.90 (d, 1.5; 3H)	1.90 (br s, 3H)
22	21.8 (q)	21.9	0.98 (d, 6.6; 3H)	0.97 (d, 6.4; 3H)
NH			5.80 (br s; 1H)	5.82 (br s; 1H)

*Groweiss *et al.*, 1983

1.2 Structure Determination of BD27 (Laulimalide)

Using antimicrotubule-guided assay, fractions (**BD12** and **BD23**) which caused the morphological change were separated to yield compound **BD27** (1.4 mg, 0.028 % w/w based on the MeOH extract).

The ^{1}H NMR spectrum of compound **BD27** (Figure 19, Table 2) was obtained using benzene-d_6 as the solvent. The overlapping signals in the spectrum, especially in the upfield region, caused difficulty in the chemical shift assignments. Attempts to conduct the 2D NMR experiments on compound **BD27** failed due to the small amount of sample. Therefore, the ^{1}H chemical shifts of **BD27** were assigned by direct comparison with the reported data. With some slight deviation, the chemical shift assignments fit well with those assigned to fijianolide B (Quinoa *et al.*, 1988) or commonly known as laulimalide (Corley *et al.*, 1988). Compound **BD27**, thus, was identified as laulimalide.
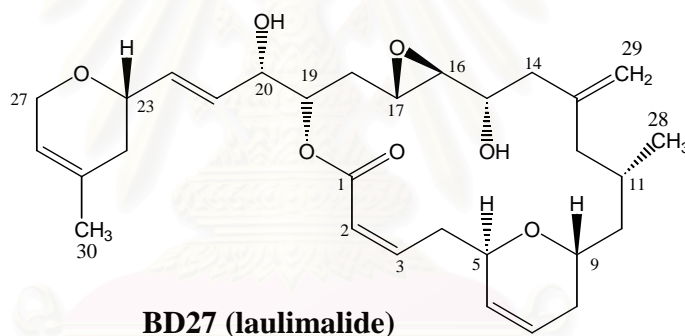
BD27 (laulimalide)

Table 2 ^{1}H (400 MHz) NMR Spectral Data of **BD27** (Laulimalide)

^{1}H	δ (mult., J in Hz) in C_6D_6	
	Fijianolide B*	**BD27**
2	5.80 (d, 12.3)	5.73 (d, 10.9; 1H)
3	6.12 (ddd, 12.3, 10.8, 4.5)	6.05 (ddd, 10.9, 9.9, 3.5; 1H)
4	3.90 (m)	3.88 (m; 1H)
	2.08 (m)	2.00 (m; 1H)
5	4.12 (m)	4.11 (m; 1H)
6	5.48 (br d, 10.2)	5.44 (br d, 10.2; 1H)
7	5.67 (br d, 10.2)	5.64 (m; 1H)
8	1.75 (m)	1.78 (m; 2H)
9	3.71 (m)	3.69 (m; 1H)
10	1.50 (m)	1.52 (m; 1H)
	1.20 (br d, 12.0)	1.19 (br d, 14.4; 1H)
11	1.75 (m)	1.78 (m; 1H)
12	2.55 (dd, 10.8, 2.4)	2.58 (dd, 13.1, 4.2; 1H)
	1.85 (dd, 10.8, 5.4)	1.89 (dd, 13.1, 9.9; 1H)
14	2.13 (br s)	2.13 (br s; 1H)
	2.14 (br s)	2.14 (br s; 1H)
15	4.04 (m)	3.92 (m; 1H)
16	2.84 (dd, 2.1, 2.1)	2.74 (br s; 1H)
17	3.10 (ddd, 11.1, 1.9, 1.9)	2.91 (dt, 6.4, 3.0; 1H)
18	2.36 (ddd, 10.8, 1.5, <1)	2.18 (m; 1H)
	1.55 (m)	1.43 (m; 1H)
19	5.25 (ddd, 10.5, 3.9, 1.8)	5.12 (m; 1H)
20	4.18 (dd, 9.3, 4.5)	3.92 (m; 1H)
21	5.81 (dd, 16.2, 5.4)	5.71 (dd, 15.8, 3.8; 1H)
22	5.94 (dd, 16.2, 5.4)	5.81 (dd, 15.8, 4.7; 1H)
23	3.90 (m)	3.86 (m; 1H)
24	2.03 (m)	1.92 (m; 1H)
	1.60 (m)	1.60 (m; 1H)
26	5.16 (br s)	5.15 (br s; 1H)
27	3.95 (br s)	4.00 (br d, 14.5; 1H)
	4.09 (br s)	4.11 (br d, 14.5; 1H)
28	0.86 (d, 6.0)	0.87 (d, 6.4; 3H)
29	4.89 (br s)	4.89 (br s; 1H)
	4.94(br s)	4.91 (br s; 1H)
30	1.50 (s)	1.50 (s; 3H)

2. Antimicrotubule Activity

The first cytotoxicity testing of laulimalide by the researcher from Hawaii showed that laulimalide was significantly active against the KB cell line in nanomolar range (IC_{50}: 5 ng/mL) while its isomer isolaulimalide showed lower activity with IC_{50}: > 200 ng/mL (Corley *et al.*, 1988). In the adjoining communication (Quinoa *et al.*, 1988), the inhibition of cell growth was investigated with synthetic laulimalide diacetate and isolaulimalide, using HT-29 (human colon tumor), P388 (murine lymphoma), A549 (human lung tumor), and HL-60 (human promyelocytic leukemia) cells. IC_{50} values in the low micromolar range, 9-14 and 0.5-6 μM, were obtained for C_{15}-O, C_{20}-O-diacetyl-laulimalide and isolaulimalide, respectively. In Higa's more recent study (Tanaka *et al.*, 1996), the same cell lines and the additional MEL28 cell line were used to determine the activity of laulimalide and its minor congener neolaulimalide. Very high activity (IC_{50} = 0.01-0.05 μM) was observed for both compounds in the same assay.

In February 1999, laulimalide and isolaulimalide were identified as new microtubule-stabilizing agents (Mooberry *et al.*, 1999). Treatment of A-10 cells (rat aortic smooth muscle cell line, a nontransformed line) with laulimalide resulted in a dose-dependent reorganization of the microtubule network in the cells and in the formation of microtubule bundles and abnormal mitotic spindles. The morphological effects on microtubules were examined by indirect immunofluorescence techniques and the result was shown in Figure 4. In A-10 cells treated with paclitaxel (1-20 μM), long thick microtubule bundles were found surrounding the nucleus with a highly organized array of microtubules. The effect of laulimalide at 2 μM concentration closely resembled that of paclitaxel. Nonetheless, at a concentration of 20 μM, treated cell exhibited short tufts of microtubule bundles.

Laulimalide and isolaulimalide also induced polymerization of purified bovine brain tubulin *in vitro*. Interestingly, while at a low concentration (2 μM) laulimalide was less potent than paclitaxel, at a higher concentration (20 μM) laulimalide became more effective, with more tubulin polymers observed. The polymers formed in the presence of laulimalide were longer, with less branching than that of paclitaxel (Mooberry *et al.*, 1999).

Like paclitaxel, laulimalide inhibited proliferation of the drug-sensitive cell lines SK-OV-3 (ovarian carcinoma) and MDA-MB-435 (human breast

adenocarcinoma), with the IC_{50} values being between 5 and 12 nM. Isolaulimalide was less potent with IC_{50} values in the low μM range. In contrast to paclitaxel, both laulimalide and isolaulimalide inhibited the proliferation of the multidrug-resistant SKVLB-1 cell line (a subline of SK-OV-3) that overexpressed the drug efflux pump P-glycoprotein (Mooberry *et al.*, 1999). These data suggested that laulimalide and isolaulimalide are poor substrates for transportation by P-glycoprotein, a property that may provide advantages over the taxanes.
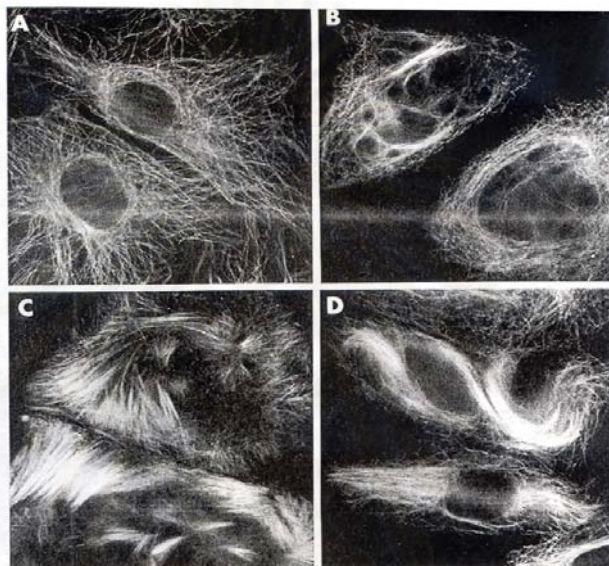
Figure 4 Effects of Laulimalide on Microtubule

; control (**A**), 2 μM laulimalide (**B**), 20 μM laulimalide (**C**), 2 μM paclitaxel (**D**) (Moobery *et al.*, 1999)

Further exciting data were recently communicated by Hamel's group (Pryor *et al.*, 2002). It was shown that laulimalide was unable to inhibit the binding of [^{3}H]-paclitaxel or a fluorescent paclitaxel derivative to tubulin. Moreover, microtubules formed in the presence of laulimalide and paclitaxel contained approximately equivalent quantities of both drugs. These findings strongly suggested the existence of a drug binding site on microtubules distinct from that occupied by taxoids. Results obtained with paclitaxel- and epothilone-resistant cell lines bearing mutated β-tubulin genes further supported this conclusion and underlined the high biological potential of laulimalide.

To date, only few initial studies concerned the effect of synthetic laulimalide derivatives on cell growth (Pryor *et al.*, 2002; Ahmed *et al.*, 2003). In recent full

account on Mulzer's laulimalide-related work, laulimalide, deoxylaulimalide [5], and the corresponding analogs with 2,3-*E*-enoate (desoxy compound [6] and its 16,17-epoxide derivative [7]) were tested for their effects on the proliferation of two drug-sensitive human breast cancer cell lines (MCF-7, MaTu) and two multidrug-resistant human breast tumor lines (NCI/ADR, MaTu/ADR), along with paclitaxel and epothilone B as the standard (Table 3). It turned out that [6] exhibited no activity at all, while [5] and [7] displayed diminishing activity.

In a very recent report from Littlefield's group, nineteen derivatives were synthesized and their activities were evaluated in the MDA-MB-435 and HT-29 cell lines. The structural modification of laulimalide was done on C2-C3-*Z*-double bond, C15-OH, C16-C17-epoxide, and C20-OH position. All the prepared analogs exhibited decreasing potencies relative to laulimalide. The C16,17-epoxide, the C-20 alcohol, and the C2-C-3 enoate all appeared to be important for activity. Also, there appeared to be some flexiblility in the stereochemistry at C15. Derivatizations of the C21-C27 side chain and C5-C9 dihydropyran were not explored in this report (Gallagher *et al.*, 2004).

Table 3 Antiproliferative Effects of Laulimalides [2], 2,3-*Z*-16,17-Deoxylaulimalide [5], 2,3-*E*-16,17-Deoxylaulimalide [6], and 2,3-*E*-Laulimalide [7], Compared with Paclitaxel and Epothilone B (Ahmed *et al.*, 2003)

Compound	IC_{50} [nM]			
	MCF-7[a]	NCI/ADR[b]	MaTU[a]	MaTu/ADR[b]
[2]	3.8	36	3.8	6.0
[5]	89	ni	43	170
[6]	ni	ni	ni	ni
[7]	54	ni	38	250
Paclitaxel	3.2	>1000	3.3	600
Epothilone B	0.59	3.5	0.46	1.2

[a]Human breast tumor cell line. [b]Human multidrug-resistant breast tumor cell line.

ni = No inhibition measured up to 100 nM.
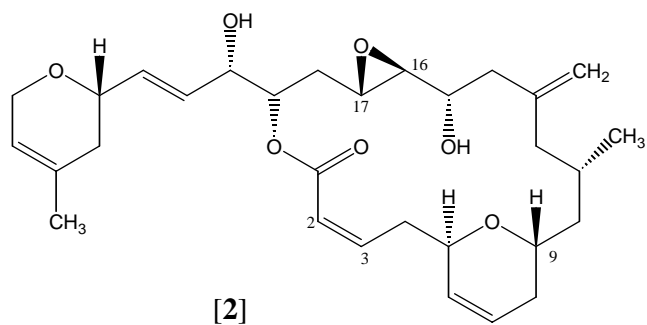
[2]
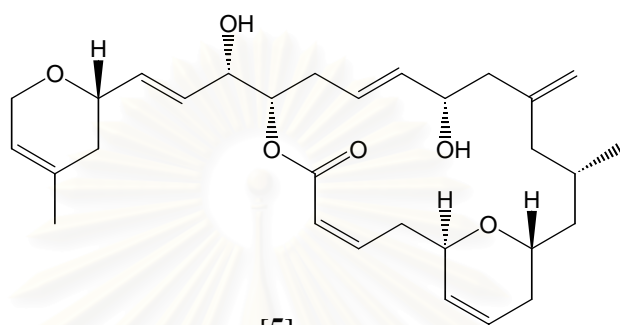
[5]
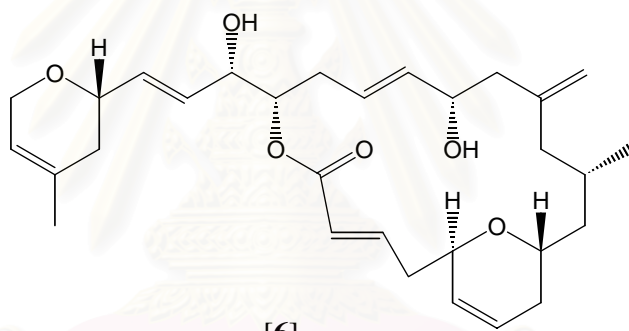
[6]
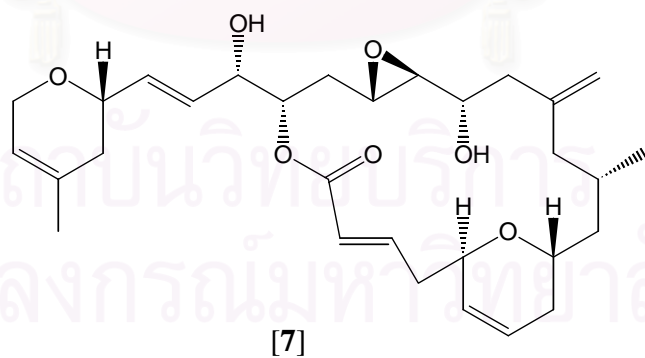
[7]

In our study, the ability of the fractions and compounds to alter cellular microtubule structures was evaluated by indirect immunofluorescence techniques. The concentration of compounds that first caused changes in mitotic spindles was determined. Table 4 shows the screening results of the fractions from the sponge *C. mycofijiensis*. The isolation based on these results yield the active antimicrotubule compound **BD27** (laulimalide), together with **BD20** (latrunculin A) in 0.02 and 0.54% w/w based on MeOH extract, respectively.

The three fragment analogs **LAU13**, **LAU14**, and **LAU16** will serve as intermediates toward further syntheses of laulimalide analogs and will be also evaluated for the antimicrotubule activity.

Table 4 Antimicrotubule Screening Results of the Fractions from the Sponge
Cacospongia mycofijiensis

Observation	Fraction (concentration*)
MT, no MF	**BD05** (1.0 μg/mL)
	BD12 (0.1 μg/mL)
	BD14 (1.0 μg/mL)
	BD23 (0.1 μg/mL)
MT, slight MF	**BD01** (10 μg/mL)
	BD15 (10 μg/mL)
Slight MT, extensive MF loss	**BD02** (10 μg/mL)
	BD16 (10 μg/mL)
MF, no MT	**BD17** (0.1 μg/mL)
	BD18 (1.0 μg/mL)
	BD20 (0.1 μg/mL)

MT = microtubule bundling activity

MF = microfilament polymerized inhibition activity

*The data is reported at the lowest concentration at which activity was observed. All samples were tested at 10, 1, and 0.1 μg/mL

3. Synthesis of the C1-C14 Fragment Analogs of Laulimalide

Apart from the significant clinical potential of laulimalide and its restricted natural supply, the attraction of laulimalide as a synthetic target originates from its unique and complex molecular architecture. Considering laulimalide's structural complexity, the production of a large and continued supply of this compound might be difficult. Specifically, its 16,17-epoxide is susceptible to nucleophilic attack from the 20-hydroxy group to form the more stable and biologically less active tetrahydrofuran isomer, isolaulimalide, and the 2,3-*cis*-enolate moiety readily undergoes *Z/E*-isomerization. Thus, an efficient and flexible synthesis is essential to provide further material for biological evaluation, along with access to novel analogs. The preparation of analogs with simplified structures that are more easily prepared would help to provide structure-activity-relationship data, when combine with information learned from studies involving other microtubule-stabilizing agents, and to prepare molecules that are equipotent with laulimalide, but more stable.

Among the known microtubule-stabilizing agents, laulimalide most resembles the epothilones, although its ring size (18-membered vs. 16-membered) is two carbons bigger. Both type of compounds contain a very similar structure motif, as highlight in Figure 5. Both laulimalide and epothilone B incorporate an epoxide ring, an unsaturated side chain bearing a methylated heterocyclic ring which is attached with the same chirality, and a lactone of a macrocyclic ring. Such similarity would seem to suggest that this motif may be important for biological activity. Furthermore, the ring bears an oxygen functionality five atoms away from the ester carbonyl and both rings contain a methyl group attached to ring with the same chirality (C11 for laulimalide; C8 for epothilone B). Differences include the geometry of the epoxide ring (*trans* in laulimalide and *cis* in epothilone B) and only laulimalide bears a cis double bond in its ring.

In this project, we have decided to synthesize three fragment analogs of the C1-C14 region of laulimalide. This portion of laulmalide's macrocyclic ring is structurally different from the epothilones, suggesting that there is flexibility within this region. Therefore, the discovery of active analogs of the fragment within the C1-C14 portion of laulimalide, which bear simplified, easier structures to synthesize would be desirable.
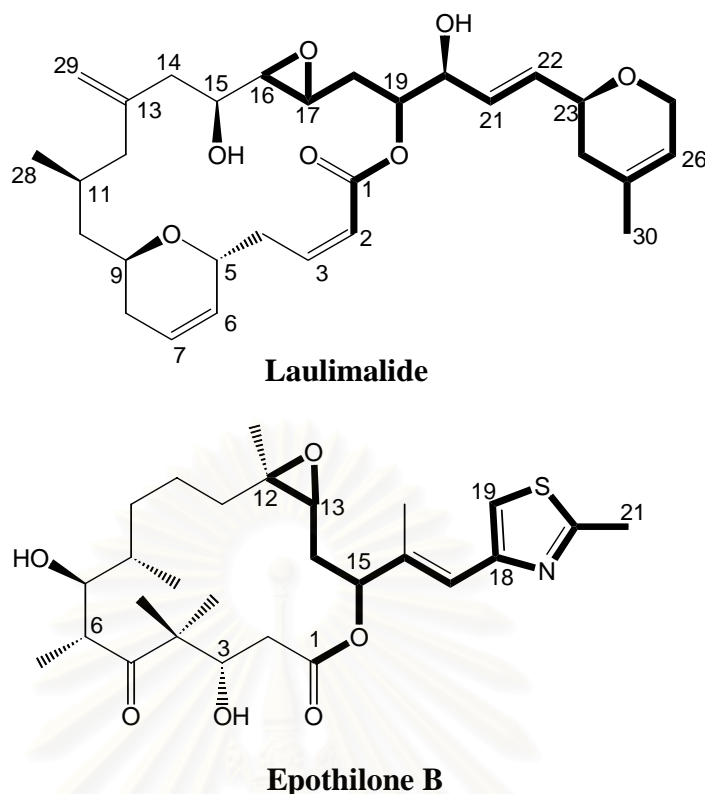
Figure 5 Structural Comparison of Laulimalide and Epothilone B

In this study, the C6-C8 carbons of the dihydropyran ring were removed, imitating epothilone B which does not have dihydropyran ring in its molecule. Modification was focused on the C1-C3 fragment. The first involved the preparation of an *E*-and *Z*-isomers, the second involved omitting C2 and C3 to obtain a product which had two carbons less than others. Furthermore, decreasing the number of carbons between the dihydropyran ring and the exomethylene was performed to form 16-membered ring analogs, which is the same size as the epothilones. Three C1-C14 fragment analogs (**LAU13**, **LAU14**, **LAU16**) of laulimalide are presented in Figure 1.

3.1 Retrosynthetic Analysis of Laulimalide and the C1-C14 Fragment Analogs

Laulimalide constitutes a significant synthetic challenge, with its 18-membered macrocyclic lactone ring, *trans*-substituted dihydropyran ring, and 9 chiral centers. To minimize the number linear steps and maximize the overall yield, a convergent approach to the synthesis of laulimalide has been devised. A retrosynthetic analysis of this study is shown in Scheme 4. The molecule of laulimalide was divided into two primary fragments; the C1-C14 fragment (fragment A) and the C15-C27 fragment (fragment B). Two fragments were coupled using asymmetric allylsilane chemistry,

either before or after epoxidation. Because of the sensitivity to basic conditions of (Z)-α,β-unsaturated ester (fragment A), we utilized a 2,4-dimethoxybenzyl (DMB) ester protecting group, envisioning simultaneous cleavage of the C19 PMB ether and the DMB ester immediately prior to macrolactonization.

The retrosynthetic plan for the C1-C14 fragment analogs is presented in Scheme 5. In these molecules, the C6-C8 carbons of the dihydropyran ring have been removed.
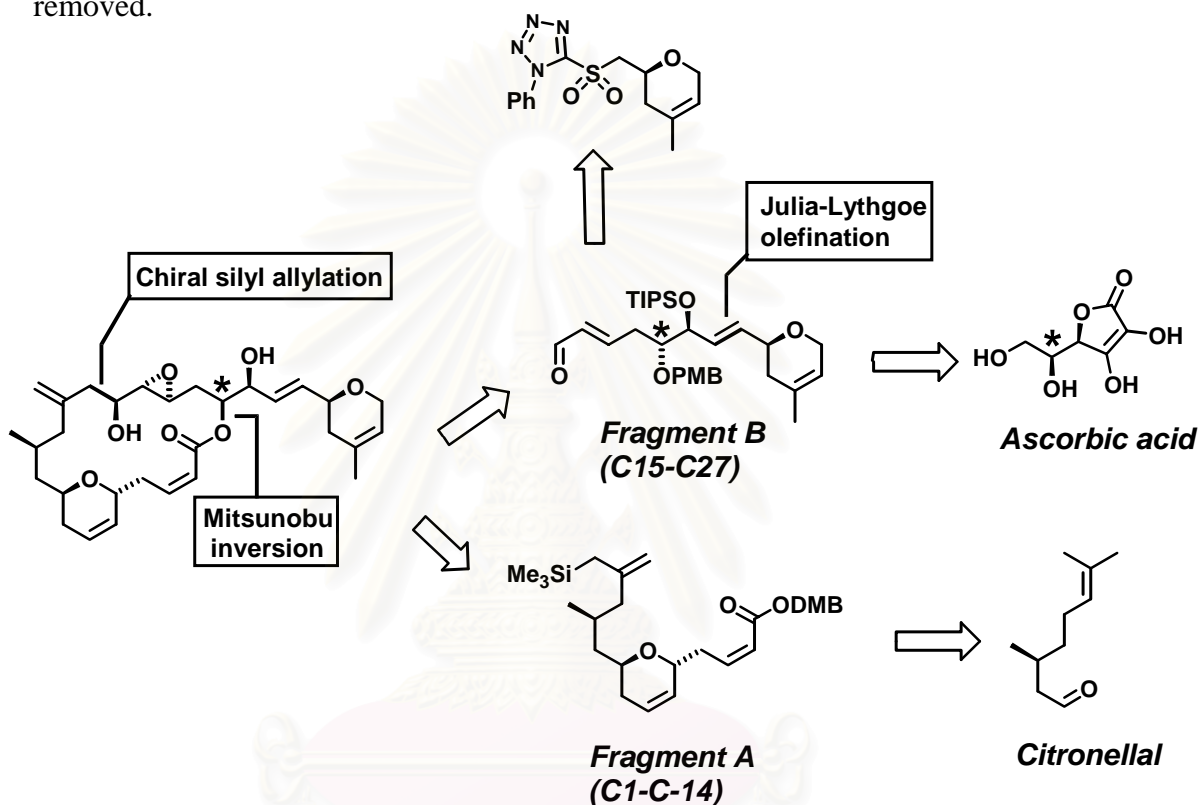
Scheme 4 Retrosynthetic Analysis of Laulimalide
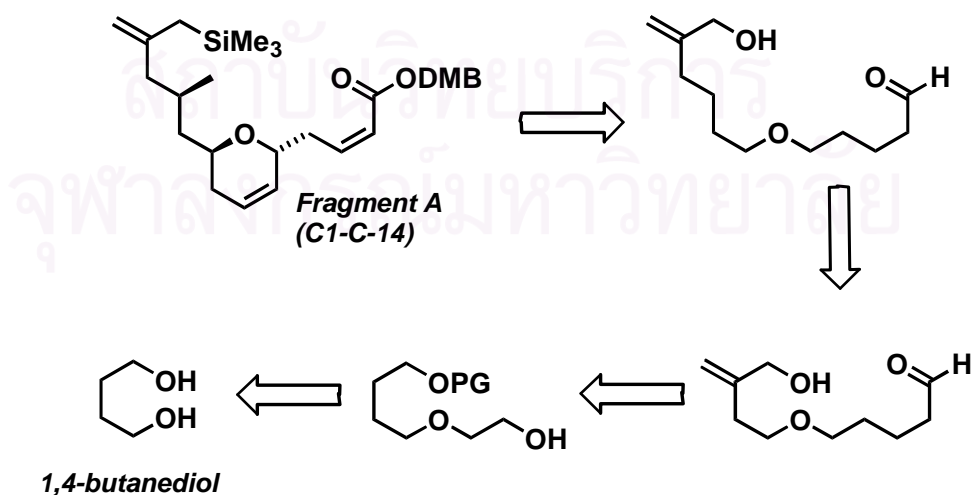
Scheme 5 Retrosyntheic Plan of the C1-C14 Fragment Analogs of Laulimalide

3.2 Chemical Synthetic Strategy of the C1-C14 Fragment Analogs of Laulimalide (LAU13, LAU14, LAU16)

This report will focus mainly on the synthesis of fragment A analogs. Three fragment analogs were prepared from the starting material 1,4 butanediol as shown in Scheme 6. The synthesis of these analogs involved two major tasks. The first task was the construction of the intermediate (**LAU12**), and the second task was the generation of each product (**LAU13, LAU14, LAU16**)

3.2.1 Synthesis of the Intermediate LAU12 3-[3-(*tert*-Butyldiphenyl silanyloxymethyl)-but-3-enyloxy]-propionaldehyde

Preparation of the three fragment analogs started with 1,4-butanediol (Scheme 6). The selective monosilylation of symmetrical primary diol was used (McDougal *et al.*, 1986). Following mono-protection of 1,4-butanediol as the TBDPS ether, the primary alcohol was oxidized with Swern oxidation to yield the aldehyde **LAU02**. Refluxing **LAU02** with 1,3-propanediol in the presence of an acid catalyst PPTS (Sterzycki, 1979) overnight gave the acetal fragment **LAU03** in 97% yield. Reductive cleavage of the acetal with an efficient method (Kotsuki *et al.*, 1986) by using $Zn(BH_4)_2$ and TMSCl led to an excellent yield of the chain-extended primary alcohol **LAU04**, which was then protected by BzCl to give **LAU05** in 93% yield. The TBDPS ether was smoothly cleaved by treatment with a 1 M solution of TBAF (Stephen and Lavallee, 1975) to generate the primary alcohol **LAU06** in 94% yield that was successively oxidized with DMSO-$(COCl)_2$ oxidation to yield the aldehyde fragment **LAU07**. This compound was converted to the unsaturated aldehyde **LAU08** using Eschenmoser's salt and Et_3N (Nadolski and Davidson, 2001) in 82% yield. Equimolar amounts of $NaBH_4$ and $CeCl_3.7H_2O$ (Luche condition) in ethanol (Luche, 1978) acted on the α,β-unsaturated aldehyde **LAU08** to deliver the allylic alcohol **LAU09** cleanly by 1,2-reduction. Silylation of **LAU09** with TBDPSCl and nucleophilic catalyst imidazole furnished the TBDPS ether **LAU10**. Subsequent benzoyl deprotection and oxidation yielded the intermediate compound **LAU12** toward the syntheses of the three fragment analogs (Scheme 7).

Scheme 6 Synthetic Strategy toward the Intermediate **LAU12** (3-[3-(*tert*-Butyldiphenyl silanyloxymethyl)-but-3-enyloxy]-propionaldehyde)

4-(*tert*-Butyldiphenylsilanyloxy)butan-1-ol [LAU01]

The monosilylation of symmetric 1,4-butanediol as TBDPS ether was carried out by the formation of an alkoxide salt with NaH. Treatment of the diol with 1 equiv. of NaH caused the formation of a voluminous precipitate of the monosodium salt. Upon the addition of silylating agent the dissolved alkoxide salt was silylated. The resulting product was obtained as an oil in excellent yield (95%).

$HO\text{-}(CH_2)_4\text{-}OH \rightarrow OH\text{-}(CH_2)_4ONa \rightarrow OH\text{-}(CH_2)_4OSiPh_2\text{-}t\text{-}Bu$

The ^{1}H NMR spectrum of **LAU01** is shown in Figure 20. The signals at δ 0.89 and 7.18-7.50 represented the *tert*-butyl and phenyl groups of the TBDPS protecting group, respectively.

4-(*tert*-Butyldiphenylsilanyloxy)butyraldehyde (LAU02)

The oxidation of primary alcohol to aldehyde was employed by using "Swern oxidation". The DMSO-oxalyl chloride (Swern reagent) has been widely used as an oxidant for the conversion of primary alcohol to the aldehyde. This reagent avoids overoxidation to carboxylic acid, and usually gives excellent yield with short reaction time and minimal formation of by-product. The addition of DMSO to $(COCl)_2$ in CH_2Cl_2 generated the active reagent (**a**) *in situ* at low temperature (-78 ^{o}C). The alcohol **LAU01** was added to (**a**) to give the alkoxysulfonium ion (**b**) which was further deprotonated by addition of an amine base (Et_3N) to yield (**c**). The intramolecular proton abstraction produced the carbonyl product **LAU02**. The reaction mechanism is shown in Figure 6.

The ^{1}H NMR spectrum of the product is shown in Figure 21. The signal at δ 9.60 (t) supported the presence of the aldehyde functionality. This aldehyde **LAU02** was prepared prior to coupling with 1,3 propanediol to give the extended alcohol.

$$Me_2S{=}O \quad + \quad (COCl)_2 \quad \longrightarrow \quad Me_2\overset{+}{S}Cl \; Cl^- \; + \; CO \; + \; CO_2$$

(**a**)

(**b**)

(**c**)

δ_H 9.60 (t)
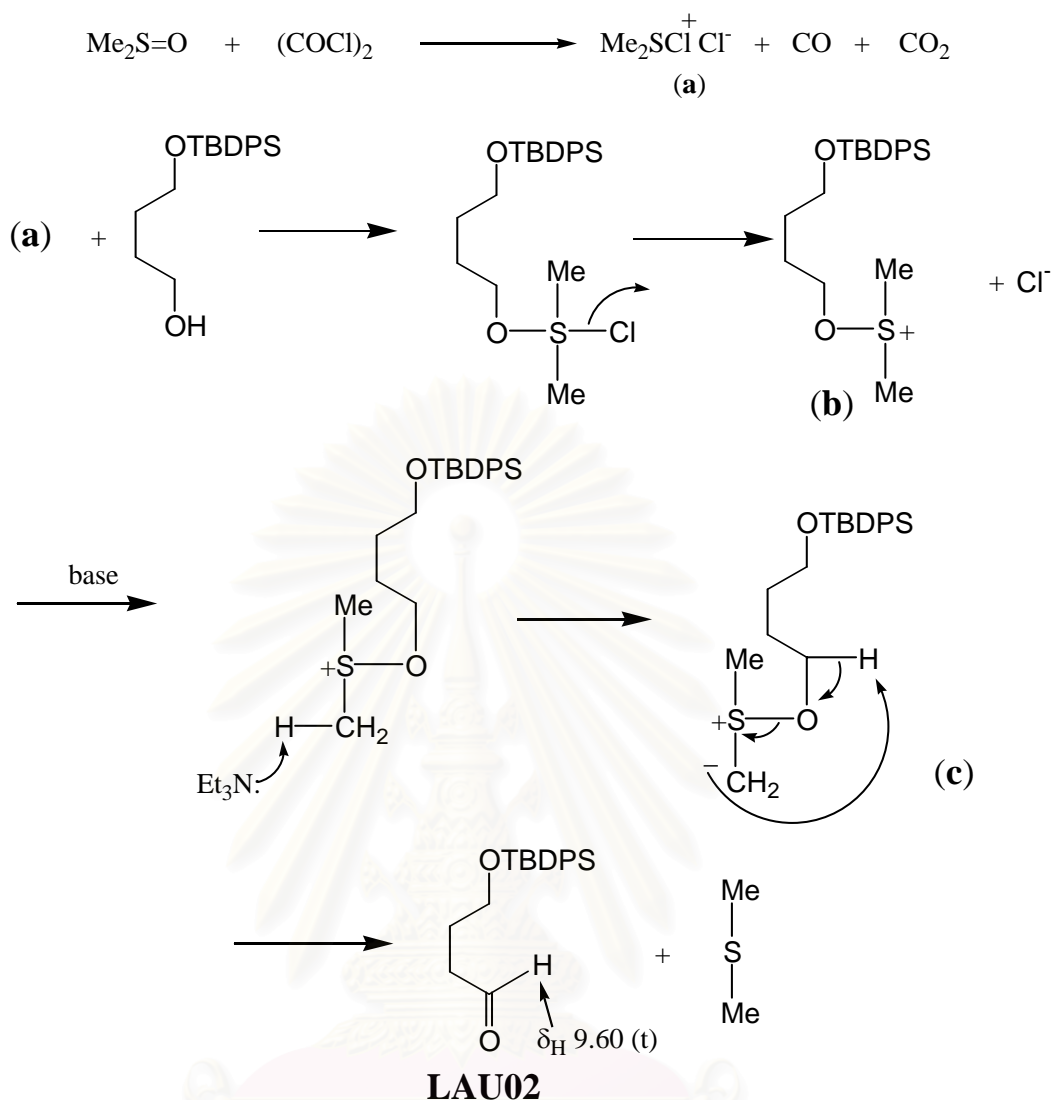
LAU02

Figure 6 Reaction Mechanism of Swern Oxidation to Synthesize **LAU02**
(4-(*tert*-Butyldiphenylsilanyloxy)butyraldehyde)

3-([1,3]Dioxan-2-yl-propoxy)- *tert*-butyldiphenylsilane (LAU03)

To synthesize the dioxolane-type acetal, the weak acidic pyridinium tosylate (pyridinium *p*-toluenesulfonate, PPTS) was chosen as the catalyst. The reaction was carried out using 20 mol% of PPTS in refluxing benzene, accompanied by the azeotropic removal of water (using Dean-Stark apparatus). The resulting product **LAU03** was obtained in excellent yield (97%) after the overnight reaction.

The ^{1}H NMR spectrum of this product is shown in Figure 22. The anomeric proton of the dioxane was presented as a triplet signal at δ 4.49 ppm.

LAU03

3-[(4-*tert*-Butyldiphenylsilanyloxy)-butoxy]-propan-1-ol (LAU04)

A number of methods for the reductive cleavage of acetal have been developed involving various reagents such as LiAlH$_4$-Lewis acids (Bonner, Lewis, and Rutter, 1981), Me$_3$SiH-Me$_3$SiOTf (Tsunoda, Suzuki, and Noyori, 1979), NaBH$_4$-CF$_3$COOH (Horne and Jordan, 1978), and H$_2$ over catalysts (Howard and Brown, 1961). In this study, we chose the efficient method of using ZnBH$_4$-TMSCl as the reagent (Kotsuki *et al.*, 1986). Zinc borohydride, prepared from zinc chloride and sodium borohydride, is a mild reducing agent because of its almost neutral character. Treatment of the acetal **LAU03** with TMSCl led to the formation of the –OSiMe$_3$. After quenching with acid, the chain-extended alcohol **LAU04** was yielded.

The reaction mechanism is illustrated in Figure 7. The ^{1}H NMR spectrum of this product is shown in Figure 23. The appearance of four methylene groups connected to oxygen atoms [δ 3.28 (t, 6.4; 2H), 3.42 (t, 5.8; 2H), 3.55 (t, 5.8; 2H), 3.60 (t, 5.6; 2H)] confirmed the cleavage of the acetal.
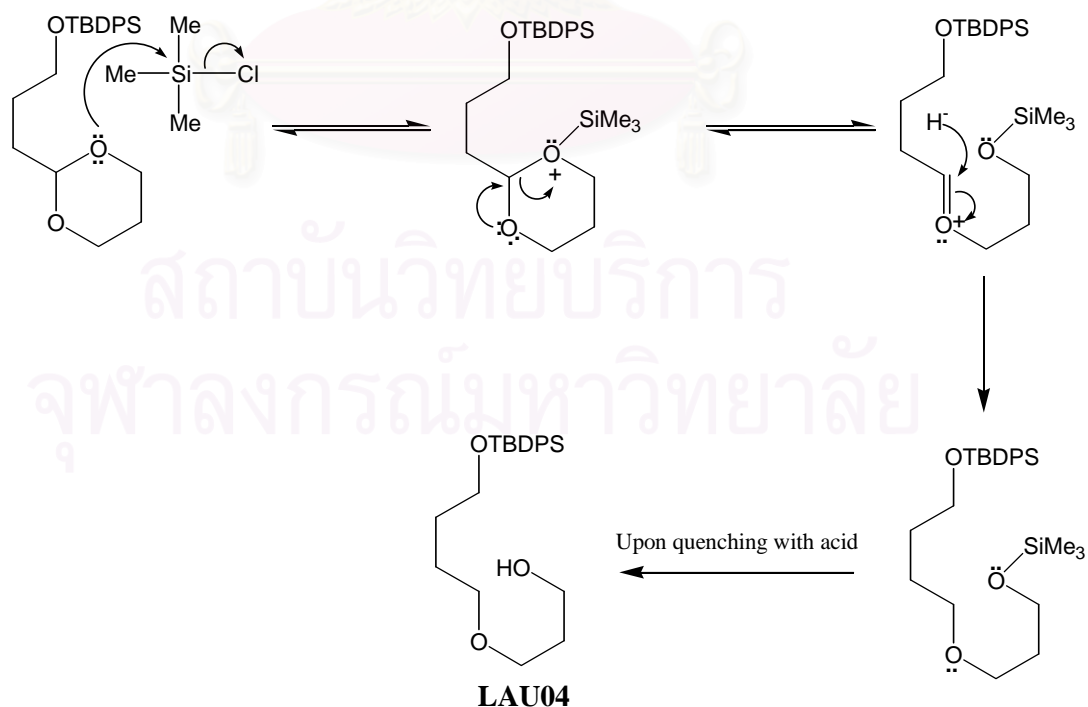
LAU04

Figure 7 Reaction Mechanism of the Reductive Cleavage of the Acetal to Synthesize
LAU04 (3-[(4-*tert*-Butyldiphenylsilanyloxy)-butoxy]-propan-1-ol)

3-(4- *tert*-Butyldiphenylsilyloxy-butoxy)-propyl benzoate (LAU05)

In order to cleave the protecting group TDBPS before being oxidized to the aldehyde in the next step, the hydroxyl group of **LAU04** had to be protected. The protection of the primary alcohol of **LAU04** was accomplished by esterification with benzoyl chloride in CH$_2$Cl$_2$ at 0 $^{\circ}$C in the presence of pyridine.

The ^{1}H NMR spectrum of this product is shown in Figure 24. The signal at δ 7.32-8.00 confirmed the presence of the benzoyl group.

3-(4-Hydroxy-butoxy)-propyl benzoate (LAU06)

Upon treatment with 1M solution of tetrabutylammonium fluoride (2 equiv.) in THF, smooth cleavage of TBDPS group occurred at room temperature to regenerate the alcohol **LAU06**, which was further oxidized to the aldehyde **LAU07** in the next step. The resulting product had R$_f$ value in TLC significantly lower than the starting material.

The ^{1}H NMR spectrum of the product is shown in Figure 25. The disappearance of the *tert*-butyl and phenyl groups of TBDPS at δ 0.97 (s; 9H) and 7.35-8.00, respectively, supported the cleavage of the protecting group.

3-(4-Oxo-butoxy)-propyl benzoate (LAU07)

The Swern oxidation was chosen again to oxidize **LAU06** to **LAU07**. The purpose of this oxidization of the hydroxyl group in **LAU06** is to generate the aldehyde group which was further subjected to Eschenmoser methylenation.

The resulting product was confirmed by the ^{1}H NMR spectrum (Figure 26) with the presence of the aldehyde proton signal at δ 9.74.

3-(3-Formyl-but-3-enyloxy)-propyl benzoate (LAU08)

Treatment of the enolizable aldehyde **LAU07** with Eschenmoser's salt ($Me_3N^+=CH_2Cl^-$) in CH_2Cl_2 for 2 days followed by addition of Et_3N yielded the unsaturated aldehyde **LAU08**. The Eschenmoser's salt was prepared from acetylation of *N,N,N′,N′* tetramethyldiaminomethane with acetylchloride (Nadolski and Davidson, 2001) and the filtered crystals were collected.
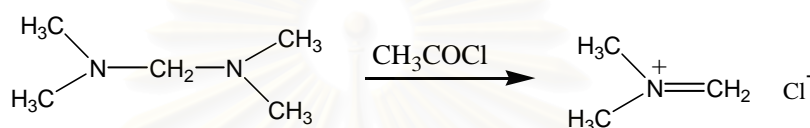
The Eschenmoser methylenation started with adding Eschenmoser's salt to the aldehyde solution in CH_2Cl_2 at room temperature for 2 days. Enolization of aldehyde to alcohol was confirmed by observing the coupling pattern of aldehyde proton in the ^{1}H NMR spectrum which changed from a triplet to a doublet peak. Addition of the base led to completion of the reaction which, again, could be monitored by the coupling pattern of aldehyde proton. The aldehyde proton of **LAU08** at δ 9.50 appeared as a singlet and the exo-methylene protons were presented at δ 6.03 and 6.34 in the ^{1}H NMR spectrum (Figure 27). The reaction mechanism is illustrated in Figure 8.
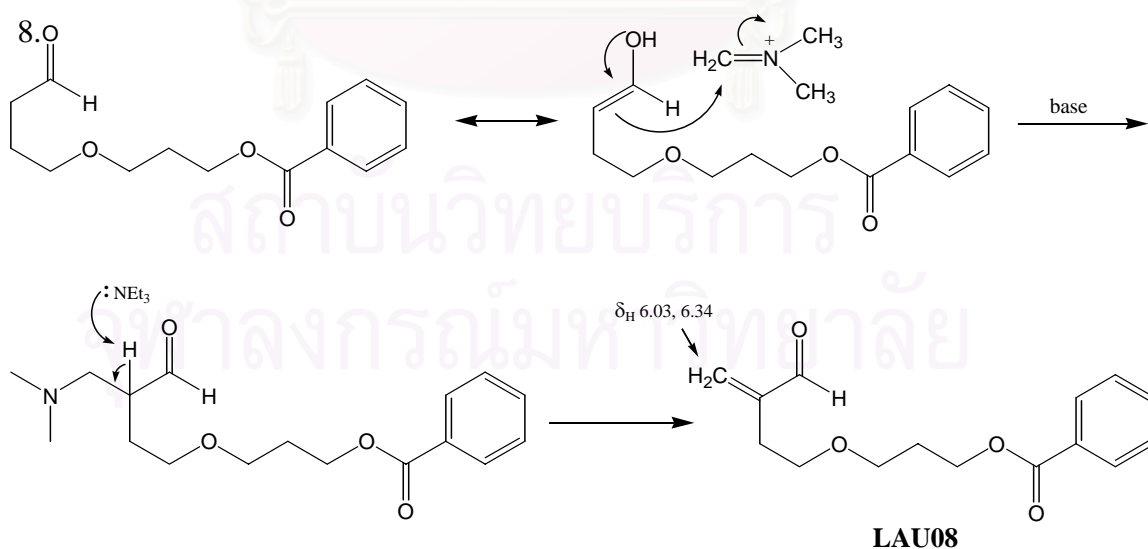
Figure 8 Reaction Mechanism of Eschenmoser Methylenation to Synthesize **LAU08** (3-(3-Formyl-but-3-enyloxy)-propyl benzoate)

3-(3-Hydroxymethyl-but-3-enyloxy)-propyl benzoate (LAU09)

Luche reduction (Luche, 1978) of the carbonyl group in **LAU08** was used to change the aldehyde to the alcohol. Equimolar amount of $CeCl_3.7H_2O$ and $NaBH_4$ in ethanol acted on α,β-unsaturated aldehyde at -78 ^oC to deliver allylic alcohol cleanly by selective 1,2-reduction in 97% yield.
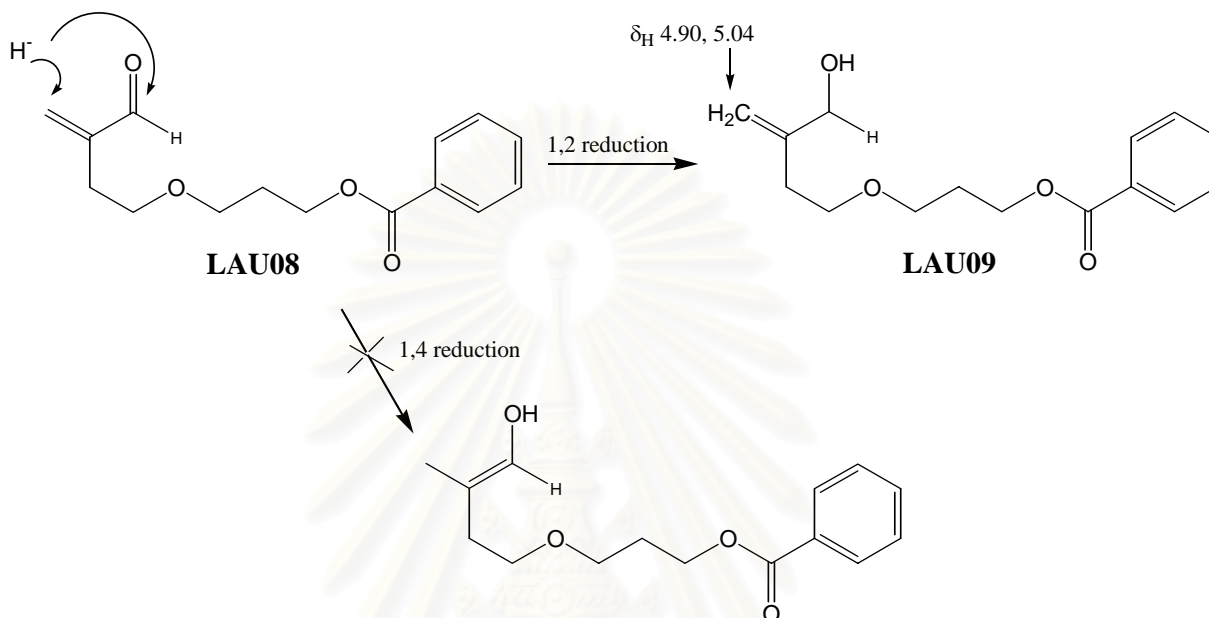
The disappearance of the aldehyde proton and the remaining exo-methylene protons at δ 4.90 and 5.04 in the ^1H NMR spectrum (Figure 28), as well as the more R_f value of **LAU09** (0.38, EtOAc:Pet. Ether, 1:4) than that of **LAU08** (0.12, EtOAc:Pet. Ether, 1:4) confirmed the 1,2-reduction.

Benzoic acid 3-[3-(*tert*-butyldiphenylsilanyloxymethyl)-but-3-enyloxy]-propyl ester (LAU10)

Silylation of **LAU09** was easily prepared by using bulky and stable silyl group, TBDPS, with the nucleophilic catalyst imidazole in CH_2Cl_2.

The ^1H NMR spectrum of the product is shown in Figure 29. The signals of the *tert*-butyl and phenyl groups in TBDPS were presented at δ 1.06 and 7.35-7.67, respectively.
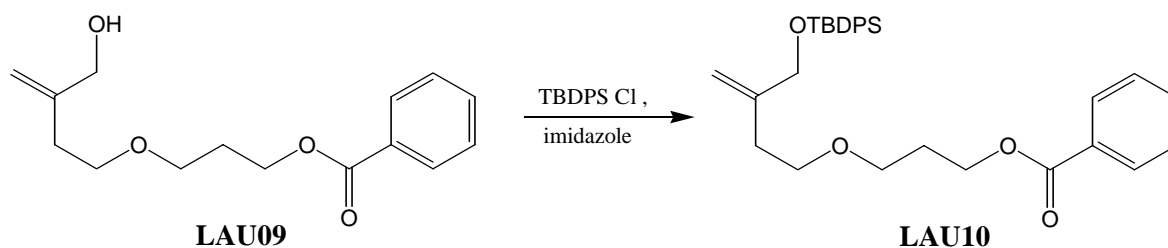
3-[3-(*tert*-Butyldiphenylsilanyloxymethyl)-but-3-enyloxy]-propan-1-ol (LAU11)

To cleave the benzoyl group, the reducing agent DIBAH was chosen. DIBAH generated hydride to react with the carbonyl carbon atom of the benzoyl group followed by loss of the benzoyl group. The reaction mechanism is shown in Figure 9. The ^{1}H NMR spectrum of the product is shown in Figure 30. The disappearance of benzoyl signal confirmed the reaction.
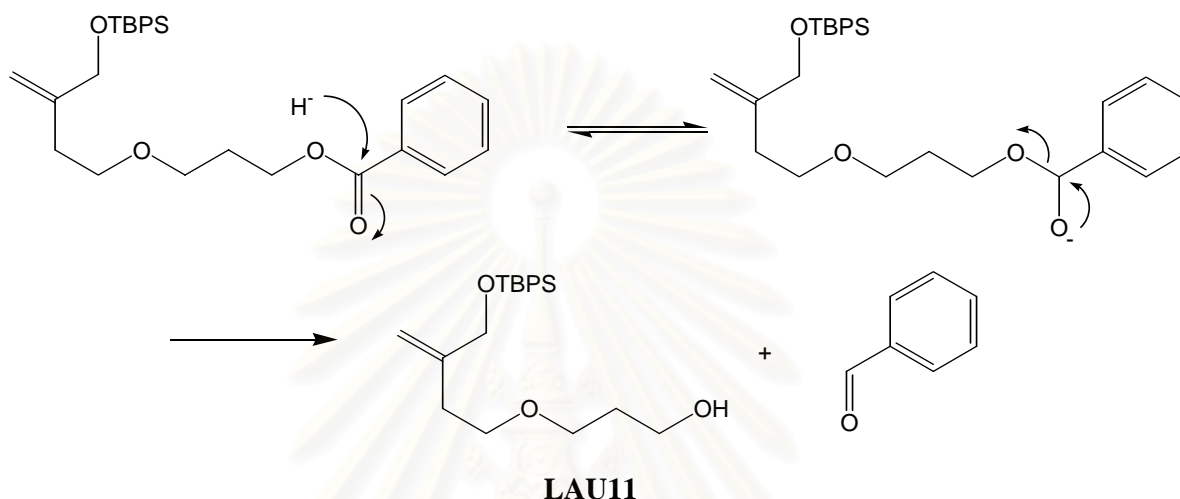
Figure 9 Reaction Mechanism of Debenzoylation to Synthesize **LAU11** (3-[3-(*tert*-Butyldiphenylsilanyloxymethyl)-but-3-enyloxy)-propan-1-ol)

3-[3-(*tert*-Butyldiphenylsilanyloxymethyl)-but-3-enyloxy]-propionaldehyde (LAU12)

The alcohol group of **LAU11** was oxidized to aldehyde in **LAU12** with Swern reagent (DMSO-(COCl)$_2$). The reaction mechanism was previously described for **LAU02**. The intermediate **LAU12** was used to prepare the three C1-C14 fragment analogs **LAU13**, **LAU14**, and **LAU16** (Scheme 7). The ^{1}H NMR spectrum of the product is shown in Figure 31. The aldehyde proton signal dappeared at δ 9.17 (t), confirming the successful Swern reaction.

intermediate LAU12
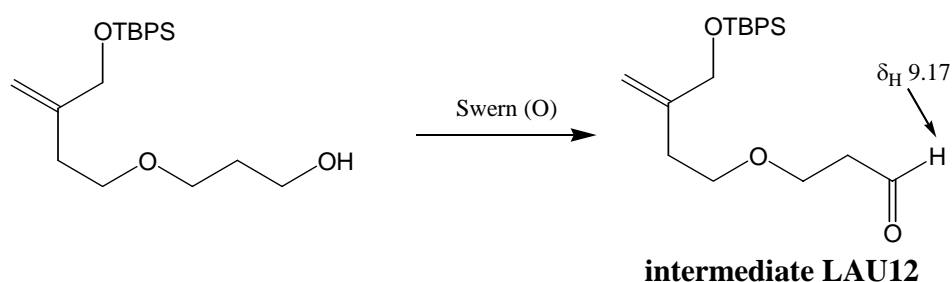
3.2.2 Synthesis of Three Fragment Analogs LAU13, LAU14, and LAU16

The intermediate aldehyde **LAU12** was converted to the three C1-C14 fragment analogs with separated routes. To enable the controlled introduction of carbon-carbon double bonds, the modified Wittig reaction (Boutagy and Thomas, 1974) was used. The (*Z*)-enolate **LAU13** was obtained from the Still-Gennari HWE application (Still and Gennari, 1983) by using electrophilic 2,4-dimethylbenzyl bis(2,2,2-trifluoroethyl phosphono)acetate and strongly dissociated base system of KN(TMS)$_2$/18-crown-6, whereas the (*E*)-enolate **LAU14** was obtained from the Horner-Emmons Olefination (Thompson and Heathcock, 1990) with 2,4-dimethylbenzyl bis(diethylphosphono)acetate and NaH. In preparing the analog **LAU16** which contains two less carbons, the intermediate **LAU12** was oxidized with NaClO$_2$-H$_2$O$_2$ oxidation (Dalcanale, 1986) and converted to **LAU16** using Steglish-Hassner esterification (Hassner and Alexanian, 1978; Neises, and Steglich, 1978).
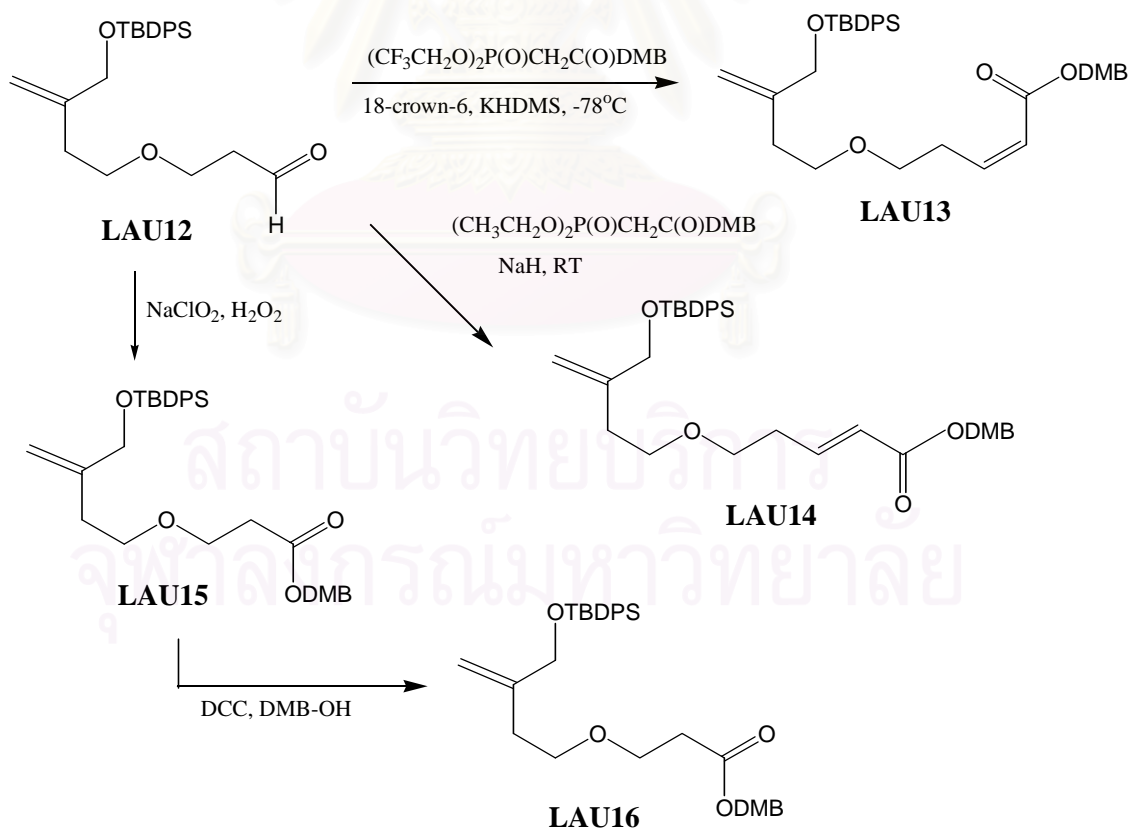
Scheme 7 Synthetic Strategy toward Three C1-C14 Fragment Analogs of Laulimalide

5-[3-(*tert*-Butyldiphenylsilanyloxymethyl)-but-3-enyloxy]-pent-2Z-ene-1-(2,4-dimethoxy)benzyl ester (LAU13) and 5-[3-(tert-Butyldiphenylsilanyloxymethyl)-but-3-enyloxy]-pent-2E-ene-1-(2,4-dimethoxy)benzyl ester (LAU14)

To synthesize the *cis*-form **LAU13** and *trans*-form **LAU14**, modification of the Wittig reaction was used. This reaction made use of resonance-stabilized phosphonate carbanion (a), where R_1 is a group capable of stabilizing the adjacent anion. This carbanion was able to react with carbonyl compound to form carbon-carbon double bond (Figure 10).
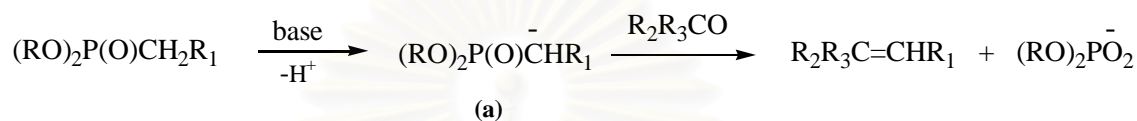
Figure 10 General Mechanism of the Modified Wittig Reaction

It appears that the stereochemical course of the reaction is governed by the same steric effects at the intermediate level as that of the conventional Wittig reaction (Figure 11). The intermediate oxyanions formed reversibly by reaction of the phosphonate carbanion and the aldehyde can exist as two diastereoisomers, where the *erythro* betaine is the precursor of the *cis* olefin via a *cis* elimination, and similarly the *threo* betaine leads to the *trans* product (Boutagy and Thomas, 1974).
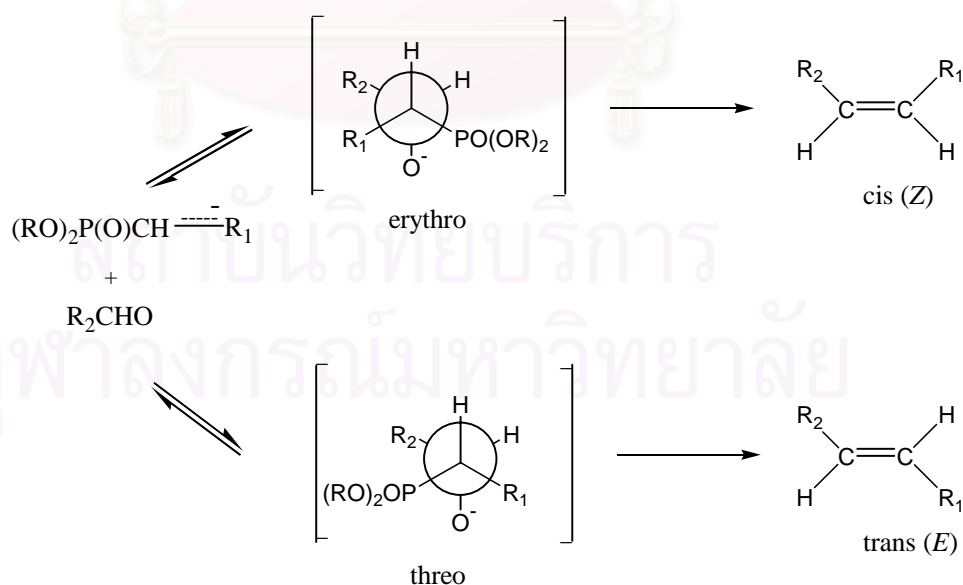
Figure 11 Proposed Stereochemical Course of the Phosphonate Modification of the Wittig Reaction

Although the modified Wittig reaction shows a preference for formation of the more stable *E*-olefins, it has been found that *Z*-selectivity can be obtained from suitable phosphonate and base system (Still and Gennari, 1983).

To obtain *cis*-form **LAU13**, Still-Gennari olefination was used (Still and Gennari, 1983). Treatment of the intermediate compound **LAU12** with 2,4-dimethyl benzyl (DMB) bis(2,2,2-trifluoroethylphosphono)acetate in the presence of $KN(TMS)_2$ and 18-crown-6 at -78 $^\circ$C yielded the compound **LAU13** as the exclusive product in 92% yield.

On the other hand, the *trans*-form **LAU14** was obtained from the Horner-Emmons Olefination (Thompson and Heathcock, 1990). The aldehyde intermediate **LAU12** was added dropwise into suspension of NaH and 2,4-dimethylbenzyl (DMB) bis(diethylphosphono)acetate at room temperature to furnish the compound **LAU14** in 85% yield.

The molecular formula of $C_{35}H_{44}O_6Si$ of both **LAU13** and **LAU14** was confirmed by EIMS, presenting the $[M+H]^+$ ion at *m/z* 612 (Figures 33 and 41).

The ^{1}H and ^{13}C NMR spectra of **LAU13** and **LAU14** are presented in Figures 36, 44, 37, and 45, respectively. The pattern of the ^{1}H and ^{13}C NMR spectra of both compounds are closely identical, except for the difference in the coupling constant values of the H-7 and H-8 olefinic protons. The olefinic coupling constants J = 11.5 and 15.0 Hz confirmed *cis* and *trans* double bonds in **LAU13** and **LAU14**, respectively. The structural assignment of both compounds (Table 5) was completed by 2D NMR using H,H-COSY (Figures 38, 46), HMQC (Figures 39, 47), and HMBC (Figures 40, 48) analyses.

LAU13

LAU14

LAU12

A

X = H or F

LAU13
cis form
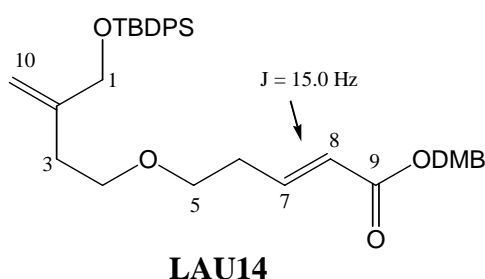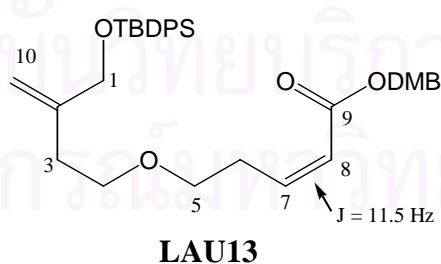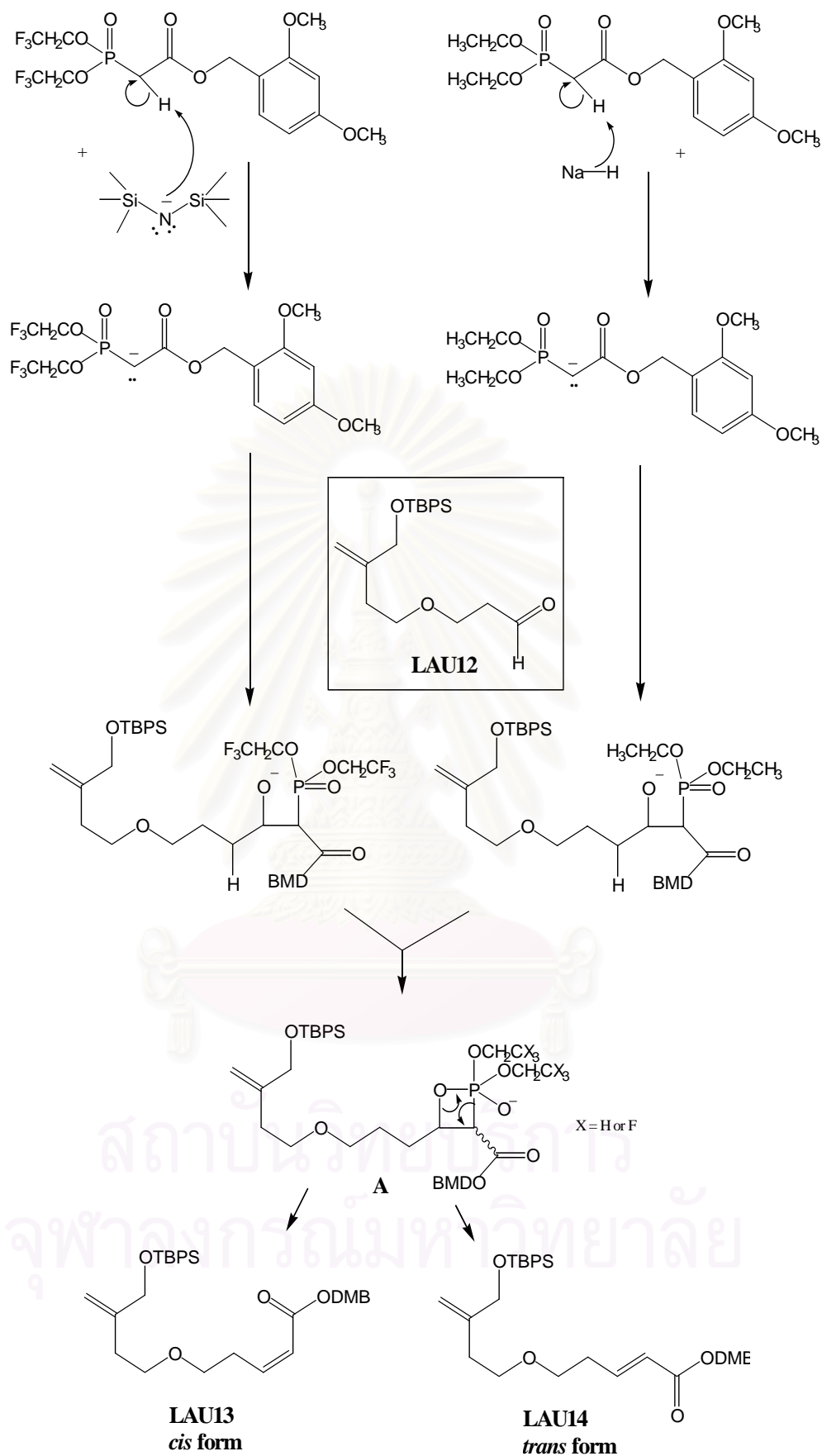
LAU14
trans form

Cis or *trans* isomers are determined by the stereochemistry in intermediate **A**

**Table 5** ^{1}H (300 MHz) and ^{13}C (75 MHz) NMR Spectral Data of **LAU13** (5-[3-(*tert*-Butyldiphenyl silanyloxymethyl)-but-3-enyloxy]-pent-2*Z*-ene-1-(2,4-dimethoxy)benzyl) ester and **LAU14** (5-[3-(*tert*-Butyldiphenylsilanyloxymethyl)-but-3-enyl oxy]-pent-2*E*-ene-1-(2,4-dimethoxy)benzyl ester)

^{1}H	δ_H (mult., *J* in Hz) in CDCl$_3$		^{13}C	δ_C (mult.) in CDCl$_3$	
	LAU13	**LAU14**		**LAU13**	**LAU14**
1	3.96 (s; 2H)	3.94 (s; 2H)	1	66.6 (t)	66.6 (t)
			2	145.2 (s)	145.0 (s)
3	2.12 (t, 6.9; 2H)	2.10 (t, 6.9; 2H)	3	33.1 (t)	33.1 (t)
4	3.31 (t, 6.9; 2H)	3.30 (t, 6.9; 2H)	4	69.5 (t)^a	68.8 (t)^b
5	3.30 (t, 6.2; 2H)	3.27 (t, 6.0; 2H)	5	69.6 (t)^a	69.9 (t)^b
6	2.74 (dq, 1.4, 6.2; 2H)	2.22 (dq, 1.5, 6.7; 2H)	6	29.7 (t)	32.7 (t)
7	6.09 (dt, **11.5**, 6.2; 1H)	6.78 (dt, **15.7**, 6.8; 1H)	7	146.7 (d)	145.4 (d)
8	5.66 (dt, **11.5**, 1.8; 1H)	5.72 (dt, **15.7**, 1.5; 1H)	8	120.8 (d)	122.7 (d)
			9	166.1 (s)	166.3 (s)
10	4.76 (br d, 1.0; 1H) 5.06 (br d, 1.0; 1H)	4.75 (br d, 1.6; 1H) 5.05 (br d, 1.6; 1H)	10	110.1 (t)	110.3 (t)
DMB	3.64 (s; 3H) 3.65 (s; 3H) 4.97 (s; 2H) 6.30 (m; 2H) 7.09 (m; 1H)	3.62 (s; 3H) 3.63 (s; 3H) 4.97 (s; 3H) 6.29 (m; 2H) 7.09 (m; 1H)	DMB	55.4 (q) 55.5 (q) 61.2 (t) 98.5 (d) 103.9 (d) 116.6 (s) 158.7 (s) 161.0 (s)	55.4 (q) 55.5 (q) 61.4 (t) 98.5 (d) 104.0 (d) 116.8 (s) 158.7 (s) 160.9 (s)
TBDPS	0.90 (s; 9H) 7.25 (m; 6H) 7.52 (m; 4H)	0.89 (s; 9H) 7.25 (m; 6H) 7.52 (m; 4H)	TBDPS	19.4 (s) 26.9 (q) 127.5 (d) 129.5 (d) 131.2 (s) 133.5 (s) 135.4 (d)	19.4 (s) 26.9 (q) 127.6 (d) 129.5 (d) 131.1 (s) 133.5 (s) 135.3 (d)

^{a,b} Values with the same superscript may be interchanged in each column

3-[3-(*tert*-Butyldiphenylsilanyloxymethyl)-but-3-enyloxy]-propionic acid (LAU15)

The aldehyde group of **LAU12** was oxidized to the acid in **LAU15** prior to coupling with DMB alcohol for generating the final product **LAU16**. Selective oxidation with sodium chlorite-hydrogen peroxide was used in this step.
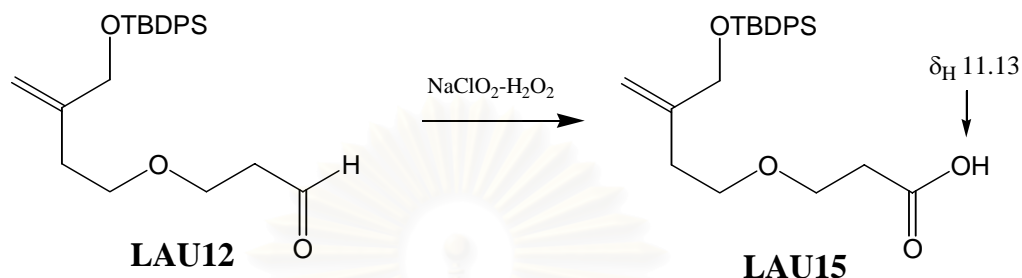
In the reaction (Dalcanale, 1986), sodium chorite will react with the aldehyde to give the carboxylic acid (**eq 1**.).

$$RCHO \ + \ HClO_2 \longrightarrow \ RCOOH \ + HOCl \qquad (\text{eq 1})$$

The hypochlorite ion must be removed in order to avoid side reactions, since the redox pair $HOCl/Cl^-$ is a more powerful oxidant than $ClO_2^-/HOCl$. Another drawback is the oxidation of ClO_2^- to ClO_2 according to the **eq 2**.

$$HOCl \ + \ 2ClO_2^- \longrightarrow 2ClO_2 \ + Cl^- \ + \ OH^- \qquad (\text{eq 2})$$

Therefore, 30 % of H_2O_2 must be added to the reaction as HOCl scavenger. The H_2O_2 will reduce HOCl according to **eq 3**, without formation of organic side products.

$$HOCl \ + \ H_2O_2 \longrightarrow \ HCl \ + O_2 \ + \ H_2O \qquad (\text{eq 3})$$

The best reaction condition was achieved by working in a weakly acidic medium, where oxidation was rapid with no competitive reduction of $HOCl_2$ to HOCl. To work up the reaction, a small amount of Na_2SO_3 was added to destroy the unreacted HOCl and H_2O_2. Acidification with 2% aqueous HCl afforded the carboxylic acid.

The [1]H (Figure 51) and ^{13}C (Figure 52) NMR spectra of the product showed broad signal at δ_H 6.2 and δ_C 175.7, suggesting the presence of the carboxylic portion in **LAU15**.

3-[3-(*tert*-Butyldiphenylsilanyloxymethyl)-but-3-enyloxy]-propionicacid-(2,4-dime-thoxy) benzyl ester (LAU16)

The Steglich-Hassner esterification allowed the conversion of the carboxylic acid **LAU15** to the ester product **LAU16**. This reaction was performed in the presence of DCC and the catalyst DMAP to couple **LAU15** with **DMB alcohol**.

The reaction mechanism is shown in Figure 12. The carboxylic acid is converted by DCC to anhydride, which forms an acylpyridinium species (**a**) with the catalyst DMAP. This is followed by the equilibration of an acylpyridinium with the alcohol to generate ion pair (**b**). Nucleophilic attack by alkoxide on the acyl group produces the ester and the catalyst. The carboxylic acid is recycled by DCC while the catalyst is reused in the formation of acylpyridinium ion.

The ^{1}H and ^{13}C NMR spectra of **LAU16** are shown in Figures 56 and 57, respectively. The comparative assignment of **LAU15** and **LAU16** was presented in Table 6. The methoxy and methylene carbons of the DMB part in **LAU16** was presented at δ_H 3.64 (s; 6H)/ δ_C 55.4, 55.5 and δ_H 4.95 (s; 6H)/ δ_C 61.7, supporting the successful reaction.

Figure 12 Reaction Mechanism of the Steglish-Hassner Esterification

Table 6 [^1]H (300 MHz) and [^13]C (75 MHz) NMR Spectral data of **LAU15** (3-[3-(*tert*-Butyl diphenyl silanyloxymethyl)-but-3-enyloxy]-propionic acid) and **LAU16** (3-[3-(*tert*-Butyldiphenylsilanyloxymethyl)-but-3-enyloxy]-propionicacid-(2,4-dimeth oxy) benzyl ester)

| ^{1}H	δ_H (mult., J in Hz) in CDCl$_3$		^{13}C	δ_C (mult.) in CDCl$_3$	
	LAU15	**LAU16**		**LAU15**	**LAU16**
1	4.10 (s; 2H)	3.95 (s; 2H)	1	65.7 (t)	66.6 (t)
			2	144.8 (s)	145.0 (s)
3	2.28 (t, 6.9; 2H)	2.11 (t, 7.0; 2H)	3	32.9 (t)	33.0 (t)
4	3.52 (t, 6.9; 2H)	3.32 (t, 7.0; 2H)	4	69.9 (t)	69.8 (t)
5	3.65 (t, 6.3; 2H)	3.48 (t, 6.6; 2H)	5	66.6 (t)	66.1 (t)
6	2.55 (t, 6.3; 2H)	2.36 (t, 6.6; 2H)	6	34.7 (t)	35.2 (t)
			7	175.7 (s)	171.4 (s)
8	4.90 (br d, 0.9; 1H) 5.19 (br d, 0.9; 1H)	4.75 (br d, 1.2; 1H) 5.05 (br d, 1.2; 1H)	8	110.4 (t)	110.1 (t)
DMB		3.62 (s; 3H) 3.63 (s; 3H) 4.95 (s; 2H) 6.29 (m; 2H) 7.05 (m; 1H)	DMB		55.4 (s) 55.5 (s) 61.7 (t) 98.5 (d) 104.0 (d) 116.6 (s) 158.7 (s) 161.0 (s)
TBDPS	1.05 (s; 9H) 7.38 (m; 6H) 7.66 (m; 4H)	0.90 (s; 9H) 7.23 (m; 6H) 7.51 (m; 4H)	TBDPS	19.4 (s) 26.9 (q) 127.5 (d) 129.5 (d) 131.2 (s) 133.4 (s) 134.6 (d) 135.4 (d)	19.4 (s) 26.9 (q) 127.5 (d) 129.5 (d) 131.1 (s) 133.4 (s) 135.2 (d) 135.3 (d)

CHAPTER V

CONCLUSION

In this investigation, bioassay-guided fractionation using antimicrotubule activity led to isolation of laulimalide from the extract of the sponge *Cacospongia mycofijensis*, along with the major compound latrunculin A. The yield of laulimalide and latrunculin A were 0.02 and 0.45 % w/w based on the methanol extract, respectively. The chemical structures of the isolated compounds were elucidated by spectroscopic techniques, mainly on NMR, and comparison with previous report.

The syntheses of three C1-C14 fragment analogs of laulimalide, **LAU13**, **LAU14**, and **LAU16**, have also been achieved in overall good yield. 1,4-Butanediol was utilized as starting material toward synthesis of the intermediate **LAU12**, which was then used in the preparation of all three analog products in separately routes. The *cis*- and *trans*- forms in the C1-C14 fragment analogs were achieved by using the modified Wittig reaction and the exomethylene carbons of the fragments were incorporated using Eschenmoser methylenation. In this study, the dihydropyran ring of the C1-C14 fragment was replaced by the ether linkage, and the number of carbon atoms was decreased to imitate the epothilones. We have incorporated 2,4-dimethoxybenzyl ester as protecting group, in order to facilitate deprotection of the ester group prior to macrolactonization.

APPENDIX C
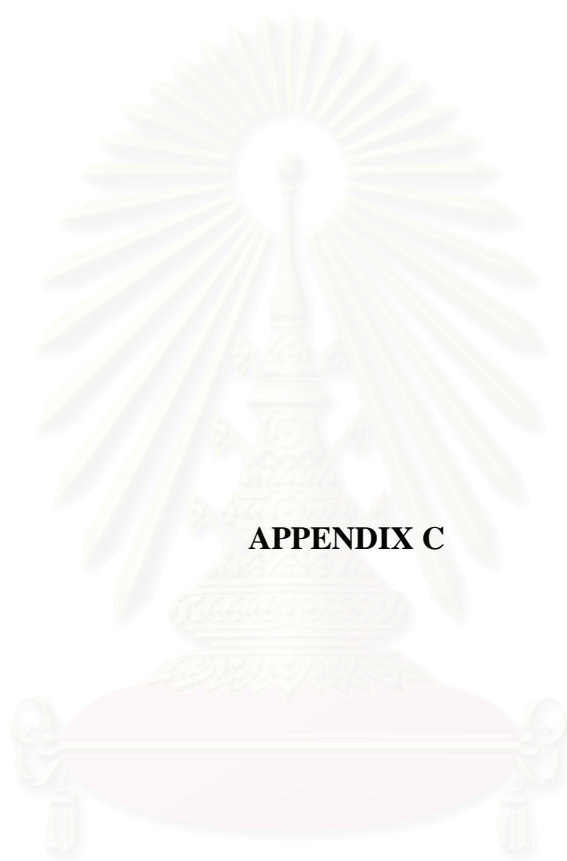
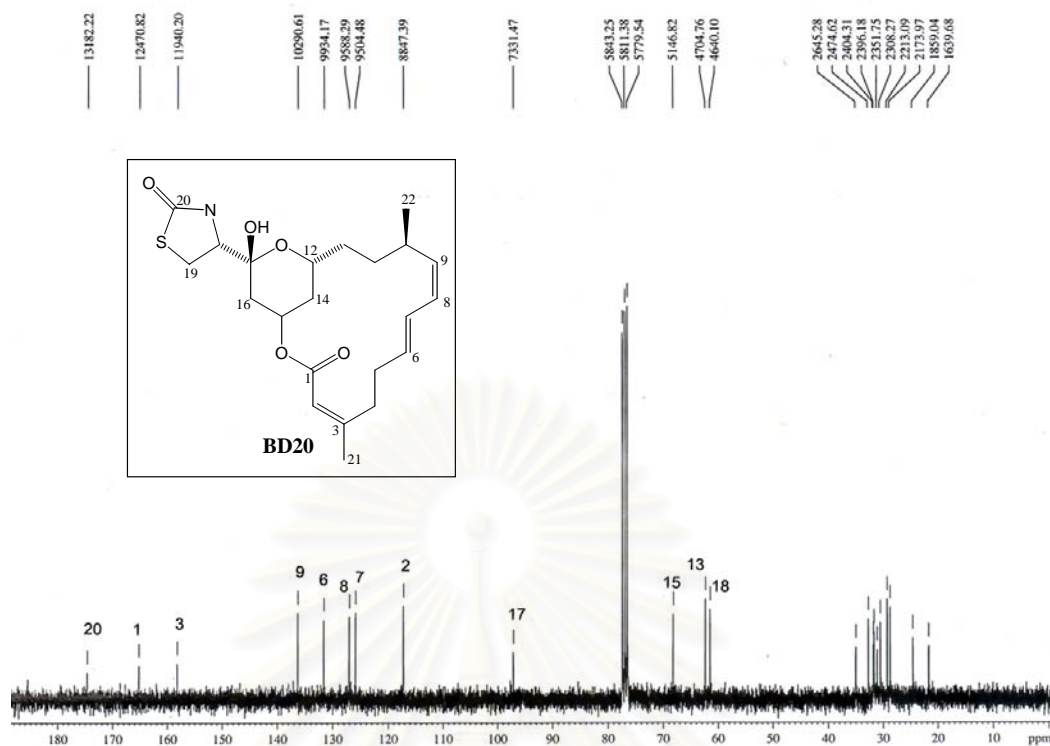**Figure 13** ^{1}H NMR (400 MHz) Spectrum of **BD20** (Latrunculin A) in CDCl$_3$

Figure 14 ^{13}C NMR (100 MHz) Spectrum of **BD20** (Latrunculin A) in CDCl$_3$
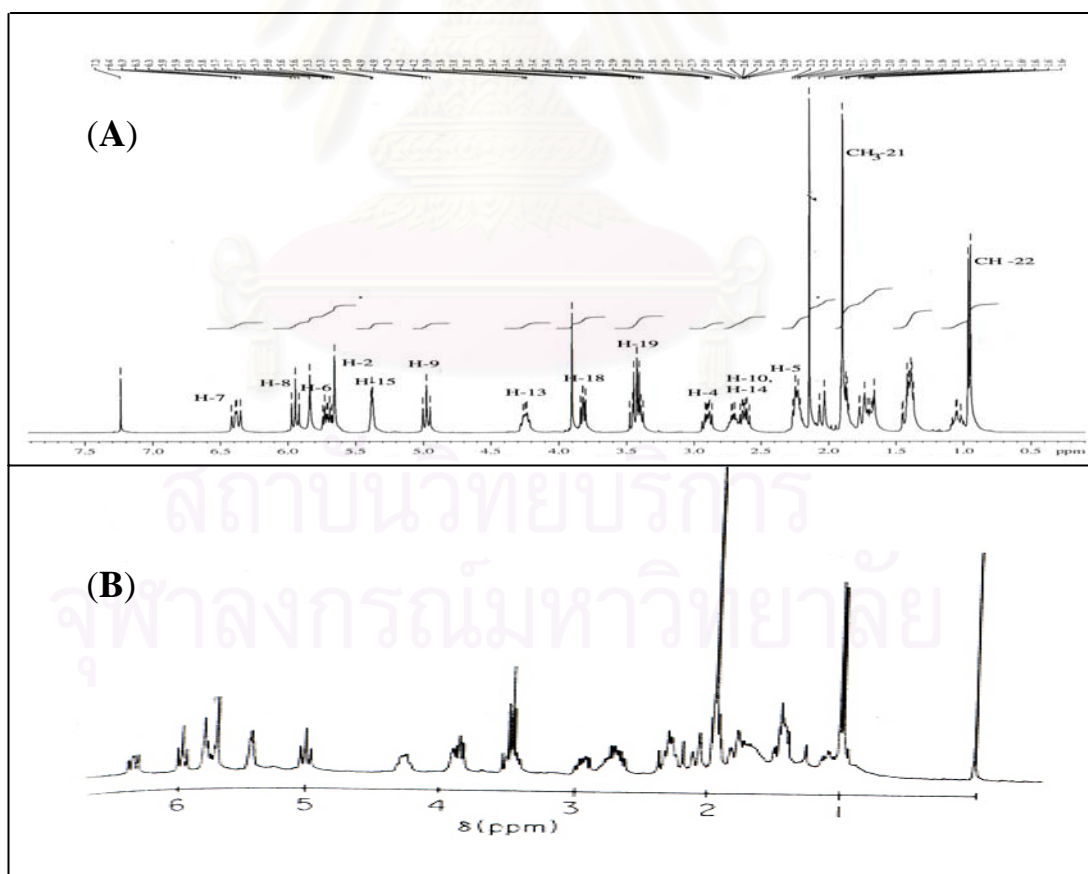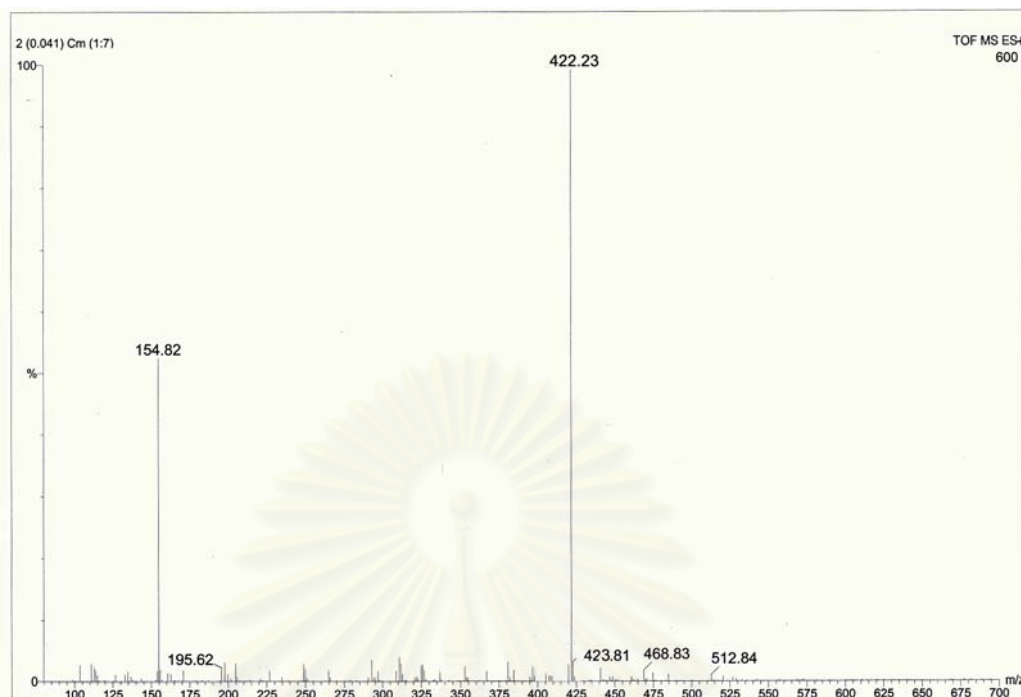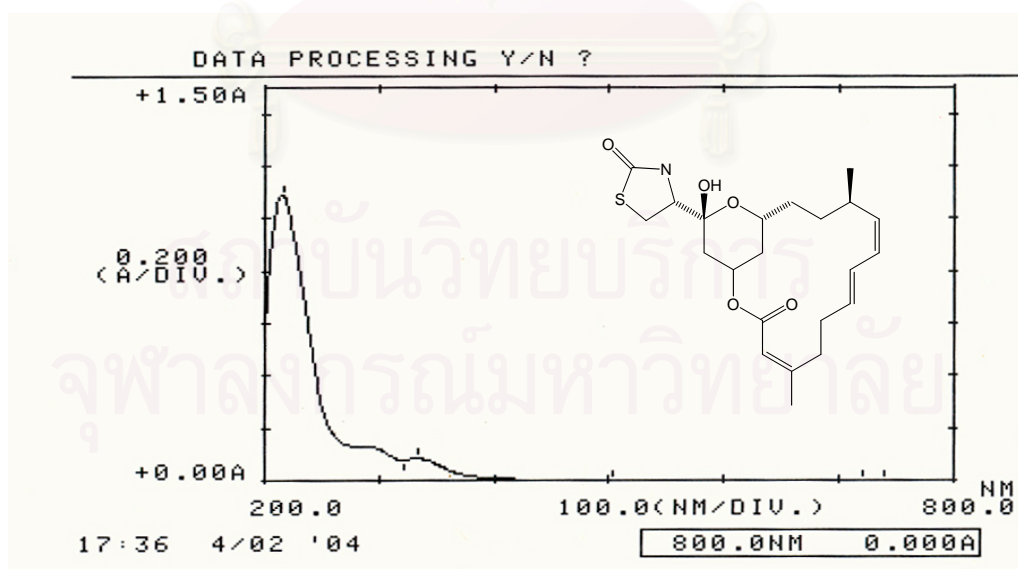

Figure 15 ^{1}H NMR (400 MHz) Spectrum of **BD20** (**A**) and Latrunculin A (**B**)
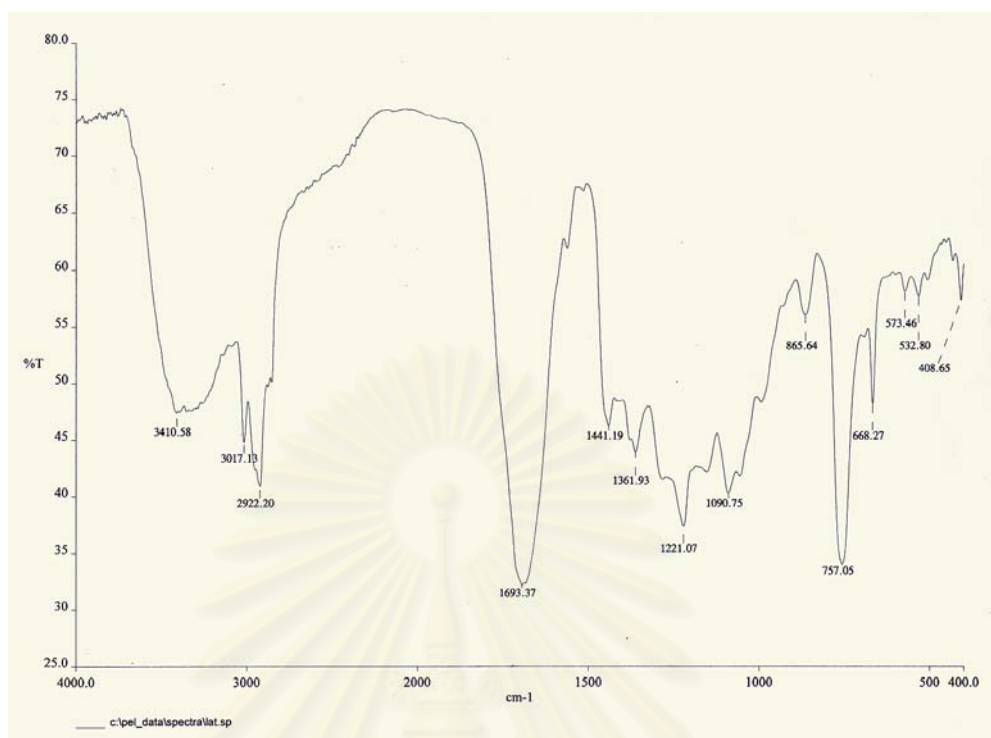
(Groweiss *et al.*, 1983)

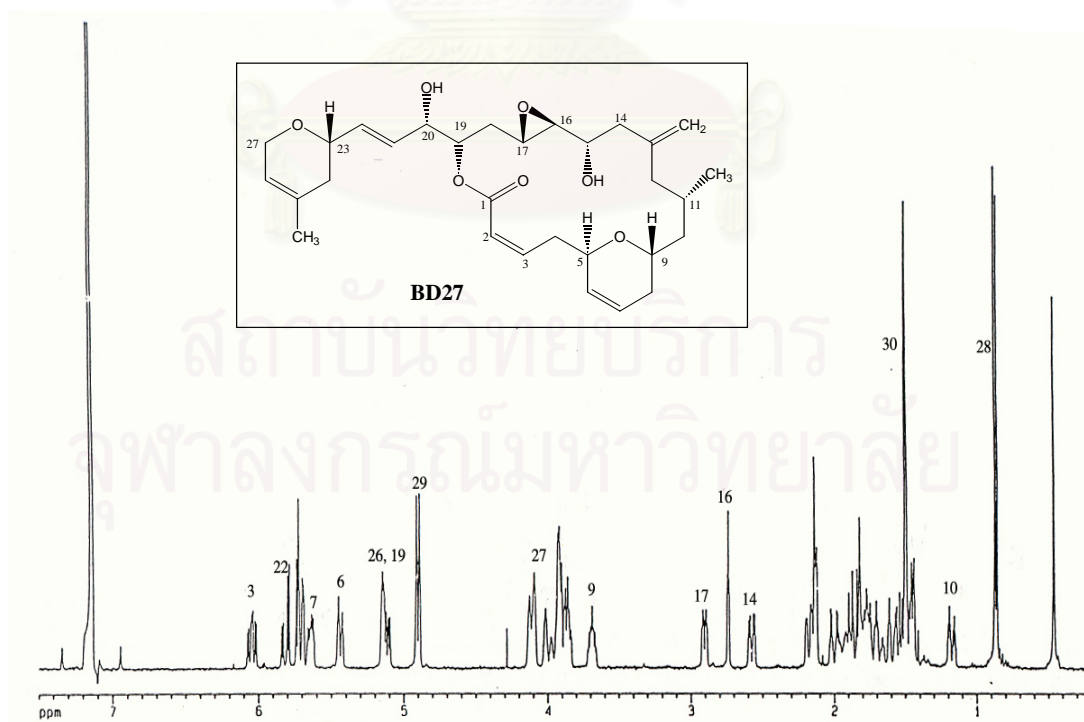**Figure 16** TOF MS Spectrum of **BD20** (Latrunculin A)

Figure 17 UV Spectrum of **BD20** (Latrunculin A) in MeOH

Figure 18 IR Spectrum (Film) of **BD20** (Latrunculin A)

Figure 19 ^{1}H NMR (400 MHz) Spectrum of **BD27** (Laulimalide) in C_6D_6

7.505
7.498
7.494
7.489
7.240
7.219
7.217
7.199
7.183

3.543
3.530
3.471
3.463

1.486

0.896
0.888

OTBDPS

OH

LAU01

t-Butyl of TBDPS

Phenyl Group of TBDPS

7.5   7.0   6.5   6.0   5.5   5.0   4.5   4.0   3.5   3.0   2.5   2.0   1.5   1.0   ppm

1.825
2.650

0.996
1.026

2.325

5.243
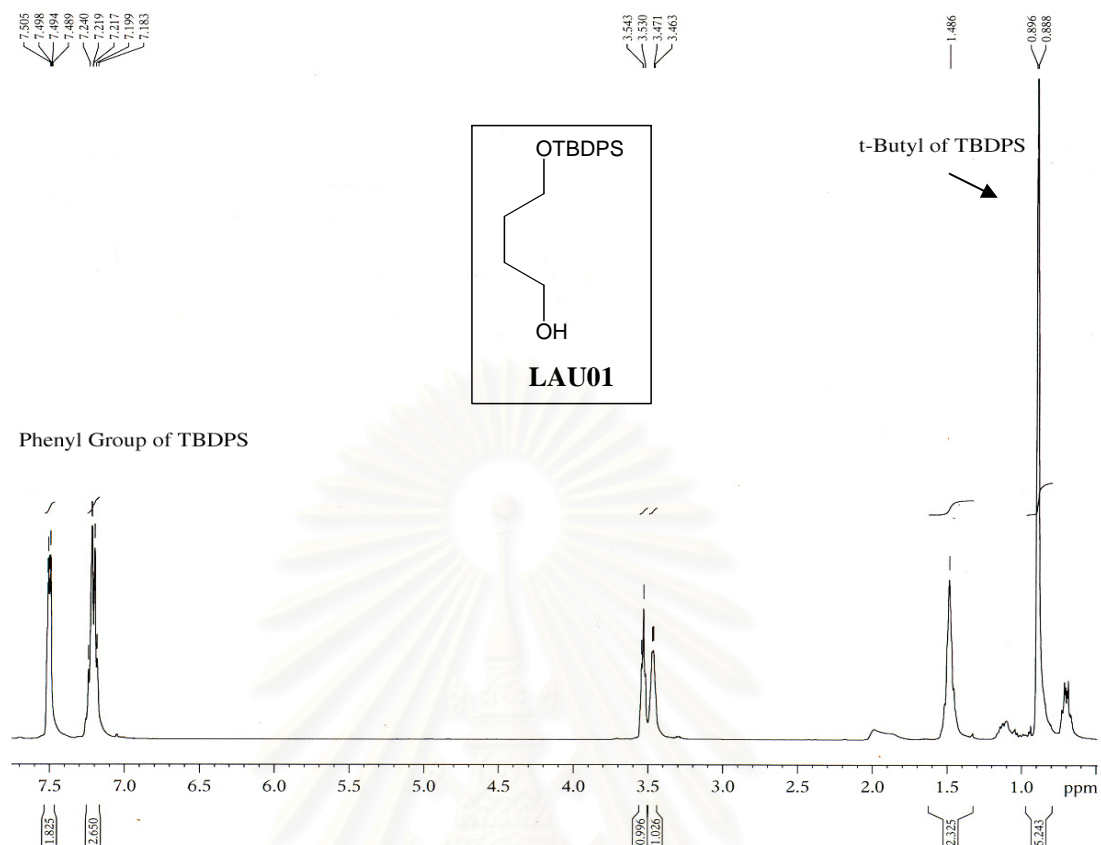
Figure 20 ^{1}H NMR (400 MHz) Spectrum of **LAU01** in CDCl$_3$

9.604
9.600
9.596

7.487
7.483
7.473
7.467
7.240
7.233
7.228
7.224
7.215
7.197
7.184
7.181
7.176

3.535
3.520
3.505

2.376
2.372
2.358
2.354
2.340
2.336
1.727
1.725
1.709
1.694
1.692

0.877

OTBDPS

H

O

LAU02

ald. proton

9.5   9.0   8.5   8.0   7.5   7.0   6.5   6.0   5.5   5.0   4.5   4.0   3.5   3.0   2.5   2.0   1.5   ppm

0.610

3.642
5.179

2.000

1.714

1.824

9.326
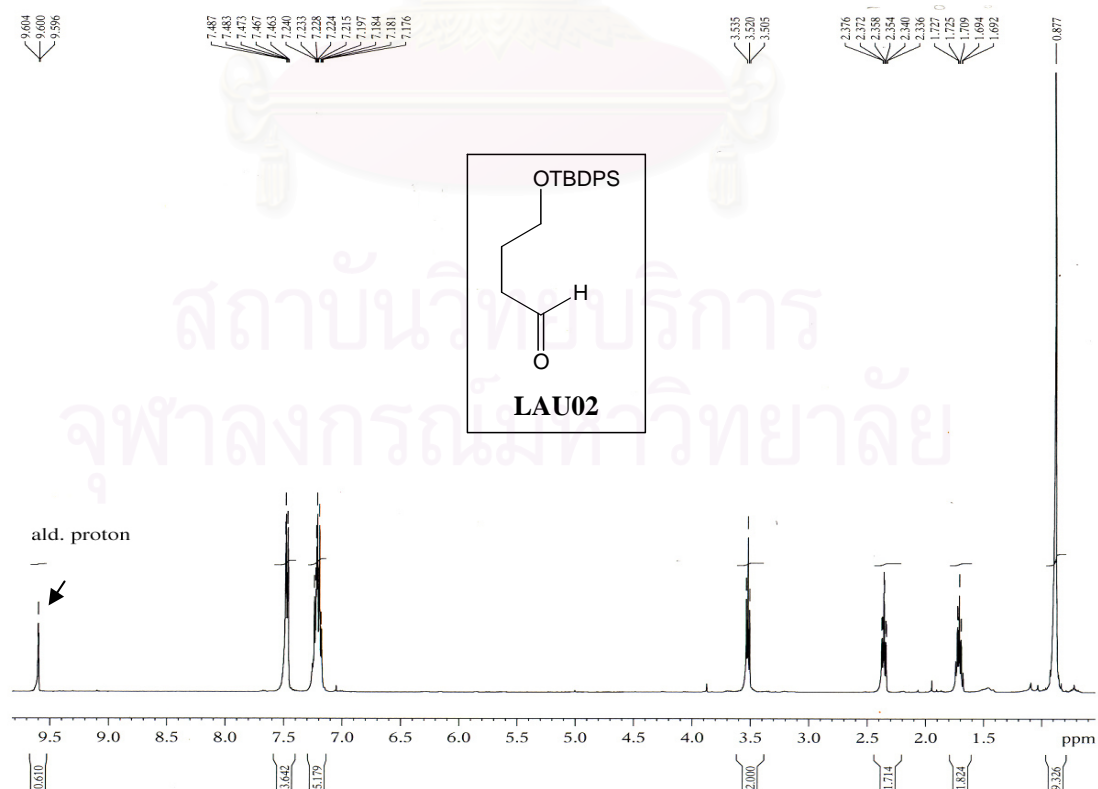
Figure 21 ^{1}H NMR (400 MHz) Spectrum of **LAU02** in CDCl$_3$
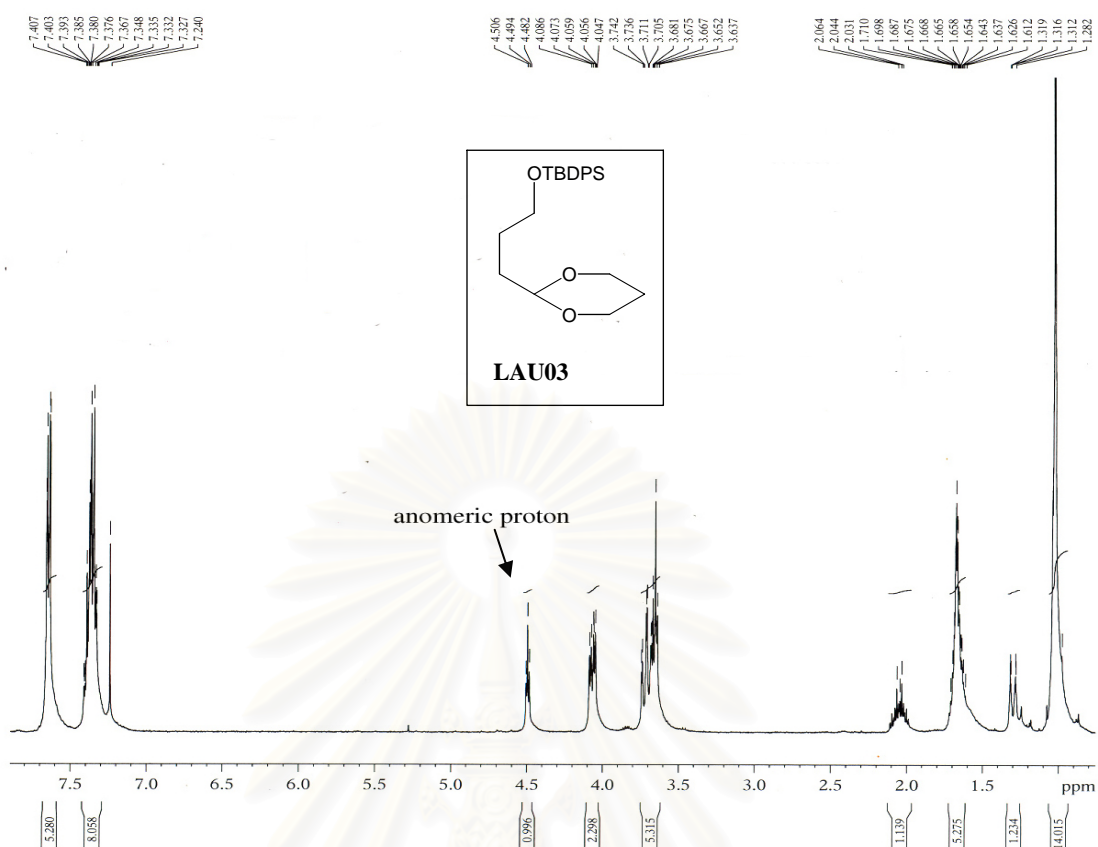
Figure 22 ^{1}H NMR (400 MHz) Spectrum of **LAU03** in CDCl$_3$
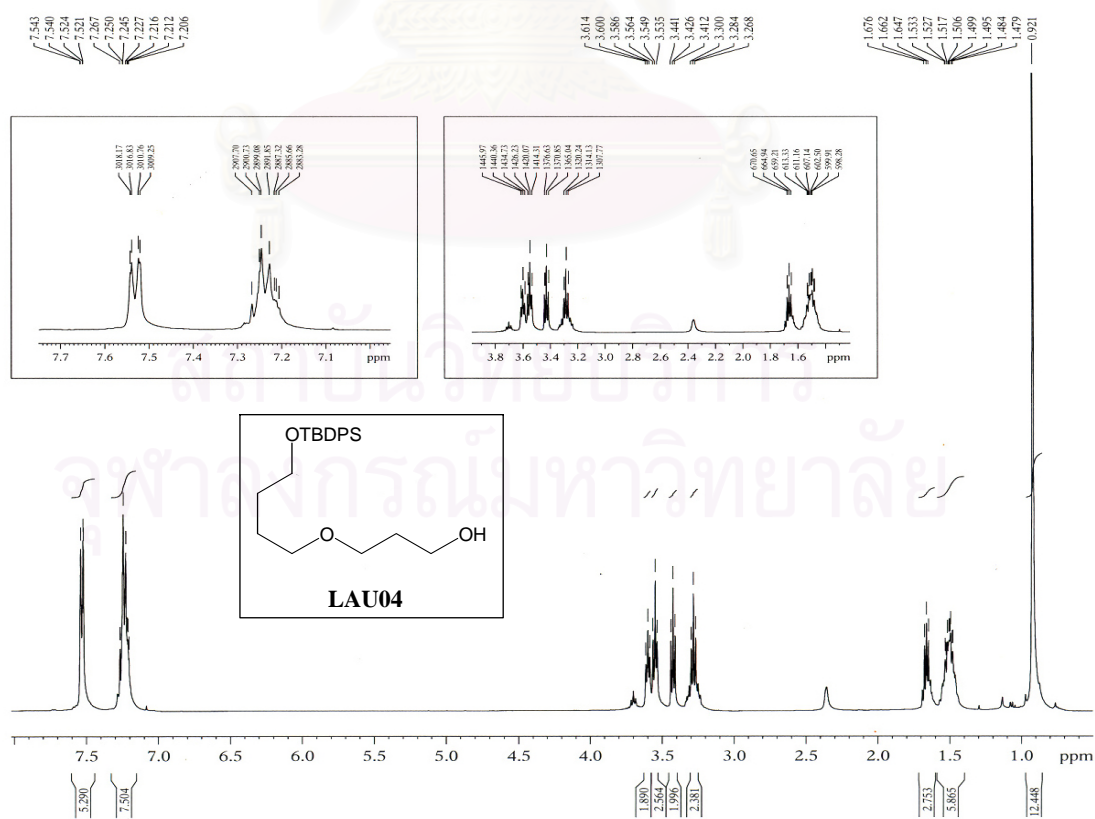
Figure 23 ^{1}H NMR (400 MHz) Spectrum of **LAU04** in CDCl$_3$

Figure 24 ^{1}H NMR (400 MHz) Spectrum of **LAU05** in CDCl$_3$

Figure 25 ^{1}H NMR (400 MHz) Spectrum of **LAU06** in CDCl$_3$
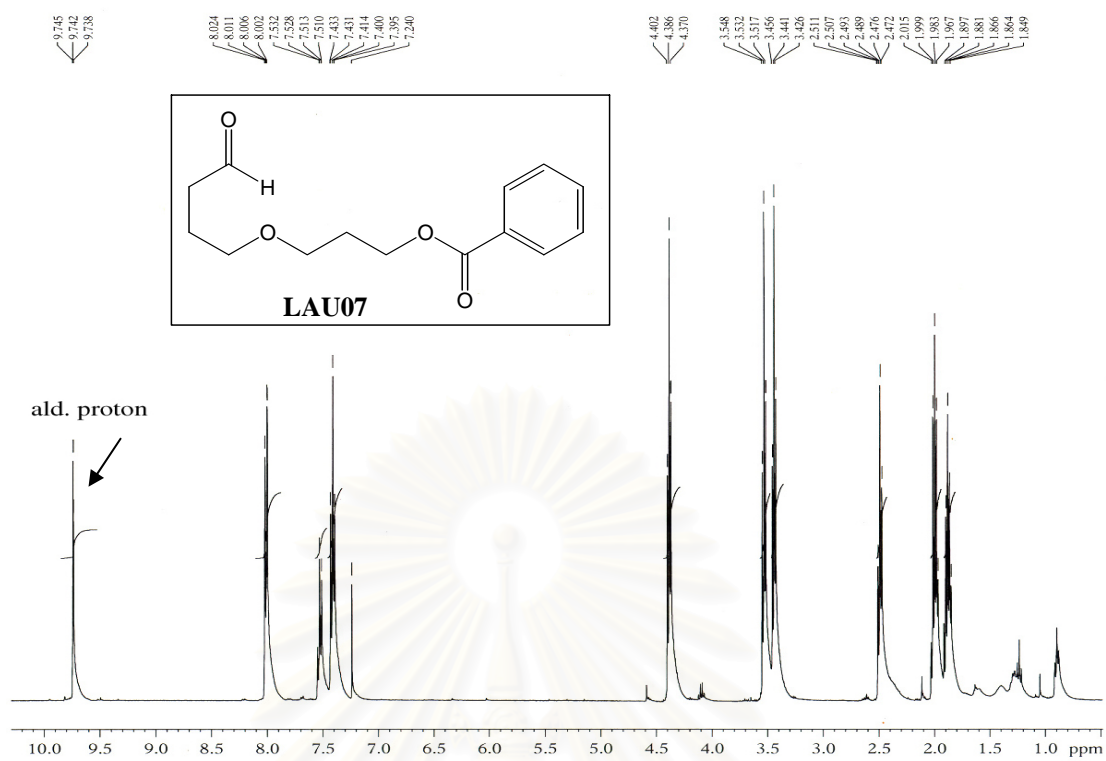
Figure 26 ^{1}H NMR (400 MHz) Spectrum of **LAU07** in CDCl$_3$
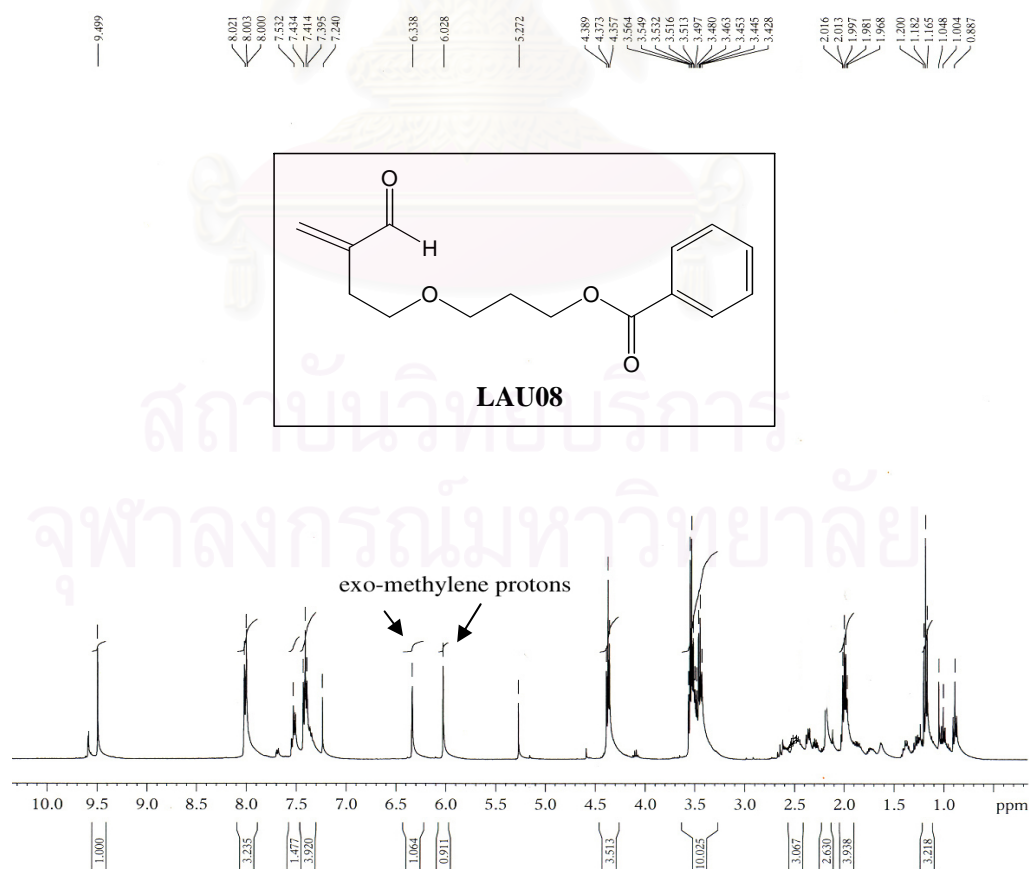
Figure 27 ^{1}H NMR (400 MHz) Spectrum of **LAU08** in CDCl$_3$

Figure 28 ^{1}H NMR (400 MHz) Spectrum of **LAU09** in CDCl$_3$

Figure 29 ^{1}H NMR (400 MHz) Spectrum of **LAU10** in CDCl$_3$
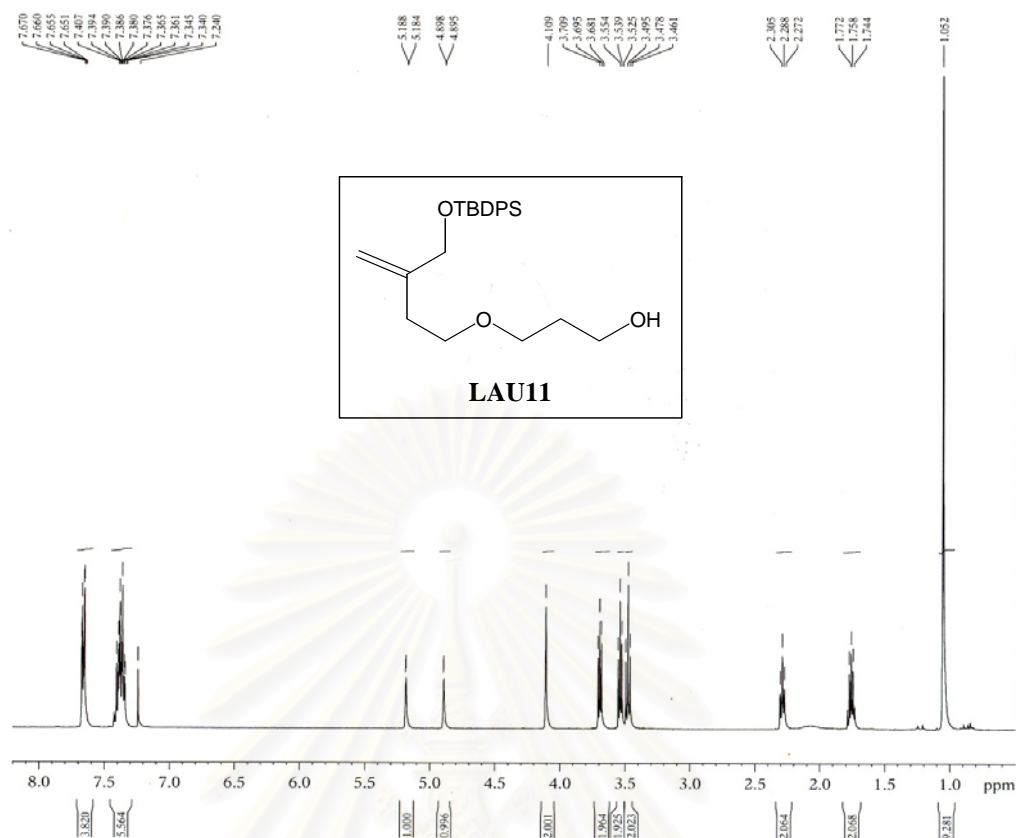
Figure 30 ¹H NMR (400 MHz) Spectrum of **LAU11** in CDCl₃
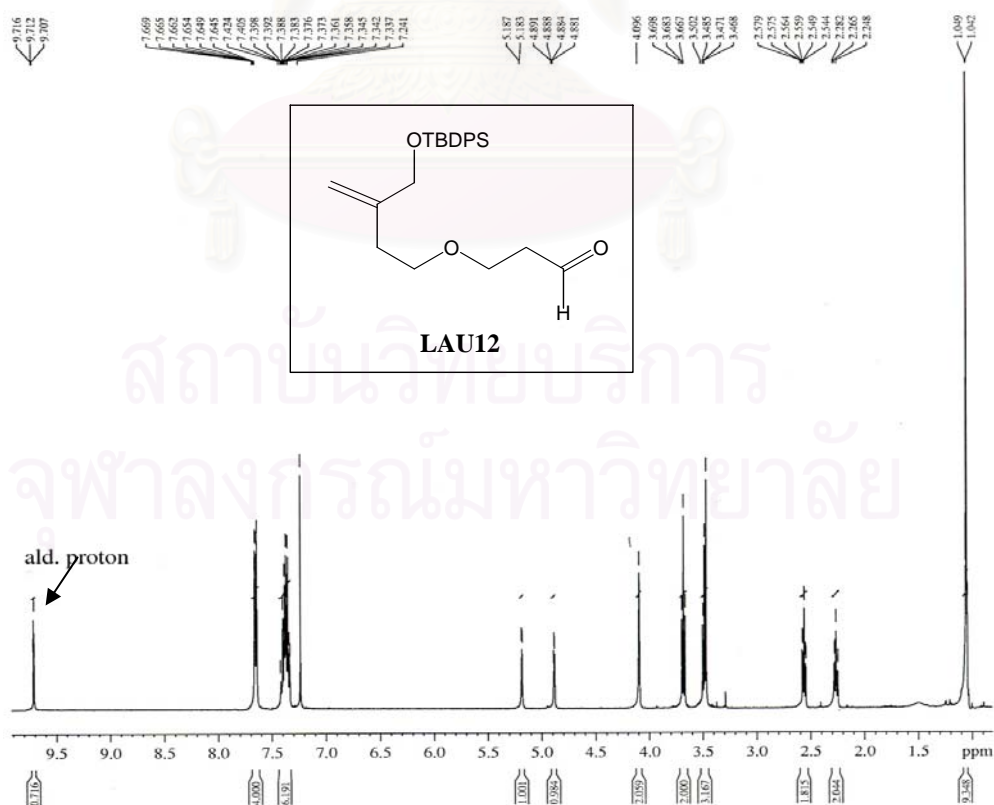
Figure 31 ¹H NMR (400 MHz) Spectrum of **LAU12** in CDCl₃

Figure 32 ^{1}H NMR (400 MHz) Spectrum of **DMB alcohol** in CDCl$_3$
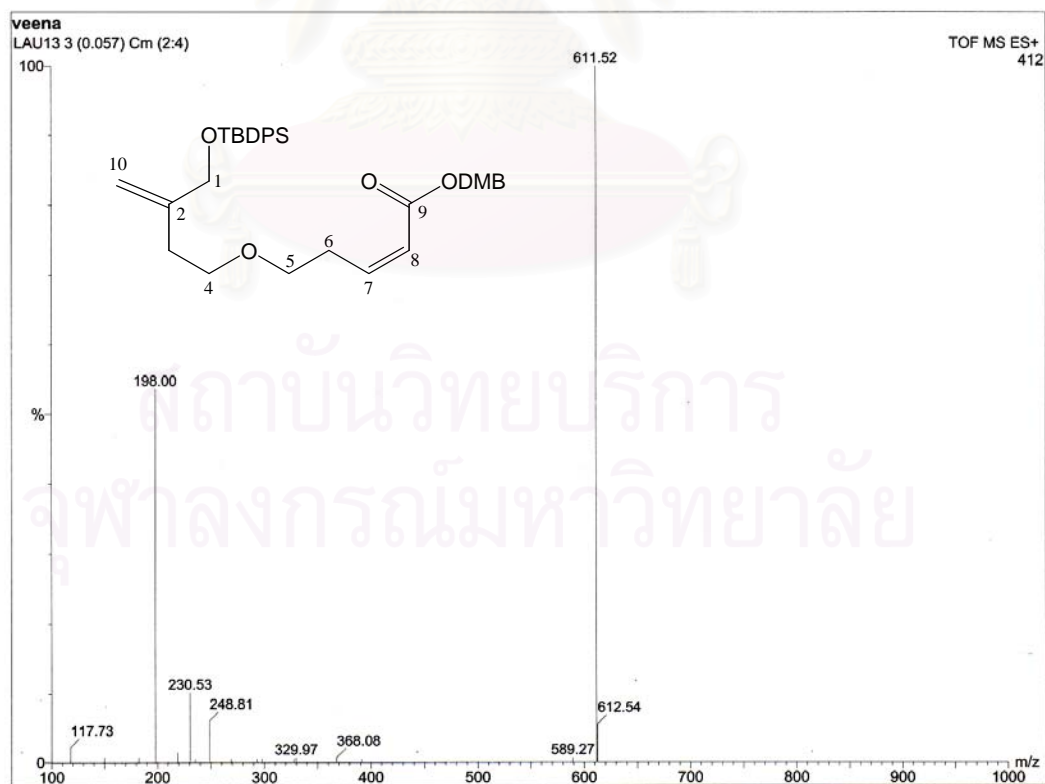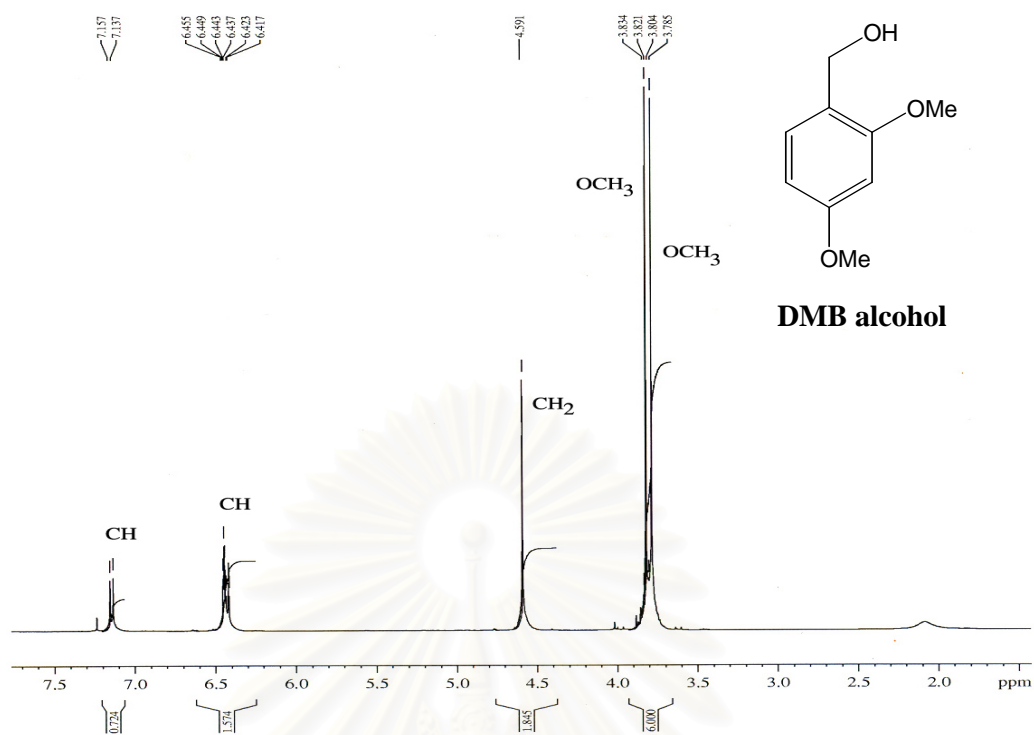
Figure 33 TOF MS Spectrum of **LAU13**
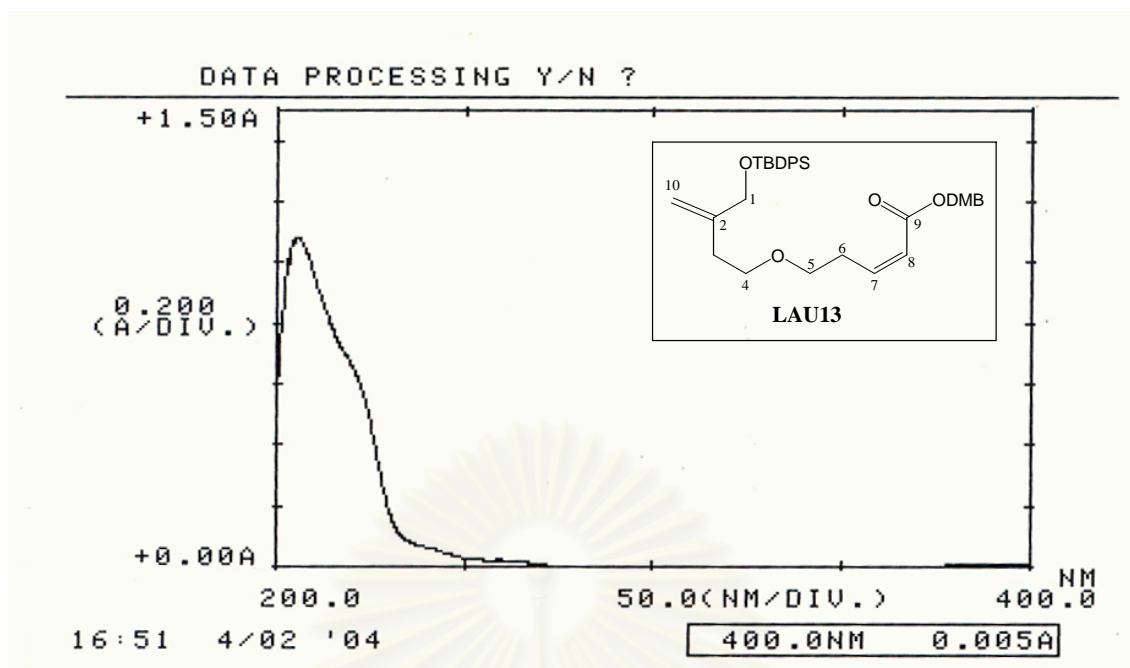
Figure 34 UV Spectrum of **LAU13** in MeOH
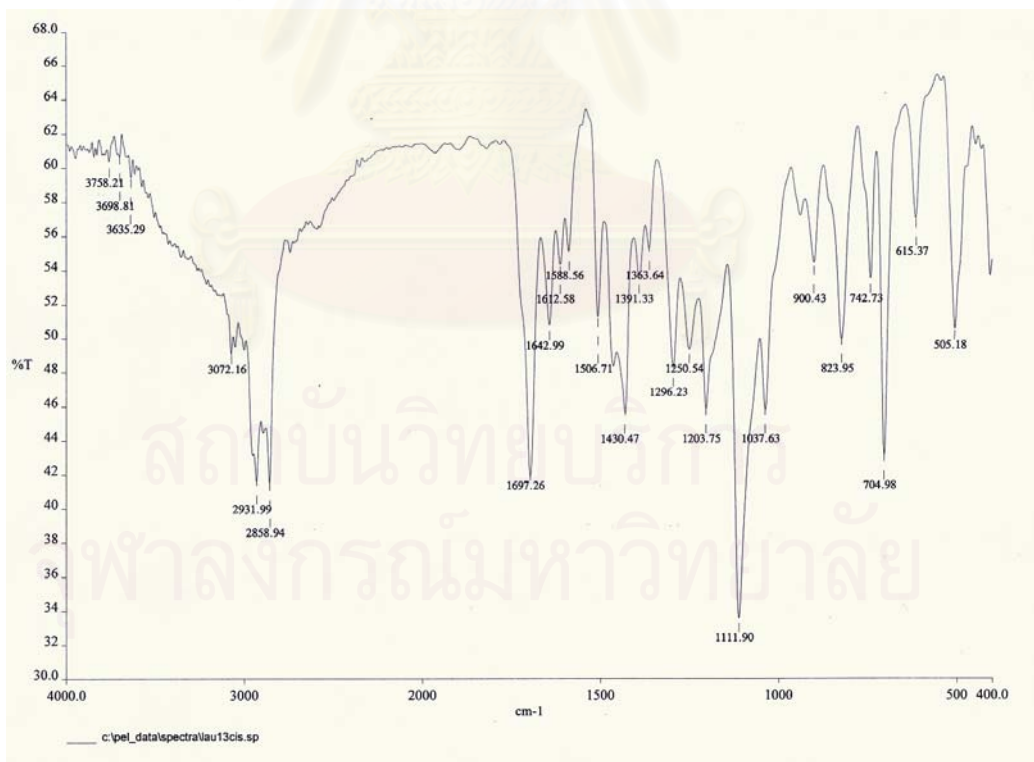
Figure 35 IR Spectrum (Film) of **LAU13**
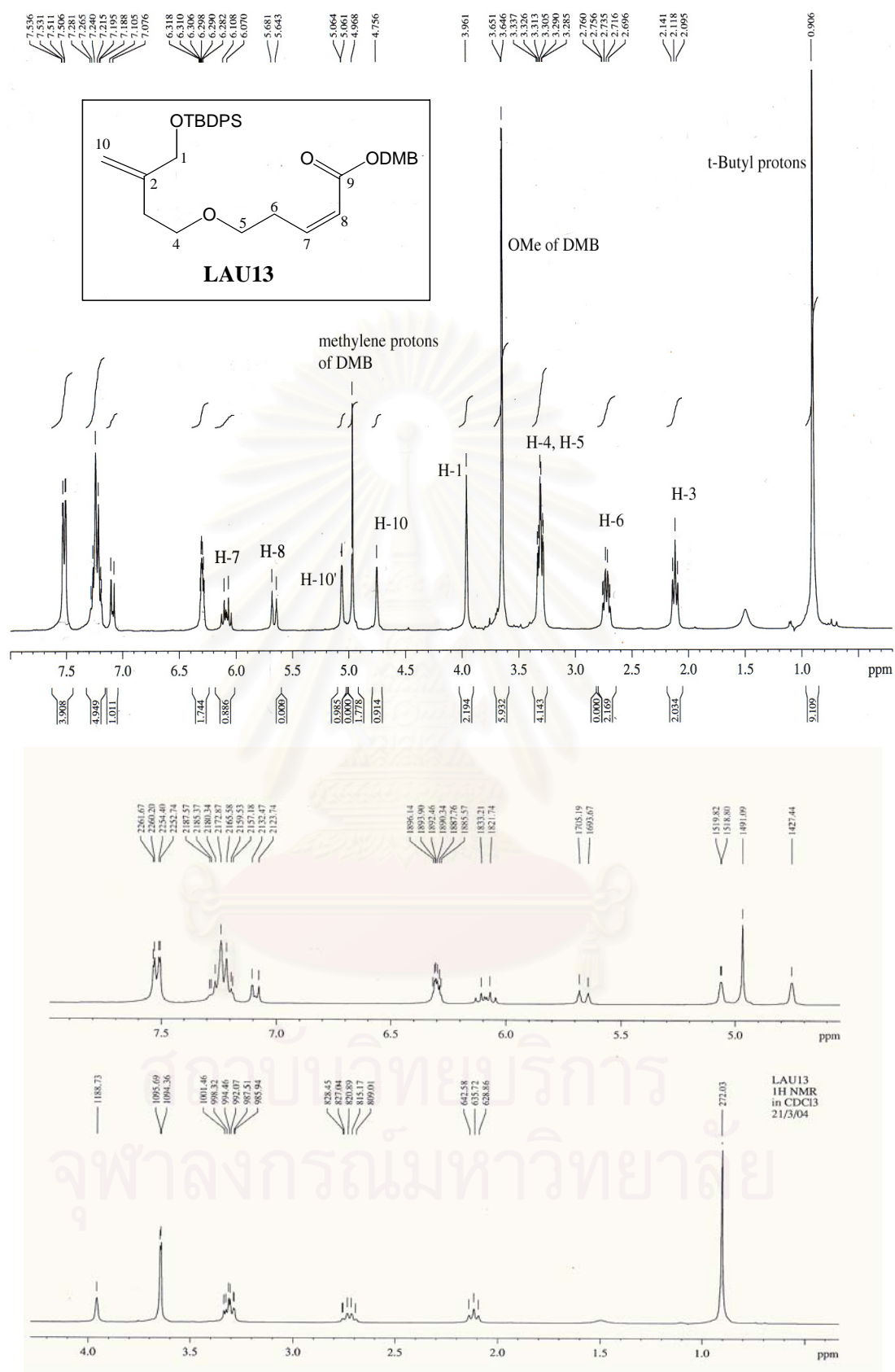
Figure 36 ^{1}H NMR (300 MHz) Spectrum of **LAU13** in CDCl$_3$
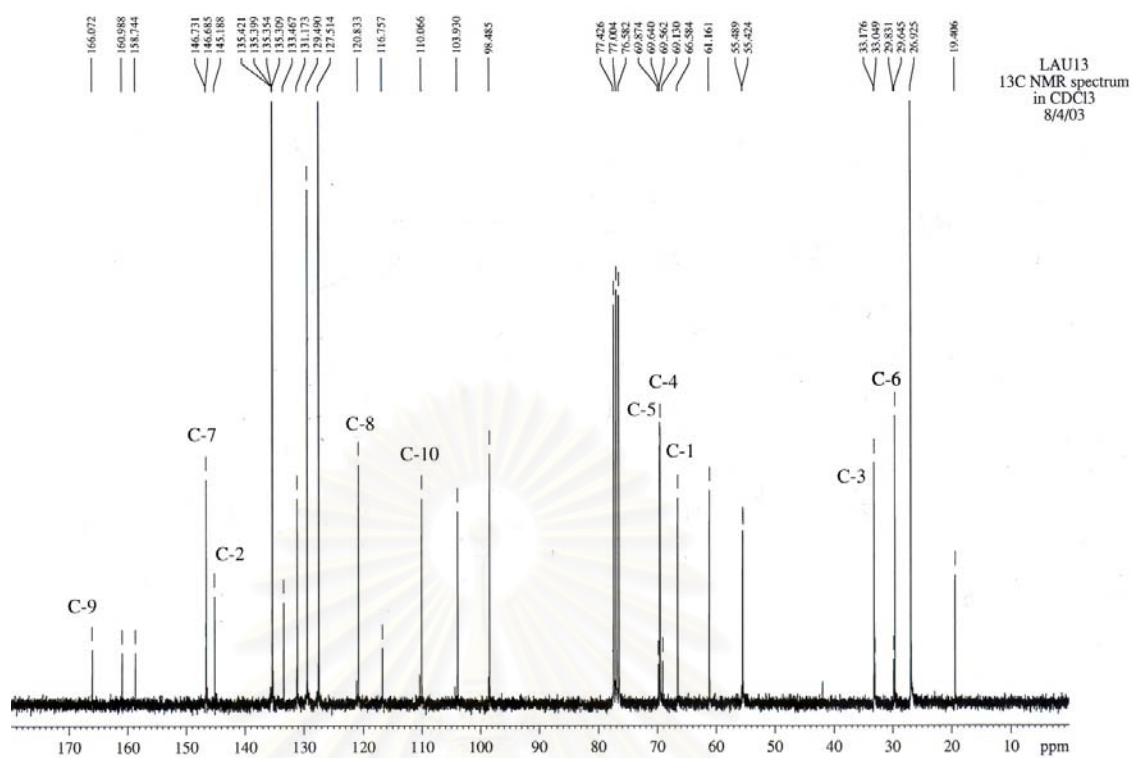
Figure 37 ^{13}C NMR (75 MHz) Spectrum of **LAU13** in CDCl$_3$
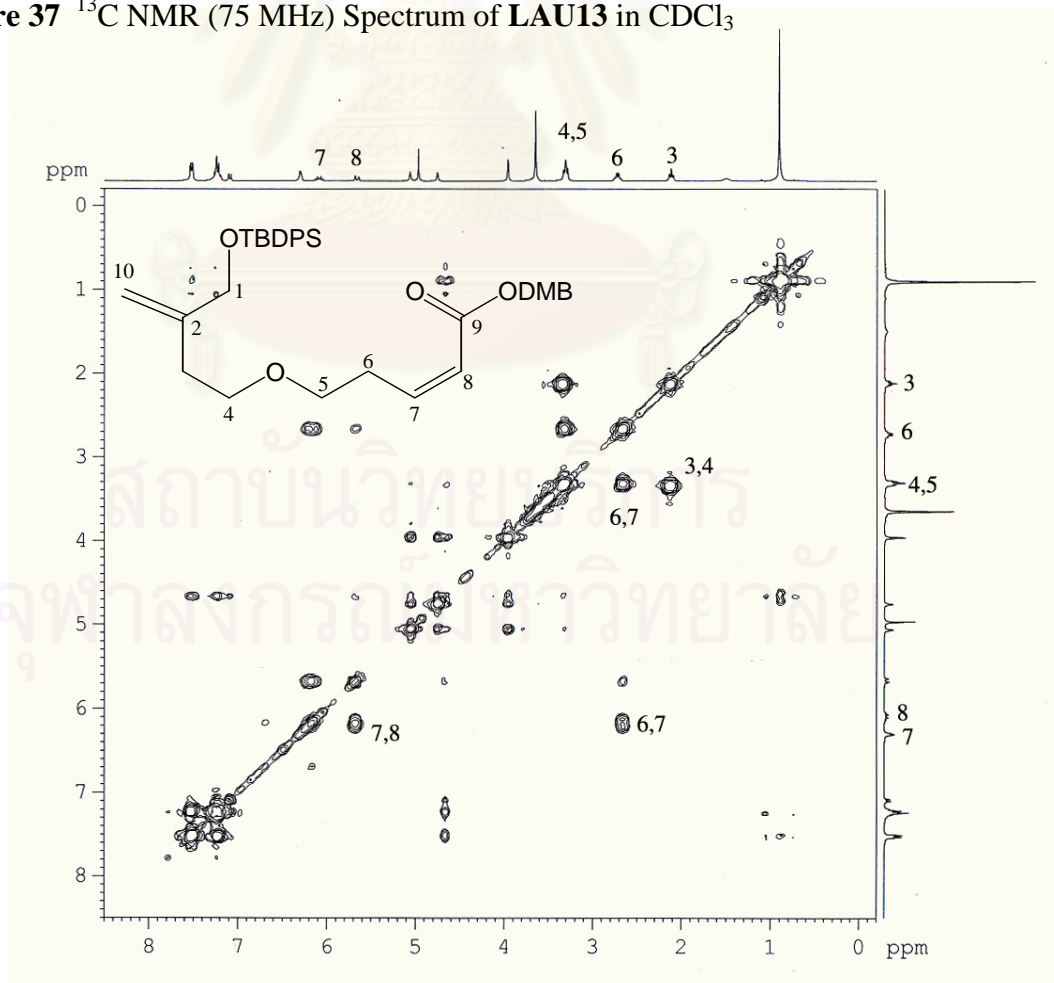
Figure 38 H,H-COSY Spectrum of **LAU13** in CDCl$_3$
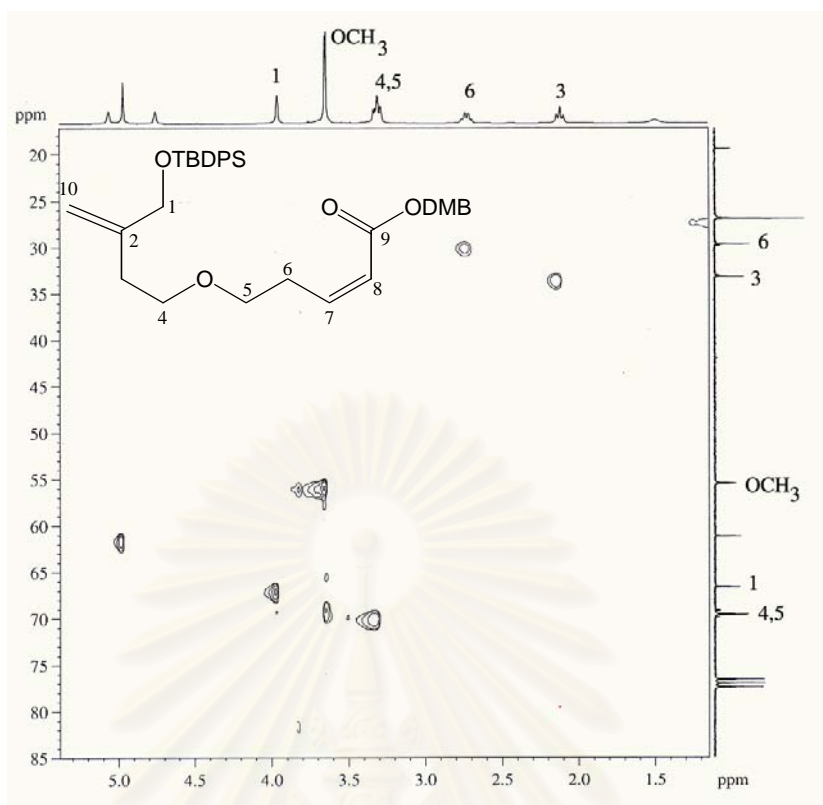
Figure 39 HMQC Spectrum of **LAU13** in CDCl₃
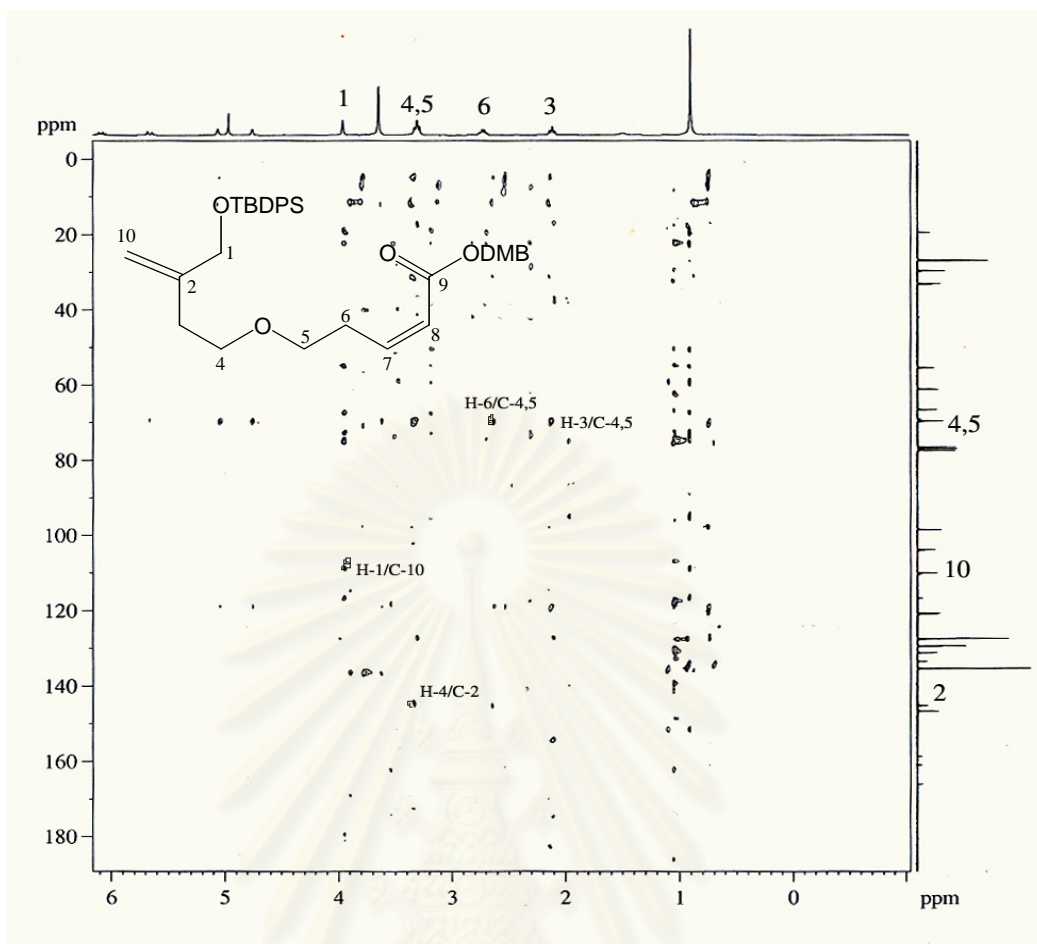
Figure 40 HMBC ($^nJ_{HC}$ = 8 Hz) Spectrum of **LAU13** in CDCl$_3$
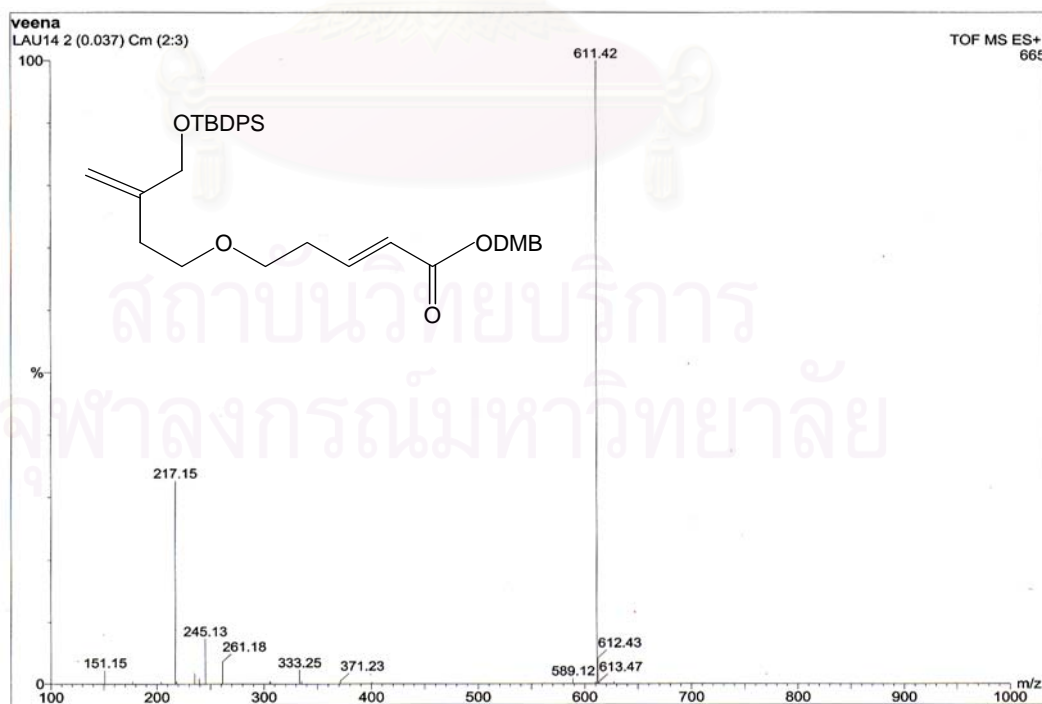
Figure 41 TOF MS Spectrum of **LAU14**
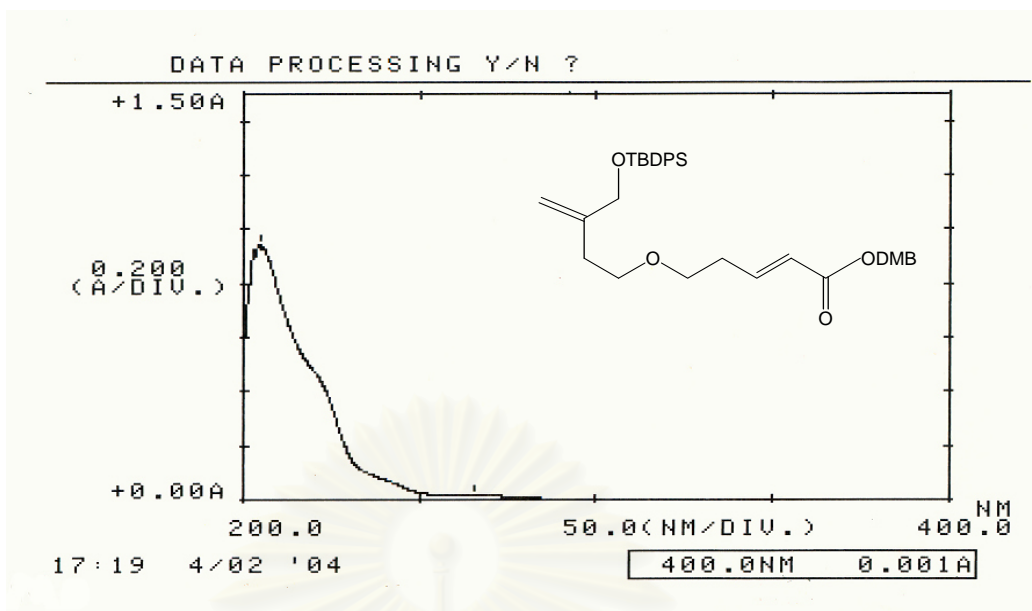
Figure 42 UV Spectrum of **LAU14** in MeOH
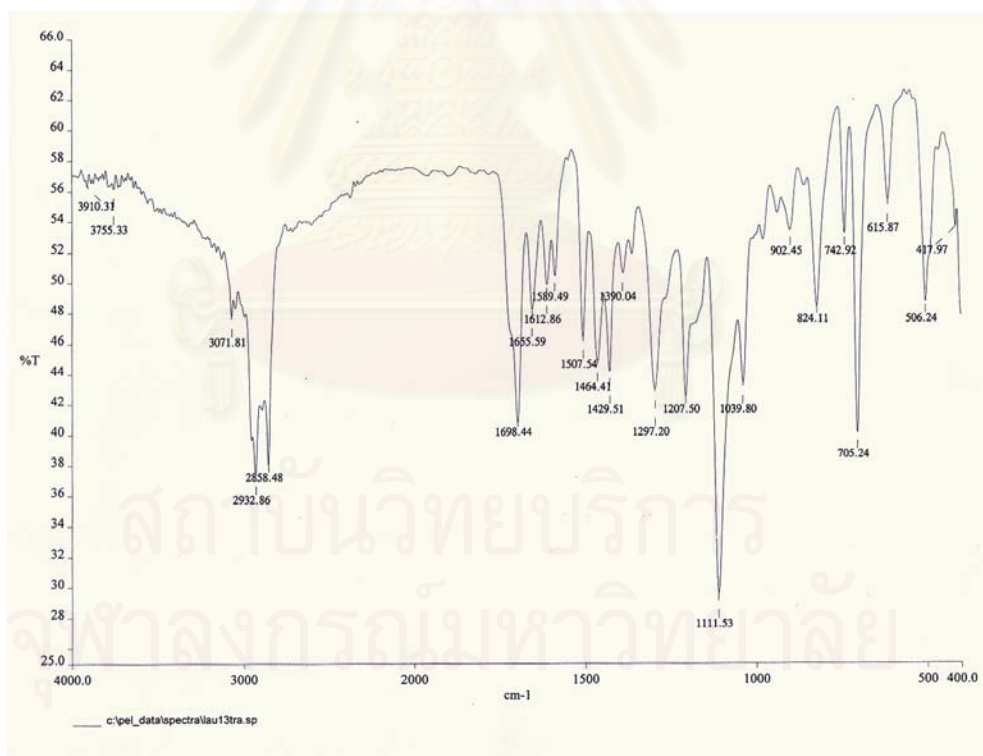
Figure 43 IR spectrum (Film) of **LAU14**
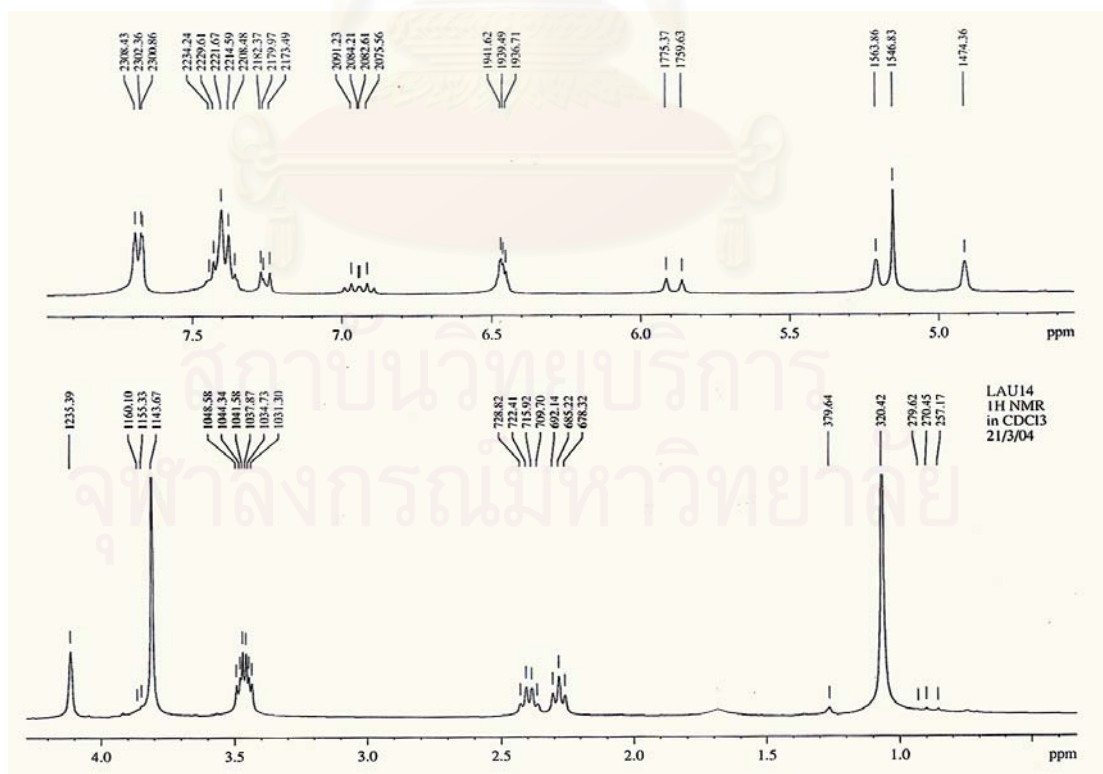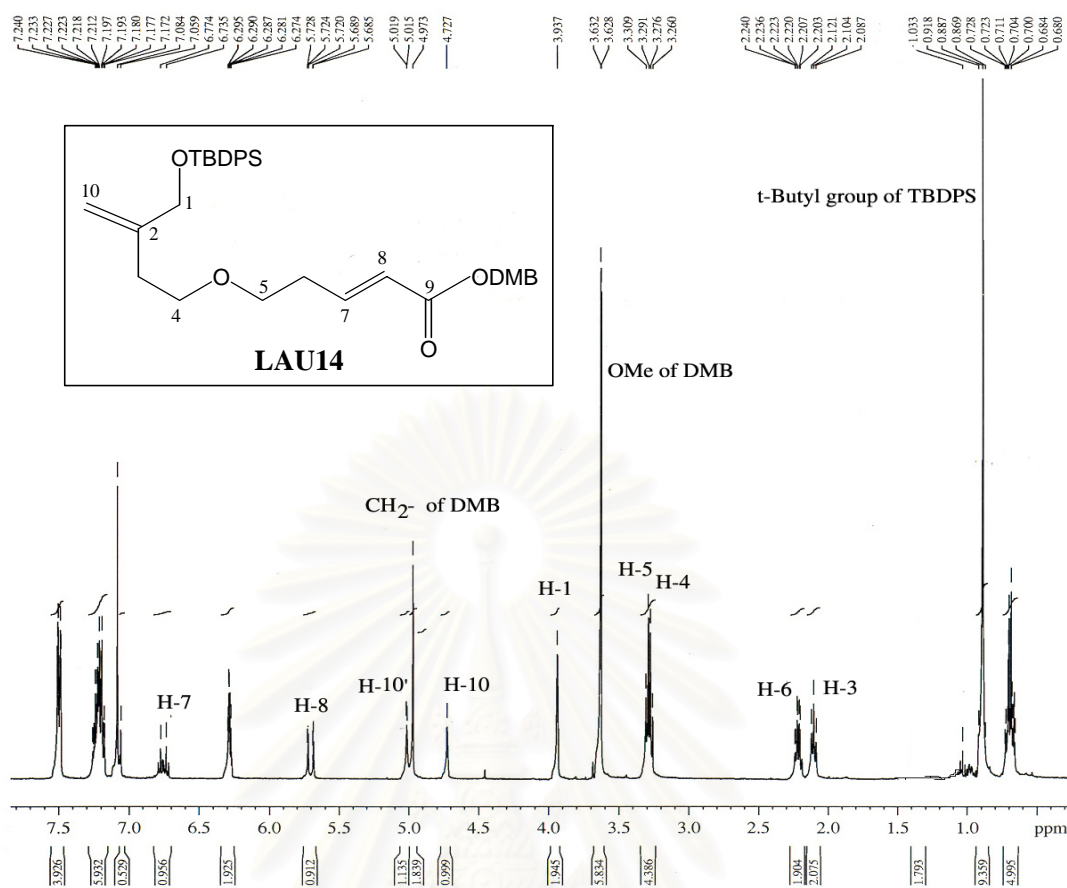
Figure 44 ^{1}H NMR (300 MHz) Spectrum of **LAU14** in CDCl$_3$
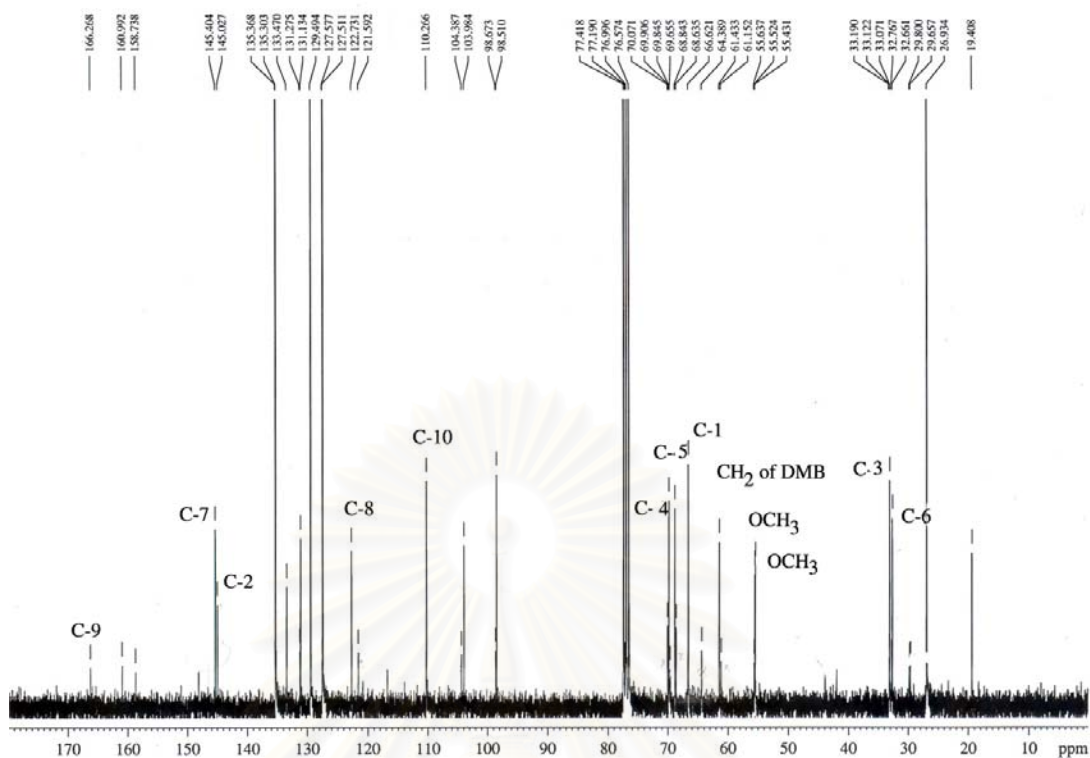
Figure 45 ^{13}C NMR (75 MHz) Spectrum of **LAU14** in CDCl$_3$
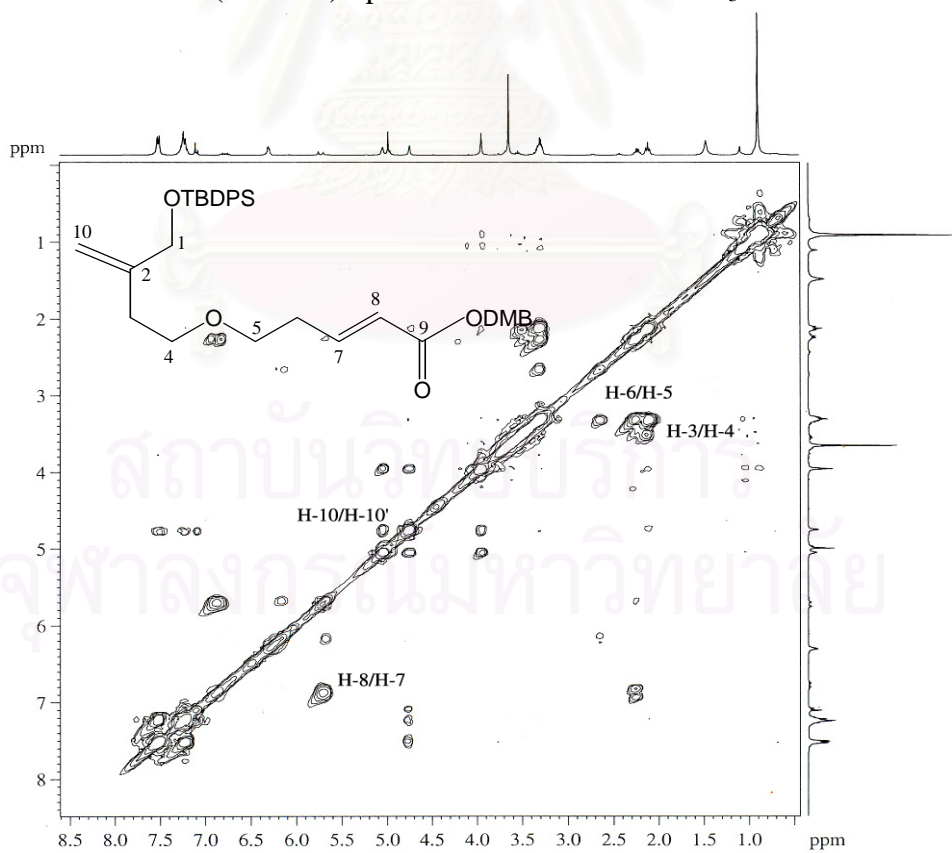
Figure 46 H,H-COSY Spectrum of **LAU14** in CDCl$_3$
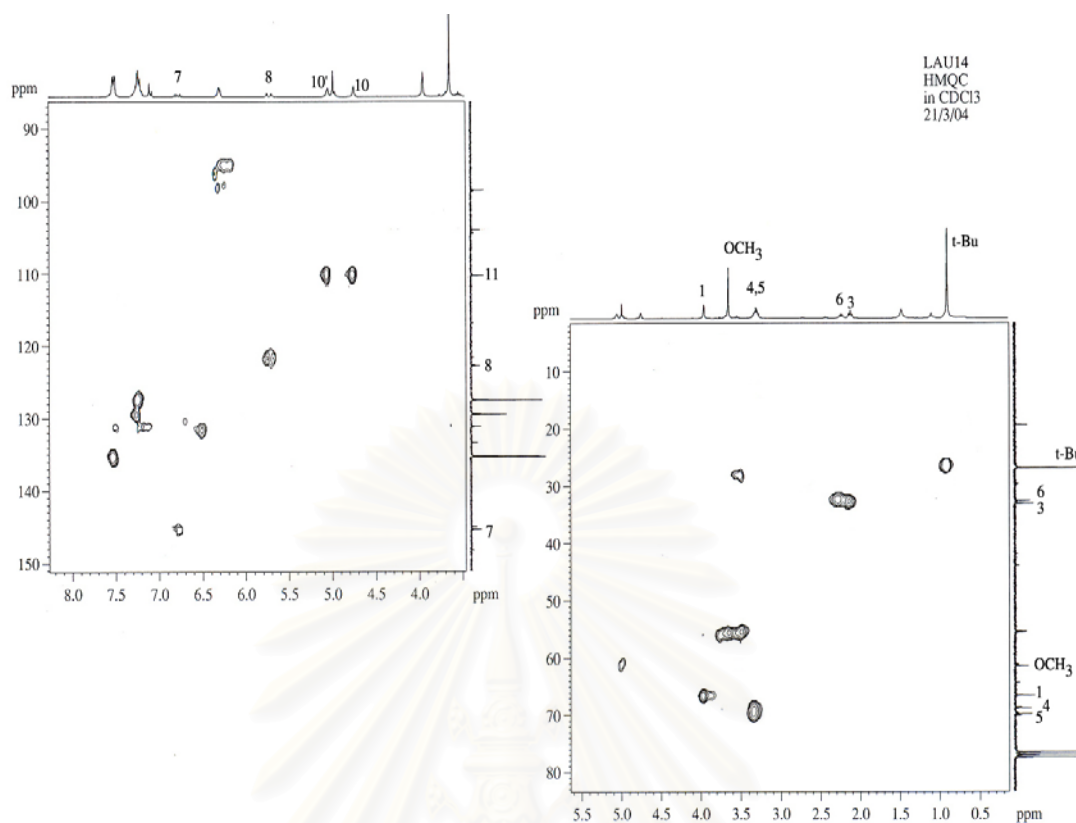
Figure 47 HMQC Spectrum of **LAU14** in CDCl₃
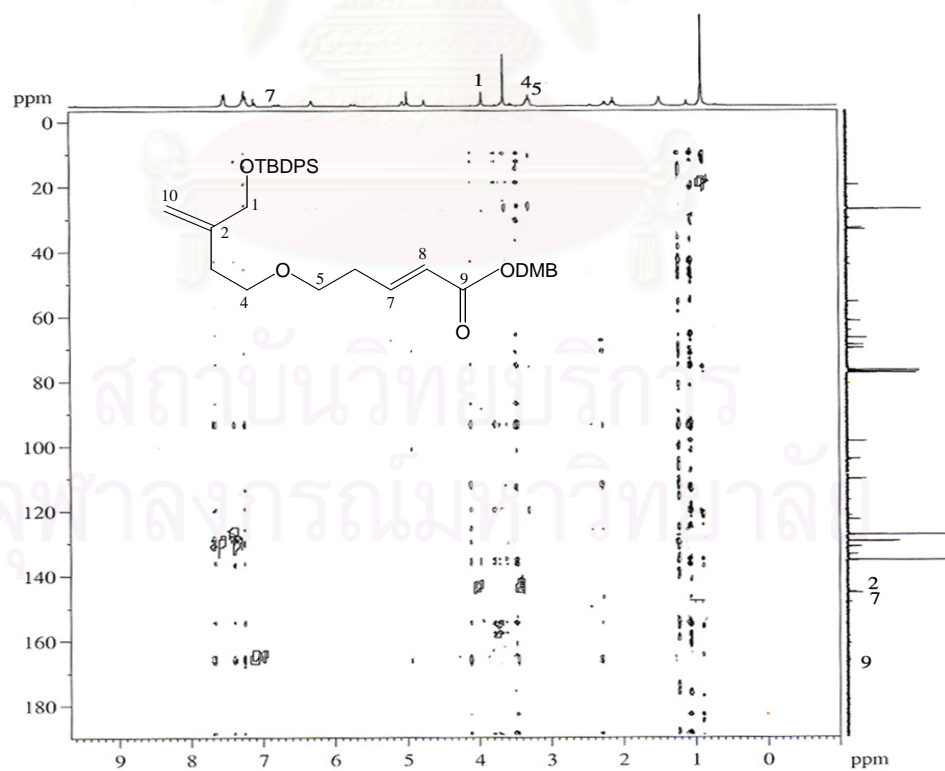
Figure 48 HMBC (ⁿJ_{HC} = 8 Hz) Spectrum of **LAU14** in CDCl₃
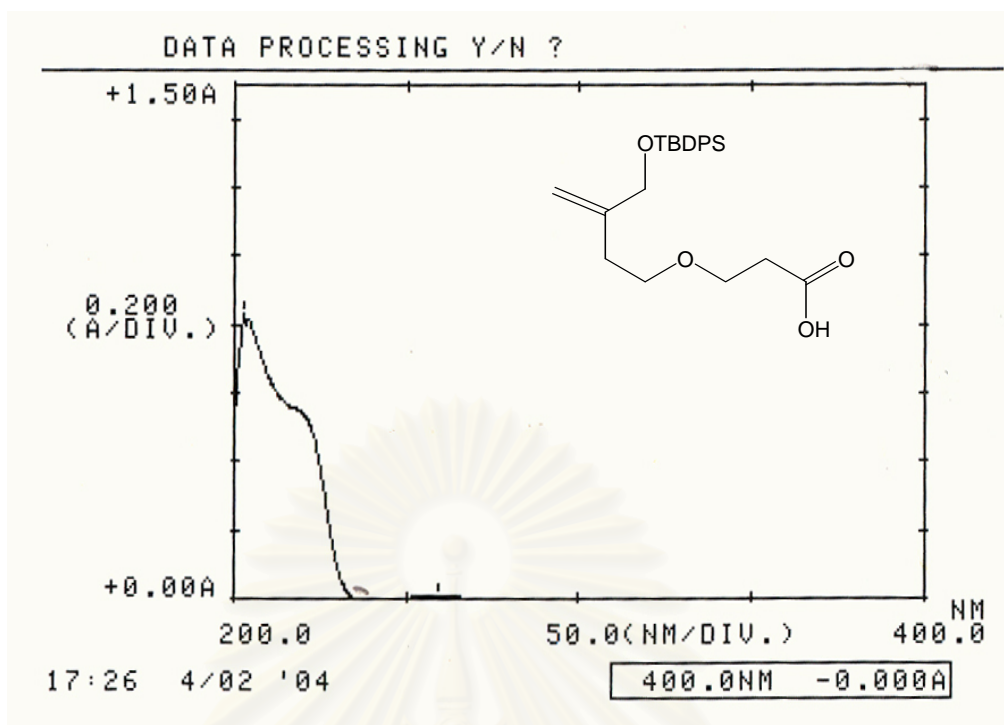
Figure 49 UV Spectrum of **LAU15** in MeOH
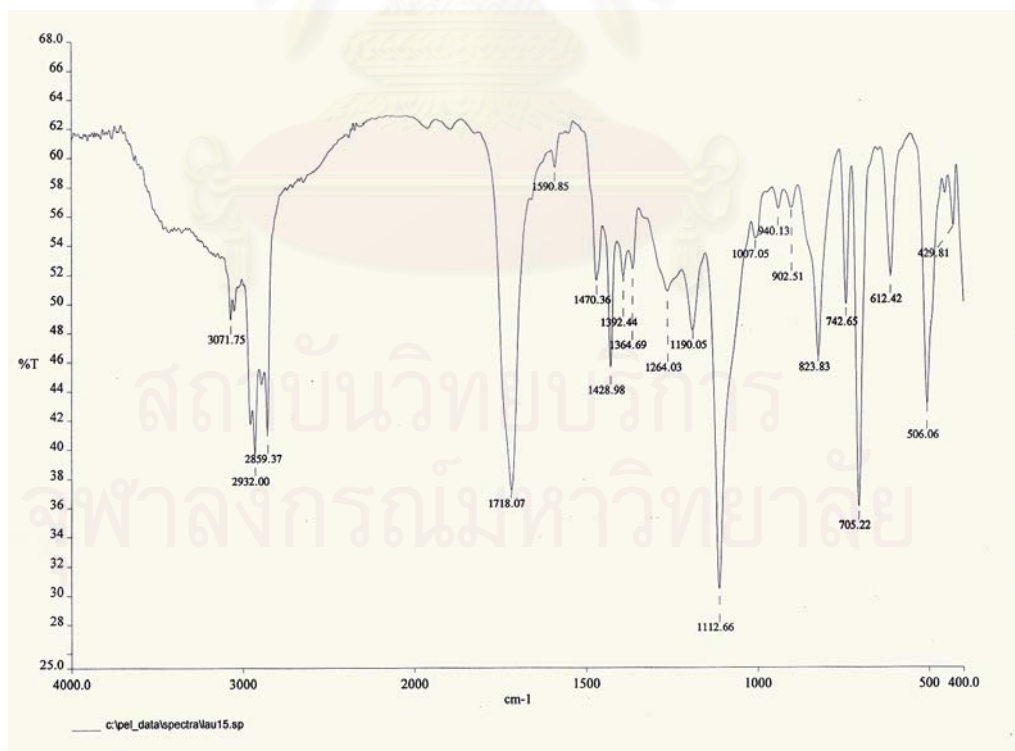
Figure 50 IR Spectrum (Film) of **LAU15**
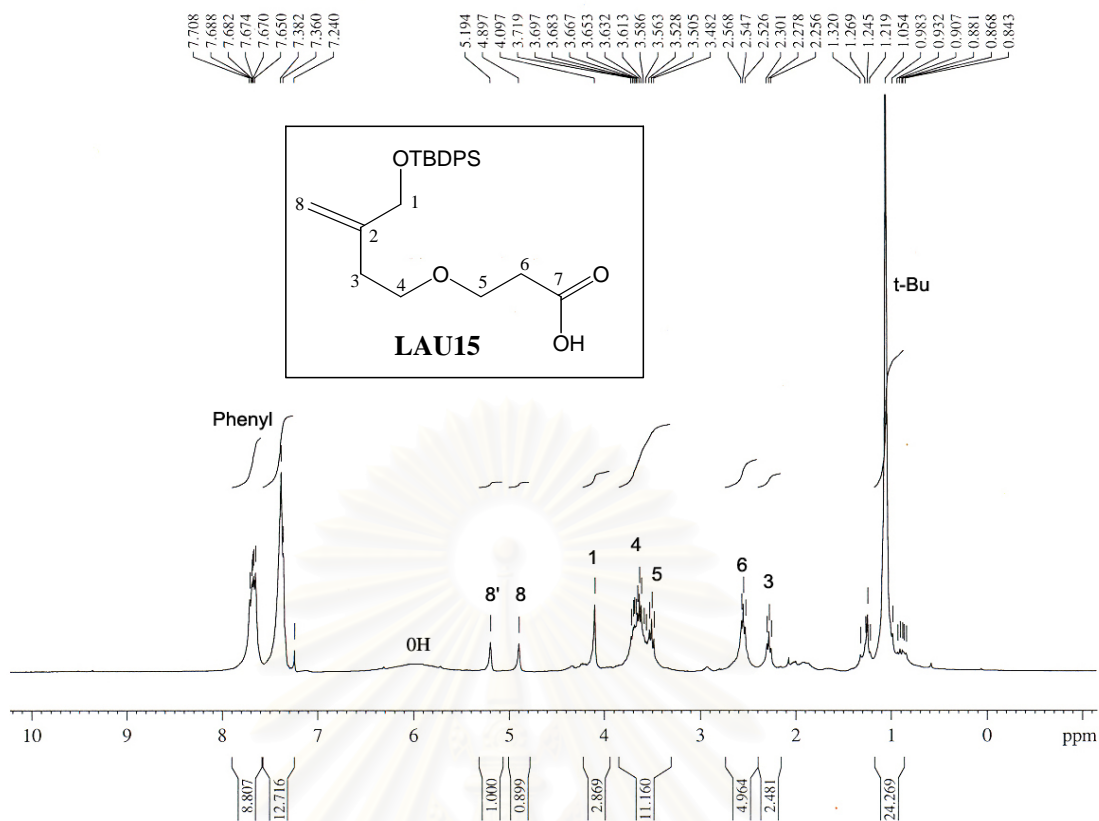
Figure 51 ^{1}H NMR (300 MHz) Spectrum of **LAU15** in CDCl$_3$
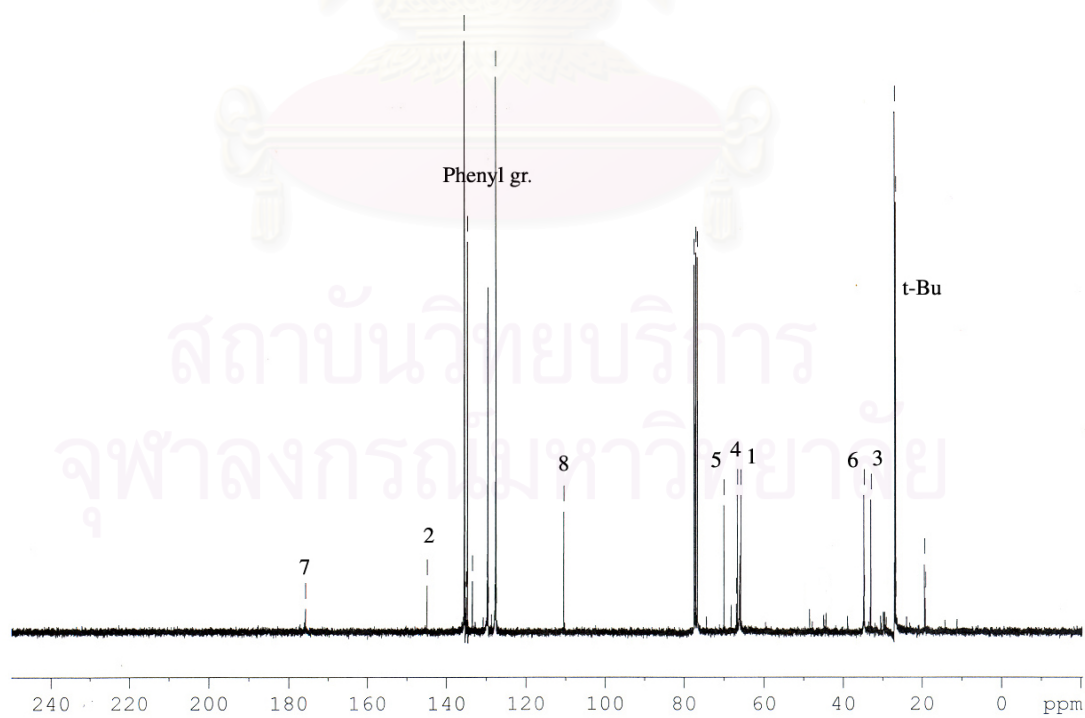
Figure 52 ^{13}C NMR (75 MHz) Spectrum of **LAU15** in CDCl$_3$
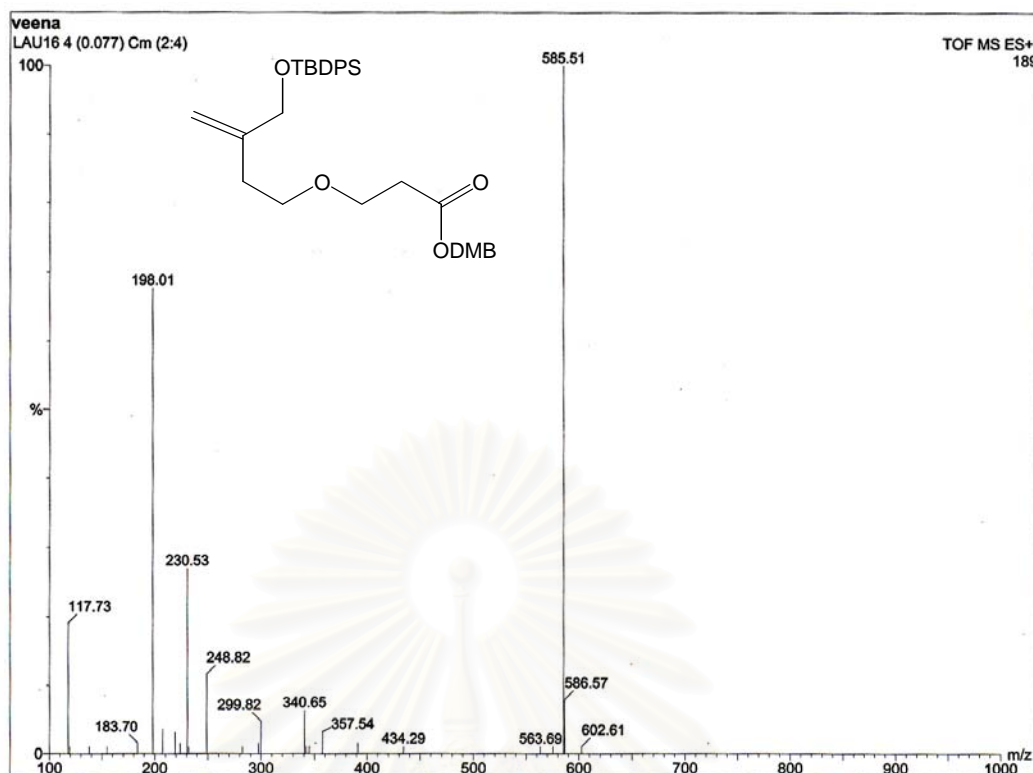
Figure 53 TOF MS Spectrum of **LAU16**
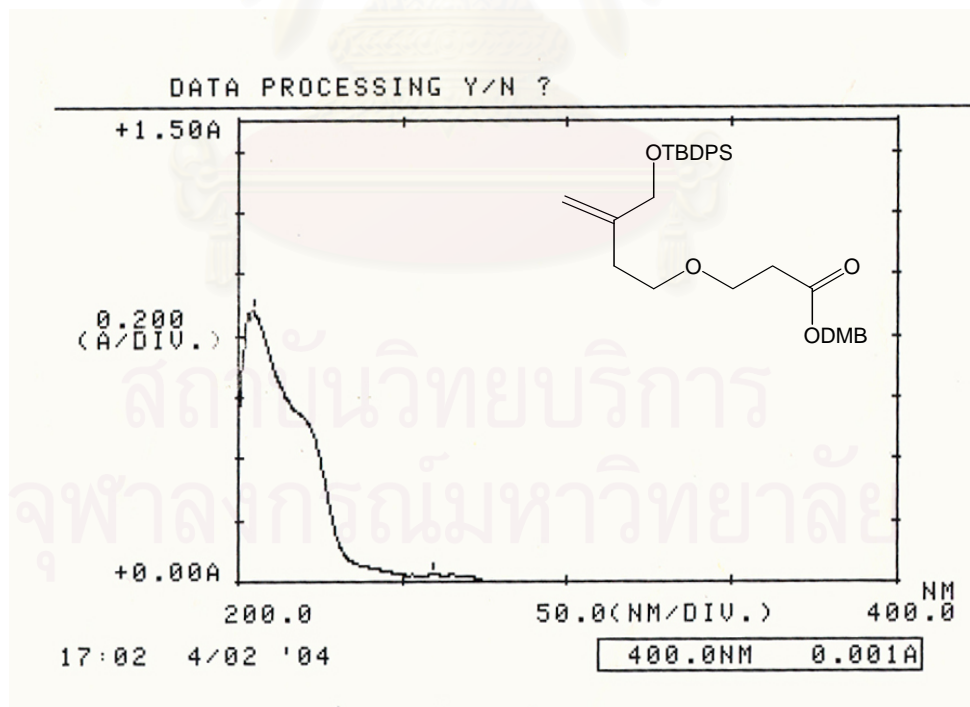
Figure 54 UV Spectrum of **LAU16** in MeOH
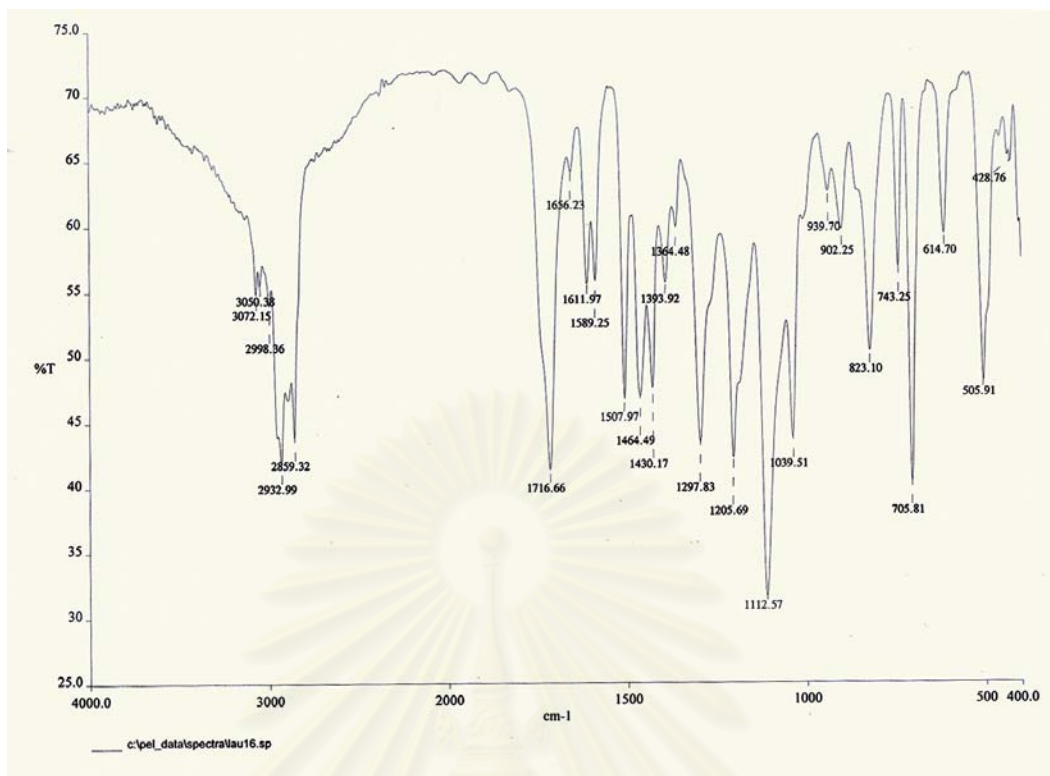
Figure 55 IR Spectrum (Film) of **LAU16**
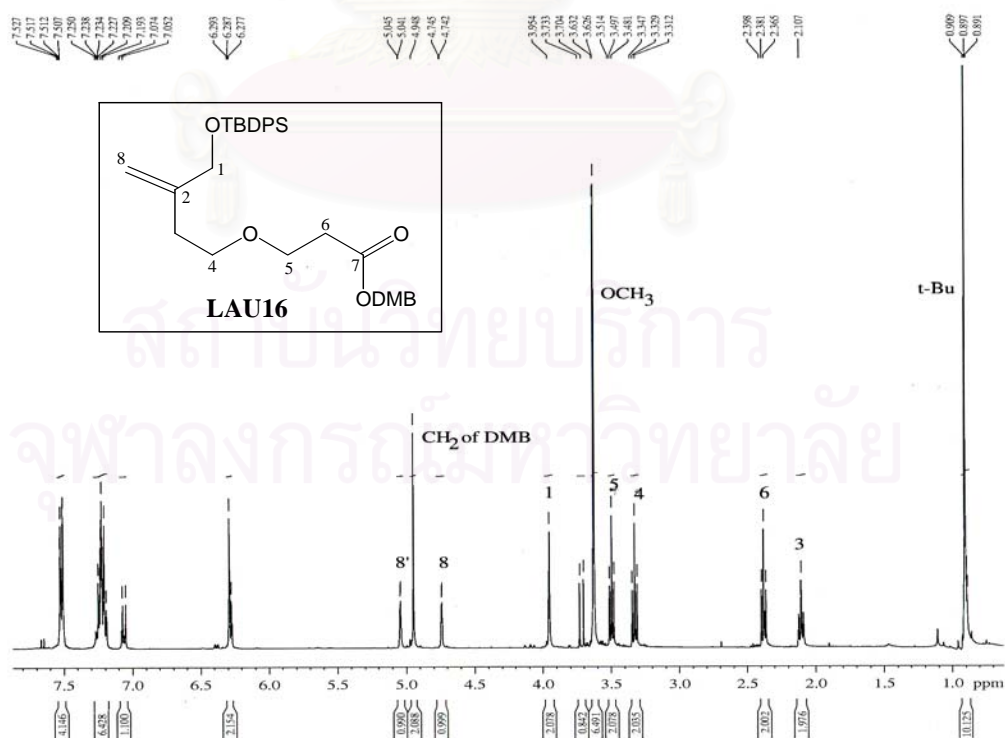
Figure 56 ^{1}H NMR (300 MHz) Spectrum of **LAU16** in CDCl$_3$

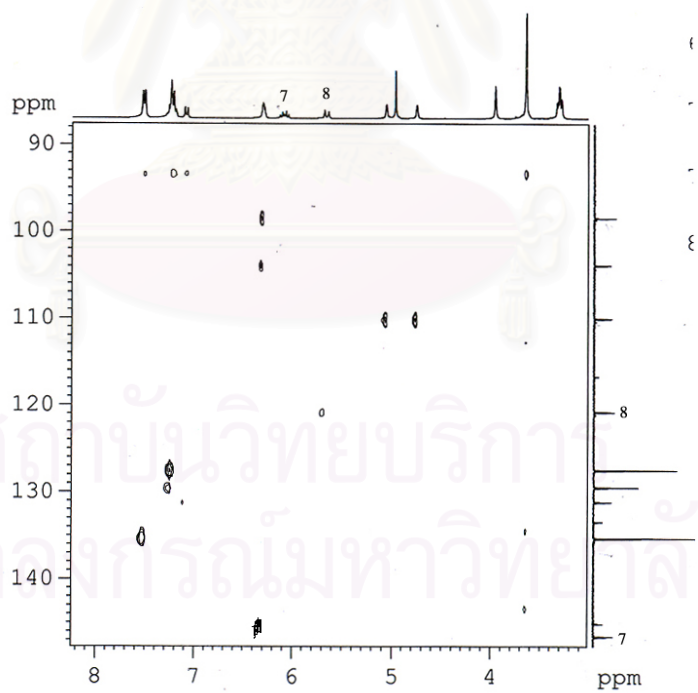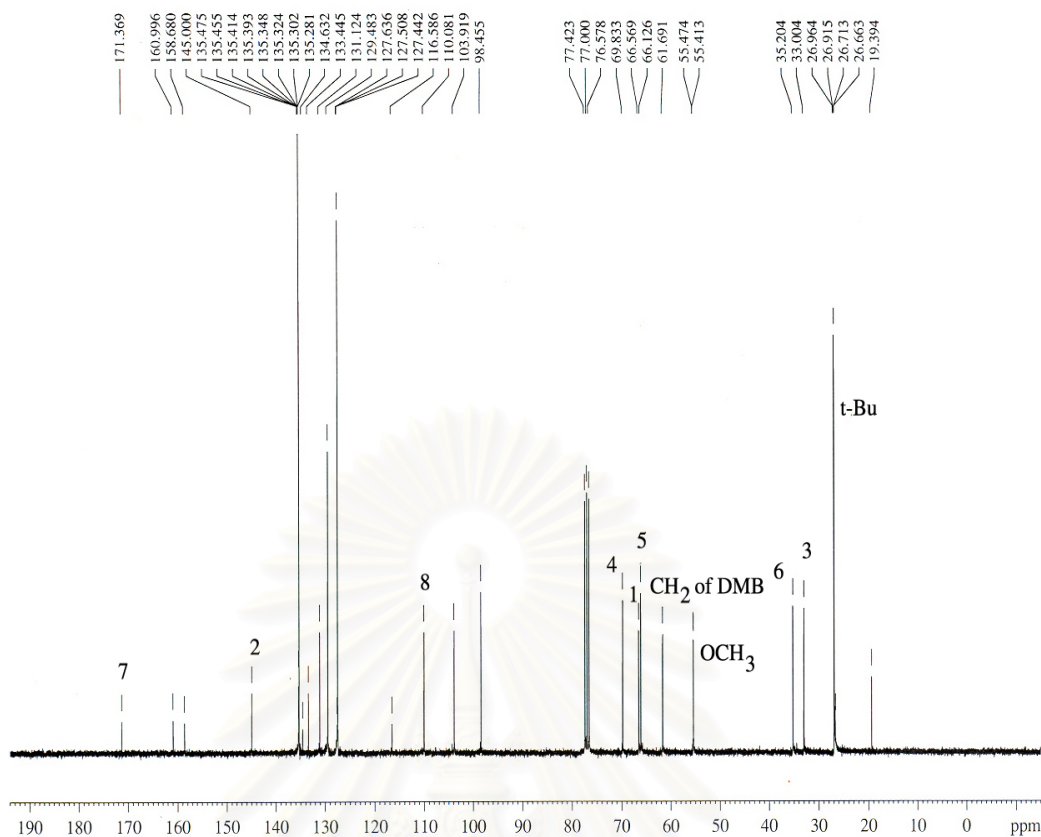**Figure 57** ^{13}C NMR (75 MHz) Spectrum of **LAU16** in CDCl$_3$
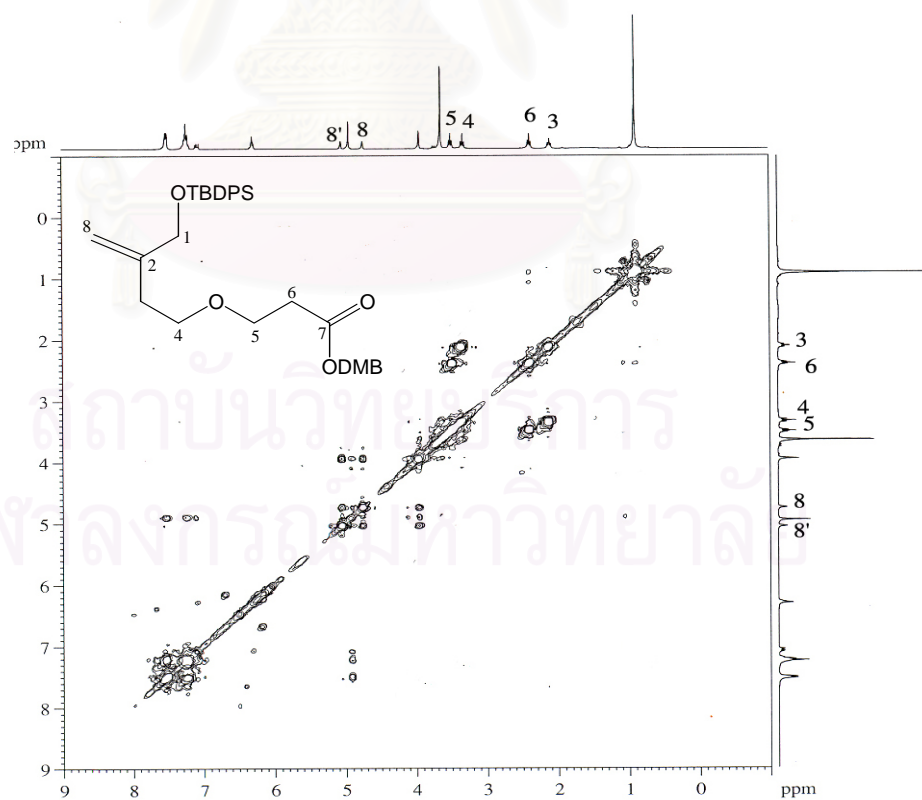
Figure 58 H,H-COSY Spectrum of **LAU16** in CDCl$_3$
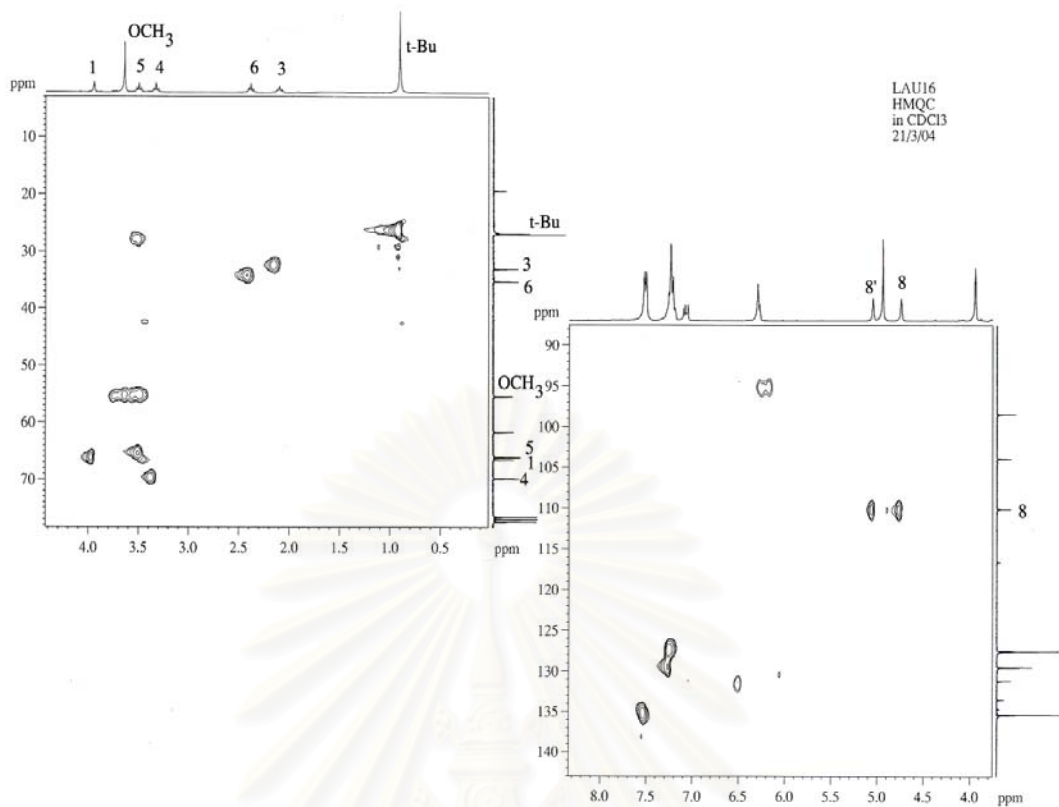
Figure 59 HMQC Spectrum of **LAU16** in CDCl$_3$
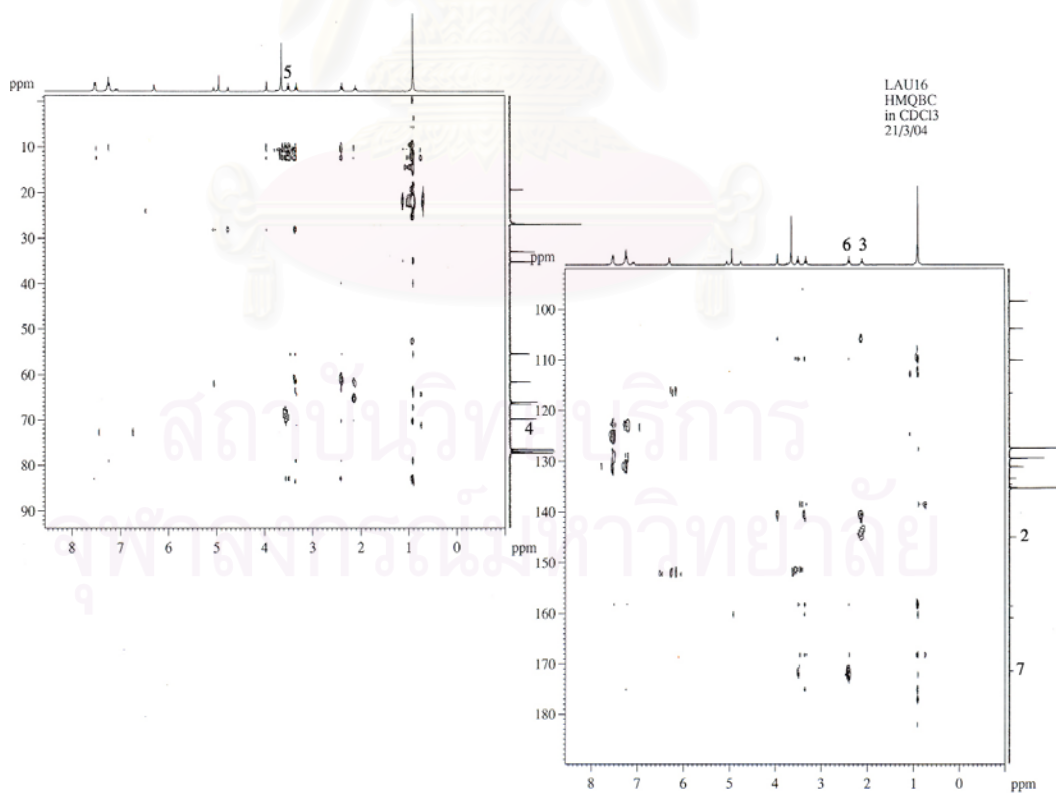
Figure 60 HMBC ($^nJ_{HC}$ = 8 Hz) Spectrum of **LAU16** in CDCl$_3$

REFERENCES

Ahmed, A., Hoegenauer, E. K., Enev, V. E., Hanbauer, M., Kahlig, H., Ohler, E., and Mulzer, J. 2003. Total synthesis of the microtubule stabilizing antitumor agent laulimalide and some nonnatural analogues: the power of sharpless' asymmetric epoxidation. J. Org. Chem. 68: 3026-3042.

Altmann, K. 2001. Microtubule-stabilizing agents: a growing class of important anticancer drugs. Curr. Opin. Chem. Biol. 5: 424-431.

Altmann, K. H., Wartmann, M., and O'Reilly, T. 2000. Epothilones and related structures-a new class of microtubule inhibitors with potent in vivo antitumor activity. Biochim. Biophys. Acta 1470: M79-M91.

Alvi, K. A., Tenenbaum, L., and Crews, P. 1991. Anthelmintic polyfunctional nitrogen-containing terpenoids from marine sponges. J. Nat. Prod. 54: 71-78.

Aoki, S., Wei, H., Matsui, K., Rachmat, R., and Kobayashi, M. 2003. Pyridoacridine alkaloids inducing neuronal differentiation in a neuroblastoma cell line, from marine sponge *Biemna fortis.* Bioorg. Med. Chem. 11: 1969-1973.

Appleton, D. R., Pearce, A. N., Lambert, G., Badcock, R. C., and Copp, B. R. 2002. I sodiplamine, cystodytin K and lissoclinidine: novel bioactive alkaloids from the New Zealand ascidian *Lissoclinum notti*. Tetrahedron 58: 9779-9783.

Bar-on, P., Millard, C. B, Harel, M., Dvir, H., Enz, A., Sussman, J. L., and Silman, I. 2002. Kinetic and structural studies on the interaction of cholinesterase with the anti-alzheimer drug rivastigmine. Biochemistry 41: 3555-3564.

Batrakov, S. G., Nikitin, D. I., Sheichenko, V. I., and Ruzhitsky, A. O. 1998. A novel sulfonic-acid analogue of ceramide is the major extractable lipid of the gram-negative marine bacterium *Cyclobacterium marinus* WH. Biochim. Biophys. Acta 1391: 79-91.

Bergmann, W., and Bruke D. C. 1955. Contribution to the study of marine products. XXXIX. The nucleosides of sponges. III. Spongothymidine and spongouridine. J. Org. Chem. 20: 1501-1507.

Bergmann, W., and Feeney, R. J. 1951. Contribution to the study of marine products. XXXII. The nucleosides of sponges. J. Org. Chem. 16: 981-987.

Bohlmann, F, Zdero, C., Robinson, H., and King, R. M. 1979. Ein neues germacren-derivat sowie ein diterpenmalonat aus *Baccharis*-arten. Phytochemistry 18: 1993-1996.

Bohlmann, F., and Ehlers, D. 1977. Ein neues *cis,cis*-germacrolid aus *Chrysanthemum poteriifolium*. Phytochemistry 16: 137-138.

Bollag, D. M., McQueney, P. A., Zhu, J., Hensens, O., Koupal, L., Liesch, J., Goetz, M., Lazarides, E., and Woods, C. M. 1995. Epothilones, a new class of microtubule-stabilizing agents with a taxol-like mechanism of action. Cancer Res. 55: 2325-2333.

Bonner, T. G., Lewis, D., and Rutter, K. 1981. Opening of cyclic acetals by trichloro-, dichloro-, and tribromo borane. J. Chem. Soc., Perkin Trans. 1 1807-1810.

Bontemps, N., Bonnard, I., Banaigs, B., Combaut, G., and Francisco, C. 1994. Cystodamine, a new cytotoxic fused polyaromatic alkaloid from the Mediterranean ascidian *Cystodytes* dellechiajei. Tetrahedron Lett. 35: 7023-7026.

Boutagy, J., and Thomas, R. 1974. Olefin synthesis with organic phosphonate carbanions. Chem. Rev. 74: 87-99.

Burreson, B. J., Christophersen, C., and Scheuer, P. J. 1975. Co-occurrence of two terpenoids isocyanide-formamide pairs in a marine sponge (*Halichondrida* sp.). Tetrahedron 31: 2015-2017.

Cafieri, F., Fattorusso, E., Mangoni, A., and Taglialatela-Scafati, O. 1995. Longamide and 3,7-dimethylisoguanine, two novel alkaloids from the marine sponge *Agelas longissima.* Tetrahedron Lett. 36: 7893-7895.

Carroll, A. R., and Scheuer, P. J. 1990. Kuanoniamines A, B, C, and D: pentacyclic alkaloids from a tunicate and its prosobranch mollusk predator *Chelynotus semperi.* J. Org. Chem. 55: 4426-4430.

Charyulu, G. A., McKee, T. C., and Ireland, C. M. 1989. Diplamine, a cytotoxic polyaromatic alkaloid from the tunicate *Diploma* sp. Tetrahedron Lett. 30: 4201-4202.

Chehade, C. C., Dias, R. L. A., Berlinck, R. G. S., Ferreira, A. G., Costa, L. V., Rangel, M., Malpezzi, E. L. A., de Fretas, J. C., and Hajdu, E. 1997. 1,3-Dimethylisoguanine, a new purine from the marine sponge *Amphimedon viridis.* J. Nat. Prod. 60: 729-731.

Chen, X. T., Zhou, B., Bhattacharya, S. K., Gutteridge, C. E., Pettus, T. R. R., and Danishefsky, S. J. 1998. The total synthesis of eleutherobin: a surprise ending. Angew. Chem. Int. Ed. Engl. 37: 789-792.

Chen, Y. L., Liston, D., Nielsen, J., Chapin, D., Dunaiskis, A., Hedberg, K., Ives, J., Johnson, J. Jr., and Jones, S. 1994. Synthesis and anticholinesterase activity of tetrahydrobenzazepine carbamates. J. Med. Chem. 37: 1996-2000.

Cho, S. J., Serrano, M. G., Bier, J., and Tropsha, A. 1996. Structure based alignment and comparative molecular field analysis of acetylcholinesterase inhibitors. J. Med. Chem. 39: 5064-5071.

Compagnone, R. S., and Faulkner, D. J. 1995. Metabolites of the palauan sponge *Axinyssa aplysinoides.* J. Nat. Prod. 58: 145-148.

Copp, B. R., Jompa, J., Tahir, A., and Ireland, C. M. 1998. Styelsamines A-D: new tetracyclic pyridoacridine alkaloids from the Indonesian ascidian *Eusynstyela latericius.* J. Org. Chem. 63: 8024-8026.

Copp, B. R., Wassvik, C. M., Lambert, G., and Page, M. J. 2000. Isolation and characterization of the new purine 1,3,7-trimethylisoguanine from the New Zealand ascidian *Pseudodistoma cereum.* J. Nat. Prod. 63: 1168-1169.

Corley, D. G., Herb, R., Scheuer, P. J., and Paul, V. J. 1988. Laulimalides: new potent cytotoxic macrolides from a marine sponge and a nudibranch predator. J. Org. Chem. 53: 3644-3646.

Cowden, C. J., Paterson, I. 1997. Cancer drugs better than taxol?. Nature 387: 238-239.

Crimmins, M. T., Stanton, M. G., and Allwein, S. P. 2002. Asymmetric total synthesis of (-)-laulimalide: exploiting the asymmetric glycolate alkylation reaction. J. Am. Chem. Soc. 124: 5958-5959.

Cutignano, A., Bruno, I., Bifulco, G., Casapullo, A., Debitus, C., Gomez-Paloma, L., and Riccio, R. 2001. Dactylolide, a new cytotoxic macrolide from the Vanuatu sponge *Dactylospongia* sp. Eur. J. Org. Chem. 2001: 775-778.

Dalcanale, E. 1986. Selective oxidation of aldehydes to carboxylic acids with sodium chlorite-hydrogen peroxide. J. Org. Chem. 51: 567-569.

Eder, C., Schupp, P., Proksch, P., Wray, V., Steube, K., Muller, C. E., Frobenius, W., Herderich, M., and van Soest, R. W. M. 1998. Bioactive pyridoacridine alkaloids from the Micronesian sponge *Oceanapia* sp. J. Nat. Prod. 61: 301-305.

Ellman, G.L., Lourtney, D.K., Andres, V., and Gmelin, G. 1961. A new and rapid colorimetric determination of acetylcholinesterase activity. Biochem. Pharmacol. 7: 88-95.

Faulkner, D. J. 1988. Marine natural products. <u>Nat. Prod. Rep.</u> 4: 613-663.

Faulkner, D. J. 2000. Highlights of marine natural products chemistry (1972-1999). <u>Nat. Prod. Rep.</u> 17: 1-6.

Faulkner, D. J. 2002. Marine natural products. <u>Nat. Prod. Rep.</u> 19: 1-48.

Fookes, C. J. R., Garson, M. J., Macleod, J. K., Skelton, B. W., and White, A. H. 1988. Biosynthesis of diisocyanoadociane, a novel diterpene from the marine sponge *Amphimedon* sp crystal structure of a monoamide derivative. <u>J. Chem. Soc., Perkin Trans. 1</u> 5:1003-1011.

Frisch, M. J., Trucks, G. W., Schlegel, H. B., Scuseria, G. E., Robb, M. A., Cheeseman, J. R., Zakrzewski, V. G., Montgomery, J. A., Stratmann, R. E., Burant, L. C., Dapprich, S., Millam, J. M., Daniels, A. D., Kudin, K. N., Strain, M. C., Farkas, O., Tomasi, J., Barone, V., Cossi, M., Cammi, R., Mennucci, B., Pomelli, C., Adamo, C., Clifford, S., Ochterski, J., Petersson, G. A., Ayala, P. Y., Cui, Q., Morokuma, K., Malick, D. K., Rabuck, A. D., Raghavachari, K., Foresman, J.B., Cioslowsko, J., Ortiz, J. V., Fox, D. J., Keith, T., Al-Laham, M. A., Peng, C. Y., Nanayakkara, A., Gonzalez, C., Challacombe, M., Gill, P. M. W., Johnson, B. G., Chen, W., Wong, M. W., Andres, J. L., Head-Gordon, M., Replogle, E. S., and Pople, J. A. 1998. <u>Gaussian 98 (Version A.1)</u>, Gaussian Inc, Pittsburgh, PA.

Gallagher, B. M., Fang, F. G., Johannes, C. W., Pesant, M., Tremblay, M. R., Zhao, H., Akasaka, K., Li, X-., Liu, J., and Littlefield, B. A. 2004. Synthesis and biological evaluation of (-)-laulimalide analogues. <u>Bioorg. Med. Chem. Lett.</u> 14: 575-579.

Ganber, D., Pollak, F. C., and Berge, R. G. 1995. A sesquiterpene alcohol from *Streptomyces citreus* CBS 109.60. <u>J. Nat. Prod.</u> 58: 1790-1793.

Gasteiger, J., and Marsili, M. 1980. Iterative partial equalization of orbital electronegativity-A rapid access to atomic charges. <u>Tetrahedron</u> 36: 3219-3288.

Ghosh, A. K., and Wang, Y. 2000. An enantioselective synthesis of the C2-C16 segment of antitumor macrolide laulimalide. <u>Tetrahedron Lett.</u> 41: 2319-2322.

Ghosh, A. K., and Wang, Y. 2000. Total synthesis of (-)-laulimalide. <u>J. Am. Chem. Soc.</u> 122: 11027-11028.

Ghosh, A. K., Mathivanan, P., and Capiello, J. 1997. Synthetic studies of antitumor macrolide laulimalide: enantioselective synthesis of the C3-C14 segment by a catalytic hetero Diels-alder strategy. Tetrahedron Lett. 38: 2427-2429.

Gilson, M. K., Straatsma, T. P., McCammon, J. A., Ripoll, D. R., Faerman, C. H., Axelsen, P. H., Silman, I., and Sussman, J. L. 1994. Open back door in a molecular-dynamics simulation of acetylcholinesterase. Science 263: 1276-1278.

Gordon, M. A., Carpenter, D. E., and Wilson, I. B. 1978. The turnover numbers of acetylcholinesterase forms. Mol. Pharmacol. 14: 266-270.

Gottesman, M. M., and Pastan, I. 1993. Biochemistry of multidrug resistance mediated by the multidrug transporter. Annu. Rev. Biochem. 62: 385-427.

Greenblatt, H. M., Kryger, G., Lewis. T., Silman. I., and Sussman. J. L. 1999. Structure of acetylcholinesterase complexed with (-)-galanthamine at 2.3 A resolution. FEBS Lett. 463: 321-326.

Groweiss, A., Shmueli, U., and Kashman, Y. 1983. Marine toxins of *Latrunculia magnifica.* J Org. Chem. 48: 3512-3516.

Gulavita, N. K., Gunasekera, S. P., Pomponi, S. A. 1992. Isolation of latrunculin A, 6,7-epoxylatrunculin A, fijianolide A, and euryfuran from a new genus of the family Thorectidae. J. Nat. Prod. 55: 506-508.

Gunasekera, S. P., Longley, R. E., and Isbrucker, R. A. 2001. Acetylated analogues of the microtubule-stabilizing agent discodermolide: preparation and biological activity. J. Nat. Prod. 64: 171-174.

Gunawardana, G. P., Koehn, F. E., Lee, A. Y., Clardy, J., He, H-., and Faulkner, D. J. 1992. Pyridoacridine alkaloids from deep-water marine sponges of the family pachastrellidae: structure revision of dercitin and related compounds and correlation with the kuanoniamines. J. Org. Chem. 57: 1523-1526.

Gunawardana, G. P., Kohmoto, S., and Burres, N. S. 1989. New cytotoxic acridine alkaloids from two deep water marine sponges of the family *Pachastrellidae.* Tetrahedron Lett. 30: 4359-4362.

Hagadone, M. R., Burrenson, B. J., Scheuer, P. J., Finer, J. S., Cardy, J. 1979. Defense allomones of the nudibranch *Phyllidia varicose* Lamarck 1801. Helv. Chim. Acta 62: 2484-2494

Hagadone, M. R., Scheuer, P. J., and Holm, A. 1984. On the origin of the isocyano function in marine sponges. J. Am. Chem. Soc. 106: 2447-2448.

Hamel, E., Sackett, D. L., Vourloumis, D., and Nicolaou, K. C. 1999. The coral-derived natural products eleutherobin and sarcodictyins A and B: effects on the assembly of purified tubulin with and without microtubule-associated proteins and binding at the polymer taxoid site. Biochemistry 38: 5490-5498.

Harel, M., Quinn, D. M., Nair, H. K., Silman, I., and Sussman, J. L. 1996. The X-ray structure of a transition state analogue complex reveals the molecular origins of the catalytic power and substrate specificity of acetylcholinesterase. J. Am. Chem. Soc. 118: 3240-3246.

Harel, M., Schalk, I., Ehret-Sabatier, L., Bouet, F., Goelgner, M., Hirth, C., Axelsen, P. H., Silman, I., and Sussman, J. L. 1993. Quarternary ligand binding to aromatic residues in the active-site gorge of acetylcholinesterase. Proc. Natl. Acad. Sci. USA 90: 9031-9035.

Hassner, A., and Alexanian, V. 1978. Direct room temperature esterification of carboxylic acids. Tetrahedron Lett. 46: 4475-4478.

He, H., and Faulkner, D. J. 1991. Eudistones A and B: two novel octacyclic alkaloids from a Seychelles tunicate, *Eudistoma* sp. J. Org. Chem. 56: 5369-5371.

He, H., Faulkner, D. J., Shumsky, J. S., Hong, K., and Clardy, J. 1989. A sesquiterpene thiocyanate and three sesquiterpene isothiocyanates from the sponge *Tachyopsis aplysinoides.* J. Org. Chem. 54: 2511-2514.

He, H., Salva, J., Catalos, R. F., and Faulkner, D. J. 1992. Sesquiterpene thiocyanates and isothiocyanates from *Axinyssa aplysinoides.* J. Org. Chem. 57: 3191-3194.

Heathcock, C. H., and Skyler, D. 2002. The pyridoacridine family tree: a useful scheme for designing synthesis and predicting undiscovered natural products. J. Nat. Prod. 65: 1573-1581.

Hofle, G., Bedorf, N., Steinmetz, H., Schemburg, D., Gerth, K., and Reichenbach, H. 1996. Epothilones A and B-novel 16-membered macrolides and cytotoxic activity: isolation, crystal structure, and conformation in solution. Angew. Chem. Int. Ed. Engl. 35: 1567-1569.

Hood, K. A., West, L. M., Rouwe, B., Northcote, P. T., Berridge, M. V., Wakefield, St. J., and Miller, J. H. 2002. Peloruside A, a novel antimitotic agent with paclitaxel-like microtubule-stabilizing activity. Cancer Res. 62: 3356-3360.

Horne,D. A., and Jordan, A. 1978. An efficient reduction of acetals and ketals to methyl ethers. Tetrhedron Lett. 19: 1357-1358.

Howard, W. L., and Brown, Jr., J. H. 1961. Hydrolysis of ketals. J. Org. Chem. 26: 1026-1028.

Iguchi, K., Shimura, H., Yang, Z., and Yamada, Y. 1993. A new 5α,8α-epidioxy sterol from the okinawan marine sponge of the *Axinyssa* genus. Steroids 58: 410-413.

Ingkaninun, K., de Best, C. M., van der Heijden, R., Hofte, A. J. P., Karabatak, B., Irth, H., Tjaden, U. R., van der Greef, J., and Verpoorte, R. 2000. High performance liquid chromatography with on-line coupled UV, mass spectrometric and biochemical detection for identification of acetylcholinesterase inhibitors from natural products. J. Chromatogr. A 872: 61-73.

Inoue, A., Kawai, T., Wakita, M., Iimura, Y., Sugimoto, H., and Kawakami, Y. 1996. The simulated binding of (±)-2,3-dihydro-5,6-dimethoxy-2-[[1-(phenyl,ethyl)-4-piperidinyl]methyl]-1H-inden-1-one hydrochloride (E2020) and related inhibitors to free and acylated acetylcholinesterase and corresponding structure-acitvity analyses. J. Med. Chem. 39: 4460-4470.

Ireland, C. M., Copp, B. R, Foster, M. P., McDonald, L. A., Radisky, D. C., and Swersey, J. C. 1993. Marine biotechnology volume 1: pharmaceutical and bioactive natural products. New York: Plenum Press.

Ishihara, Y., Kato, K., and Goto, G. 1991. Central cholinergic agents. I. potent acetylcholinesterase inhibitors, 2-[ω-[N-alkyl-N-(ω-phenylalkyl)amino]alkyl]-1H-isoindole-1,3(2H)-diones, based on a new hypothesis of the enzyme's active site. Chem. Pharm. Bull. 39: 3225-3235.

Ishitsuka, M., Kusumi, T., Kakisawa, H., Kawakami, Y., Nagai, Y., and Sato, T. 1986. Structural elucidation and conformational analysis of germacrane-type diterpenoids from the brown alga Pachydictyon coriaceum. Tetrahedron Lett. 27: 2639-2642.

Jefford, C. W., Bernardinelli, G., Tanaka, J., and Higa, T. 1996. Structures and absolute configuration of marine toxins, latrunculin A and laulimalide. Tetrahedron Lett. 37: 156-162.

Jordan, M. A., Wendell, K., Gardiner, S, Derry, W. B., Copp, H., and Wilson, L. 1996. Mitotic block induced in HeLa cells by low concentrations of paclitaxel

(taxol) results in abnormal mitotic exit and apoptotic death. Cancer Res. 56: 816-825.

Kakou, Y., Crews, P., Bakus, G. J. 1987. Dendrolasin and latrunculin A from the Fijian sponge *Spongia mycofijiensis* and an associated nudibranch *Chromodoris lochi.* J. Nat. Prod. 50: 482-484.

Karuso, P., and Scheuer, P. J. 1989. Biosynthesis of isocyanoterpenes in sponges. J. Org. Chem. 54: 2092-2095.

Kashman, Y., Groweiss, A., and Shmueli, U. 1980. Latrunculin A, a new 2-thiazolidinone macrolide from the marine sponge Latrunculia magnifica. Tetrahedron Lett. 21: 3629-3632.

Kavallaris, M., Verrills, N. M., and Hill, B. T. 2001. Anticancer therapy with novel tubulin-interacting drugs. Drug Resist. Updates 4: 392-401.

Kawakami, Y., Inoue, A., Kawai, T., Wakita, M., Sugimoto, H., and Hopfinger, A. J. 1996. The rationale for E2020 as a acetylcholinesterase inhibitor. Bioorg. Med. Chem. 4: 1429-1446.

Kim, J., Pordesimo, E. O., Toth, S. I., Schmitz, F. J., and van Altena, I. 1993. Pantherinine, a cytotoxic aromatic alkaloid, and 7-deazainosine from the ascidian *Aplidium pantherinum.* J. Nat. Prod. 56: 1813-1816.

Kim, Y. H., Nachman, R. J., Pavelka, L., and Mosher, H. S. 1981. Dorisidone, 1-methylisoguaninosine, from *Anisodoris nobilis*; structure, pharmacological properties and synyhesis. J. Nat. Prod. 44: 206-214.

Kobayashi, J., Cheng, J., Nakamura, H., Ohizumi, Y., Hirata, Y., Sasaki, T. Ohta, T., and Nozoe, S. 1988. Ascididemin, a novel pentacyclic aromatic alkaloid with potent antileukemic activity from the okinawan tunicate *Didemnum* sp. Tetrahedron Lett. 29: 1177-1180

Kobayashi, J., Cheng, J., Walchli, M. R., Nakamura, N., Hirata, Y., Sasaki, T., and Ohizumi, Y. 1988. Cystodytins A, B, and C, novel tetracyclic aromatic alkaloids with potent antineoplastic activity from the Okinawan tunicate *Cystodytes dellechiajei.* J. Org. Chem. 53: 1800-1804.

Kodama, K., Higushi, R., Miyamoto, T., and van Soest, R. W. M. 2003. (-)-Axinyssene: a novel cytotoxic diterpene from a Japanese marine sponge *Axinyssa* sp. Org. Lett. 5: 169-171.

Koren-Goldshlager, G., Aknin, M., Gaydou, E. M., and Kashman, Y. 1998. Three new alkaloids from the marine tunicate *Cystodytes*. J. Org. Chem. 63: 4601-4603.

Kotsuki, H., Ushio, Y., Yoshimura, N., and Ochi, M. 1986. Efficient method for the reduction cleavage acetals and ketals with $Zn(BH_4)_2$/Me_3SiCl. J. Org. Chem. 52: 2594-2596.

Kowalski, R. J., Giannakakou, P., Gunasekera, S., Longley, R. E., Day, B. W., and Hamel, E. 1997. The microtubule-stabilizing agent discodermolide competitively inhibits the binding of paclitaxel (taxol) to tubulin polymers, enhances tubulin nucleation reactions more potently than paclitaxel, and inhibits the growth of paclitaxel-resistant cells. Mol. Pharmacol. 52: 613-622.

Kozikowski, A. P., Miller, C. P., Yamada, F., Pang, Y. P., Miller, J. H., McKinney, M., and Ball, R. G. 1991. Delineating the pharmacophoric elements of huperzine A. Importance of the unsaturated 3-carbon bridge to its AChE inhibitory activity. J. Med. Chem. 34: 3399-3402.

Kryger, G., Silman, I., and Sussman, J. L. 1998. Three-dimensional structure of a complex of E2020 with acetylcholinesterase from *Torpedo californica*. J. Physiol. Paris 92: 191-194.

Lee, F. Y. F., Borzilleri, R., Fairchild, C. R., Kim, S. H., Long, B. H., Reventos-Suarez, C., Vite, G. D., Rose, W. C., and Kramer, R. A. 2001. BMS-247550: a novel epothilone analog with a mode of action similar to paclitaxel but possessing superior antitumor efficacy. Clin. Cancer Res. 7: 1429-1437.

Li, C., Schmitz, F. J., and Kelly, M. 1999. New nitrogenous bisabolene-type sesquiterpenes from a Micronesian marine sponge, *Axinyssa* species. J. Nat. Prod. 62: 1330-1332.

Lindsay, B. S., Battershill, C. N., and Copp, B. R. 1999. 1,3-dimethylguanine, a new purine from the New Zealand ascidian *Botrylloides leachi*. J. Nat. Prod. 62: 638-639.

Long, B. H., Carboni, J. M., Wasserman, A. J., Cornell, L. A., Casazza, A. M., Jensen, P. R., Lindel, T., Fenical, W., and Fairchild, C. R. 1998. Eleutherobin, a novel cytotoxic agent that induces tubulin polymerization, is similar to paclitaxel (Taxol). Cancer Res. 58: 1111-1115.

Lorian, V. 1980. Antibiotics in laboratory medicine. Baltimore: The Williams & Wilkins Co.

Luche, J. 1978. Lanthanides in organic chemistry. 1. Selective 1,2 reductions of conjugated ketones. J. Am. Chem. Soc. 100: 2226-2227.

MacPhee-Quigley, K., Taylor, P., and Taylor, S. 1985. Primary structures of the catalytic subunits from two molecular forms of acetylcholinesterase, a comparison of NH2-terminal and active center sequence. J. Biol. Chem. 260: 12185-12189.

Marcus, A. H., Molinski, T. F., Fahy, E., and Faulkner, D. J. 1989. 5-Isothiocyanatopupukeanane from a sponge of the genus *Axinyssa*. J. Org. Chem. 54: 5184-5186.

Mayer, A. M. S. 1999. Marine pharmacology in 1998: antitumor and cytotoxic compounds. The Pharmacologist 41: 159-164.

McCarthy, P. J., Pitis, T. P., Gunawardana, G. P., Kelly-Borges, M., and Pomponi, S. A. 1992. Antifungal activity of meridine, a natural product from the marine sponge *Corticium* sp. J. Nat. Prod. 55: 1664-1668.

McDonald, L. A., Eldredge, G. S., Barrows, L. R., Ireland, C. M. 1994. Inhibition of topoisomerase II catalytic activity by pyridoacridine alkaloids from a *Cystodytes* sp. ascidian: a mechanism for the apparent intercalator-induced inhibition of topoisomerase II. J. Med. Chem. 37: 3819-3827.

McDougal, P. G., Rico, J. G., Oh, Y., and Condon, B. D. 1986. A convenient procedure for the monosilylation of symmetric 1,n-diols. J. Org. Chem. 51: 3388-3390.

Minnard, A. J., Wijnberg, J. B. P. A., and de Groot, A. 1994. The synthesis of (+)-Hedycaryol, starting from natural (-)-Guaiol. Tetrahedron 50: 4755-4764.

Mitchell, S. S., Whitehill, A. B., Trapido-Rosenthal, H. G., and Ireland, C. M. 1997. Isolation and characterization of 1,3-dimethylisoguanine from the Bermudian sponge *Amphimedon viridis*. J. Nat. Prod. 60: 727-728.

Molinski, T. F. 1993. Marine pyridoacridine alkaloids: structure, synthesis, and biological chemistry. Chem. Rev. 93: 1825-1838.

Molinski, T. F., and Ireland, C. M. 1989. Veramines A and B, new cytotoxic thioalkaloids from *Lissoclinum vareau*. J. Org. Chem. 54: 4256-4259.

Molinski, T. F., Fahy, E., Faulkner, D. J., Duyne, G. D., and Clardy, J. 1988. Petrosamine, a novel pigment from the marine sponge *Petrosia* sp. J. Org. Chem. 53: 1340-1341.

Mooberry, S. L., Tien, G., Hemandez, A. H., Plubrukarn, A., and Davidson, B. S. 1999. Laulimalide and isolaulimalide, new paclitaxel-like microtubule-stabilizing agents. Cancer Res. 120: 10814-10826.

Morris, G. M., Goodsell, D. S., Halliday, R. S., Huey, R., Hart, W. E., Belew, R. K., and Olson, A. J. 1998. Automated docking using a lamarckian genetic algorithm and an empirical binding free energy function. J. Comput. Chem. 19: 1639-1662.

Mulzer, J., and Ohler, E. 2003. Microtubule-stabilizing marine metabolite laulimalide and its derivatives: synthetic approaches and antitumor activity. Chem. Rev. 103: 3753-3786.

Mulzer, J., Hanbauer, M. 2000. Synthesis of the C1-C-12 dihydropyran segment of the antitumor agent laulimalide by ring closing metathesis. Tetrahedron Lett. 41: 33-36

Nadolski, G. T., and Davidson, B. S. 2001. Synthetic studies toward the microtubule-stabilizing agent laulimalide: synthesis of the C1-C14 fragment. Tetrahedron Lett. 42: 797-800.

Neises, B., and Steglich, W. 1978. Simple method for the esterification of carboxylic acids. Angew. Chem. Int. Ed. Engl. 17: 522-524.

Nelson, S. G., Cheung, W. S., Kassick, A. J., and Hilfiker, M. A. 2002. A de novo enantioselective total synthesis of (-)-laulimalide. J. Am. Chem. Soc. 124: 13654-13655

Nicolaou, K. C., Dai, W. M., and Guy, R. K. 1994. Chemistry and biology of taxol. Angew. Chem. Int. Ed. Engl. 33: 15-44.

Nicolaou, K. C., Roschanger, F., and Vourloumis, D. 1998. Chemistry biology of epothilone. Angew. Chem. Int. Ed. Engl. 37: 2014-2045.

Nicolaou, K. C., Xu, J. Y., Kim, S., Pfefferkorn, J., Oshima, T., Vourloumis, D., and Hosokawa, S. 1998. Total synthesis of sarcodictyins A and B. J. Am. Chem. Soc. 120: 8661-8673.

Nilar, Sidebottom, P. J., Carte, B. K., and Butler, M. S. 2002. Three new pyridoacridine type alkaloids from a Singaporean ascidian. J. Nat. Prod. 65: 1198-1200.

Nogales, E., Wolf, S. G., Downing, K. H. 1998. Structure of the $\alpha\beta$ tubulin dimmer by electron crystallography. Nature 391: 199-203.

Ojima, I., Chakravarty, S., Inoue, T., Lin, S., He, L., Horwitz, S. B., Kuduk, S. D., and Danishesky, S. J. 1999. A common pharmacophore for cytotoxic natural products that stabilize microtubule. Proc. Natl. Acad. Sci. USA 96: 4256-4261.

Okuda, R. K., Scheuer, P. J. 1985. Latrunculin A, ichthyotoxic constituent of the nudibranch *Chromodoris elisabethina*. Experientia 41: 1355-1356.

Osinga, R., Tramper, J., and Wijffels, R. H. 1998. Cultivation of marine sponges for metabolite production: applications for biotechnology. Trends Biotechnol. 16:130-134.

Patil, A. D., Freyer, A. J., Reichwein, R., Bean, M. F., Faucette, L., and Johnson, R. K. 1997. Two new nitrogenous sesquiterpenes from the sponge *Axinyssa aplysinoides*. J. Nat. Prod. 60: 507-510.

Perry, N. B., Blunt, J. W., and Munro, M. H. G. 1987. 1,3,7-Trimethylguanine from the sponge *Latrunculia brevis*. J. Nat. Prod. 50: 307-308.

Pettit, G. R., Herald, C. L., Doubek, D. L., Herald, D. L., Arnold, E., and Clardy, J. 1982. Isolation and structure of bryostatin 1. J. Am. Chem. Soc. 104: 6846-6848.

Pilger, C., Bartolucci, C., Lamba, D., Tropsha, A., and Fels, G. 2001. Accurate prediction of the bound conformation of galanthamine in the active site gorge of *Torpedo Californica* acetylcholinesterase using molecular docking. J. Mol. Graphics. Modell. 19: 288-296.

Plubrukarn, A., and Davidson, B. S. 1998. Arnoamines A and B, new cytotoxic pentacyclic pyridoacridine alkaloids from the ascidian *Cystodytes* sp. J. Org. Chem. 63: 1657-1659.

Pryor, D. E., O'Brate, A., Bilcer, G., Diaz, J. F., Wang, Yu, Wang, Yo, Kabaki, M., Jung, M. K., Andreu, J. M., Ghosh, A. K., Giannakakou, P., and Hamel, E. 2002. The Microtubule stabilizing agent laulimalide does not bind in the taxoid site, kills cells resistant to paclitaxel and epothilones, and may not require its epxide moiety for activity. Biochemistry 41: 9109-9115.

Quinn, D. M. 1987. Acetylcholinesterase: enzyme structure, reaction dynamics, and virtual transition states. Chem. Rev. 87: 955-979.

Quinoa, E., Kakou, Y., and Crews, P. 1988. Fijianolides, polyketide heterocycles from a marine sponge. J. Org. Chem. 53: 3642-3644.

Ravelli, R. B. G., Raves, M. L., Ren, Z., Bourgeois, D., Roth, M., Kroon, J., Silman, I., Sussman, J. L. 1998. Static Laue diffraction studies on acetylcholinesterase. Acta Crystallogr. D54: 1359-1366.

Rhee, I. K., van de Meent, M., Ingkaninan, K., and Verpoorte, R. 2001. Screening for acetylcholinesterase inhibitors from Amaryllidaceae using silica gel thin-layer chromatography in combination with bioactivity staining. J. Chromatogr. A 915: 217-223.

Rogers, D., Moss, G. P., and Neidle, S. 1972. Proposed conventions for describing germacranolide sesquiterpenes. J. Chem. Soc., Chem. Commun. 142-143.

Salomon, C. E., and Faulkner, D. J. 1996. Sagitol, a pyridoacridine alkaloid from the sponge *Oceanapia sagittaria*. Tetrahedron Lett. 37: 9147-9148.

Schiff, P. B., and Horwitz, S. B. 1980. Taxol stabilizes microtubule in mouse fibroblast cells. Proc. Natl. Acad. Sci. USA 77: 1561-1565.

Schiff, P. B., Fant, J., and Horwitz, S. B. 1979. Promotion of microtubule assembly in vitro taxol. Nature 277: 665-667.

Schmitz, F. J, DeGuzman, F. S., Hossain, M. B., and van der Helm, D. 1991. Cytotoxic aromatic alkaloids from the ascidian *Amphicarpa meridiana* and *Leptoclinides* sp.: meridine and 11-hydroxyascididemin. J. Org. Chem. 56: 804-808.

Schmitz, F. J., Agarwal, S. K., and Gunasekera, S. P. 1983. Amphimedine, new aromatic alkaloid from a pacific sponge, *Amphimedon*sp. Carbon connectivity determination from natural abundance ^{13}C-^{13}C coupling constants. J. Am. Chem. Soc. 105: 4835-4836.

Searle, P. A., and Molinski, T. F. 1994. Five new alkaloids from the tropical ascidian, *Lissoclinum* sp. lissoclinotoxin A is chiral. J. Org. Chem. 59: 6600-6605.

Segawa, M., Kimiaki, Y., and Shirahama, H. 1990. A gremacrane-type sesquiterpene from the brown alga *Dictyopteris divaricata.* Phytochemistry 29: 973-974.

Shimizu, A., Nishiyama, S. 1997. Synthesis of the C1-C16 fragment of marine toxin, laulimalide. Tetrahedron Lett. 38:6011-6014.

Shimizu, A., Nishiyama, S. 1997. Synthetic approaching towards laulimalide: synthesis of the C12-C-29 fragment. Synlett. 1209-1210.

Siddiqui, M F., and Levey, A. I. 1999. Cholinergic therapies in Alzheimer's disease. Drugs of the Future 24: 417-424.

Simpson, J. S., and Garson, M. J. 1998. Thiocyanate biosynthesis in the tropical marine sponge *Axinyssa* n. sp. Tetrahedron Lett. 39: 5819-5822.

Simpson, J. S., and Garson, M. J. 2001. Advanced precursors in marine biosynthetic study. Part 2: the biosynthesis of isocyanides and isothiocyanates in the tropical marine sponge *Axinyssa* n. sp. Tetrahedron Lett. 42: 4267-4269.

Simpson, J. S., Hooper, J. N. A., Cline, E. I., Angerhofer, C. K., and Garson, M. J. 1997. Terpene metabolites from the tropical marine sponge, *Axinyssa* sp. Aust. J. Chem. 50, 1123-1127.

Skehan, P., Storeng, R., Scudiero, D., Monks, A., McMahon, J., Vistica, D., Warren, J. T., Bokesch, H., Kenney, S., and Boyed, M. R. 1990. New colorimetric cytotoxicity assay for anticancer-drug screening. J. Natl. Cancer Inst. 82: 1107-1112.

Smith, A. B. III., Beauchamp, T. J., LaMarche, M. J., Kaufman, M. D., Qiu, Y., Arimoto, H., Jones, D. R., and Kobayashi, K. 2000. Evolution of a gram-scale synthesis of (+)-discodermolide. J. Am. Chem. Soc. 122: 8654-8664.

Spector, I., Shochet, N. R., Kashman, Y., Groweiss, A. 1983. Latrunculins: novel marine toxins that disrupt microfilament organization in cultured cells. Science 219: 493-495.

Stanslas, J., Hagan, D. J., Ellis, M. J., Turner, C., Carmichael, J., Ward, W., Hammonds, T. R., and Stevens, M. F. G. 2000. Antitumor polycyclic acridines. 7. synthesis and biological properties of DNA affinic tetra- and pentacyclic acridines. J. Med. Chem. 43: 1563-1572.

Stephen, H., and Lavallee, P. 1975. The preparation and synthetic utility of *tert*-butyldiphenylsilyl ethers. Can. J. Chem. 53: 2975-2977.

Sterzycki, R. 1979. Pyridinium tosylate, a mild catalyst for formation and cleavage of dioxolane-type acetals. Synthesis 724-725.

Still, W. C., and Gennari, C. 1983. Direct synthesis of Z-unsaturated esters. A useful modification of the Horner-Emmons olefination. Tetrahedron Lett. 24: 4405-4408.

Sugimoto, H., Iimura, Y., Yamanishi, Y., and Yamatsu, K. 1995. Synthesis and structure-activity relationships of acetylcholinesterase inhibitors: 1-benzyl-4-[5,6-dimethoxy-1-oxoindan-2-yl)methyl]piperidine hydrochloride and related compounds. J. Med. Chem. 38: 4821-4829.

Sun, H. H., and Fenical, W. 1979. Hydroxydilophol, a new monocyclic diterpenoid from the brown alga *Dictyota masonii*. J. Org. Chem. 44: 1354-1356.

Sussman, J. L., Harel, M., Frolow, F., Oefner, C., Goldman, A., Toker, L., and Silman, I. 1991. Atomic structure of acetylcholinesterase from *Torpedo californica*: a prototypic acetylcholine-binding protein. Science 253: 872-879.

Suzuki, M., Kowata, N., Kobayashi, H., and Tanaka, I. 1990. The structure of a germacrane-type sesquiterpene alcohol, a possible precursor of guanine-type sesquiterpenes from the brown alga *Dictyopteris divaricata*. Chem. Lett. 2187-2190.

Tanaka, J., Higa, T., Bernardinelli, G., and Jefford, C. W. 1996. New cytotoxic macrolides from the sponge *Fasciospongia rimosa*. Chem. Lett. 255-256.

Taraporewala, I. B., Cessac, J. W., Chanh, T. C., Delgado, A. V., and Schinazi, R. F. 1992. HIV-1 neutralization and tumor cell proliferation inhibition in vitro by simplified analogues of pyrido[4,3,2-mn]thiazolo[5,4-b]acridine marine alkaloids. J. Med. Chem. 35: 2744-2752.

Tasdemir, D., Marshall, K. M., Mangalindan, G. C., Concepcion, G. P., Barrows, L. R., Harper, M. K., and Ireland, C. M. 2001. Deoxyamphimedine, a new pyridoacridine alkaloid from two tropical *Xestospongia* sponges. J. Org. Chem. 66: 3246-3248.

Taylor, P., and Lappi, S. 1975. Interaction of fluorescence probes with acetylcholinesterase site and specificity of propidium binding. Biochemistry 14: 1989-1997.

ter Haar, E., Kowalski, R. J., Hamel, E., Lin, C. M., Longley, R. E., Gunasekera, S. P., Rosenkranz, H. S., and Day, B. W. 1996. Discodermolide, a cytotoxic marine agent that stabilizes microtubules more potently than taxol. Biochemistry 35: 243-250.

Thompson, S. K., and Heathcock, C. H. 1990. Effect of cation, temperature, and solvent on the stereoselectivity of the Horner-Emmons reaction of trimethyl phosphonoacetate with aldehydes. J. Org. Chem. 55: 3386-3388.

Torres, Y. R., Bugni, T. S., Berlinck, R. G. S., Ireland, C. M., Magalhaes, A., Ferreira, A. G., and de Rocha, R. M. 2002. Sebastianines A and B, novel biologically active pyridoacridine alkaloids from the Brazilian ascidian *Cystodytes dellechiajei*. J. Org. Chem. 67: 5429-5432.

Tsunoda,T., Suzuki, M., and Noyori, R. 1979. Reaction of acetals and trialkylsilanes catalyzed by trimethylsilyl trifluoromethane sulfonate. A simple method for conversion of a acetals to ethers. Tetrahedron Lett. 20: 4679-4680.

Wani, M. C., Taylor, H. L., Wall, M. E., Coggan, P., and McPhail, A. T. 1971. Plant antitumor agents VI. The isolation and structure of taxol, a novel antileukemic and antitumor agent from *Taxus brevifolia*. J. Am. Chem. Soc. 93: 2325-2327.

Weinheimer, A. J., Youngblood, W. W., Wasecheck, P. H., Karns, T. K. B., and Ciereszko, L. S. 1970. Isolation of the elusive (-)-germacrene A from the gorgonian, *Eunicea mimosa*. Tetrahedron Lett. 7: 497-500.

Wenzel, P. J., and Crews, P. 2003. Probing biotransformation relationships among pyridoacridines by focusing on oxygenated analogues. J. Nat. Prod. 66: 873-875.

Williams, D. R., Mi, L., Mullins, R. J., and Stites, R. E. 2002. Synthesis of (-)-laulimalide: an agent for microtubule stabilization. Tetrahedron Lett. 43: 4841-4844.

Wlodek, S. T., Clark, T. W., Scott, L. R., and McCammon, J. A. 1997. Molecular dynamics of acetylcholinesterase dimmer complexed with tarcine. J. Am. Chem. Soc. 119: 9513-9522.

Yagi, H., Matsunaga, S., and Fusetani, N. 1994. Isolation of 1-methylherbipoline, a purine base from a marine sponge, *Jaspis* sp. J. Nat. Prod. 57: 837-838.

Yoshikawa, M., Morikawa, T., Toguchida, I., Harima, S., and Matsuda, H. 2000. Medicinal flowers. II. Inhibitors of nitric oxide production and absolute stereostructures of five new germacrane-type sesquiterpenes, kikkanols D, D monoacetate, E, F, and F monoacetate from the flowers of *Chrysanthemum indicum* L. Chem. Pharm. Bull. 48: 651-656.

Zaheer-ul-haq, Wellenzohn, B., Liedl, K. R., and Rode, B. M. 2003. Molecular docking studies of natural cholinesterase-inhibiting steroidal alkaloids from *Sarcococca saligna*. J. Med. Chem. 46: 5087-5090.

Zdero, C., Bohlmann, F, Solomon, J. C., King, R. M., and Robinson, H. 1989. *ent*-Clerodanes and other constituents from bolivian *Baccharis*. Phytochemistry 28: 531-542.

Zeng, C., Ishibashi, M., Matsumoto, K., Nakaike, S., and Kobayashi, J. 1993. Two new polycyclic aromatic alkaloids from the okinawan marine sponge *Biemna* sp. Tetrahedron 49: 8337-8342.

VITA

Miss Veena Satitpatipan was born on November 3, 1973 in Bangkok, Thailand. She received her Bachelor's Degree of Science in Pharmacy (2nd class honor) from the Faculty of Pharmacy, Mahidol University in 1996. She was granted a 1998 Royal Golden Jubilee Ph.D. Scholarship from the Thailand Research Fund (TRF).

Publications

Satitpatipan, V. and Suwanborirux, K. 2004. "New Nitrogenous Germacranes from a Thai Marine Sponge, *Axinyssa* n. sp." **J. Nat. Prod.** 67(3): 503-505.

Satitpatipan,V., Saen-oon, S., Ingkaninan, K., Hannongbua, S., Davidson, B. S., and Suwanborirux, K. Petrosamine, a Pyridoacridine Alkaloids, from a Thai Marine Sponge, *Petrosia* n. sp., as a New Acetylcholinesterase Inhibitor. (in preparation)

Satitpatipan,V., Ingkaninan, K., and Suwanborirux, K. 1,3,9-Trimethyl-8-hydroxyisoguanine, a New Isoguanine Base from a Thai Marine Sponge, *Petrosia* n. sp. (in preparation)

Oral presentations

Satitpatipan, V. "Chemical investigation of marine sponges" 22nd RGJ Seminar Series: Research Progress in Pharmacognosy and Phytochemistry, Febuary 11, 2003, Faculty of Pharmaceutical Sciences, Chulalongkorn University, Bangkok, Thailand.

Satitpatipan, V. "Chemical investigation of marine sponges" RGJ-Ph.D. Congress IV, April 25-27, 2003, Pattaya, Thailand. [Best presentation award in Chemistry]

Poster presentations

Satitpatipan, V., Suwanborirux, K., and Davidson, B. S. "Synthesis of the C_1-C_{14} fragment analogs of laulimalide" p. 147. The 28th Congress on Science and Technology of Thailand. October 24-26, 2002, Bangkok, Thailand.

Satitpatipan, V., Suwanborirux, K., and Davidson, B. S. "Synthesis of the C_1-C_{14} fragment analogs of laulimalide" p.13. The 19th Annual Research Meeting in Pharmaceutical Sciences. December 4, 2002, Faculty of Pharmaceutical Sciences, Chulalongkorn University, Bangkok, Thailand.

Satitpatipan, V. and Suwanborirux, K. "New antimicrobial germacranes from a Thai marine sponge, *Axinyssa* sp." p88. International Symposium: Chemistry and Biology of Marine Organisms. September 21-26, 2003, Crete, Greece.

Satitpatipan, V., Ingkaninan, K., Davidson, B. S, and Suwanborirux, K. "Secondary metabolites from a Thai marine sponge, *Petrosia* sp." p159. The 6th JSPS_NRCT Joint Seminar: Recent Advances in Natural Medicine Research. December 2-4, 2003, Faculty of Pharmaceutical Sciences, Chulalongkorn University, Bangkok, Thailand.